

**LIBRARY
Michigan State
University**

This is to certify that the
dissertation entitled

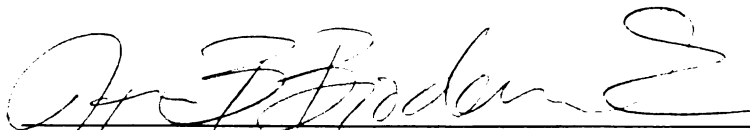
**INVESTIGATION OF PYRUVATE FORMATE-LYASE AND
PYRUVATE FORMATE-LYASE ACTIVATING ENZYME**

presented by

JIAN YANG

has been accepted towards fulfillment
of the requirements for the

Ph.D. degree in Chemistry



Major Professor's Signature

December 4, 2007

Date

PLACE IN RETURN BOX to remove this checkout from your record.
TO AVOID FINES return on or before date due.
MAY BE RECALLED with earlier due date if requested.

DATE DUE	DATE DUE	DATE DUE

**INVESTIGATION OF PYRUVATE FORMATE-LYASE AND PYRUVATE
FORMATE-LYASE ACTIVATING ENZYME**

By

Jian Yang

A DISSERTATION

**Submitted to
Michigan State University
In partial fulfillment of the requirements
for the degree of**

DOCTOR OF PHILOSOPHY

Department of Chemistry

2007

ABSTRACT

INVESTIGATION OF PYRUVATE FORMATE-LYASE AND PYRUVATE FORMATE-LYASE ACTIVATING ENZYME

By

Jian Yang

Pyruvate formate-lyase (PFL) and pyruvate formate-lyase activating enzyme (PFL-AE) are critical for facultative anaerobes to survive anaerobic conditions because they represent the key step in a major anaerobic metabolic pathway, namely glucose metabolism. PFL-AE contains a [4Fe-4S] cluster and utilizes S-adenosylmethionine (AdoMet) to generate the catalytically essential glycy radical of PFL. The [4Fe-4S]⁺ cluster of PFL-AE provides the electron required for reductive cleavage of AdoMet and generation of an intermediate 5'-deoxyadenosyl radical intermediate; this radical intermediate abstracts the pro-S hydrogen of Gly734 of PFL to generate the active enzyme. The resulting activated PFL then reversibly converts pyruvate and coenzyme A (CoA) into formate and acetyl-CoA.

Our *in vivo* investigation of PFL-AE yields evidence for [2Fe-2S]²⁺ ↔ [4Fe-4S]²⁺ cluster interconversions occurring in PFL-AE in growing *E. coli* cells, with only [4Fe-4S] clusters present under anaerobic conditions but both cluster types present under aerobic conditions. Such cluster interconversions may be physiologically relevant for PFL-AE since more of the catalytically relevant [4Fe-4S] state is produced under anaerobic culture conditions. Our results also provide unequivocal evidence for the presence of an unusual, valence-localized

$[4\text{Fe-4S}]^{2+}$ in PFL-AE in whole cells. Protein crystallography study in collaboration with Drennan lab at MIT reveals the first holo and substrate-bound structures of PFL-AE. These structures provide important insight into the possible modes of interaction in the full physiological complex. We present herein the first evidence for the activation of PFL-AE by potassium ion. The electronic structure of the $[4\text{Fe-4S}]^+$ cluster, as well as the enzyme activity, changes in the presence of K^+ , regardless of the presence of other components in the buffer. We also demonstrate that the mandatory homolytic cleavage of the S-C bond of SAM can proceed in the absence of its protein substrate PFL.

The interaction between PFL-AE and PFL employing various PFL mutants provide no evidence for the presence of a tight complex with PFL-AE. Several PFL cysteine mutants have been successfully constructed in an effort to investigate the roles of two cysteines (C418 and C419) in the PFL catalytic reaction. H/D exchange of these activated PFL cysteine mutants in D_2O indicates that C419 is not acetylated in the presence of excess pyruvate, suggesting C419 serves as a radical shuttle between G734 and C418, and that it is the C418 thiyl radical that attacks pyruvate to initiate the PFL catalytic reaction.

MoaA, another important member of the Radical SAM superfamily, has also been successfully cloned from *E. coli* genomic DNA. Subsequent transformation produces high-yield overexpressing strain. However, the overexpressed MoaA is found in inclusion bodies and various posttranslational improvements do not yield soluble MoaA, therefore preventing us from further characterizing this enzyme.

I dedicate this work to my parents Fasheng Yang and Yonglan Cao who have always been there for me in anyway possible. I dedicate this work to my beautiful and intelligent wife Fang Sheng who offered unconditional love and support thorough my life no matter what. Thank you for keeping my spirits up. Without all of you, I never would have made this far.

ACKNOWLEDGEMENTS

I would like to express sincere and heartfelt appreciation to my advisor Dr. Joan Broderick, who has provided me with academic guidance through my whole graduate program. Thank you for everything and my best wishes to your aspirations, academically and personally.

I would also like to thank my graduate committee members, Dr. Thomas J. Pinnavaia, Dr. David P. Weliky and Dr. James H. Geiger. Your guidance and support make my graduate study fruitful.

I appreciate all my collaborators. Dr. Vincent Huyhn, Dr. Ricardo Garcia, and Dr. Danilo Ortillo are the best experts to help me with Mössbauer studies. Dr. Catherine Drennan and Dr. Jessica Vey are the best experts in protein crystallography studies. Nobody is better than Dr. Brian Hoffman and Dr. Nick Lees when ENDOR studies are required. Thank you all for your support.

I would like to thank my lifelong friends in China, Xinyan Li, Dong Wang, and Peng Zhang. Thank you for your friendship and support. I am looking forward to sharing the rest of my life with you.

I would also like to thank lab friends. Dr. Jennifer Cheek provided training to help me settle down in the field. Dr. Mbako Nnyepi taught me how to perform the basic enzymatic assay. Hope you are having a good time with your family in Botswana. My thanks also go to Dr. Danilo Ortillo and Dr. Jeff Buis for your help in using the lab equipments. Dan's cake makes everyone's birthday memorable. I acknowledge Dr. Will Broderick for showing me the basic anaerobic techniques and I will always remember the road trip from Lansing to Bozeman with you. I

have a great time collaborating with Yi. It is always a pleasure to talk with Dr. Tilak Chandra about everything. Wish Meng Li find a good job in Madison. I would also like to thank my other lab friends, Magdalena Makowska-Gryska, Ziyang Su, Efthalia Kalliri, Dr. Susan Veneziano, Kaitlin Duschene, Sunshine Silver, Racheal Undelhoven and Dr. Eric Sheperd. It has been always a pleasure to work with you.

I would also like to thank the members from Dr. Dave Dooley's lab and Dr. John Peter's lab. Doreen is extremely helpful whenever bad things happen to the EPR instruments. Arathi help me setup the screening trials for the PFL R753K mutants.

TABLE OF CONTENTS

LIST OF TABLES.....	xii
LIST OF SCHEMES.....	xiii
LIST OF FIGURES	xiv
LIST OF ABBREVIATIONS	xviii

CHAPTER I

INTRODUCTION	1
I.1 Iron-Sulfur Clusters for Life	1
I.2 Radical SAM Superfamily	5
I.3 Pyruvate Formate Lyase (PFL) and Pyruvate Formate Lyase-Activating Enzyme (PFL-AE).....	17
I.4 Molybdenum Cofactor (Moco) Biosynthesis.....	27
I.5 References	29

CHAPTER II

INVESTIGATION ON THE <i>IN VIVO</i> STATES OF PFL-AE	42
II.1 Introduction	42
II.2 Materials and methods.....	49
II.3 Results and Discussion.....	55
II.3.1 Construction of overexpressing and control cells.....	55
II.3.2 Iron-sulfur cluster interconversions in PFL-AE in whole cells.....	57
II.3.3 Valence-localized $[4\text{Fe-4S}]^{2+}$ in PFL-AE in whole cells.....	64
II.3.4 Valence-localized $[4\text{Fe-4S}]^{2+}$ in purified PFL-AE	65
II.3.5 Stability of the $[4\text{Fe-4S}]^{2+}$ clusters and the valence-localized site in whole cells.....	74

II.4 Conclusions	76
II.5 References.....	78
CHAPTER III	
SPECIFIC ACTIVATION OF PFL-AE BY POTASSIUM ION	81
III.1 Introduction	81
III.2 Materials and methods.....	83
III.3 Results and Discussion.....	87
III.3.1 Effect of buffer conditions on the EPR spectra of PFL-AE	87
III.3.2 Effect of cations on PFL and PFL-AE activity.....	101
III.3.3 K_D for potassium ion on PFL-AE	105
III.4 Conclusions	109
III.5 References.....	114
CHAPTER IV	
X-RAY STRUCTURAL CHARACTERIZATION OF PFL-AE	118
VIII.1 Introduction.....	118
VIII.2 Materials and methods	120
VIII.3 Results and Discussion	123
VIII.3.1 Crystal structure of PFL-AE	123
VIII.3.2 Crystal Structure of PFL-AE with SAM and 7-mer peptide.	124
VIII.3.3 Comparison of the crystal structures of PFL-AE alone and with substrates bound.....	126
VIII.4 Conclusions	128
VIII.5 References	129
CHAPTER V	

SAM CLEAVAGE ASSAYS OF PFL-AE	131
V.1 Introduction.....	131
V.2 Materials and methods	134
V.3 Results and Discussion	138
V.3.1 SAM cleavage by PFL-AE occurs in the absence of PFL.....	138
V.3.2 One SAM is cleaved per [4Fe-4S] ¹⁺ cluster in PFL-AE.....	139
V.3.3 Effects of buffer components and substrates on rates of SAM cleavage.....	144
V.3.4 PFL mutants affect SAM cleavage by PFL-AE.....	148
V.4 Conclusions	151
V.5 References	152
CHAPTER VI	
INVESTIGATION ON THE INTERACTION OF PFL-AE AND PFL.....	154
VI.1 Introduction.....	154
VI.2 Materials and methods	159
VI.3 Results and Discussion	177
VI.3.1 Overexpression and purification of PFL G734A.....	177
VI.3.2 Activity Assay of PFL and PFL G734A	181
VI.3.3 EPR and ENDOR spectroscopy of PFL-AE/PFL G734A/(¹³ C-Methyl)-SAM.....	181
VI.3.4 Mutagenesis, transformation, overexpression, and purification of PFL R753K.....	186
VI.3.5 Binding assay of PFL-AE with PFL R753K.....	188
VI.3.6 EPR of PFL-AE with PFL R753K.....	190
VI.3.7 Attempted crystallization of PFL R753K by Microdialysis	194
VI.3.8 Construction of plasmids to express YfiD and YfiD R120K.....	194

VI.3.9 Expression and purification of YfiD and YfiD R120K	195
VI.3.10 Binding assay of PFL-AE with YfiD and YfiD R120K	196
VI.3.11 Salvage of PFL by YfiD: EPR and activity assays	198
VI.4 Conclusions	202
VI.5 References	204

CHAPTER VII

INVESTIGATION ON THE MECHANISM OF PFL BY VARIOUS CYSTEINE

MUTANTS: PFL C418A, PFL C419A, AND PFL C418A/C419A..... 206

VII.1 Introduction.....	206
VII.2 Materials and methods	210
VII.3 Results and Discussion	214
VII.3.1 Mutagenesis of PFL to produce PFL C418A, PFL C419A, and PFL C418A/C419A.....	214
VII.3.2 Expression and purification of PFL mutants	214
VII.3.3 D ₂ O exchange in the PFL cysteine mutants	217
VII.3.4 Photolysis to generate thiyl radicals on PFL cysteine mutants	225
VII.4 Conclusions	228
VII.5 References	229

CHAPTER VIII

INVESTIGATION ON THE FIRST STEP OF THE BIOSYNTHESIS OF MOCO230

VIII.1 Introduction.....	230
VIII.2 Materials and methods	237
VIII.3 Results and Discussion	247
VIII.3.1 Purification of genomic DAN from <i>E. coli</i> BL21 cells	247
VIII.3.2 Construction of the recombinant plasmids JYI58 and JYIII139.....	247

VIII.3.3 Transformation and overexpression of plasmids JYI58 and JYIII139 into Tuner(DE3)placI cells	249
VIII.3.4 Solubilization and purification of MoaA	249
VIII.3.5 Purification of denatured MoaA	252
VIII.3.6 Construction of plasmid JYIV145 for maltose binding purification	254
VIII.3.7 Transformation and overexpression of the fusion protein MBP-MoaA, and the following characterization of the fusion protein by western blotting.....	256
VIII. Conclusions	259
VIII.5 References	261

LIST OF TABLES

Table I.1.1. Functions and [Fe-S] cluster types of a few iron-sulfur cluster containing enzymes.	4
Table I.2.1. CX ₃ CX ₂ C conserved motif of the radical SAM superfamily.	8
Table III.3.2.1. Time course of the generation of glycy radical in the presence of different cations.....	103
Table V.3.3.1. Components and corresponding concentrations for each of the sample in Figure V.3.3.1.	147
Table V.3.4.1. Linear fitting of the time course of the SAM cleavage by PFL-AE in the presence of PFL, YfiD, and PFL mutants.....	150
Table VIII.4.1. Genes involved in the first step of biosynthesis of Moco.....	233
Table VIII.2.7.1 The variance of columns and buffering conditions for purification of MoaA.	243

LIST OF SCHEMES

Scheme I.1.1. A rare case of the two-electron transfer process found in nitrogenases.	3
Images in this thesis/dissertation are presented in color.	
Scheme I.2.1. Selected reactions catalyzed by radical SAM enzymes.	7
Scheme I.2.2. Structure of the 5'-deoxyadenosyl radical and its generation from AdoCbl and AdoMet.	11
Scheme I.2.3. Cleavage of AdoMet by radical SAM superfamily enzymes yields a 5'-deoxyadenosyl radical.	13
Scheme I.3.1. The overall reaction catalyzed by PFL including the two independent steps.	18
Scheme I.3.2. Proposed mechanism for iron-sulfur cluster and AdoMet-mediated radical generation catalyzed by PFL-AE.	26
Scheme VI.2.2.1. Schematic depiction of the coupled enzymatic assay for PFL activity.	163
Scheme VII.1.1. Summary of two PFL mechanisms.	209
Scheme VII.3.3.1. Theoretical results of C418A and C419A mutants reaction with pyruvate followed by buffer exchange with D ₂ O assuming the initial attack is from C418 thiyl radical.	223
Scheme VII.3.3.2. Theoretical results of C418A and C419A mutants reaction with pyruvate followed by buffer exchange with D ₂ O assuming the initial attack is from C419 thiyl radical.	224
Scheme VIII.4.1. Biosynthesis of Moco.	232
Scheme VIII.4.2. Comparision of pterin biosynthesis pathways.	234

LIST OF FIGURES

Figure I.1.1. The three major categories of iron-sulfur clusters.	2
Figure I.2.1. Crystal structures of HemN, MoaA, BioB, and LAM.	16
Figure I.3.1. Cartoon representation of the PFL-dimer in complex with pyruvate and CoA in sticks.	20
Figure I.4.1. Structure of molybdenum cofactor.	28
Figure II.3.1.1. Construction of PFL-AE-overexpressing and control cells.	56
Figure II.3.2.1. X-band EPR spectra of the control cells under different conditions.	59
Figure II.3.2.2. X-band EPR spectra of the PFL-AE cells under different conditions.	60
Figure II.3.2.3. X-band EPR spectra subtraction of the PFL-AE cells from the control cells.	61
Figure II.3.2.4. Mössbauer spectra of PFL-AE-overexpressing and control cells under different growth conditions.	63
Figure II.3.4.1. Representative Mössbauer data for the purified PFL-AE in the absence and presence of 5'-dAdo.	69
Figure II.3.4.2. Representative Mössbauer data for samples in which the added small molecule induces a valence-localized $[4\text{Fe-4S}]^{2+}$ cluster.	70
Figure II.3.4.3. Representative Mössbauer data for samples in which the added small molecule does not induce valence-localization of the $[4\text{Fe-4S}]^{2+}$ cluster. ...	71
Figure II.3.4.4. Effects of different small molecules on the X-band EPR spectra of the photoreduced $[4\text{Fe-4S}]^{1+}$ cluster of PFL-AE.	72
Figure II.3.4.5. Effects of different small molecules on the X-band EPR spectra of the photoreduced $[4\text{Fe-4S}]^{1+}$ cluster of PFL-AE.	73
Figure II.3.5.1. Mössbauer spectra of whole cell PFL-AE in the presence of SAM.	75
Figure III.3.1.1. X-band EPR spectra of reduced PFL-AE and PFL-AE/AdoMet.	88

Figure III.3.1.2. Effects of different cations on the X-band EPR spectra of the photoreduced [4Fe-4S] ¹⁺ cluster of PFL-AE.....	91
Figure III.3.1.3. Effects of oxamate or pyruvate on the X-band EPR spectra of the photoreduced [4Fe-4S] ¹⁺ cluster of PFL-AE.....	93
Figure III.3.1.4. Effects of different glassing agents on the X-band EPR spectra of the photoreduced [4Fe-4S] ¹⁺ cluster of PFL-AE.....	95
Figure III.3.1.5. Effects of different cations on the X-band EPR spectra of the photoreduced [4Fe-4S] ¹⁺ cluster of PFL-AE in the presence of glycerol.	98
Figure III.3.1.6. Effects of different glassing agents on the X-band EPR spectra of the photoreduced [4Fe-4S] ¹⁺ cluster of PFL-AE in the presence of oxamate and KCL.....	100
Figure III.3.2.1. Time course of PFL activation in the presence of different cations.	103
Figure III.3.3.1.a. EPR titration of the photoreduced [4Fe-4S] ¹⁺ cluster of PFL-AE with potassium ion.....	106
Figure III.3.3.1.b. EPR titration of the photoreduced [4Fe-4S] ¹⁺ cluster of PFL-AE with potassium ion in the presence of AdoMet.....	107
Figure III.3.3.2. Plot of EPR intensity at g = 1.86 vs. [K ⁺] for PFL-AE/[4Fe-4S] ¹⁺ in the presence of AdoMet (Figure III.3.3.1.b.)	108
Figure IV.3.1.1. A ribbons diagram of the PFL-AE holoenzyme at 2.25Å resolution.	124
Figure IV.3.2.1. A ribbons diagram of the SAM and peptide bound form of PFL-AE at 2.88 Å resolution.	126
Figure IV.3.3.1. Structural comparison of the holoform and SAM/peptide bound form of PFL-AE.	127
Figure V.3.1.1. HPLC chromatograms of SAM cleavage assays in the absence of PFL.	139
Figure V.3.2.1. Stoichiometry of SAM cleavage by PFL-AE [4Fe-4S] ¹⁺	142
Figure V.3.2.2. Time course for SAM cleavage by reduced PFL-AE.....	143
Figure V.3.3.1. Effects of various components on the SAM cleavage activity.	146

Figure V.3.4.1. Time course of the SAM cleavage by PFL-AE in the presence of PFL, YfiD, and PFL mutants.	150
Figure VI.1.1. Sequence and structural comparison of the C-terminal domains of PFL and GD.	156
Figure VI.1.2. Top, sequence comparison of the C-terminal domains of PFL and the YfiD.	158
Figure VI.3.1.1. Purification of PFL G734A by ion exchange chromatography.	179
Figure VI.3.1.2. Purification of PFL G734A by hydrophobic interaction chromatography.	180
Figure VI.3.3.1. X-band EPR spectrum of PFL-AE/SAM/PFL G734A complex.	183
Figure VI.3.3.2. Q-band EPR spectrum of PFL-AE/SAM/PFL G734A complex.	184
Figure VI.3.3.3. The field dependence data comparison of the PFL-AE/(¹³ C-Methyl)-SAM/PFL G734A complex and the PFL-AE/(¹³ C-Methyl)-SAM complex.	185
Figure VI.3.4.1. The structural topology of the local residues surrounding glycine loop of PFL.	187
Figure VI.3.5.1. Gel filtration chromatography of PFL R753K and PFL-AE mixture on a Sepharose 12 column.	190
Figure VI.3.6.1. X-band EPR spectrum of the single turnover before and after addition of PFL R753K to photoreduced PFL-AE/SAM complex.	192
Figure VI.3.6.2. X-band EPR spectrum of the multiple turnover containing photoreduced PFL-AE, SAM and PFL R753K under three different conditions.	193
Figure VI.3.9.1. Purification of YfiD by ion exchange chromatography.	196
Figure VI.3.10.1. Gel filtration chromatography of YfiD and PFL-AE mixture on a Sepharose TM 12 column.	198
Figure VI.3.10.2. SDS-PAGE analysis of fractions off the gel filtration column showing separation of PFL-AE and YfiD.	198
Figure VI.3.11.1. Plot of PFL specific activity as a function of YfiD/PFL ratio.	200
Figure VI.3.11.2. X-band EPR spectra of the PFL1-733, a 5-fold excess of YfiD and the mixture of both after "activation" by PFL-AE.	201

Figure VII.1.1. Catalytic site of PFL.....	207
Figure VII.3.1.1. Purification of PFL C418A by ion exchange chromatography.....	215
Figure VII.3.1.2. Purification of PFL C418A by hydrophobic interaction chromatography.....	216
Figure VII.3.3.1. X-band EPR spectra of activated PFL C418A with different amount of pyruvate and D ₂ O.....	219
Figure VII.3.3.2. X-band EPR spectra of activated PFL C419A with different amount of pyruvate and D ₂ O.....	220
Figure VII.3.4.1. X-band EPR spectra of thiyl radicals of PFL cysteine mutants generated by UV photolysis.	227
Figure VIII.3.2.1. PCR products of <i>moaA</i> and <i>moaC</i> genes from <i>E. coli</i> genomic DNA.	248
Figure VIII.3.2.2. Confirmatory DNA fingerprints of plasmids JYI58 (<i>pETBlue-1-Ecoli-moaA</i>) and JYIII139 (<i>pETBlue-1-Ecoli-moaC</i>).	248
Figure VIII.3.3.1. SDS-PAGE of MoaA and MoaC from <i>E. coli</i> cells.	249
Figure VIII.3.4.1. SDS-PAGE of MoaA Denaturation by 6M Urea.....	251
Figure VIII.3.5.1. Purification of denatured MoaA by ion exchange chromatography.....	253
Figure VIII.3.6.1. PCR of <i>moaA</i> from <i>E. coli</i> genomic DNA and confirmatory DNA fingerprints of plasmids JYIV145.....	255
Figure VIII.3.7.1. SDS-PAGE of the overexpression of the MoaA-MBP fusion protein in whole cells.....	258
Figure VIII.3.7.2. SDS-PAGE and western blotting of whole cells containing MoaA-MBP fusion protein.	258

LIST OF ABBREVIATIONS

2'dAdo.....	2'-deoxyadenosine
5'dAdo.....	5'-deoxyadenosine
Ado	adenosine
AdoCbl	adenosylcobalamin
AdoMet	S-adenosyl-L-methionine
ADP	adenosine diphosphate
AMP	adenosine monophosphate
anRNR	anaerobic ribonucleotide reductase
APS.....	ammonium persulfate
ATP	adenosine triphosphate
BioB	Biotin Synthase
β-ME	β-mercaptoethanol
BSA.....	bovine serum albumin
cAMP	adenosine 3',5'-cyclic monophosphate
CPM.....	counts per minute
DFT	density functional theory
DNA	deoxyribonucleic acid
DTT	dithiothreitol
<i>E.coli</i>	<i>Escherichia coli</i>
EDTA	Ethylenedinitrolo)tetra-acetic acid disodium salt dehydrate
ENDOR	electron nuclear double resonance
EPR	electron paramagnetic resonance

EXAFSextended x-ray absorbtion fine structure

FAD.....flavin adenine dinucleotide

FPLC.....fast protein liquid chromatography

HemN..... oxygen independent coproporphyrinogen-III-oxidase

Hepes 4-(2-Hydroxyethyl)piperazine-1-ethanesulfonic acid

HPLChigh performance liquid chromatography

IPTGisopropyl- β -D-thiogalactopyranoside

LAM lysine 2,3 –aminomutase

LB Luria-Bertani

LMCT ligand to metal charge transfer

MM.....minimal media

MOPS 3-(N-morpholino) propanesulfonic acid

MTAdo Methyl thiol adenosine

NAD⁺.....nicotinamide adenine dinucleotide (oxidized form)

NADH.....nicotinamide adenine dinucleotide (reduced form)

NMR.....nuclear magnetic resonance

PFLpyruvate formate lyase

PFL-AE pyruvate formate lyase activating enzyme

PMSFphenylmethyl sulfonyl fluoride

RNA ribonucleic acid

SAM..... S-adenosyl-L-methionine

SDS-PAGE sodium dodecyl sulfate-polyacrylamide gel electrophoresis

SPL.....spore photoproduct lyase

SASPsmall acid soluble protein

TFAtrifluoroacetic acid

Tris.....tromethamine

CHAPTER I

INTRODUCTION

I.1 Iron-sulfur Clusters for Life

An iron-sulfur cluster is a structural motif found in certain metalloproteins and is among the most versatile and ubiquitous structures found in biological systems. It has been proposed that these metal-containing clusters are associated with the appearance of early life on earth.¹

Depending on the number of irons in the iron-sulfur cluster, these metalloproteins can be separated into three major categories (the [2Fe-2S], [3Fe-4S], and [4Fe-4S] clusters) as shown in Figure I.1.1. These clusters consist of 2, 3, or 4 irons, with inorganic sulfide ions (2 or 4) acting as bridging ligands. The sulfurs from protein cysteine side chains usually form additional covalent bonds with the irons to locate these clusters in the protein. Although the most common ligand to the iron-sulfur clusters is the side chain sulfur atom of cysteinate residues, backbone amide or side chains from other amino acids (histidine, serine, or aspartate) are also known to bind the irons in some iron-sulfur clusters.² Minor modification of these common clusters and more complicated iron-sulfur clusters can also be observed in nature, such as the [8Fe-7S] cluster in nitrogenase and [Ni-4Fe-5S] cluster in acetyl CoA synthase.^{3, 4}

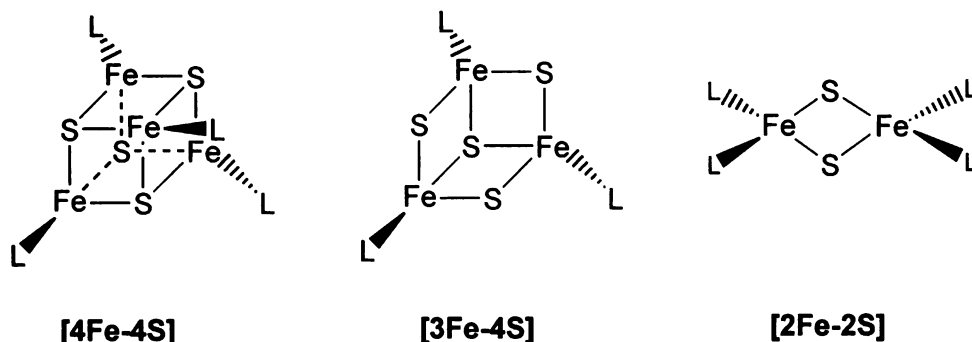
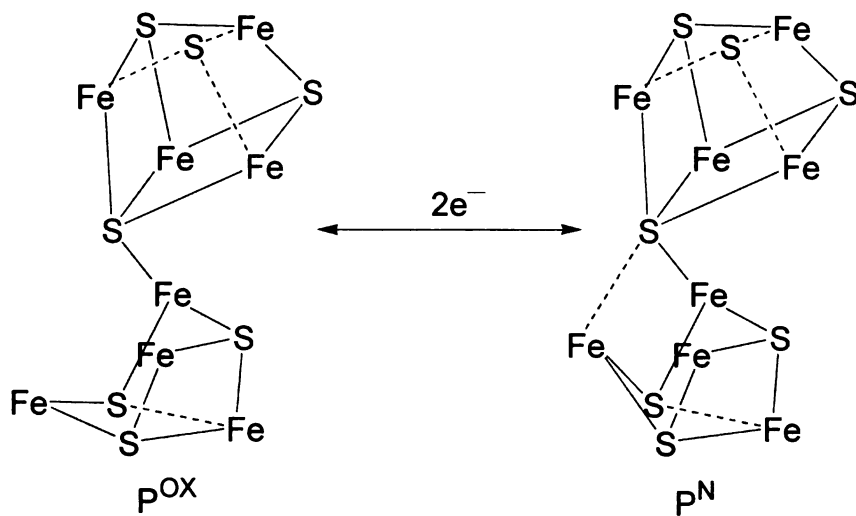


Figure I.1.1. The three major categories of iron-sulfur clusters. Irons and bridging sulfides are shown as black balls and gray balls respectively.

A direct consequence of so many versatile structures of the iron-sulfur clusters is the corresponding diverse chemistry in which they are involved. Electron transfer is the first recognized and most common function of these iron-sulfur clusters in biology. Both the irons and the sulfides of the iron-sulfur cluster are capable of delocalizing electron density; as a result, the redox potentials of the cluster in different proteins can be greatly modified making the cluster suitable for mediating biological electron transfer.^{5, 6} One electron transfer is the most common mode among enzymes containing [2Fe-2S], [3Fe-4S] and [4Fe-4S] clusters, which include the arsenite oxidases, rubredoxins, rieske proteins, and ferredoxins.⁷⁻¹⁰ In contrast, two electron transfer is rare and found only in nitrogenases, where a rearrangement of the double cubane [8Fe-7S] cluster is involved (Scheme I.1).¹¹



Scheme I.1.1 A rare case of the two-electron transfer process found in nitrogenases. P^{OX}: Oxidized form; P^N: Reduced form.

Although earlier work on iron-sulfur cluster proteins was focused on electron transfer, more recent discoveries of both new versatile structures and novel functions of these iron-sulfur clusters have put the iron-sulfur clusters in a much wider and promising position in biology.¹²⁻¹⁴ These new functions cover almost the entire range of major enzymatic reactions as well as other biological functions and have prompted a new round of interest in these ancient structures. Table I.1.1 contains a few examples of these iron-sulfur proteins with “novel” functions.

Selected Functions	Cluster type	Examples
Coupled electron/proton transfer	[8Fe-7S]	Nitrogenase ^{3, 15}
Regulation of gene expression	[2Fe-2S] and [4Fe-4S]	IRE-BP ^{16, 17} FNR ¹⁸⁻²⁰ SoxR ²¹⁻²³
regulation of enzyme activity	[4Fe-4S]	Glutamine PRPP amidotransferase ²⁴
Redox catalysis	[4Fe-4S]	Carbon monoxide dehydrogenase ²⁵ Hydrogenase ²⁶
non-redox catalysis	[4Fe-4S]	Aconitase ^{27, 28}
Structural	[4Fe-4S]	Endonuclease III ²⁹ MutY ³⁰
Sulfur donor	[2Fe-2S]	BioB ^{31, 32}
Substrate binding and activation	[4Fe-4S]	Radical SAM enzymes ³³⁻⁴³

Table I.1.1. Functions and [Fe-S] cluster types of a few iron-sulfur cluster containing enzymes.

One of the most intriguing new functions for iron-sulfur clusters has been their involvement in the initiation of radical catalysis in the radical SAM superfamily, which will be discussed in greater detail in the next section.

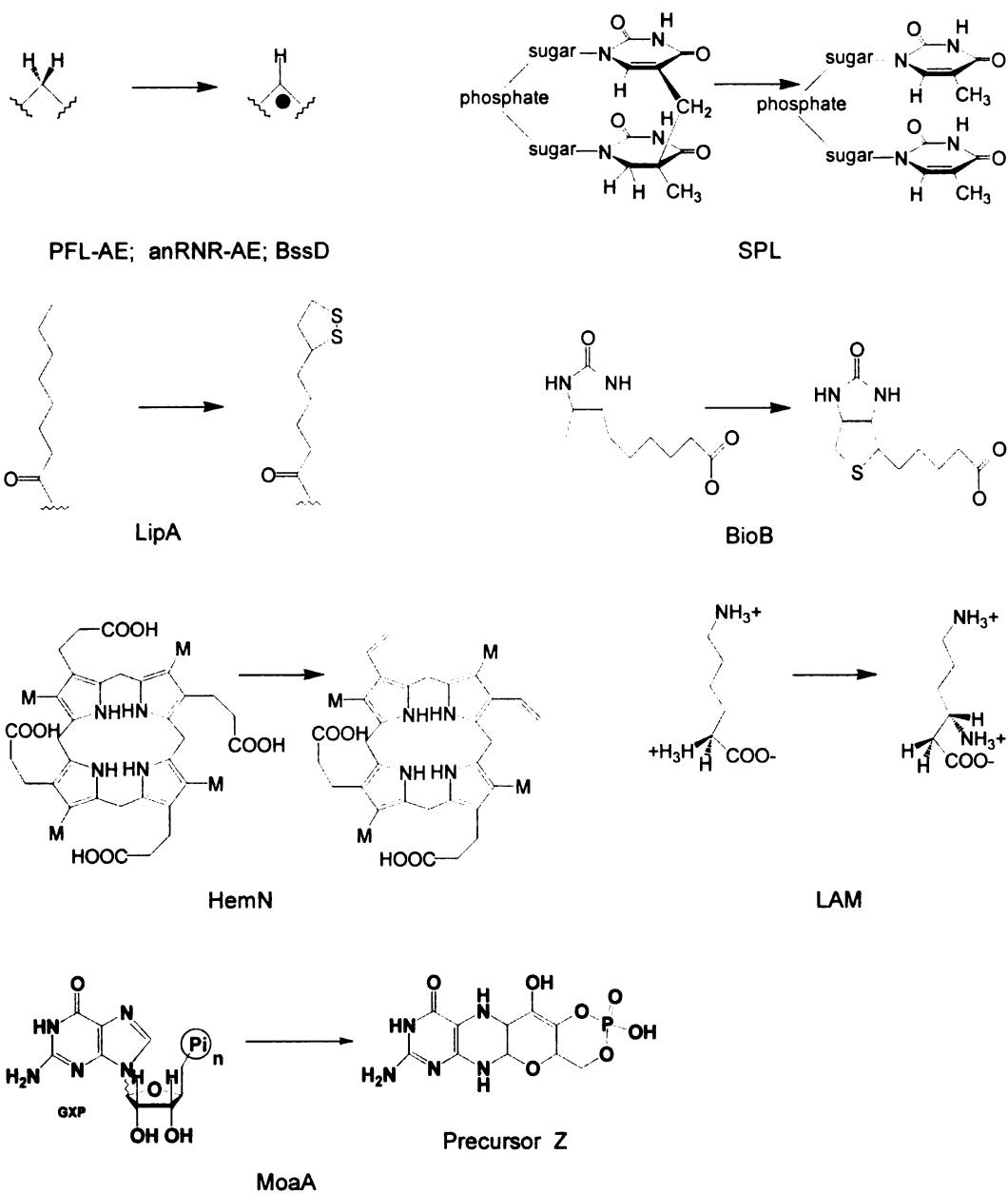
To summarize, iron-sulfur cluster containing proteins are diverse with a relatively wide range of functions. The functions of these enzymes are closely associated with corresponding [Fe-S] cluster structures. It will not be surprising to see in the near future more enzymes and more novel functions discovered in this field.

I.2 Radical SAM Superfamily

In 2001, Sofia and coworkers identified a superfamily of enzymes with 645 unique sequences from 126 species using powerful bioinformatics and information visualization methods.³³ These enzymes are classified into the Radical SAM Superfamily because they utilize S-adenosyl-methionine (AdoMet or SAM) and catalyze radical reactions. They contain a common characteristic CX₃CX₂C motif and all are proposed to generate the same radical species to initiate individual reactions.

The actual study of many Radical SAM enzymes had started long before and the characteristic CX₃CX₂C motif had been noted.⁴⁴ In the late 1960's and early 1970's, Barker and co-workers, who had been studying lysine 2,3 aminomutase isomerase, discovered that the reaction required SAM rather than adenosylcobalamin (AdoCbl), used by many other isomerases, to catalyze the interconversion of L-lysine and L-β-lysine.⁴⁵ Thereafter, research on other members of the radical SAM superfamily has rapidly expanded. Scheme I.2.1 lists reactions catalyzed by some radical SAM enzymes. Biotin synthase (BioB) catalyzes the radical-mediated insertion of sulfur into dethiobiotin to form biotin.^{31, 32, 46} Lipote synthase (LipA) catalyzes the insertion of sulfur into octanoic acid bound to acyl carrier protein (octanoyl-ACP) to generate lipoyl-ACP.^{47, 48} Spore photoproduct lyase (SPL) catalyzes the repair of SP dimers to thymine monomers.⁴⁹⁻⁵² Lysine 2,3-aminomutase (LAM) catalyzes the interconversion of L-lysine and L-β-lysine.^{53, 54} The oxygen-independent coproporphyrinogen-III oxidase (HemN) catalyzes an oxygen-independent oxidation in anaerobic heme

biosynthesis.^{55, 56} Pyruvate formate lyase-activating enzyme (PFL-AE),⁵⁷⁻⁵⁹ anaerobic ribonucleotide reductase activating enzyme (anRNR-AE),⁶⁰⁻⁶² glycerol dehydratase activating enzyme (GD-AE),⁶³⁻⁶⁵ and benzylsuccinate synthase activating enzyme (BssD)⁶⁶⁻⁶⁸ can activate their respective protein substrates by abstracting a hydrogen from a specific glycine residue. MoaA, together with the MoaC protein, is involved in the first step of Moco biosynthesis.⁶⁹⁻⁷¹ ThiH, together with the ThiG protein, is required for the biosynthesis of the thiazole moiety of thiamine (vitamin B(1)).⁷²⁻⁷⁴ HydE and HydG have been recently found to be involved in the maturation of FeFe-hydrogenase.⁷⁵⁻⁷⁸



Scheme I.2.1 Selected reactions catalyzed by radical SAM enzymes.

Despite the fact that members of radical SAM superfamily catalyze a variety of reactions covering almost all enzyme classifications, there are a few common features. Firstly, they all share a highly conserved cysteine motif CX₃CX₂C. (Table I.1)^{33-36, 42, 43, 79} Cysteine is a naturally occurring, sulfur-containing amino acid that has a thiol group and is found in most proteins. The common modified forms of this residue in peptides and proteins include thiols, thiolates, thiyl radicals, disulfides, sulfenic, sulfinic, sulfonic acids, disulfide-S-oxides and selenodisulfides. As a result of such flexibility, cysteine can serve to stabilize protein structure, participate in metal binding and be involved in catalysis and redox chemistry.⁸⁰

• PFL-AE	24	ITFFQGCLMRCLYCHNRDT
• aRNR-AE	20	VLFTVIGCLHKCEGCYNRST
• BssD	68	TIFLKGCONYKCGFCFHTIN
• SPL	86	IPFATGCMGHCHYCYLQTT
• BioB	47	SIKTGACPDCKYCPQTSR
• LipA	48	MILGAICTRRCPFDVAHG
• LAM	132	LLITDMCSMYCRHCTRRRF
• HemN	53	YFHIPFCQSMCLYGCSEIH
• MoeA	15	IAVTPECNLDCCFFCHMEFK
• ThiH	90	LYLSNYCNSKCVYCGFQIL

Table I.2.1. CX₃CX₂C conserved motif of the radical SAM superfamily.

The CX₃CX₂C motif in the radical SAM proteins is proposed to coordinate an iron-sulfur cluster. However, in many cases the elucidation of the actual form of this cluster does not come easily due to the intrinsic instability of the iron-sulfur cluster. For example, the early studies of PFL-AE and BioB, two of the radical SAM enzymes, show a mixture of different forms including [2Fe-2S], [3Fe-4S], and [4Fe-4S] clusters. However, upon reduction, all the clusters are

converted into [4Fe-4S] clusters.⁸¹⁻⁸⁴ Later EPR experiment done by Broderick and coworkers correlate the consumption of the [4Fe-4S]¹⁺ of PFL-AE with equimolar production of the organic glycy radical of PFL, therefore suggesting that the [4Fe-4S]¹⁺ cluster is the physiologically active species.⁸⁵ Other experiments on LAM and anRNR also show that the [4Fe-4S]¹⁺ cluster is proportionally related to the final results of the reaction.^{61, 86} As a result, the [4Fe-4S] cluster is believed to be the catalytically active species and the different oxidation states are associated with various stages of the reaction or with cluster oxidation and degradation.

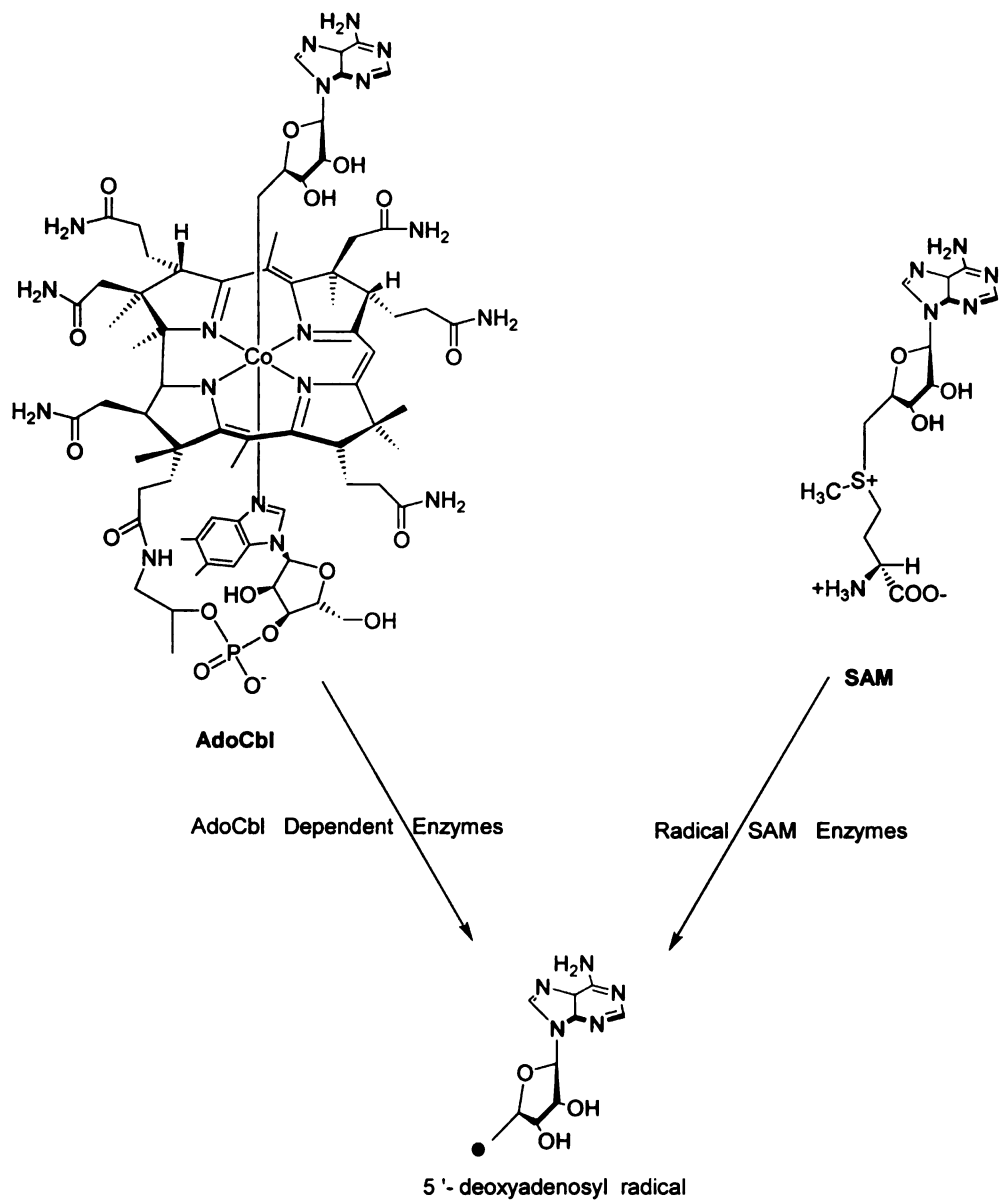
One interesting aspect of the radical SAM iron-sulfur cluster is the site-differentiated coordination of the [4Fe-4S] cluster due to the insufficient number of cysteines in the CX₃CX₂C motif. The [4Fe-4S] cluster consists of four irons and four sulfides placed at the vertices of a cubane-type structure. Three of the irons form additional covalent bonds with conserved cysteine residues while the fourth iron does not. This fourth iron is designated as the unique iron, and is believed to be conserved for the binding of cofactor/cosubstrate AdoMet during catalysis. Such arrangement has been seen in aconitase, an iron-sulfur cluster containing enzyme but not a member of radical SAM superfamily. Aconitase contains a similar site-differentiated [4Fe-4S] cluster and uses its unique iron to coordinate the carboxyl oxygens of the substrate citrate.⁸⁷⁻⁸⁹ In contrast, the radical SAM enzymes use their unique irons to interact the amino nitrogen and carboxyl oxygen of AdoMet. This configuration was first discovered by Broderick, Hoffman, and coworkers, who used ENDOR to investigate the interaction of AdoMet with

PFL-AE.^{90, 91} This coordination of AdoMet to the unique iron was further confirmed by several crystal structures of radical SAM enzymes, including LAM, BioB, HemN and MoaA.^{55, 69, 92, 93}

A third common feature of the radical SAM enzymes is that a 5'-deoxyadenosyl radical intermediate is believed to be involved. The radical is extremely reactive and is generated by homolytic S-C bond cleavage in AdoMet when AdoMet receives one electron from the coordinated $[4\text{Fe-4S}]^{1+}$ cluster. The most direct evidence for the presence of this extremely reactive adenosyl radical comes from the study of LAM, reacting with an allylic analog of AdoMet to generate an allylically stabilized adenosyl radical intermediate.^{94, 95}

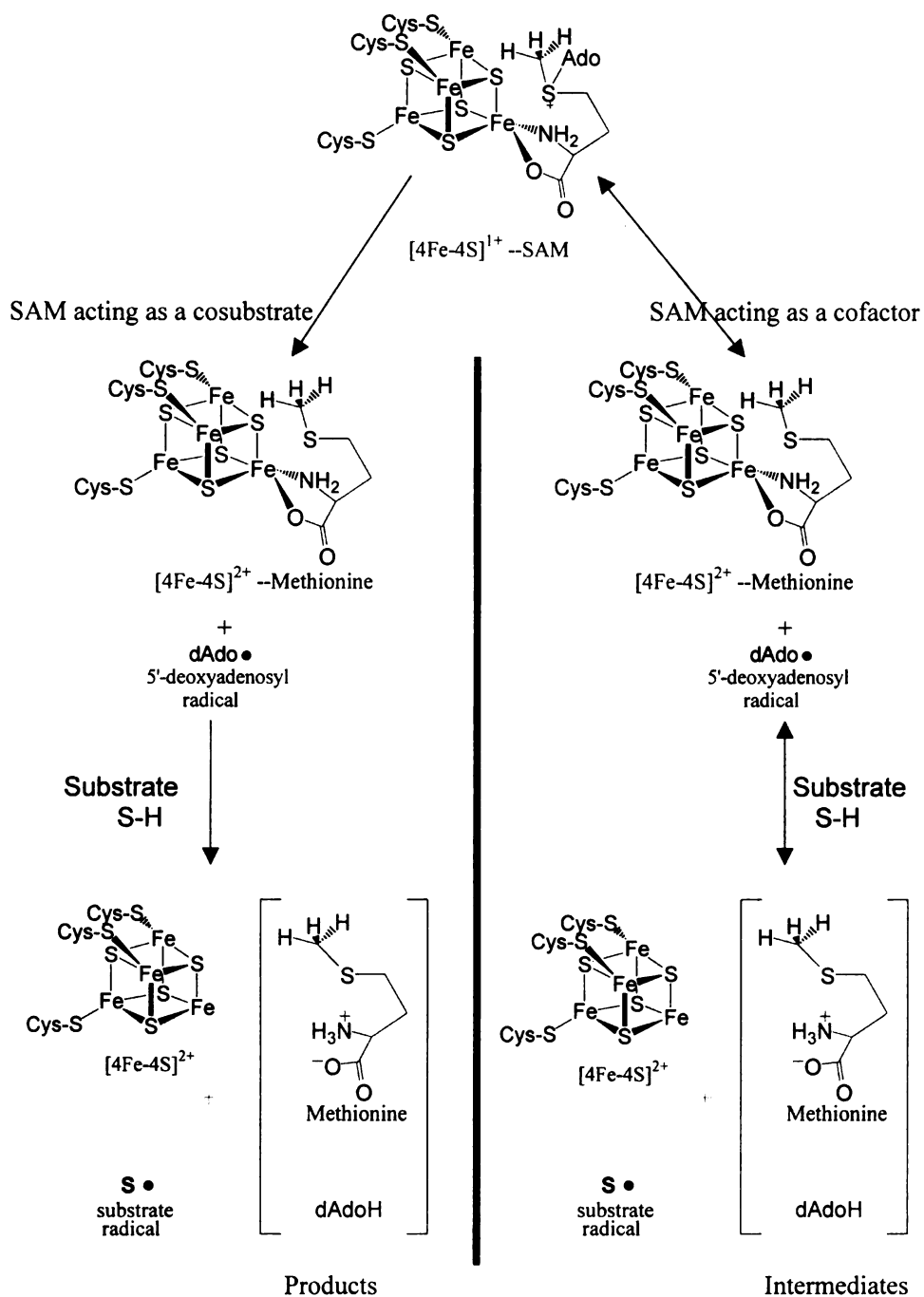
Adenosylcobalamin (AdoCbl) containing enzymes also use an adenosyl radical intermediate, produced by the homolytic cleavage of the Co-C bond.^{34, 36, 41-43, 96-98} Scheme 1.2.2 summarizes the generation of the 5'-deoxyadenosyl radical from AdoCbl and AdoMet.

AdoMet is a naturally occurring molecule found in all body tissues and fluids. AdoMet acts as methyl donor in the methylation of the phospholipids, proteins, DNA, RNA and other molecules, and is actively involved in a number of biochemical reactions including enzymatic transmethylation, as well as contributing to the synthesis, activation and/or metabolism of such compounds as hormones, neurotransmitters, nucleic acids, proteins, phospholipids and certain drugs.⁹⁹⁻¹⁰¹ The involvement of AdoMet in the radical SAM superfamily was, however, totally unexpected.^{33, 34, 36, 41}



Scheme I.2.2 Structure of the 5'-deoxyadenosyl radical (bottom) and its generation from AdoCbl (top left) and AdoMet (top right).

A common mechanism involving radical-based hydrogen atom abstraction by the 5'-deoxyadenosyl radical intermediate, has been proposed as the first step of all of the radical SAM reactions. The unique iron of the [4Fe-4S] cluster coordinates the amino nitrogen and carboxyl oxygen of AdoMet to anchor this molecule in the catalytic site; as a result of this interaction, the sulfonium of AdoMet forms close interaction with the cluster, causing orbital overlap between the sulfonium of AdoMet and the cluster.^{59, 90, 91} Therefore, an inner sphere electron transfer pathway has been proposed to result in the homolytic scission of the C-S bond of AdoMet.^{58, 59, 91, 102, 103} As a result of this homolytic cleavage of the C-S bond of AdoMet, the 5'-deoxyadenosyl radical intermediate is produced. This radical is then either consumed stoichiometrically to produce 5'-deoxyadenosine and methionine as products (AdoMet acting as a cosubstrate) or is regenerated at the end of the reaction (AdoMet acting as a cofactor). In the latter case, the two transient AdoMet cleavage products, 5'-deoxyadenosine and methionine, reform back into AdoMet after catalysis. Both routes are summarized in Scheme I.2.3.

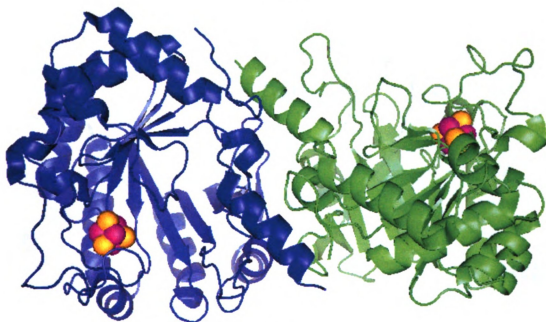


Scheme 1.2.3 Cleavage of AdoMet by radical SAM superfamily enzymes yields a 5'-deoxyadenosyl radical. Top: AdoMet acts as a cosubstrate. Bottom: AdoMet acts as a cofactor.

So far, crystal structures of four radical SAM enzymes (HemN, BioB, MoaA, and LAM) have been solved (Figure 1.2.1). Despite the different substrates acted on by these radical SAM enzymes and the different multimeric forms in which they are crystallized (HemN as monomer, BioB and MoaA as homodimer, and LAM as tetramer), they show striking similarities in the core protein structures.^{55, 69, 92, 93} In terms of their peptide backbones, they all form a typical TIM barrel and share a $(\beta/\alpha)_6$ repeat motif in their structural cores. BioB has two additional β/α repeats to completely close the TIM barrel; in contrast, the other enzymes (HemN, MoaA, and LAM) form a large crescent channel along the surface of these enzymes due to the incomplete TIM barrel. The [4Fe-4S] cluster is located at the N terminal end of the barrels in all these structures, with three of the irons coordinated by the highly conserved CX₃CX₂C motif and the unique iron coordinated by the amino nitrogen and carboxyl oxygen of AdoMet, confirming previous ENDOR results.^{90, 91}

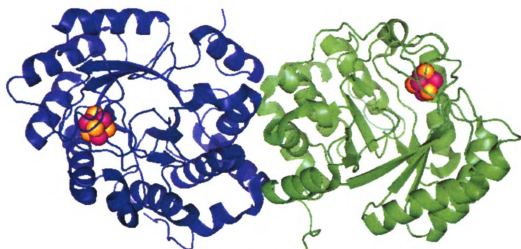


HemN

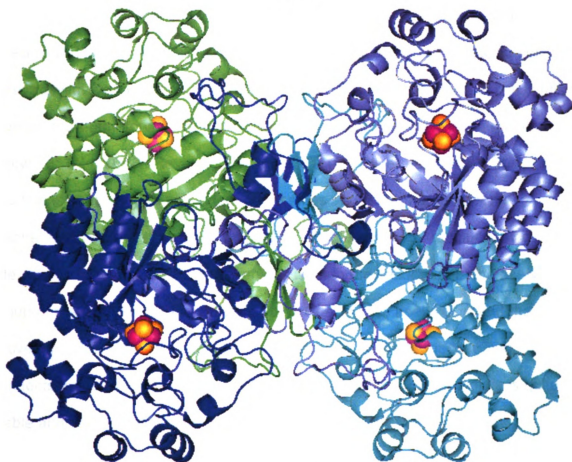


MoaA

Figure I.2.1. Crystal structures of HemN, MoaA, BioB, and LAM. These structures are made from PDB files (1OLT, 1TV7, 1R3O, and 2A5H respectively).



BioB



LAM

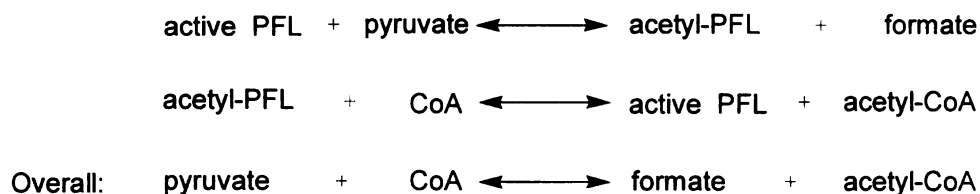
Figure 1.2.1. (continued) Crystal structures of HemN, MoaA, BioB, and LAM. These structures are made from PDB files (1OLT, 1TV7, 1R3O, and 2A5H respectively).

I.3 Pyruvate Formate-Lyase (PFL) and Pyruvate Formate-Lyase

Activating Enzyme (PFL-AE)

E. coli contains three enzyme systems to convert the glycolysis product pyruvate into acetyl-CoA, the latter being a key intermediate in the production of ATP. Two systems, the pyruvate dehydrogenase multienzyme complex and pyruvate:ferredoxin / flavodoxin oxidoreductase, function in the presence of oxygen. The third system, the pyruvate formate-lyase, catalyses the reaction when the environment becomes anaerobic.¹⁰⁴

The actual recognition of the PFL enzymatic function can be dated back as early as 1943 by Kalnitsky and Werkman.¹⁰⁵ PFL catalyzes the reaction of pyruvate with CoA to formate and acetyl CoA. (Scheme I.3.1) The reaction is fully reversible with the forward reaction slightly favorable over the reverse reaction (Forward: $TN=770s^{-1}$, Reverse: $TN=260s^{-1}$; TN =turnover number).¹⁰⁶ The reaction is composed of two independent steps and follows a “ping-pong” mechanism. In the first step, the active PFL attacks pyruvate, resulting in an intermediate acetylated PFL and formate. Then in the second step, the acetyl group of the acetylated PFL is picked up by CoA to form acetyl CoA and the active form PFL. The acetylated PFL is a very important intermediate and connects these two steps. Surprisingly, this acetylated PFL intermediate is quite stable and can be easily generated by mixing active PFL with pyruvate.¹⁰⁷



Scheme I.3.1. The overall reaction catalyzed by PFL including the two independent steps.

PFL is catalytically inactive following aerobic expression and purification. It is a homodimer with a molecular weight of 170kDa and contains no cofactors. Several crystal structures have been published since 1999, including wild type PFL (wt-PFL), wt-PFL with pyruvate or oxamate, wt-PFL with both pyruvate and CoA, and PFL cysteine mutants.¹⁰⁸⁻¹¹¹ Little structural difference has been found between PFL crystallized as holoenzyme (wt-PFL) or in complex with its substrates. These structures provide a lot of structural information, however, they are all structures of the inactive form of PFL. The active form of PFL contains a glycy radical on residue G734, and as a result, the active site of PFL may adopt a different local configuration.

The inactive form of PFL is crystallized as a homodimer forming a nearly perfect two-fold rotation. The tight contact between the two monomers is mainly in the helical region of residues 131-155 and 200-232. Each monomer is assembled in an antiparallel manner from two parallel five-stranded β -sheets. The active site residues G734, C418 and C419 are found at the tips of two opposing hairpin loops, which are designated as the glycine loop and the cysteine loop respectively. Both loops protrude from either the top or the bottom surfaces of PFL into the center of this barrel. The distance between G734 Ca and

C419 Ca, which receives the radical from G734, is 4.8Å. The overall architecture is strikingly similar to that of ribonucleotide reductases, which also contains a glycy radical in the active form. Pyruvate, as well as its structural analogue oxamate, binds in the active site of each protomer with its carbonyl C 2.6Å away from C418 Sy. Interestingly, the binding of either pyruvate or oxamate causes no significant overall structural change of PFL. Likewise, the binding of CoA, the other substrate of PFL reaction, also makes no change to the overall structure of PFL. The CoA molecule is found to bind at the surface of PFL with the adenine moiety located 15Å away from the active site. CoA assumes a syn glycosidic configuration and places its pantetheine chain extending away from the active site toward the opposing monomer. The thiol group at the tip of this pantetheine chain is 30 Å away from either active site. However, rotation around the N-glycosidic bond will relocate the ribose-pantetheine moiety and place the thiol group within 5 Å of the active site. As a result of this movement, the thiol group of CoA is presumably able to “fish out” the acetyl group from the acetylated PFL.

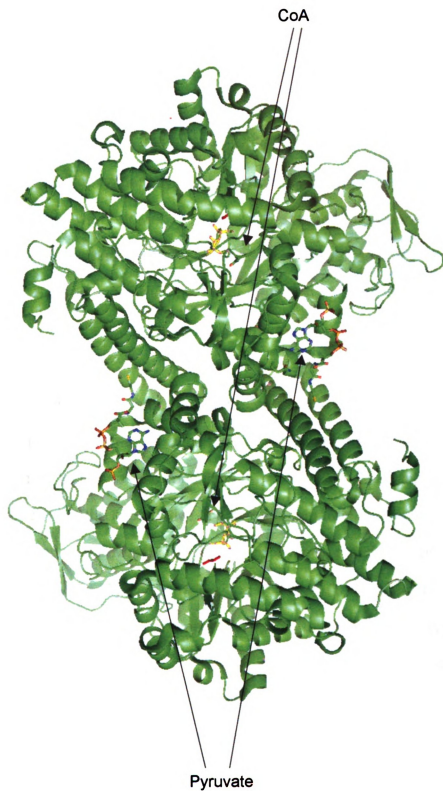


Figure 1.3.1. Cartoon representation of the PFL-dimer in complex with pyruvate and CoA in sticks. The vicinal C418, C419, and G734 are in yellow, yellow, and red sticks respectively. CoA and pyruvate are indicated in the figure.

PFL has to be activated in order to perform its enzymatic function. Activation involves hydrogen atom abstraction from G734 of PFL, and is catalyzed by PFL-AE.¹¹²⁻¹¹⁴ Two lines of experimental evidence published by Knappe and co-workers show that it is the pro-S hydrogen on PFL G734 that is abstracted by the 5'-deoxyadenosyl radical intermediate, which is generated by PFL-AE in a reaction with AdoMet.¹¹²⁻¹¹⁴ First, the adenosyl radical intermediate is trapped by C-adenosylation of the dehydroalanyl octapeptide mimic of the PFL glycine loop.¹¹⁴ Second, when the pro-S hydrogen of the glycine loop mimic peptides is replaced by a methyl group (e.g. a normal Ala), no hydrogen atom abstraction occurs.¹¹²

Interestingly, only one of the PFL protomers can be activated at a time even though it is a homodimer.¹¹⁵ Once the G734 radical is generated, it remains very stable under strict anaerobic conditions ($t_{1/2} > 24\text{hr}$).^{59, 116} This stability is believed to result from the captodative effect, the summation of effects of resonance electron withdrawal by the glycyI-carbonyl group and resonance electron donation by the adjacent amide nitrogen through the lone electron pair. This glycyI radical is, however, extremely susceptible to reaction with oxygen, which results in protein cleavage.^{115, 117, 118} Whether there is an enzyme to quench this glycyI radical and reduce the active form PFL back to its inactive form to avoid this unfavorable degradation is still under investigation.^{116, 119, 120}

The glycyI radical shows a doublet EPR signal ($A_{\text{iso}} = 15\text{G}$) centered at $g = 2.0037$; the splitting of the signal is due to hyperfine coupling to the remaining α -hydrogen of the G734 residue.¹¹⁸ Surprisingly, the remaining α -hydrogen of

the G734 residue of the active PFL is in constant exchange with solvent, a rapid hydrogen exchange reaction mediated by the free thiol group of the residue C419.¹²¹ EPR results have shown that the active form of PFL loses its hyperfine coupling in D₂O in just a few minutes ($t_{1/2}$ =5min) due to the hydrogen exchange reaction.¹²¹

Although the glycyl radical is initially generated on residue G734 of PFL, G734 is not believed to be directly involved in catalysis. Instead, G734 is able to relay the glycyl radical to the adjacent cysteine residues to form a C418 thiyl radical or a C419 thiyl radical. Depending on which thiyl radical is directly involved in the homolytic cleavage of the pyruvate C-C bond, two mechanisms have been proposed for the PFL-catalyzed reaction.^{108, 110, 111, 121} These two mechanisms will be discussed in detail in the following chapter.

PFL-AE is a monomeric protein containing an iron-sulfur cluster with a molecular weight of 28 KDa. It activates PFL under strict anaerobic conditions in the presence of AdoMet, pyruvate, and an external electron, which can be supplied by NADPH *in vivo* or dithionite or photoreduced 5-deazariboflavin *in vitro*.^{113, 122}

PFL-AE was first purified aerobically from (non-overexpressing) *E. coli* by Knappe and co-workers and had a broad absorbance from 310 to 550 nm suggesting the presence of covalently bound cofactor.¹¹³ Kozarich and co-workers overexpressed PFL-AE, however the protein was present largely in inclusion bodies, thus necessitating complete denaturation followed by refolding after purification. Although many divalent metals were shown to be able to bind

this refolded protein, only Fe(II) in the presence of DTT restored enzymatic activity.¹²³ The presence of thiophilic metals inhibited PFL-AE activity, leading to a suggestion that the iron was bound in a cysteinal coordination environment. In addition, site directed mutagenesis studies of PFL-AE identified three cysteine residues (C29, C33, and C36) that were required for the incorporation of this metal cofactor,¹²⁴ a fact that is consistent with the later proposed CX₃CX₂C iron-sulfur cluster binding motif for the radical SAM superfamily.

In an effort to avoid solubility issues and to identify the native metal center of PFL-AE, Broderick and co-workers pursued anaerobic purification of PFL-AE. By modifying expression and purification conditions, they were able to identify the metal cofactor in PFL-AE as a [4Fe-4S] cluster and showed that exogenous iron is not necessary for its enzymatic activity.⁸³ Their initial purification methods were performed under anaerobic conditions without DTT, resulting in a mixture of [4Fe-4S], [3Fe-4S] and [2Fe-2S] clusters and suggesting that PFL-AE was an iron-sulfur cluster containing protein.⁸²⁻⁸⁵ However, upon reduction by dithionite, all clusters were converted into [4Fe-4S] clusters. To further improve the purification, the isolation was later carried out under anaerobic condition in the presence of DTT. In this case only [4Fe-4S]²⁺ clusters are present and PFL-AE has the highest observed enzymatic activity.⁵⁹

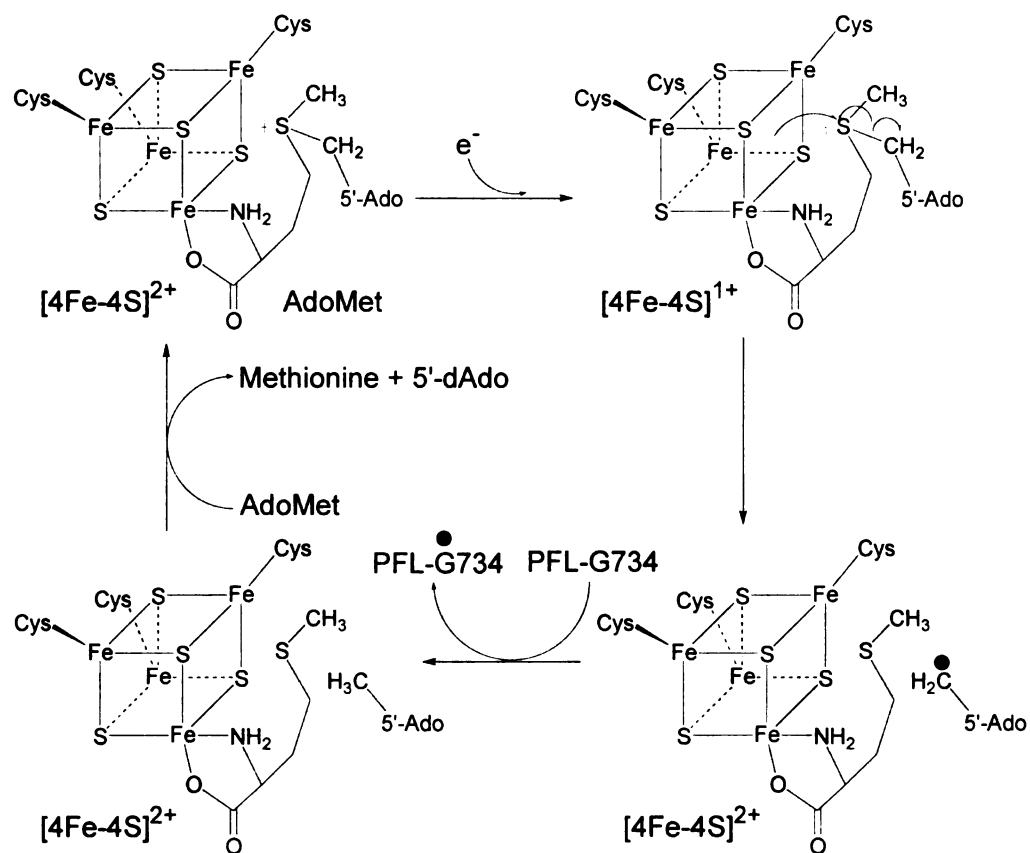
Although many different types of iron-sulfur clusters have been observed in PFL-AE, only the [4Fe-4S] cluster is believed to be catalytically relevant because only this cluster is observed under reducing conditions.⁸⁴ The catalytically active species [4Fe-4S]¹⁺ cluster was determined by using a "single

turnover" experiment, in which the $[4\text{Fe-4S}]^{1+}$ cluster of PFL-AE produces equal molar amount of glycyl radical on PFL.⁸⁵ The $[4\text{Fe-4S}]^{2+}$ cluster has been proposed to be the catalytic counterpart of the $[4\text{Fe-4S}]^{1+}$ cluster because the $[4\text{Fe-4S}]^{2+}$ cluster is the concomitant product with glycyl radical generation and it can be reactivated back into $[4\text{Fe-4S}]^{1+}$ cluster after the first catalytic cycle.^{59, 85}

This paragraph summarizes a few key results that lead to a proposal of the PFL-AE mechanism. First, EPR results have shown that the $[4\text{Fe4S}]^{1+}$ cluster signal is greatly altered in the presence of AdoMet, suggesting the direct interaction between AdoMet and the $[4\text{Fe-4S}]^{1+}$ cluster. Second, ENDOR studies, in which the isotopically labeled AdoMet is used to measure the binding distance and mode to the $[4\text{Fe-4S}]^{1+}$ cluster, demonstrate that the amino nitrogen and carboxylate oxygen act as ligands to the unique iron of the iron sulfur cluster and the sulfonium of AdoMet provides orbital overlap with the cluster. Together, these results support an inner-sphere electron transfer from the $[4\text{Fe-4S}]^{1+}$ cluster to the sulfonium center of AdoMet followed by cleavage of AdoMet and formation of the 5'-deoxyadenosyl radical. Although similar experiments can not be used directly to probe the interaction between AdoMet with the diamagnetic $[4\text{Fe4S}]^{2+}$ cluster, a modified method was successfully utilized to solve this question. The diamagnetic $[4\text{Fe-4S}]^{2+}$ cluster was first frozen together with AdoMet, trapping the geometry of the $[4\text{Fe-4S}]^{2+}$ /AdoMet complex. Cryoreduction of this frozen solution converts the $[4\text{Fe-4S}]^{2+}$ /AdoMet complex to the $[4\text{Fe4S}]^{1+}$ /AdoMet complex, which is EPR active and can be measured by ENDOR. The resulting data are essentially identical to that of the $[4\text{Fe-4S}]^{1+}$ /AdoMet complex,

suggesting both reduced ($[4\text{Fe-4S}]^{1+}$) and oxidized form ($[4\text{Fe-4S}]^{2+}$) of PFL-AE have the same binding mode with AdoMet.

Currently, the mechanism for PFL activation by PFL-AE is proposed as follows (Scheme I.3.2).⁵⁹ The $[4\text{Fe-4S}]^{2+}$ cluster of PFL-AE, the resting state of this enzyme under anaerobic conditions, situates AdoMet in the catalytic site of PFL-AE by forming a classic five-member chelate ring between the unique iron of the cluster and the methionine moiety of AdoMet. Such interaction brings the sulfonium of AdoMet into orbital overlap with the $[4\text{Fe-4S}]^{2+}$ cluster. The $[4\text{Fe-4S}]^{1+}$ -AdoMet complex is the product of one-electron reduction of the $[4\text{Fe-4S}]^{2+}$ cluster by a reducing agent (reduced flavodoxin *in vivo*). Surprisingly, this complex remains quite stable until the substrate PFL is introduced into the system. The presence of PFL induces the reaction to move forward, resulting inner-sphere electron transfer from the $[4\text{Fe-4S}]^{1+}$ cluster to the sulfonium of AdoMet to initiate the homolytic S-C bond cleavage. Methionine, one of the two cleavage products of AdoMet, is left bound to the unique site of the oxidized $[4\text{Fe-4S}]^{2+}$ cluster, while the 5'-deoxyadenosyl radical intermediate, the other AdoMet cleavage product and the universal radical throughout the radical SAM superfamily, activates PFL by abstracting the pro-S H from its residue G734. The catalytic cycle is then repeated upon displacement of methionine and 5'-deoxyadenosine with a new AdoMet molecule. The activated PFL will then catalyze the conversion of pyruvate and CoA to acetyl CoA and formate by a mechanism that is still under debate^{108, 110, 111, 121}.



Scheme I.3.2. Proposed mechanism for iron-sulfur cluster and AdoMet-mediated radical generation catalyzed by PFL-AE.

I.4 Molybdenum Cofactor (Moco) Biosynthesis

As the only second and third row transition elements with known biological function, Mo and W have received much attention since the identification of their biological roles almost 75 and 25 years ago respectively.¹²⁵⁻
¹²⁷ The existence of these trace elements in biological systems is known to play a key role in the global circulation of carbon, oxygen, hydrogen, nitrogen and sulfur.¹²⁶ These metalloenzymes exist not only in lower organisms, such as bacteria, archaea and fungi, but also in higher organisms, like plants, animals and even in human beings.^{71, 128-131} Since the development of modern techniques to analyze diseases on the molecular level, more and more well known and fatal phenomena had been associated with the malfunction of Mo and W enzymes. Stunted growth, chlorosis of leaves as well as small narrow crinkled leaves are the most visible damages to the plants due to the deficiency of Mo and W enzymes.¹³² In humans, by the end of year 2000, more than 80 diseases were known to be induced by the combined malfunction of one or more Mo and W enzymes.¹³³ These diseases are autosomal recessive and can be found in all races worldwide.¹³⁴ Patients having these kinds of diseases experience neonatal seizures, severe neurological abnormalities, dislocated ocular lenses, feeding difficulties, and dysmorphic features of the brain and head of the adult, and are generally fatal to new born babies.^{135, 136}

For molybdenum enzymes, of which over 40 have been identified up to now, all except nitrogenases contain Mo bound to a unique tricyclic pyranopterin

containing a cis-dithiolene group in its pyran ring. This most common biological Mo structure is called molybdenum cofactor (Moco) (Figure I.4.1).¹³⁷

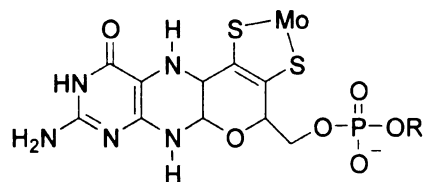


Figure I.4.1. Structure of molybdenum cofactor.

Without question, the studying of the biosynthesis of this cofactor will be of pivotal importance, helping in the treatment of this type of diseases worldwide.

I.5 References

1. Huber, C.; Wachtershauser, G., Activated acetic acid by carbon fixation on (Fe,Ni)S under primordial conditions. *Science* **1997**, 276, (5310), 245-7.
2. Link, T. A., The structures of Rieske and Rieske-type proteins. *Advances in Inorganic Chemistry* **1999**, 47, 83-157.
3. Igarashi, R. Y.; Seefeldt, L. C., Nitrogen fixation: the mechanism of the Mo-dependent nitrogenase. *Critical Reviews in Biochemistry and Molecular Biology* **2003**, 38, (4), 351-384.
4. Harrop, T. C.; Mascharak, P. K., Structural and spectroscopic models of the A-cluster of acetyl coenzyme A synthase/carbon monoxide dehydrogenase: Nature's Monsanto acetic acid catalyst. *Coordination Chemistry Reviews* **2005**, 249, (24), 3007-3024.
5. Glaser, T.; Hedman, B.; Hodgson, K. O.; Solomon, E. I., Ligand K-edge X-ray absorption spectroscopy: a direct probe of ligand-metal covalency. *Accounts of chemical research* **2000**, 33, (12), 859-68.
6. Noodleman, L.; Case, D. A., Density-functional theory of spin polarization and spin coupling in iron-sulfur clusters. *Advances in Inorganic Chemistry* **1992**, 38, 423-70.
7. Lee, W.-Y.; Brune, D. C.; LoBrutto, R.; Blankenship, R. E., Isolation, characterization, and primary structure of rubredoxin from the photosynthetic bacterium, *Heliobacillus mobilis*. *Archives of Biochemistry and Biophysics* **1995**, 318, (1), 80-8.
8. Mason, J. R.; Cammack, R., The electron-transport proteins of hydroxylating bacterial dioxygenases. *Annual review of microbiology* **1992**, 46, 277-305.
9. Cowan, J. A., *Inorganic Biochemistry: An Introduction*. 1993; p 349 pp.
10. Lebrun, E.; Brugna, M.; Baymann, F.; Muller, D.; Lievremont, D.; Lett, M.-C.; Nitschke, W., Arsenite oxidase, an ancient bioenergetic enzyme. *Molecular Biology and Evolution* **2003**, 20, (5), 686-693.
11. Peters, J. W.; Stowell, M. H.; Soltis, S. M.; Finnegan, M. G.; Johnson, M. K.; Rees, D. C., Redox-dependent structural changes in the nitrogenase P-cluster. *Biochemistry* **1997**, 36, (6), 1181-7.

12. Beinert, H.; Meyer, J.; Lill, R., Iron-sulfur proteins. *Encyclopedia of Biological Chemistry* **2004**, 2, 482-489.
13. Johnson, D. C.; Dean, D. R.; Smith, A. D.; Johnson, M. K., Structure, function, and formation of biological iron-sulfur clusters. *Annual Review of Biochemistry* **2005**, 74, 247-281.
14. Beinert, H., Iron-sulfur proteins: ancient structures, still full of surprises. *JBIC, Journal of Biological Inorganic Chemistry* **2000**, 5, (1), 2-15.
15. Burgess, B. K.; Lowe, D. J., Mechanism of Molybdenum Nitrogenase. *Chem. Rev.* **1996**, 96, 2983-3011.
16. Haile, D. J.; Rouault, T. A.; Harford, J. B.; Kennedy, M. C.; Blondin, G. A.; Beinert, H.; Klausner, R. D., *Proceedings of the National Academy of Sciences of the United States of America* **1992**, 89, 11735-11739.
17. Hentze, M. W.; Kuhn, L. C., *Proceedings of the National Academy of Sciences of the United States of America* **1996**, 93, 8175-8182.
18. Khoroshilova, N.; Beinert, H.; Kiley, P. J., Association of a polynuclear iron-sulfur center with a mutant FNR protein enhances DNA binding. *Proceedings of the National Academy of Sciences of the United States of America* **1995**, 92, (7), 2499-503.
19. Khoroshilova, N.; Popescu, C.; Munck, E.; Beinert, H.; Kiley, P. J., Iron-sulfur cluster disassembly in the FNR protein of *Escherichia coli* by O₂: [4Fe-4S] to [2Fe-2S] conversion with loss of biological activity. *Proceedings of the National Academy of Sciences of the United States of America* **1997**, 94, (12), 6087-6092.
20. Popescu, C. V.; Bates, D. M.; Beinert, H.; Munck, E.; Kiley, P. J., Moessbauer spectroscopy as a tool for the study of activation/inactivation of the transcription regulator FNR in whole cells of *Escherichia coli*. *Proceedings of the National Academy of Sciences of the United States of America* **1998**, 95, (23), 13431-13435.
21. Hildago, E.; Ding, H.; Demple, B., *Trends Biochem. Sci.* **1997**, 22, 207-210.
22. Demple, B., *Science* **1998**, 279, 1655-1656.
23. Huhta, M. S.; Ciceri, D.; Golding, B. T.; Marsh, E. N., A novel reaction between adenosylcobalamin and 2-methyleneglutarate catalyzed by glutamate mutase. *Biochemistry* **2002**, 41, (9), 3200-6.

24. Muchmore, C. R.; Krahn, J. M.; Kim, J. H.; Zalkin, H.; Smith, J. L., Crystal structure of glutamine phosphoribosylpyrophosphate amidotransferase from *Escherichia coli*. *Protein Sci* **1998**, 7, (1), 39-51.
25. Drennan, C. L.; Heo, J.; Sintchak, M. D.; Schreiter, E.; Ludden, P. W., *Proceedings of the National Academy of Sciences of the United States of America* **2001**, 98, 11973-11978.
26. Vignais, P. M.; Colbeau, A., Molecular biology of microbial hydrogenases *Curr. Issues Mol. Bio.* **2004**, 6, (2), 159-188.
27. Beinert, H.; Kennedy, M. C.; Stout, C. D., Aconitase as Iron-Sulfur Protein, Enzyme, and Iron Regulatory Protein. *Chemical Reviews (Washington, D. C.)* **1996**, 96, (7), 2335-2373.
28. Beinert, H.; Kennedy, M. C., Aconitase, a two-faced protein: enzyme and iron regulatory factor. *FASEB J.* **1993**, 7, 1442-1449.
29. Holland-Staley, C. A.; Lee, K.; Clark, D. P.; Cunningham, P. R., Aerobic activity of *Escherichia coli* alcohol dehydrogenase is determined by a single amino acid. *Journal of bacteriology* **2000**, 182, (21), 6049-54.
30. Porello, S. L.; Cannon, M. J.; David, S. S., *Biochemistry* **1998**, 37, 6465-6475.
31. Lotierzo, M.; Bui, B. T. S.; Florentin, D.; Escalettes, F.; Marquet, A., Biotin synthase mechanism: an overview. *Biochemical Society Transactions* **2005**, 33, (4), 820-823.
32. Jarrett, J. T., Biotin Synthase. *Chemistry & Biology* **2005**, 12, (4), 409-410.
33. Sofia, H. J.; Chen, G.; Hetzler, B. G.; Reyes-Spindola, J. F.; Miller, N. E., Radical SAM, a novel protein superfamily linking unresolved steps in familiar biosynthetic pathways with radical mechanisms: functional characterization using new analysis and information visualization methods. *Nucleic Acids Research* **2001**, 29, (5), 1097-1106.
34. Cheek, J.; Broderick, J. B., Adenosylmethionine-dependent iron-sulfur enzymes: versatile clusters in a radical new role. *Journal of biological inorganic chemistry : JBIC : a publication of the Society of Biological Inorganic Chemistry* **2001**, 6, (3), 209-26.
35. Frey, P. A., Radical mechanisms of enzymatic catalysis. *Annual Review of Biochemistry* **2001**, 70, 121-148.

36. Frey, P. A.; Magnusson, O. T., S-adenosylmethionine: A wolf in sheep's clothing, or a rich man's adenosylcobalamin? *Chemical Reviews (Washington, DC, United States)* **2003**, 103, (6), 2129-2148.
37. Fonetcave, M.; Mulliez, E.; Ollagnier de-Choudens, S., *Curr. Opin. Chem. Biol.* **2001**, 5, 506-511.
38. Jarrett, J. T., *Curr. Opin. Chem. Biol.* **2003**, 7, 174-182.
39. Broderick, J. B., Iron-sulfur clusters in enzyme catalysis. *Comprehensive Coordination Chemistry II* **2004**, 8, 739-757.
40. Marsh, E. N. G.; Patwardhan, A.; Huhta, M. S., S-Adenosylmethionine radical enzymes. *Bioorganic Chemistry* **2004**, 32, (5), 326-340.
41. Frey, P. A.; Booker, S. J., Radical mechanisms of S-adenosylmethionine-dependent enzymes. *Advances in Protein Chemistry* **2001**, 58, (Novel Cofactors), 1-45.
42. Fontecave, M.; Mulliez, E.; Ollagnier-de-Choudens, S., Adenosylmethionine as a source of 5'-deoxyadenosyl radicals. *Current Opinion in Chemical Biology* **2001**, 5, (5), 506-512.
43. Jarrett, J. T., The generation of 5'-deoxyadenosyl radicals by adenosylmethionine-dependent radical enzymes. *Current Opinion in Chemical Biology* **2003**, 7, (2), 174-182.
44. Duin, E. C.; Lafferty, M. E.; Crouse, B. R.; Allen, R. M.; Sanyal, I.; Flint, D. H.; Johnson, M. K., [2Fe-2S] to [4Fe-4S] Cluster Conversion in Escherichia coli Biotin Synthase. *Biochemistry* **1997**, 36, (39), 11811-11820.
45. Chirpich, T. P.; Zappia, V.; Costilow, R. N.; Barker, H. A., Lysine 2,3-aminomutase. Purification and properties of a pyridoxal phosphate and S-adenosylmethionine-activated enzyme. *J Biol Chem* **1970**, 245, (7), 1778-89.
46. Jarrett, J. T., The novel structure and chemistry of iron-sulfur clusters in the adenosylmethionine-dependent radical enzyme biotin synthase. *Archives of Biochemistry and Biophysics* **2005**, 433, (1), 312-321.
47. Ollagnier-de Choudens, S.; Fontecave, M., The lipoate synthase from Escherichia coli is an iron-sulfur protein. *FEBS Letters* **1999**, 453, (1,2), 25-28.
48. Marquet, A.; Bui, B. T. S.; Florentin, D., Biosynthesis of biotin and lipoic acid. *Vitamins and Hormones (San Diego, CA, United States)* **2001**, 61, 51-101.

49. Rebeil, R.; Sun, Y.; Chooback, L.; Pedraza-Reyes, M.; Kinsland, C.; Begley, T. P.; Nicholson, W. L., Spore photoproduct lyase from *Bacillus subtilis* spores is a novel iron-sulfur DNA repair enzyme which shares features with proteins such as class III anaerobic ribonucleotide reductases and pyruvate-formate lyases. *J Bacteriol* **1998**, 180, (18), 4879-85.
50. Rebeil, R.; Nicholson, W. L., The subunit structure and catalytic mechanism of the *Bacillus subtilis* DNA repair enzyme spore photoproduct lyase. *Proceedings of the National Academy of Sciences of the United States of America* **2001**, 98, (16), 9038-9043.
51. Cheek, J.; Broderick, J. B., Direct H atom abstraction from spore photoproduct C-6 initiates DNA repair in the reaction catalyzed by spore photoproduct lyase: evidence for a reversibly generated adenosyl radical intermediate. *J Am Chem Soc* **2002**, 124, (12), 2860-1.
52. Buis, J. M.; Cheek, J.; Kalliri, E.; Broderick, J. B., Characterization of an active spore photoproduct lyase, a DNA repair enzyme in the radical S-adenosylmethionine superfamily. *J Biol Chem* **2006**, 281, (36), 25994-6003.
53. Frey, P. A.; Booker, S., Radical intermediates in the reaction of lysine 2,3-aminomutase. *Advances in Free Radical Chemistry (Greenwich, Connecticut)* **1999**, 2, 1-43.
54. Frey, P. A., Radical reactions featuring lysine 2,3-aminomutase. *Comprehensive Natural Products Chemistry* **1999**, 5, 205-223.
55. Layer, G.; Moser, J.; Heinz, D. W.; Jahn, D.; Schubert, W. D., Crystal structure of coproporphyrinogen III oxidase reveals cofactor geometry of Radical SAM enzymes. *Embo J* **2003**, 22, (23), 6214-24.
56. Layer, G.; Kervio, E.; Morlock, G.; Heinz, D. W.; Jahn, D.; Retey, J.; Schubert, W.-D., Structural and functional comparison of HemN to other radical SAM enzymes. *Biological Chemistry* **2005**, 386, (10), 971-980.
57. Knappe, J.; Wagner, A. F. V., Stable glycy radical from pyruvate formate-lyase and ribonucleotide reductase (III). *Advances in Protein Chemistry* **2001**, 58, (Novel Cofactors), 277-315.
58. Buis, J. M.; Broderick, J. B., Pyruvate formate-lyase activating enzyme: elucidation of a novel mechanism for glycy radical formation. *Archives of Biochemistry and Biophysics* **2005**, 433, (1), 288-296.
59. Walsby, C. J.; Ortillo, D.; Yang, J.; Nnyepi, M. R.; Broderick, W. E.; Hoffman, B. M.; Broderick, J. B., Spectroscopic Approaches to Elucidating Novel

Iron-Sulfur Chemistry in the "Radical-SAM" Protein Superfamily. *Inorganic Chemistry* **2005**, 44, (4), 727-741.

60. Stubbe, J., Ribonucleotide reductases: the link between an RNA and a DNA world? *Current Opinion in Structural Biology* **2000**, 10, (6), 731-736.

61. Tamarit, J.; Gerez, C.; Meier, C.; Mulliez, E.; Trautwein, A.; Fontecave, M., The activating component of the anaerobic ribonucleotide reductase from *Escherichia coli*. An iron-sulfur center with only three cysteines. *Journal of Biological Chemistry* **2000**, 275, (21), 15669-15675.

62. Tamarit, J.; Mulliez, E.; Meier, C.; Trautwein, A.; Fontecave, M., The anaerobic ribonucleotide reductase from *Escherichia coli*. The small protein is an activating enzyme containing a $[4\text{Fe-4S}](2+)$ center. *J Biol Chem* **1999**, 274, (44), 31291-6.

63. O'Brien, J. R.; Raynaud, C.; Croux, C.; Girbal, L.; Soucaille, P.; Lanzilotta, W. N., Insight into the Mechanism of the B12-Independent Glycerol Dehydratase from *Clostridium butyricum*: Preliminary Biochemical and Structural Characterization. *Biochemistry* **2004**, 43, (16), 4635-4645.

64. Sun, L.; Warncke, K., Comparative model of EutB from coenzyme B12-dependent ethanolamine ammonia-lyase reveals a b8a8, TIM-barrel fold and radical catalytic site structural features. *Proteins: Structure, Function, and Bioinformatics* **2006**, 64, (2), 308-319.

65. Lehtio, L.; Grossmann, J. G.; Kokona, B.; Fairman, R.; Goldman, A., Crystal structure of a glycyl radical enzyme from *Archaeoglobus fulgidus*. *Journal of Molecular Biology* **2006**, 357, (1), 221-235.

66. Leuthner, B.; Leutwein, C.; Schulz, H.; Horth, P.; Haehnel, W.; Schiltz, E.; Schagger, H.; Heider, J., Biochemical and genetic characterization of benzylsuccinate synthase from *Thauera aromatica*: a new glycyl radical enzyme catalysing the first step in anaerobic toluene metabolism. *Mol Microbiol* **1998**, 28, (3), 615-28.

67. Achong, G. R.; Rodriguez, A. M.; Spormann, A. M., Benzylsuccinate synthase of *Azoarcus* sp. strain T: cloning, sequencing, transcriptional organization, and its role in anaerobic toluene and m-xylene mineralization. *Journal of Bacteriology* **2001**, 183, (23), 6763-6770.

68. Hermuth, K.; Leuthner, B.; Heider, J., Operon structure and expression of the genes for benzylsuccinate synthase in *Thauera aromatica* strain K172. *Arch Microbiol* **2002**, 177, (2), 132-8.

69. Haenzelmann, P.; Schindelin, H., Crystal structure of the S-adenosylmethionine-dependent enzyme MoaA and its implications for molybdenum cofactor deficiency in humans. *Proceedings of the National Academy of Sciences of the United States of America* **2004**, 101, (35), 12870-12875.
70. Hanzelmann, P.; Schindelin, H., Binding of 5'-GTP to the C-terminal FeS cluster of the radical S-adenosylmethionine enzyme MoaA provides insights into its mechanism. *Proceedings of the National Academy of Sciences of the United States of America* **2006**, 103, (18), 6829-6834.
71. Wuebbens, M. M.; Liu, M. T.; Rajagopalan, K.; Schindelin, H., Insights into molybdenum cofactor deficiency provided by the crystal structure of the molybdenum cofactor biosynthesis protein MoaC. *Structure (London)* **2000**, 8, (7), 709-718.
72. Vander Horn, P. B.; Backstrom, A. D.; Stewart, V.; Begley, T. P., Structural genes for thiamine biosynthetic enzymes (thiCEFGH) in Escherichia coli K-12. *J Bacteriol* **1993**, 175, (4), 982-92.
73. Leonardi, R.; Fairhurst, S. A.; Kriek, M.; Lowe, D. J.; Roach, P. L., Thiamine biosynthesis in Escherichia coli: isolation and initial characterisation of the ThiGH complex. *FEBS Lett* **2003**, 539, (1-3), 95-9.
74. Martinez-Gomez, N. C.; Robers, M.; Downs, D. M., Mutational analysis of ThiH, a member of the radical S-adenosylmethionine (AdoMet) protein superfamily. *J Biol Chem* **2004**, 279, (39), 40505-10.
75. Rubach, J. K.; Brazzolotto, X.; Gaillard, J.; Fontecave, M., Biochemical characterization of the HydE and HydG iron-only hydrogenase maturation enzymes from Thermatoga maritima. *FEBS Letters* **2005**, 579, (22), 5055-5060.
76. Posewitz, M. C.; King, P. W.; Smolinski, S. L.; Zhang, L.; Seibert, M.; Ghirardi, M. L., Discovery of Two Novel Radical S-Adenosylmethionine Proteins Required for the Assembly of an Active [Fe] Hydrogenase. *Journal of Biological Chemistry* **2004**, 279, (24), 25711-25720.
77. Hallenbeck, P. C., Integration of hydrogen evolving systems with cellular metabolism: The molecular biology and biochemistry of electron transport factors and associated reductases. *Biohydrogen II: An Approach to Environmentally Acceptable Technology, [Workshop on Biohydrogen], 2nd, Tsukuba, Japan, June, 1999* **2001**, 171-181.
78. McGlynn, S. E.; Ruebush, S. S.; Naumov, A.; Nagy, L. E.; Dubini, A.; King, P. W.; Broderick, J. B.; Posewitz, M. C.; Peters, J. W., In vitro activation of [FeFe]

hydrogenase: new insights into hydrogenase maturation. *J Biol Inorg Chem* **2007**, 12, (4), 443-7.

79. Broach, R. B.; Jarrett, J. T., Role of the [2Fe-2S]²⁺ Cluster in Biotin Synthase: Mutagenesis of the Atypical Metal Ligand Arginine 260. *Biochemistry* **2006**, 45, (47), 14166-14174.

80. Giles, N. M.; Giles, G. I.; Jacob, C., Multiple roles of cysteine in biocatalysis. *Biochem Biophys Res Commun* **2003**, 300, (1), 1-4.

81. Sanyal, I.; Cohen, G.; Flint, D. H., Biotin Synthase: Purification, Characterization as a [2Fe-2S] Cluster Protein, and in vitro Activity of the Escherichia coli bioB Gene Product. *Biochemistry* **1994**, 33, (12), 3625-31.

82. Broderick, J. B.; Henshaw, T. F.; Cheek, J.; Wojtuszewski, K.; Smith, S. R.; Trojan, M. R.; McGhan, R. M.; Kopf, A.; Kibbey, M.; Broderick, W. E., Pyruvate formate-lyase-activating enzyme: Strictly anaerobic isolation yields active enzyme containing a [3Fe-4S]⁺ cluster. *Biochemical and Biophysical Research Communications* **2000**, 269, (2), 451-456.

83. Broderick, J. B.; Duderstadt, R. E.; Fernandez, D. C.; Wojtuszewski, K.; Henshaw, T. F.; Johnson, M. K., Pyruvate formate-lyase activating enzyme is an iron-sulfur protein. *Journal of the American Chemical Society* **1997**, 119, (31), 7396-7397.

84. Krebs, C.; Henshaw, T. F.; Cheek, J.; Huynh, B. H.; Broderick, J. B., Conversion of 3Fe-4S to 4Fe-4S Clusters in Native Pyruvate Formate-Lyase Activating Enzyme: Moessbauer Characterization and Implications for Mechanism. *Journal of the American Chemical Society* **2000**, 122, (50), 12497-12506.

85. Henshaw, T. F.; Cheek, J.; Broderick, J. B., The [4Fe-4S]¹⁺ Cluster of Pyruvate Formate-Lyase Activating Enzyme Generates the Glycyl Radical on Pyruvate Formate-Lyase: EPR-Detected Single Turnover. *Journal of the American Chemical Society* **2000**, 122, (34), 8331-8332.

86. Petrovich, R. M.; Ruzicka, F. J.; Reed, G. H.; Frey, P. A., Characterization of iron-sulfur clusters in lysine 2,3-aminomutase by electron paramagnetic resonance spectroscopy. *Biochemistry* **1992**, 31, (44), 10774-81.

87. Telser, J.; Emptage, M. H.; Merkle, H.; Kennedy, M. C.; Beinert, H.; Hoffman, B. M., ¹⁷O electron nuclear double resonance characterization of substrate binding to the [4Fe-4S]¹⁺ cluster of reduced active aconitase. *J Biol Chem* **1986**, 261, (11), 4840-6.

88. Werst, M. M.; Kennedy, M. C.; Houseman, A. L.; Beinert, H.; Hoffman, B. M., Characterization of the [4Fe-4S]⁺ cluster at the active site of aconitase by ⁵⁷Fe, ³³S, and ¹⁴N electron nuclear double resonance spectroscopy. *Biochemistry* **1990**, 29, (46), 10533-40.
89. Werst, M. M.; Kennedy, M. C.; Beinert, H.; Hoffman, B. M., ¹⁷O, ¹H, and ²H electron nuclear double resonance characterization of solvent, substrate, and inhibitor binding to the [4Fe-4S]⁺ cluster of aconitase. *Biochemistry* **1990**, 29, (46), 10526-32.
90. Walsby, C. J.; Ortillo, D.; Broderick, W. E.; Broderick, J. B.; Hoffman, B. M., An Anchoring Role for FeS Clusters: Chelation of the Amino Acid Moiety of S-Adenosylmethionine to the Unique Iron Site of the [4Fe-4S] Cluster of Pyruvate Formate-Lyase Activating Enzyme. *Journal of the American Chemical Society* **2002**, 124, (38), 11270-11271.
91. Walsby, C. J.; Hong, W.; Broderick, W. E.; Cheek, J.; Ortillo, D.; Broderick, J. B.; Hoffman, B. M., Electron-Nuclear Double Resonance Spectroscopic Evidence That S-Adenosylmethionine Binds in Contact with the Catalytically Active [4Fe-4S]⁺ Cluster of Pyruvate Formate-Lyase Activating Enzyme. *Journal of the American Chemical Society* **2002**, 124, (12), 3143-3151.
92. Berkovitch, F.; Nicolet, Y.; Wan, J. T.; Jarrett, J. T.; Drennan, C. L., Crystal structure of biotin synthase, an S-adenosylmethionine-dependent radical enzyme. *Science (Washington, DC, United States)* **2004**, 303, (5654), 76-80.
93. Lepore, B. W.; Ruzicka, F. J.; Frey, P. A.; Ringe, D., The x-ray crystal structure of lysine-2,3-aminomutase from *Clostridium subterminale*. *Proceedings of the National Academy of Sciences of the United States of America* **2005**, 102, (39), 13819-13824.
94. Magnusson, O. T.; Reed, G. H.; Frey, P. A., Characterization of an allylic analogue of the 5'-deoxyadenosyl radical: an intermediate in the reaction of lysine 2,3-aminomutase. *Biochemistry* **2001**, 40, (26), 7773-82.
95. Magnusson, O. T.; Reed, G. H.; Frey, P. A., Spectroscopic Evidence for the Participation of an Allylic Analogue of the 5'-Deoxyadenosyl Radical in the Reaction of Lysine 2,3-Aminomutase. *Journal of the American Chemical Society* **1999**, 121, (41), 9764-9765.
96. Frey, P. A., Lysine 2,3-aminomutase: is adenosylmethionine a poor man's adenosylcobalamin? *Faseb J* **1993**, 7, (8), 662-70.
97. Halpern, J., Mechanisms of coenzyme B12-dependent rearrangements. *Science* **1985**, 227, (4689), 869-75.

98. Banerjee, R., Radical peregrinations catalyzed by coenzyme B12-dependent enzymes. *Biochemistry* **2001**, 40, (21), 6191-8.
99. Chiang, P. K.; Gordon, R. K.; Tal, J.; Zeng, G. C.; Doctor, B. P.; Pardhasaradhi, K.; McCann, P. P., S-Adenosylmethionine and methylation. *Faseb J* **1996**, 10, (4), 471-80.
100. Grillo, M. A.; Colombatto, S., S-Adenosylmethionine and protein methylation.. *Amino Acids* **2005**, 28, 357-362.
101. Loenen, W. A. M., S-Adenosylmethionine: jack of all trades and master of everything? *Biochemical Society Transactions* **2006**, 34, (2), 330-333.
102. Chen, D.; Walsby, C.; Hoffman, B. M.; Frey, P. A., Coordination and Mechanism of Reversible Cleavage of S-Adenosylmethionine by the [4Fe-4S] Center in Lysine 2,3-Aminomutase. *Journal of the American Chemical Society* **2003**, 125, (39), 11788-11789.
103. Cosper, N. J.; Booker, S. J.; Ruzicka, F.; Frey, P. A.; Scott, R. A., Direct FeS cluster involvement in generation of a radical in lysine 2,3-aminomutase. *Biochemistry* **2000**, 39, (51), 15668-73.
104. Knappe, J.; Sawers, G., A radical-chemical route to acetyl-CoA: the anaerobically induced pyruvate formate-lyase system of Escherichia coli. *FEMS Microbiology Reviews* **1990**, 75, (4), 383-98.
105. Kalnitsky, G.; Werkman, C. H., The anaerobic dissimilation of pyruvate by a cell-free extract of Escherichia Coli. *Arch Biochem Biophys* **1943**, 2, 113-124.
106. Knappe, J.; Blaschkowski, H. P.; Groebner, P.; Schmitt, T., Pyruvate formate-lyase of Escherichia coli. Acetyl-enzyme intermediate. *European Journal of Biochemistry* **1974**, 50, (1), 253-63.
107. Parast, C. V.; Wong, K. K.; Kozarich, J. W.; Peisach, J.; Magliozzo, R. S., Electron Paramagnetic Resonance Evidence for a Cysteine-Based Radical in Pyruvate Formate-lyase Inactivated with Mercaptopyruvate. *Biochemistry* **1995**, 34, (17), 5712-17.
108. Becker, A.; Fritz-Wolf, K.; Kabsch, W.; Knappe, J.; Schultz, S.; Wagner, A. F. V., Structure and mechanism of the glycyl radical enzyme pyruvate formate-lyase. *Nature Structural Biology* **1999**, 6, (10), 969-975.
109. Leppanen, V.-M.; Parast, C. V.; Wong, K. K.; Kozarich, J. W.; Goldman, A., Purification and crystallization of a proteolytic fragment of Escherichia coli pyruvate formate-lyase. *Acta Crystallographica, Section D: Biological Crystallography* **1999**, D55, (2), 531-533.

110. Lehtioe, L.; Leppaenen, V. M.; Kozarich, J. W.; Goldman, A., Structure of Escherichia coli pyruvate formate-lyase with pyruvate. *Acta Crystallographica, Section D: Biological Crystallography* **2002**, D58, (12), 2209-2212.
111. Becker, A.; Kabsch, W., X-ray Structure of Pyruvate Formate-Lyase in Complex with Pyruvate and CoA. *Journal of Biological Chemistry* **2002**, 277, (42), 40036-40042.
112. Frey, M.; Rothe, M.; Wagner, A. F. V.; Knappe, J., Adenosylmethionine-dependent synthesis of the glycyl radical in pyruvate formate-lyase by abstraction of the glycine C-2 pro-S hydrogen atom. Studies of [2H]glycine-substituted enzyme and peptides homologous to the glycine 734 site. *Journal of Biological Chemistry* **1994**, 269, (17), 12432-7.
113. Conradt, H.; Hohmann-Berger, M.; Hohmann, H. P.; Blaschkowski, H. P.; Knappe, J., Pyruvate formate-lyase (inactive form) and pyruvate formate-lyase activating enzyme of Escherichia coli: isolation and structural properties. *Archives of Biochemistry and Biophysics* **1984**, 228, (1), 133-42.
114. Wagner, A. F. V.; Demand, J.; Schilling, G.; Pils, T.; Knappe, J., A dehydroalanyl residue can capture the 5'-deoxyadenosyl radical generated from S-adenosylmethionine by pyruvate formate-lyase-activating enzyme. *Biochemical and Biophysical Research Communications* **1999**, 254, (2), 306-310.
115. Unkrig, V.; Neugebauer, F. A.; Knappe, J., The free radical of pyruvate formate-lyase. Characterization by EPR spectroscopy and involvement in catalysis as studied with the substrate-analogue hypophosphite. *European Journal of Biochemistry* **1989**, 184, (3), 723-8.
116. Nnyepi, M. R.; Peng, Y.; Broderick, J. B., Inactivation of E. coli pyruvate formate-lyase: role of AdhE and small molecules. *Arch Biochem Biophys* **2007**, 459, (1), 1-9.
117. Knappe, J.; Neugebauer, F. A.; Blaschkowski, H. P.; Gaenzler, M., Post-translational activation introduces a free radical into pyruvate formate-lyase. *Proceedings of the National Academy of Sciences of the United States of America* **1984**, 81, (5), 1332-5.
118. Wagner, A. F. V.; Frey, M.; Neugebauer, F. A.; Schaefer, W.; Knappe, J., The free radical in pyruvate formate-lyase is located on glycine-734. *Proceedings of the National Academy of Sciences of the United States of America* **1992**, 89, (3), 996-1000.

119. Kessler, D.; Herth, W.; Knappe, J., Ultrastructure and pyruvate formate-lyase radical quenching property of the multienzymic AdhE protein of *Escherichia coli*. *Journal of Biological Chemistry* **1992**, 267, (25), 18073-9.
120. Kessler, D.; Leibrecht, I.; Knappe, J., Pyruvate-formate-lyase-deactivase and acetyl-CoA reductase activities of *Escherichia coli* reside on a polymeric protein particle encoded by adhE. *FEBS Letters* **1991**, 281, (1-2), 59-63.
121. Parast, C. V.; Wong, K. K.; Lewisch, S. A.; Kozarich, J. W.; Peisach, J.; Magliozzo, R. S., Hydrogen Exchange of the Glycyl Radical of Pyruvate Formate-Lyase Is Catalyzed by Cysteine 419. *Biochemistry* **1995**, 34, (8), 2393-9.
122. Roedel, W.; Plaga, W.; Frank, R.; Knappe, J., Primary structures of *Escherichia coli* pyruvate formate-lyase and pyruvate-formate-lyase-activating enzyme deduced from the DNA nucleotide sequences. *European Journal of Biochemistry* **1988**, 177, (1), 153-8.
123. Wong, K. K.; Murray, B. W.; Lewisch, S. A.; Baxter, M. K.; Ridky, T. W.; Ulissi-DeMario, L.; Kozarich, J. W., Molecular properties of pyruvate formate-lyase activating enzyme. *Biochemistry* **1993**, 32, (51), 14102-10.
124. Kulzer, R.; Pils, T.; Kappl, R.; Huttermann, J.; Knappe, J., Reconstitution and characterization of the polynuclear iron-sulfur cluster in pyruvate formate-lyase-activating enzyme. Molecular properties of the holoenzyme form. *Journal of Biological Chemistry* **1998**, 273, (9), 4897-4903.
125. Maynard, R. H.; Premakumar, R.; Bishop, P. E., Mo-independent nitrogenase 3 is advantageous for diazotrophic growth of *Azotobacter vinelandii* on solid medium containing molybdenum. *Journal of bacteriology* **1994**, 176, (17), 5583-6.
126. Hille, R., The Mononuclear Molybdenum Enzymes. *Chemical Reviews (Washington, D. C.)* **1996**, 96, (7), 2757-2816.
127. Sigel, H.; Sigel, A.; Editors, *Metal Ions in Biological Systems, Vol. 31: Vanadium and Its Role in Life*. 1995; p 779 pp.
128. Wuebbens, M. M.; Rajagopalan, K. V., Investigation of the early steps of molybdopterin biosynthesis in *Escherichia coli* through the use of in vivo labeling studies. *Journal of Biological Chemistry* **1995**, 270, (3), 1082-7.
129. Unkles, S. E.; Smith, J.; Kanan, G. J. M. M.; Millar, L. J.; Heck, I. S.; Boxer, D. H.; Kinghorn, J. R., The *Aspergillus nidulans* cnxABC locus is a single gene encoding two catalytic domains required for synthesis of precursor Z, an intermediate in molybdenum cofactor biosynthesis. *Journal of Biological Chemistry* **1997**, 272, (45), 28381-28390.

130. Hoff, T.; Schnorr, K. M.; Meyer, C.; Caboche, M., Isolation of two Arabidopsis cDNAs involved in early steps of molybdenum cofactor biosynthesis by functional complementation of Escherichia coli mutants. *Journal of Biological Chemistry* **1995**, 270, (11), 6100-7.
131. Reiss, J.; Cohen, N.; Dorche, C.; Mandel, H.; Mendel, R. R.; Stallmeyer, B.; Zabot, M.-T.; Dierks, T., Mutations in a polycistronic nuclear gene associated with molybdenum cofactor deficiency. *Nature Genetics* **1998**, 20, (1), 51-53.
132. Gabard, J.; Pelsy, F.; Marion-Poll, A.; Caboche, M.; Saalbach, I.; Grafe, R.; Mueller, A. J., Genetic analysis of nitrate reductase deficient mutants of Nicotiana plumbaginifolia: evidence for six complementation groups among 70 classified molybdenum cofactor deficient mutants. *Molecular and General Genetics* **1988**, 213, (2-3), 206-13.
133. Reiss, J., Genetics of molybdenum cofactor deficiency. *Human genetics* **2000**, 106, (2), 157-63.
134. McKusick, V. A.; (Assistant), S. E. A.; (Assistant), C. A. F.; (Assistant), O. H.; (Assistant), A. F. S.; (Assistant), M. S.; (Assistant), D. V., *Mendelian Inheritance in Man: A Catalog of Human Genes and Genetic Disorders*. The Johns Hopkins University Press: 1998; p 3972.
135. Johnson, J. L.; Waud, W. R.; Rajagopalan, K. V.; Duran, M.; Beemer, F. A.; Wadman, S. K. *Inborn errors of molybdenum metabolism: combined deficiencies of sulfite oxidase and xanthine dehydrogenase in a patient lacking the molybdenum cofactor*, United States, 1980; pp 3715-9.
136. Johnson, J. L.; Rajagopalan, K. V.; Wadman, S. K., Human molybdenum cofactor deficiency. *Advances in experimental medicine and biology* **1993**, 338, 373-8.
137. Rajagopalan, K. V., Novel aspects of the biochemistry of the molybdenum cofactor. *Advances in enzymology and related areas of molecular biology* **1991**, 64, 215-90.

CHAPTER II

INVESTIGATION ON THE *IN VIVO* STATES OF PFL-AE

II.1 Introduction

The iron-sulfur cluster in purified PFL-AE has been shown to be oxygen-sensitive, labile, and extremely sensitive to purification and handling conditions. The first report of an iron-sulfur cluster in PFL-AE provided evidence for a mixture of $[4\text{Fe-4S}]^{2+}$ and $[2\text{Fe-2S}]^{2+}$ clusters in the enzyme as-isolated, with reduction in the presence of AdoMet yielding a mixture of $[4\text{Fe-4S}]^+$ and $[4\text{Fe-4S}]^{2+}$ clusters.¹ Later reports showed that PFL-AE isolated under modified conditions contained primarily $[3\text{Fe-4S}]^+$ clusters, with a mixture of $[4\text{Fe-4S}]^{2+/+}$ clusters obtained upon reduction.² The best purification, using anaerobic conditions in the presence of DTT, yielded only the $[4\text{Fe-4S}]^{2+}$ cluster in the purified protein.³ Although the proposed mechanism has assigned the $[4\text{Fe-4S}]^{2+}$ cluster to the catalytically oxidized form and the $[4\text{Fe-4S}]^{1+}$ clusters to the reduced form,⁴ little is known about the resting states of the iron-sulfur clusters *in vivo* under different conditions and whether these clusters have their own specific functions.

In this chapter we are going to investigate the homologously overexpressed recombinant *E. coli* PFL-AE in whole cells using EPR and Mössbauer techniques. The objectives are to investigate the cluster composition of PFL-AE in the cell under different conditions in order to understand the relevance of different clusters present in previous *in vitro* studies.^{1, 2, 5} We also want to understand how the cosubstrate SAM interacts with PFL-AE clusters *in vivo* as well as any other possible function. The other interesting question we want to address is how the unique iron interacts with SAM. Whether it is going to be the same as *in vitro* studies.⁴

In 1944, Soviet physicist Yevgeniy Zavoyskiy was the first to discover the phenomenon of electron paramagnetic resonance (EPR). Since then, significant developments in this technique have been achieved. EPR has been used in a wide range of studies of organic free radicals and inorganic complexes with unpaired electrons.

The physical basics of EPR are analogous to those of nuclear magnetic resonance (NMR). Instead of detecting nuclear spin transitions as in NMR, EPR monitors the transition between electron spin states. When an electron is placed inside an external magnetic field with strength B_0 , the electron's magnetic moment aligns itself either parallel ($m_s = -1/2$) or antiparallel ($m_s = +1/2$) to the field. Each alignment is associated with a specific energy level, with the parallel alignment corresponding to the lower energy state and the antiparallel alignment to the higher energy. The energy separation (ΔE) between the two states is depicted according to equation II.1.1.

$$\Delta E = g_e \mu_B B_0, \quad \text{Equation II.1.1.}$$

where g_e is the electron's so-called g-factor and μ_B is Bohr magneton. The splitting of the energy levels is therefore directly proportional to the magnetic field's strength, as shown above.

In order for the electron to transition between the two energy levels, an amount energy equal to the difference in energy levels (ΔE) is required. The energy of electromagnetic radiation (E) is defined as in equation II.1.2.

$$E = h\nu \quad \text{Equation II.1.2.}$$

where ν is the frequency of electromagnetic radiation and h is Planck's constant.

Substituting in $E = h\nu$ and $\Delta E = g_e \mu_B B_0$ leads to the fundamental equation of EPR spectroscopy (Eq. II.1.3).

$$h\nu = g_e \mu_B B_0 \quad \text{Equation II.1.3.}$$

Theoretically, EPR spectra can be generated by either varying the frequency of electromagnetic radiation while holding the magnetic field constant, or doing the reverse. In practice, it is usually the frequency that is kept fixed. Depending on the microwave frequencies used, the spectrometers are defined as L-band (1-2 GHz), S-band (2-4 GHz), X-Band (8-10 GHz), Q-band (35 GHz), and W-band (95 GHz). Among these, X-band EPR is the most commonly used in biochemical studies.

In the case of a free electron in the external magnetic field, g_e is a constant with a value of 2.0023. However, in real systems the electron is not solitary, but is associated with the surrounding environment, and is thus subject to an effective field (B_{eff}) that is the combination of the spectrometer's applied

magnetic field (B_0) and the local magnetic field produced by surrounding atoms (σ), as shown by equation II.1.4.

$$B_{\text{eff}} = B_0(1 - \sigma) \quad \text{Equation II.1.4.}$$

Therefore, the resonance condition for an electron in a given environment can be rewritten as follows (Equation II.1.5.):

$$h\nu = g_e\mu_B B_{\text{eff}} = g_e\mu_B B_0(1 - \sigma) \quad \text{Equation II.1.5.}$$

The quantity $g_e(1 - \sigma)$ is re-defined as the g-factor (g). Therefore, the final resonance equation becomes

$$h\nu = g\mu_B B_0 \quad \text{Equation II.1.6.}$$

Knowledge of the g-factor for an unpaired electron can give information about a paramagnetic center's electronic structure. The g-factor may be anisotropic, or orientation dependent, thus providing information about the orbital containing the electron. The line shape of the EPR spectrum can also be used to study the interaction of an unpaired electron with its environment.

EPR is an appropriate technique to probe the electronic structures of paramagnetic species, such as the iron-sulfur cluster of PFL-AE. The formal oxidation states for iron in iron-sulfur clusters is generally Fe^{2+} with $S = 2$ and Fe^{3+} with $S = 5/2$. For example, a typical $[\text{4Fe-4S}]^{1+}$ cluster contains formally 3 Fe^{2+} and 1 Fe^{3+} . The 1 Fe^{2+} and 1 Fe^{3+} on the same face of the iron sulfur cluster ferromagnetically couple, producing an $\text{Fe}^{+2.5}\text{Fe}^{+2.5}$ pair with $S = 9/2$. Similarly, the other two Fe^{2+} forms an $\text{Fe}^{2+}\text{Fe}^{2+}$ pair with $S = 4$. The resulting two dimer pairs antiferromagnetically couple with each other to produce an overall spin of $S = 1/2$. Similarly, a typical $[\text{4Fe-4S}]^{2+}$ cluster, contains 2 Fe^{2+} and 2 Fe^{3+} , exhibits

an overall spin of $S = 0$ due to antiferromagnetic coupling of the two $\text{Fe}^{+2.5}\text{Fe}^{+2.5}$ pairs. This cluster is EPR silent, while the $[\text{4Fe-4S}]^{1+}$ cluster is EPR active. EPR can provide powerful insight into the properties of paramagnetic iron-sulfur clusters, such as the type of the cluster, the oxidation state of the cluster, and the surrounding environment of the cluster.^{6, 7}

^{57}Fe Mössbauer spectroscopy is another powerful and widely used technique for examining iron-sulfur cluster containing proteins. Unlike EPR, which can only detect paramagnetic species, Mössbauer spectroscopy takes advantage of the recoilless nuclear gamma resonance, the transition between the nuclear ground state and nuclear excited state. Therefore, this technique can detect all types of the iron-sulfur clusters regardless of the oxidation state or magnetic properties of the irons as long as the cluster is enriched with the ^{57}Fe isotope. Like EPR, Mössbauer spectroscopy is also capable of differentiating the surrounding environment of the ^{57}Fe species and each iron-sulfur cluster can be identified by its own characteristic spectrum. The study of the iron-sulfur clusters of purified PFL-AE is one of the best examples regarding how well different clusters can be assigned according to their Mössbauer spectra.^{5, 7, 8} In 1998, Popescu et al successfully apply the Mössbauer spectroscopy to the *in vivo* behavior of the iron-sulfur clusters of the overexpressed FNR, discovering the *in vivo* interconversion of the $[\text{4Fe-4S}]^{2+}$ and the $[\text{2Fe-2S}]^{2+}$.⁹ Since then, several iron-sulfur enzymes have been successfully studied *in vivo* by this technique, including aRNR,¹⁰ BioB,^{11, 12} and thioredoxin reductase.¹³

To acquire a ^{57}Fe Mössbauer absorption spectrum, a solid sample containing ^{57}Fe in question is exposed to a beam of gamma radiation produced by the excited state of ^{57}Fe (14.4 KeV). The energy of this incident gamma radiation is then finely tuned by moving the source toward and away from the solid sample. Because of the Doppler effect, this spectrum of gamma-rays centered at 14.4 KeV arrives at the sample. A detector then measures the intensity of the beam that is transmitted through the sample. In the case of a bare ^{57}Fe nucleus, a single absorption line corresponding to the difference between the nuclear excited state and the ground state would be observed. However, the ^{57}Fe nucleus is usually embedded in an environment defined by interacting atoms. The symmetry of this environment is usually lower than spherical, tetrahedral or cubic. As a result, the degeneracy of the nuclear excited state is lifted by the quadrupole moment interaction with this asymmetric electric field, resulting in the characteristic doublet associated with a Mössbauer spectrum. The splitting of the excited states is called the quadrupole splitting energy (ΔE_Q), a very important Mössbauer factor. The other factor is the isomer shift (δ), centroid of the spectrum. It arises from the non-zero volume of the nucleus and the electron charge density due to s-electrons within it. As a result, the isomer shift (δ) is a good indicator of the oxidation state.¹⁴

Taken together, the combination of powerful EPR and Mössbauer spectroscopies can provide a fairly complete picture of the cluster content of simple or complex iron-sulfur proteins. This study is designed to investigate the

type and properties of the iron–sulfur clusters present in homologously expressed recombinant *E. Coli* PFL-AE in whole cells.

II.2. MATERIALS AND METHODS

Photoreducing agent 5-deazariboflavin was synthesized according to the published procedures.¹⁵ Competent cells were purchased from Novagen. Restriction endonucleases and DNA markers were purchased from NEB. Compass DNA purification kit was purchased from American Bioanalytical. Wizard plus SV minipreps DNA purification system was purchased from Promega.

II.2.1. Construction of PFL-AE Expression and Control Vectors.

The pCAL-n-EK/*pflA* vector (hereafter designated pTHVI47) was constructed as previously described.² For construction of the control vector, pTHVI47 was digested with NdeI and HindIII. The fragments were separated on an agarose gel, and the large fragment was purified using a Compass DNA Purification Kit. The ends were trimmed by using the End Conversion Mix from the PETBlue-1 Perfectly Blunt Cloning Kit; following end-conversion, the blunt fragment was ligated to generate the control plasmid containing no *pflA* gene. The control plasmid was verified by DNA fingerprinting using EcoRV and XbaI, as well as by DNA sequencing, and was designated pJYVI119.

II.2.2. Growth, Induction, and Cycling of PFL-AE and Control Cultures.

The vectors pTHVI47 and pJYVI119 were transformed into BL21(DE3)plysS Singles Competent Cells to generate PFL-AE expressing and control cells, respectively. Both PFL-AE and control cells were grown overnight in

LB at 37° C with shaking, and 5 mL of these overnight cultures were used to inoculate 1 L of defined minimal media in a 2800 mL Fernbach flask. The PFL-AE and control cultures were grown with shaking (250 rpm) at 37° C to an OD₆₀₀ ~ 0.7. At this point, IPTG was added to both cultures to a final concentration of 1 mM. The cultures were grown for two more hours under aerobic conditions with shaking. Both cultures were then transferred to a 4°C cold box and made anaerobic by bubbling N₂ gas through for 16 hours. To make the culture aerobic again, air was bubbled through the culture for 6 hours. Further cycling of aerobic/anaerobic conditions simply followed the same procedure. For preparation of Mössbauer samples, both PFL-AE and control cells were prepared in the same way as just described except that the growth medium was enriched with ⁵⁷Fe. At specific time points after induction, or after transition from aerobic to anaerobic or anaerobic to aerobic conditions, aliquots (15 mL for EPR and/or 60 mL for Mössbauer) were removed for analysis by EPR and Mössbauer spectroscopy.

II.2.3. Preparation of Whole-Cell, Lysed-Cell, and Clear Lysate

Mössbauer samples.

The aliquots taken during cycling between aerobic and anaerobic conditions were centrifuged to collect cell paste (~0.8 g per 60 mL aliquot). The cell pastes were resuspended in 200 mL wash buffers (50 mM NaCl, 40 mM MOPS pH 7.0 and 22.2 mM glucose) and then centrifuged to collect the cell paste, which was transferred to Mössbauer cups. To investigate the effect of

SAM on the spectroscopic properties of PFL-AE in whole cells, whole cell samples prepared as described above were resuspended in AE lysis buffer (50 mM HEPES pH 7.5, 200 mM NaCl, 5% (w/v) glycerol, 1% (w/v) Triton X-100, 10 mM MgCl₂) (~0.4 g whole cell + 300 µL AE lysis buffer), and SAM was added to 2.5 mM. The sample was incubated at room temperature for 15 mins before transferring to a Mössbauer cup and freezing in liquid nitrogen. In addition, separate whole cell samples were resuspended in AE lysis buffer (~2 g whole cell + 1.5 mL AE lysis buffer) and lysed by addition of lysozyme/DNase/RNase, followed by addition of SAM to 2.5 mM. After incubation at room temperature for 15 min, the sample was transferred to a Mössbauer cup and flash-frozen in liquid nitrogen. The lysed PFL-AE cells in the presence of added SAM were also exposed to air at room temperature for various amounts of time before freezing in liquid nitrogen. Samples of unpurified overexpressed PFL-AE in the presence of SAM, PFL, and/or YfiD were also made by lysis as described above, followed by centrifugation to obtain a clear lysate. The clear lysate was mixed with SAM (final concentration 1.7 – 1.9 mM), YfiD (final concentration 0.19 mM), or PFL (final concentration 0.17 mM). The resulting samples were incubated at room temperature for 30 minutes before transferring to Mössbauer cups and freezing in liquid nitrogen.

II.2.4. Preparation of Mössbauer Samples of Purified PFL-AE.

⁵⁷Fe-labeled PFL-AE was expressed and purified as previously described.^{2, 5} To purified [⁵⁷Fe]-PFL-AE (0.64 mM in 50 mM Hepes pH 7.5, 200

mM NaCl, and 1 mM DTT) was added ATP, ADP, AMP, 5'-deoxyadenosine, methylthioadenosine, adenine, ribose, pyruvate, formate, CoA, or Acetyl-CoA (all at 6.4 mM final concentration). The samples were frozen in liquid nitrogen immediately after mixing. After collecting the Mössbauer spectra, the samples were thawed and SAM was added to each (to 6.4 mM final concentration). The samples were flash-frozen for collection of additional Mössbauer spectroscopy.

II.2.5. Preparation of EPR Samples of Purified PFL-AE.

Purified PFL-AE (100 μ M) in buffer containing 100 μ M 5-deazariboflavin, 1 mM DTT, 100 mM Tris-HCl pH 7.6, 100 mM KCl, and 20 mM oxamate was illuminated for 1 h at 0°C to reduce the [4Fe-4S] cluster to the 1+ state. The reduced enzyme was then divided into 10 aliquots, and one of (ATP, ADP, AMP, cAMP, 5'-deoxyadenosine, 2'-deoxyadenosine, adenosine, methylthioadenosine, methionine) was added to each aliquot to 2 mM final concentration. The EPR samples were then frozen in liquid nitrogen. After measuring the EPR spectra, the samples were thawed and SAM was added to 2 mM final concentration followed by flash-freezing the samples again.

II.2.6. Effects of ATP, ADP, and AMP on PFL-AE Activity Assay.

The PFL-AE activity was measured using modifications of previously published procedures.² Anaerobic PFL-AE reaction mixes all contained in a final volume 500 μ L: 0.1 M Tris-HCl pH 7.6, 0.1 M KCl, 10 mM oxamate, 8 mM DTT, ~0.06 μ M PFL-AE, ~6 μ M PFL, 0.2 mM AdoMet, and 50 μ M 5-deazariboflavin.

Some assays also contained 0.2 mM ATP, ADP or AMP. For each PFL-AE activity assay, 5-deazariboflavin was added last, in the dark, and the reaction was initiated by illumination of the sample in an ice water bath with a 300 W halogen bulb. At time intervals after initiation of the reaction, typically 5 to 30 min, an aliquot (5 μ L) was removed for assay of active PFL through the coupling assay.

The coupling assay mix contained 0.1 M Tris-HCl pH 8.1, 3 mM NAD, 55 mM CoA, 0.1 mg BSA, 10 mM pyruvate, 10 mM malate, 20 units citrate synthase, 300 units malic dehydrogenase, and 10 mM DTT in a final volume of 20 mL. To assay PFL activity, 895 μ L of the coupling assay mix and 5 μ L of the PFL-AE activity mix were combined in a quartz cuvette, which was then sealed with a septum and brought out of the chamber to monitor the production of NADH by the increase in absorbance at 340 nm.

II.2.7. Mössbauer and EPR Spectroscopy.

Mössbauer spectra were recorded in either weak-field spectrometer equipped with a Janis 8 DT variable-temperature cryostat or a strong-field spectrometer furnished with a Janis CNDT/SC SuperVaritemp cryostat encasing an 8-T superconducting magnet. Both spectrometers operate in a constant acceleration mode in a transmission geometry. The zero velocity of the spectra refers to the centroid of a room-temperature spectrum of a metallic iron foil. EPR spectra were recorded in a Bruker EPR spectrometer cooled to 12 K with a liquid

He cryostat and a temperature controller from Oxford Instruments. The samples were measured at 2 mW microwave power and 10 G modulation amplitude.

II.3. Results and Discussion

II.3.1. Construction of Overexpressing and Control Cells.

The PFL-AE overexpression vector was constructed as previously described, and when transformed into *E. coli* BL21(DE3)pLysS cells provided a high level of overexpression of PFL-AE (Figure II.3.1.1). A control vector was constructed by using restriction digestion and ligation to remove the *pflA* gene from the PFL-AE expression vector. This vector, when transformed into the same *E. coli* strain, showed no evidence for overexpression of PFL-AE (Figure II.3.1.1).

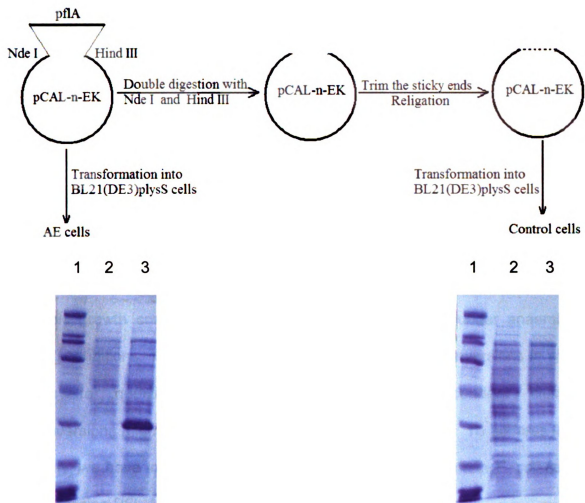


Figure II.3.1.1. Construction of PFL-AE-overexpressing and control cells. The PFL-AE expression vector, constructed as indicated in the figure and described in the text, was transformed into *E. coli* BL21(DE3)pLysS cells. The control vector, the PFL-AE expression vector with the PFL-AE gene removed, was transformed into the same cell line. SDS-PAGE gels showing the results of growth and induction of the PFL-AE (left) and control (right) cells is shown. Lanes on each gel are 1) MW standard, 2) pre-induction, and 3) 2 h post-induction.

II.3.2. Iron-Sulfur Cluster Interconversions in PFL-AE in Whole Cells.

Purified PFL-AE has been shown previously to undergo cluster interconversions. An early report suggested a $[2\text{Fe-2S}]^{2+} \rightarrow [4\text{Fe-4S}]^{2+/+}$ interconversion upon reduction of PFL-AE,¹ while more recent results point to a facile $[3\text{Fe-4S}]^+ \rightarrow [4\text{Fe-4S}]^{2+/+}$ conversion under reducing conditions, with the corresponding $[4\text{Fe-4S}]^{2+/+} \rightarrow [3\text{Fe-4S}]^+$ occurring upon oxidation.^{2, 5} The physiological relevance of these cluster conversions, if any, has yet to be identified. PFL-AE is constitutively expressed in *E. coli* under both aerobic and anaerobic growth conditions, however it activates PFL only under anaerobic reducing conditions. Our observation of PFL-AE cluster interconversions *in vitro* led us to question whether cellular redox-state-dependent cluster interconversions might play a role in regulating PFL-AE activity. To address this possibility, we have investigated PFL-AE cluster interconversions in *E. coli* cells overexpressing PFL-AE.

Figure II.3.2.1 and Figure II.3.2.2 summarized the EPR spectra of both PFL-AE and the control samples. The control cells showed very good background information at a region between 3350 to 3450 Gauss. In comparison, the PFL-AE cells showed not only the background signals but also the shoulder signals at a region between 3300 to 3350 Gauss. This shoulder signal reached its maximal strength 1hr after the PFL-AE cells were changed from anaerobic to aerobic conditions. Interestingly, longer incubation of this culture under aerobic conditions weakened this signal. Deconvolution (subtraction) of PFL-AE cells from the control cells exhibited a typical $[3\text{Fe-4S}]^{1+}$ cluster signal ($g=2.02, 2.04$).

However, spin quantification of this difference signal accounted for only 0.3% of the total iron-sulfur cluster present in the PFL-AE cells, suggesting the $[3\text{Fe-4S}]^{1+}$ cluster is not the major species of PFL-AE in the whole cells. Most (99.7 %) of the iron-sulfur clusters of PFL-AE were in the diamagnetic states that can not be observed by EPR spectroscopy. In order to investigate these diamagnetic species *in vivo*, Mössbauer spectroscopy was used and results will be discussed in the next paragraph.

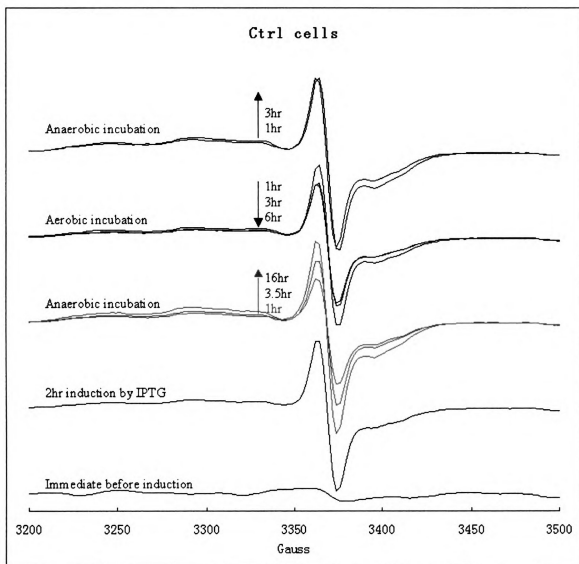


Figure II.3.2.1. X-band EPR spectra of the control cells under different conditions. Each sample contained ~ 0.2 g cell paste and were resuspended in 0.2 mL wash buffer (50 mM NaCl, 40 mM MOPS pH 7.0, and 22.2 mM glucose). Conditions of measurement, $T = 12\text{ K}$; microwave power, 2 mW; modulation amplitude, 10 G.

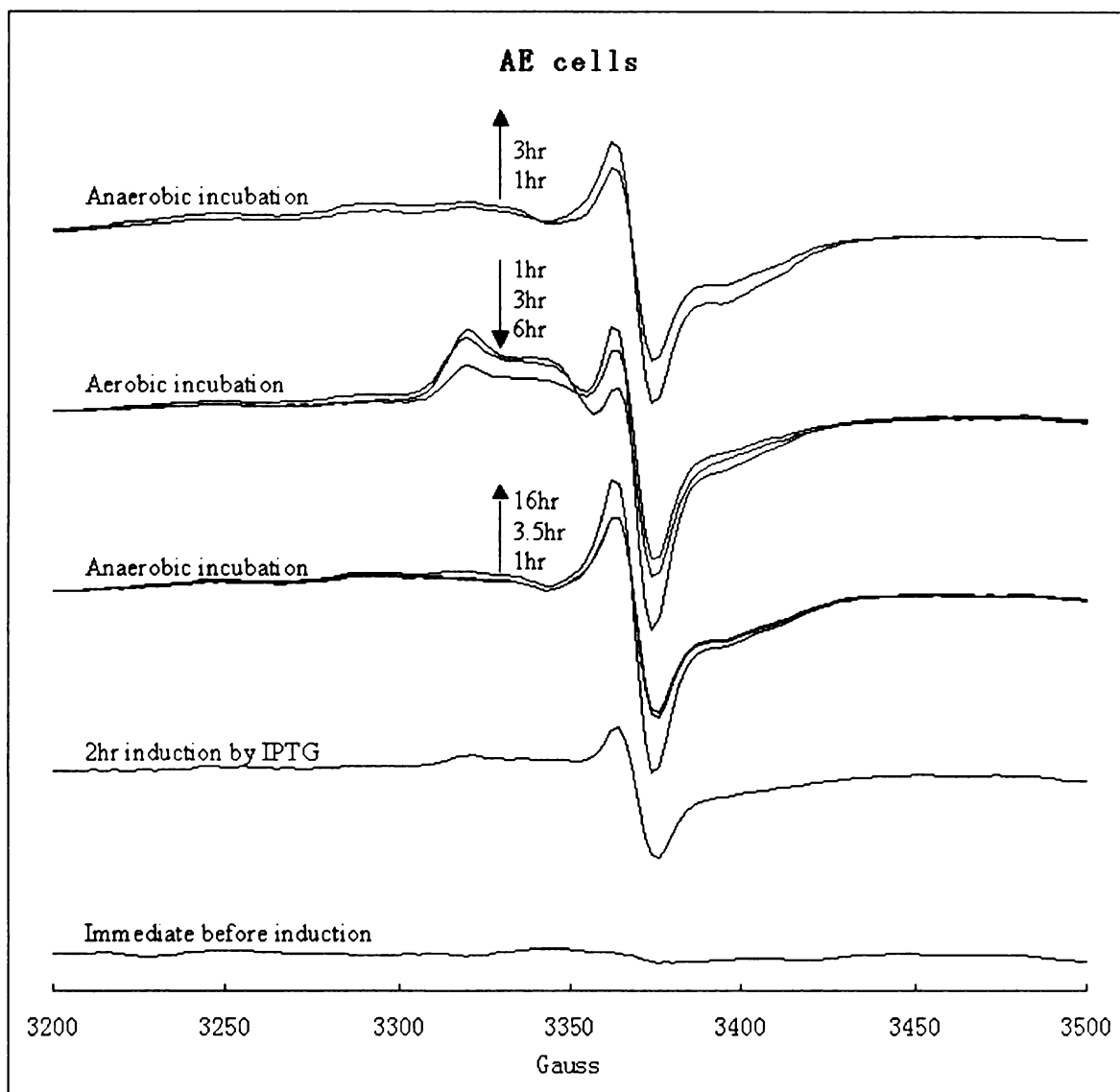


Figure II.3.2.2. X-band EPR spectra of the PFL-AE cells under different conditions. Each sample contained ~ 0.2 g cell paste and were resuspended in 0.2 mL wash buffer (50 mM NaCl, 40 mM MOPS pH 7.0, and 22.2 mM glucose). Conditions of measurement, $T = 12$ K; microwave power, 2 mW; modulation amplitude, 10 G.

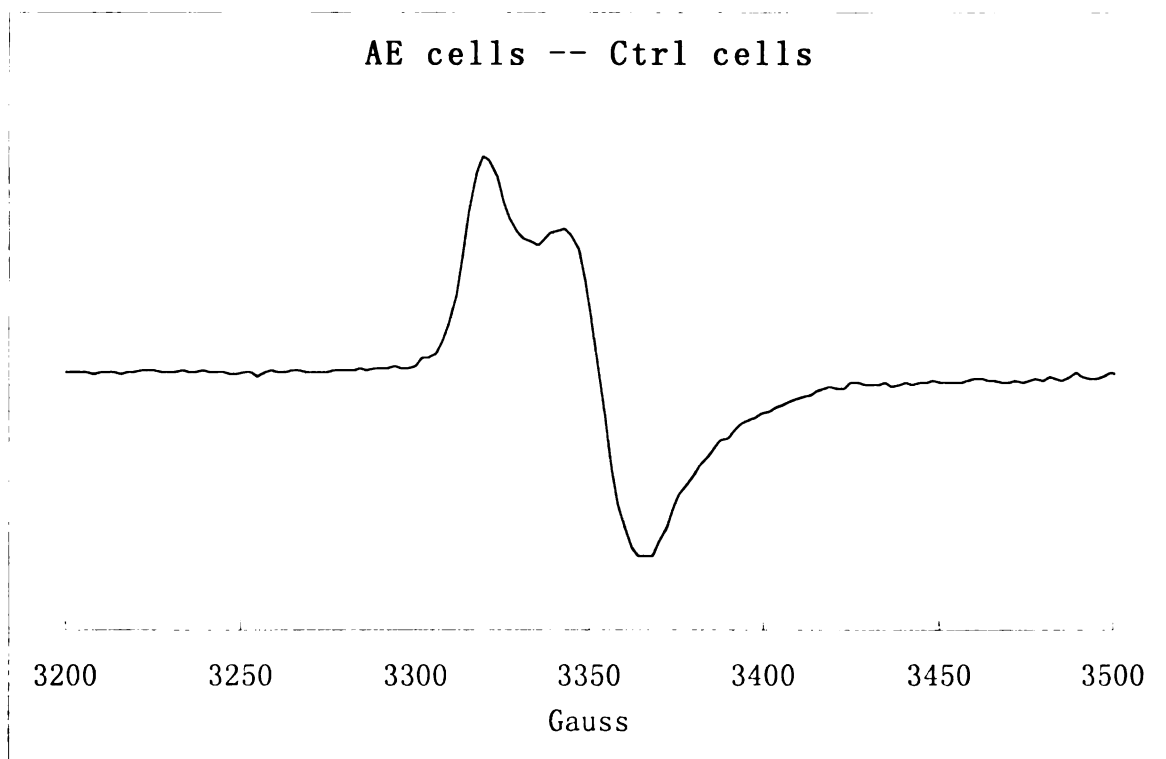


Figure II.3.2.3. X-band EPR spectra subtraction of the PFL-AE cells from the control cells. Both PFL-AE and the control samples have been incubated under aerobic condition for 1 hr. This signal represents a typical $[3\text{Fe}4\text{S}]^{1+}$ cluster ($g = 2.02, 2.04$) and accounts for only 0.3% of the total iron present in the PFL-AE cells.

After 2 h induction under aerobic conditions, the ^{57}Fe -Mössbauer spectra of *E. coli* cells overexpressing PFL-AE are comprised of four components, including $[4\text{Fe}4\text{S}]^{2+}$ clusters (~50% of total iron), $[2\text{Fe}2\text{S}]^{2+}$ clusters (~6% of total iron), Fe(III) (~24.5% of total iron), and Fe(II) (~7% of total iron) (Figure II.3.2.4). The corresponding control sample exhibits signals only for Fe(III) (~61% of total iron) and Fe(II) (~41% of total iron), with no cluster signals observed, thereby providing evidence that the cluster signals observed in the PFL-AE cells are due solely to PFL-AE iron-sulfur clusters (Figure II.3.2.4). After 16 hours of subsequent anaerobic incubation, the iron speciation of the PFL-AE cells changes dramatically, such that $[4\text{Fe}4\text{S}]^{2+}$ (77% of total iron) and Fe(II) (6%

of total iron) are the only species observed. Further aerobic incubation resulted in the PFL-AE cells containing again ~50% total iron as $[4\text{Fe-4S}]^{2+}$, 10% total iron as $[2\text{Fe-2S}]^{2+}$, with some Fe(III) ~15%) and Fe(II) (8%) also present. The corresponding control cells show some variation in the relative amount of Fe(III) and Fe(II) present, with Fe(III) increasing under aerobic growth conditions and decreasing under anaerobic growth conditions. It should be noted that the amount of signal attributed to Fe(II) in the PFL-AE cells changes little in response to the change in oxygen availability, while the amount of the Fe(III), $[2\text{Fe-2S}]^{2+}$, and $[4\text{Fe-4S}]^{2+}$ changes dramatically. In fact, the sum of the quantities of iron present in these three signals in aerobic cultures (50 + 6 + 24.5 % of total iron) is approximately equal to the amount of iron in the $[4\text{Fe-4S}]^{2+}$ (77% of total iron) after anaerobic incubation of the culture. This provides support for the hypothesis that under anaerobic conditions, additional $[4\text{Fe-4S}]^{2+}$ clusters are assembled in PFL-AE at the expense of the $[2\text{Fe-2S}]^{2+}$ clusters and Fe(III) present under aerobic growth conditions. Together, these results provide support for oxygen-dependent cluster interconversions occurring in PFL-AE *in vivo*, with a mixture of $[4\text{Fe-4S}]^{2+}$ and $[2\text{Fe-2S}]^{2+}$ clusters present under aerobic growth conditions, converting to all $[4\text{Fe-4S}]^{2+}$ under anaerobic conditions.

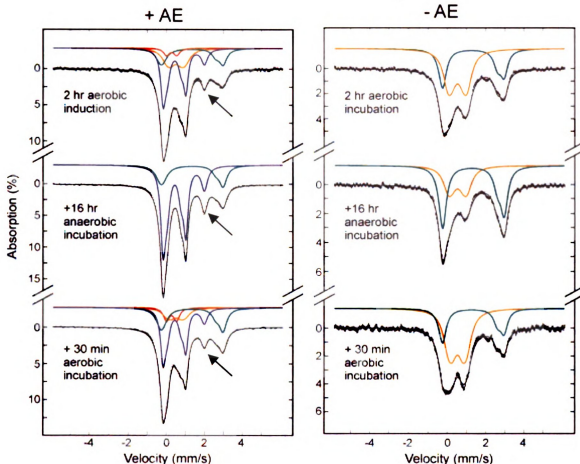


Figure II.3.2.4. Mössbauer spectra of PFL-AE-overexpressing and control cells under different growth conditions. The colored lines are the theoretical simulations of component spectra that sum to a theoretical spectrum (black solid lines overlaying experimental data) in good agreement with the experimental data (black hatched lines). Component spectral simulations are color-coded as non-cluster Fe(II) (green), non-cluster Fe(III) (orange), $[2\text{Fe-2S}]^{2+}$ (red), and $[4\text{Fe-4S}]^{2+}$ (blue). The control cells (right) exhibit a mixture of Fe(II) and Fe(III) after 2 h aerobic induction which becomes more weighted toward the ferrous state after anaerobic incubation and more weighted to the ferric state after aerobic incubation. No signals due to iron-sulfur cluster signals are observed. The PFL-AE-expressing cells show, in addition to the ferrous and ferric signals, strong signals attributed to $[2\text{Fe-2S}]^{2+}$ and $[4\text{Fe-4S}]^{2+}$ clusters. After anaerobic incubation, the $[2\text{Fe-2S}]^{2+}$ cluster is no longer present, and the $[4\text{Fe-4S}]^{2+}$ cluster signal increases in intensity. After aerobic incubation, the $[4\text{Fe-4S}]^{2+}$ cluster signal decreases in intensity and the $[2\text{Fe-2S}]^{2+}$ cluster signal reappears. Spectral parameters and signal quantitation are provided in the text.

II.3.3. Valence-Localized $[4\text{Fe-4S}]^{2+}$ in PFL-AE in Whole Cells.

The $[4\text{Fe-4S}]^{2+}$ cluster in PFL-AE in whole cells contains a valence-localized $\text{Fe}^{2+}\text{-Fe}^{3+}$ pair, as indicated by the prominent peak at approximate +1.9 mm/s; this peak is one-half of a quadrupole doublet ($\delta_3 = 0.967$, $\Delta E_{Q3} = 2.075$) assigned to a localized Fe(II) site in the $[4\text{Fe-4S}]^{2+}$ cluster (Figure II.3.2.4, arrow). The magnetic field dependence of this signal demonstrates that it arises from an iron that is part of a diamagnetic cluster, and thus is not attributable to free Fe(II). The large isomer shift and quadrupole splitting, however, are indicative of an unusual coordination environment that is not the typical FeS_4 environment found in $[4\text{Fe-4S}]$ clusters. Two other quadrupole doublets ($\delta_1 = 0.431$, $\Delta E_{Q1} = 1.2$, $\delta_2 = 0.428$, $\Delta E_{Q2} = 0.709$) arise from the $[4\text{Fe-4S}]^{2+}$ cluster of PFL-AE in whole cells. The first quadrupole doublet has parameters ($\delta_1 = 0.431$, $\Delta E_{Q1} = 1.2$) consistent with its assignment to a delocalized $\text{Fe}^{2.5+}\text{-Fe}^{2.5+}$ pair in a $[4\text{Fe-4S}]^{2+}$ cluster. The second quadrupole doublet ($\delta_2 = 0.428$, $\Delta E_{Q2} = 0.709$) we assign to the Fe^{3+} of the valence-localized pair. The relative signal intensity of the three quadrupole doublets (2:1:1 for δ_1 : δ_2 : δ_3) supports their assignment as the delocalized pair and the two localized sites, respectively, and also suggests that 100% of the $[4\text{Fe-4S}]^{2+}$ clusters are in this valence-localized state.

The Mössbauer spectral features of the $[4\text{Fe-4S}]^{2+}$ cluster of PFL-AE in whole cells are distinct from those previously reported for the purified protein. The $[4\text{Fe-4S}]^{2+}$ cluster of the purified protein exhibits a typical $[4\text{Fe-4S}]^{2+}$ Mössbauer spectrum, with site 1 ($\delta = 0.45$, $\Delta E_{Q1} = 1.15$) and site 2 ($\delta = 0.45$, $\Delta E_{Q1} = 1.00$) giving rise to equal-intensity quadrupole doublets, each assigned to a

valence-delocalized $\text{Fe}^{2.5+}/\text{Fe}^{2.5+}$ pair.⁵ Addition of S-adenosylmethionine (AdoMet) to the purified protein results in the appearance of a shoulder to the high-field side of these quadrupole doublets. Detailed characterization of the AdoMet-bound form of purified PFL-AE required a dual iron-isotope method, in which the unique site of the $[\text{4Fe-4S}]^{2+}$ cluster of PFL-AE was labeled with ^{57}Fe , and changes to this site alone were monitored upon addition of AdoMet. In the absence of AdoMet, this unique site gave rise to a Mössbauer spectrum typical for a $[\text{4Fe-4S}]^{2+}$ cluster, with ($\delta = 0.42$, $\Delta E_{\text{Q1}} = 1.12$).¹⁶ Upon addition of AdoMet, a dramatic increase in the isomer shift ($\delta = 0.72$, $\Delta E_{\text{Q1}} = 1.15$) of this unique site signaled an increase in coordination number and/or binding of more ionic ligands, suggesting that the substrate AdoMet coordinated the unique Fe site;¹⁶ subsequent ENDOR studies provided further support for direct coordination of AdoMet to the unique Fe site.^{3, 17}

The large isomer shift of site 3 of the $[\text{4Fe-4S}]^{2+}$ cluster in PFL-AE in whole cells is indicative of not only valence-localization at that site, but also of an unusual coordination that is atypical for Fe in an iron-sulfur cluster; the requirement for unusual coordination implicates the unique site of the $[\text{4Fe-4S}]^{2+}$ cluster, which has the demonstrated ability to exchange ligands, as the valence-localized Fe(II) site. The large isomer shift, however, does not appear to be a result of AdoMet binding, since AdoMet bound to the purified protein gives rise to an isomer shift of 0.72, not 0.97, at the unique site.

II.3.4. Valence-Localized $[\text{4Fe-4S}]^{2+}$ cluster in purified PFL-AE.

In an effort to explore the factors associated with valence-localization in the $[4\text{Fe-4S}]^{2+}$ cluster, Mössbauer spectra were obtained for purified PFL-AE in the presence of a series of small molecules, including potential AdoMet degradation products (methylthioadenosine, 5'-deoxyadenosine, methionine, adenine, and ribose), substrates and products of PFL (pyruvate, formate, CoA, and acetyl-CoA), and abundant cellular metabolites (ATP, ADP, and AMP). The valence-localized state was produced by addition of methylthioadenosine, 5'-deoxyadenosine, AMP, or ADP to PFL-AE, as evidenced by the appearance of a prominent peak in the Mössbauer spectra at approximately 2 mm/s. Representative data for the PFL-AE/5'-dAdo sample is shown in Figure II.3.4.1, lower panel, with the Mössbauer spectrum of purified PFL-AE alone shown in the upper panel for comparison. In the presence of 6.4 mM 5'-dAdo, 80% of the PFL-AE $[4\text{Fe-4S}]^{2+}$ cluster is in the "bound" state, with a Mössbauer spectrum consisting of three distinct quadrupole doublets ($\delta_1 = 0.443$, $\Delta E_{Q1} = 1.203$; $\delta_2 = 0.997$, $\Delta E_{Q2} = 2.067$; $\delta_3 = 0.385$, $\Delta E_{Q3} = 0.518$) in a 2:1:1 ratio of relative intensities. Sites 1, 2, and 3 are assigned to a valence-delocalized $\text{Fe}^{2.5+}/\text{Fe}^{2.5+}$ pair, a valence-localized Fe^{2+} (the unique iron site), and a valence-localized Fe^{3+} site, respectively. The 20% of the PFL-AE $[4\text{Fe-4S}]^{2+}$ cluster in the unbound state has parameters identical to that observed for the as-purified PFL-AE ($\delta_1 = 0.443$, $\Delta E_{Q1} = 1.203$; $\delta_2 = 0.437$, $\Delta E_{Q2} = 0.978$). Similar results are observed upon addition of methylthioadenosine, AMP, and ADP to purified PFL-AE, (Figure II.3.4.2) with a fraction of the $[4\text{Fe-4S}]^{2+}$ exhibiting the bound state Mössbauer spectrum with a valence-localized site, and the remainder of the

cluster being in the unbound state; the fraction of cluster in the bound state varied with the identity of the small molecule and in no cases was 100%. The remaining molecules examined for the ability to produce the valence localized state had no significant impact on the Mössbauer spectrum of PFL-AE (Figure II.3.4.3); it is concluded that these molecules either do not bind PFL-AE, or do not bind in such a way as to produce a valence-localized site.

Samples prepared in parallel to those just described and then photoreduced to the $[4\text{Fe-4S}]^+$ state were examined by EPR spectroscopy (Figure II.3.4.4). The molecules that induce valence localization of the $[4\text{Fe-4S}]^{2+}$ of PFL-AE also induce a slight perturbation of the EPR spectrum of the $[4\text{Fe-4S}]^+$ cluster of PFL-AE, from the normal PFL-AE/ $[4\text{Fe-4S}]^+$ g values of ($g_{\parallel} = 2.02$, $g_{\perp} = 1.93$) to new g values of the complexes (ADP($g_{\parallel} = 2.01$, $g_{\perp} = 1.92$); AMP($g_{\parallel} = 2.01$, $g_{\perp} = 1.91$); MTAdo($g_{\parallel} = 2.01$, $g_{\perp} = 1.91$); 5dAdo($g_{\parallel} = 2.01$, $g_{\perp} = 1.91$), cAMP($g_{\parallel} = 2.01$, $g_{\perp} = 1.92$), 2dAdo($g_{\parallel} = 2.01$, $g_{\perp} = 1.92$), Ado($g_{\parallel} = 2.01$, $g_{\perp} = 1.90$). These results suggest that these molecules bind to and perturb the electronic structure of the cluster. In contrast, the molecules that do not induce valence localization as observed by Mössbauer also do not significantly perturb the EPR spectrum of PFL-AE/ $[4\text{Fe-4S}]^+$ (Figure II.3.4.4). Subsequent addition of SAM to the PFL-AE/small molecule samples resulted in appearance of the normal PFL-AE/ $[4\text{Fe-4S}]^+$ /AdoMet EPR spectrum (Figure II.3.4.5), demonstrating that AdoMet is capable of displacing any of these small molecules that do bind to PFL-AE.

Together, these results demonstrate that the valence-localized state observed for PFL-AE in whole cells can be reproduced in the purified protein by

addition of certain adenosyl-containing molecules, including ADP, AMP, 5'-deoxyadenosine, and methylthioadenosine. The appearance of a valence-localized site with a large isomer shift of approximately 0.97 mm/s can best be explained by a change in coordination of the unique site of the $[4\text{Fe-4S}]^{2+}$ of PFL-AE upon addition of these molecules. It is curious that none of these molecules contains the carboxylate and amino groups found to coordinate the unique site in the AdoMet complexes of several radical-SAM enzymes. Whether the adenosyl moieties coordinate the unique site, or whether their binding in a proximal pocket somehow changes the coordination of the unique site, remains to be determined. Regardless of the mechanism by which the valence-localization occurs, it seems likely that an abundant intracellular molecule containing an adenosyl moiety is responsible for the valence-localization observed in PFL-AE in whole cells. Of the molecules that cause valence localization in the purified protein, only AMP would be considered to be abundant in *E. coli* cells (estimated to be over 1 mM),¹⁸⁻²⁰ and thus we consider AMP the most likely candidate for binding to PFL-AE in whole cells and generating the valence-localized state.

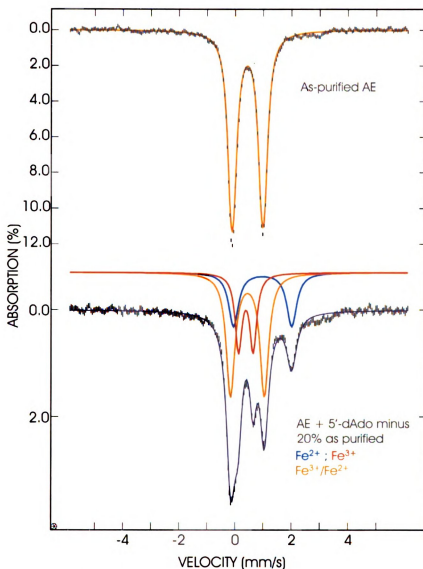


Figure II.3.4.1. Representative Mössbauer data for the purified PFL-AE in the absence (upper panel) and presence (lower panel) of 5'-dAdo. The colored lines are the theoretical simulations of component spectra that sum to a theoretical spectrum (black solid lines overlaying experimental data) in good agreement with the experimental data (black hatched lines). Upper Panel: Purified PFL-AE contains $[4\text{Fe-4S}]^{2+}$ clusters accounting for 97 % of total iron. The quadrupole doublets are: 48.4 % ($\text{Fe}^{2+}/\text{Fe}^{3+}$ pair): $\delta=0.443$; $\Delta E_Q = 1.203$; 48.4 % ($\text{Fe}^{2+}/\text{Fe}^{3+}$ pair): $\delta= 0.437$; $\Delta E_Q = 0.978$). Lower Panel: In the presence of 5'-dAdo, the 5'-dAdo-bound $[4\text{Fe-4S}]^{2+}$ clusters account for 79% of total iron. The data shown is after subtracting 20 % of the as-purified spectrum so that a spectrum of the bound-species remains. The quadrupole doublets are: 39.5 % ($\text{Fe}^{2+}/\text{Fe}^{3+}$ pair): ($\delta= 0.443$; $\Delta E_Q = 1.203$) (orange solid lines); 19.5 % (Fe^{2+} "unique iron"): ($\delta= 0.977$; $\Delta E_Q = 2.067$) (red solid lines); 19.5 % (Fe^{3+}): ($\delta= 0.385$; $\Delta E_Q = 0.518$) (blue solid lines).

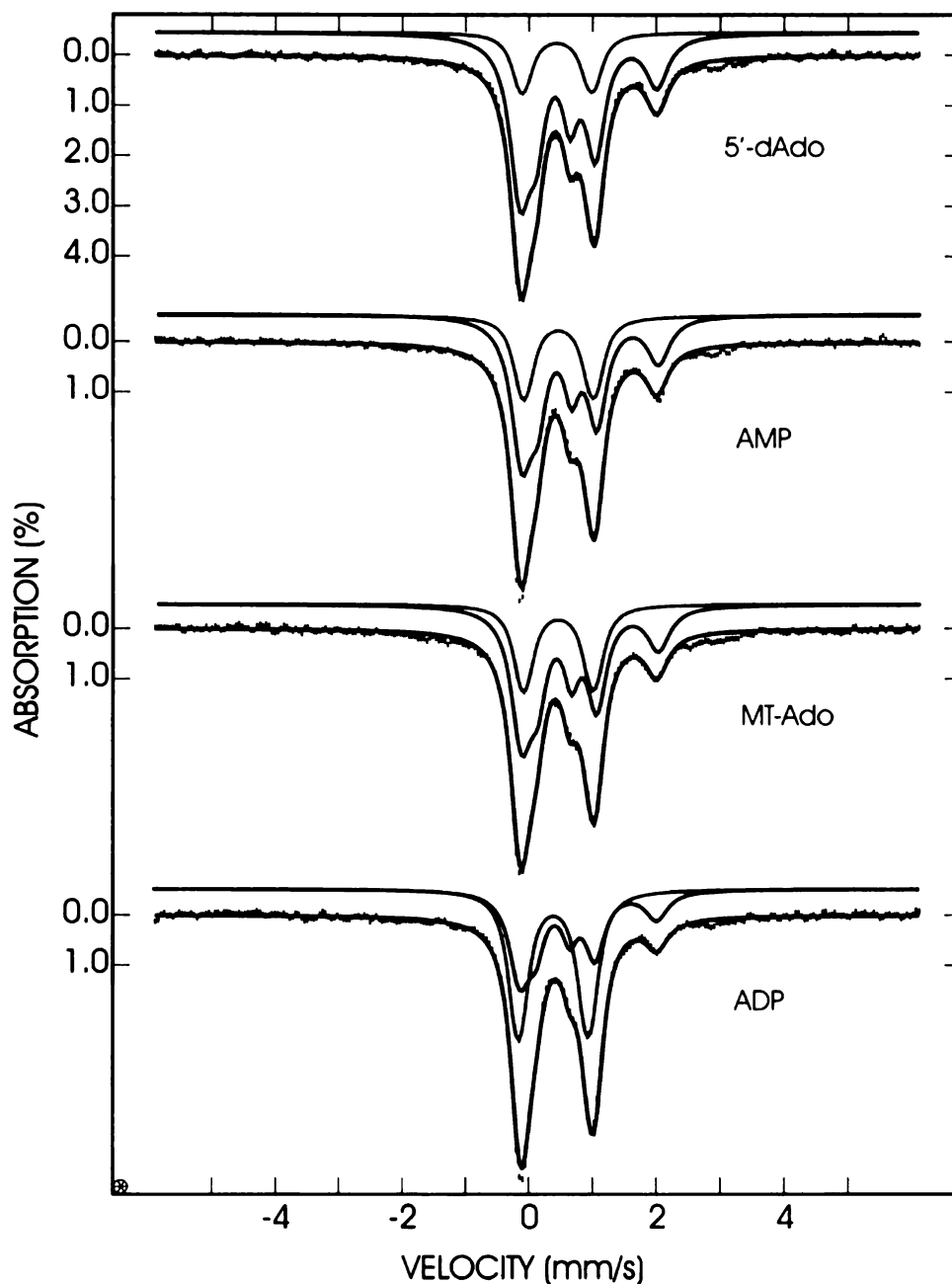


Figure II.3.4.2. Representative Mössbauer data for samples in which the added small molecule induces a valence-localized $[4\text{Fe-4S}]^{2+}$ cluster. The colored lines are the theoretical simulations of component spectra that sum to a theoretical spectrum (black solid lines overlaying experimental data) in good agreement with the experimental data (black hatched lines). The composite is broken down into two components. The orange and blue lines show the unbound and bound clusters respectively, normalized to their percentage in the sample. 5dAdo (20 % unbound, 79 % bound); AMP (28 % unbound, 72 % bound); MTAdo (29 % unbound, 69 % bound); ADP (47 % unbound, 53 % bound).

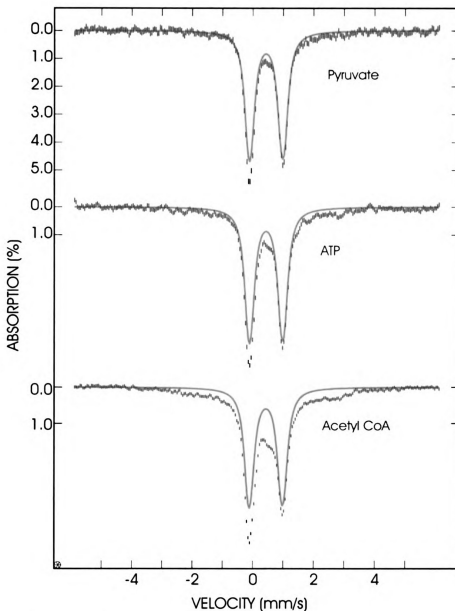


Figure II.3.4.3. Representative Mössbauer data for samples in which the added small molecule does not induce valence-localization of the $[4\text{Fe-4S}]^{2+}$ cluster. The colored lines are the theoretical simulations of the $[4\text{Fe-4S}]^{2+}$ cluster comprising the majority of iron-containing species in the sample. The black hatched lines are the actual experimental data. Pyruvate (90 % $[4\text{Fe-4S}]^{2+}$); ATP (80 % $[4\text{Fe-4S}]^{2+}$); Acetyl CoA (66 % $[4\text{Fe-4S}]^{2+}$).

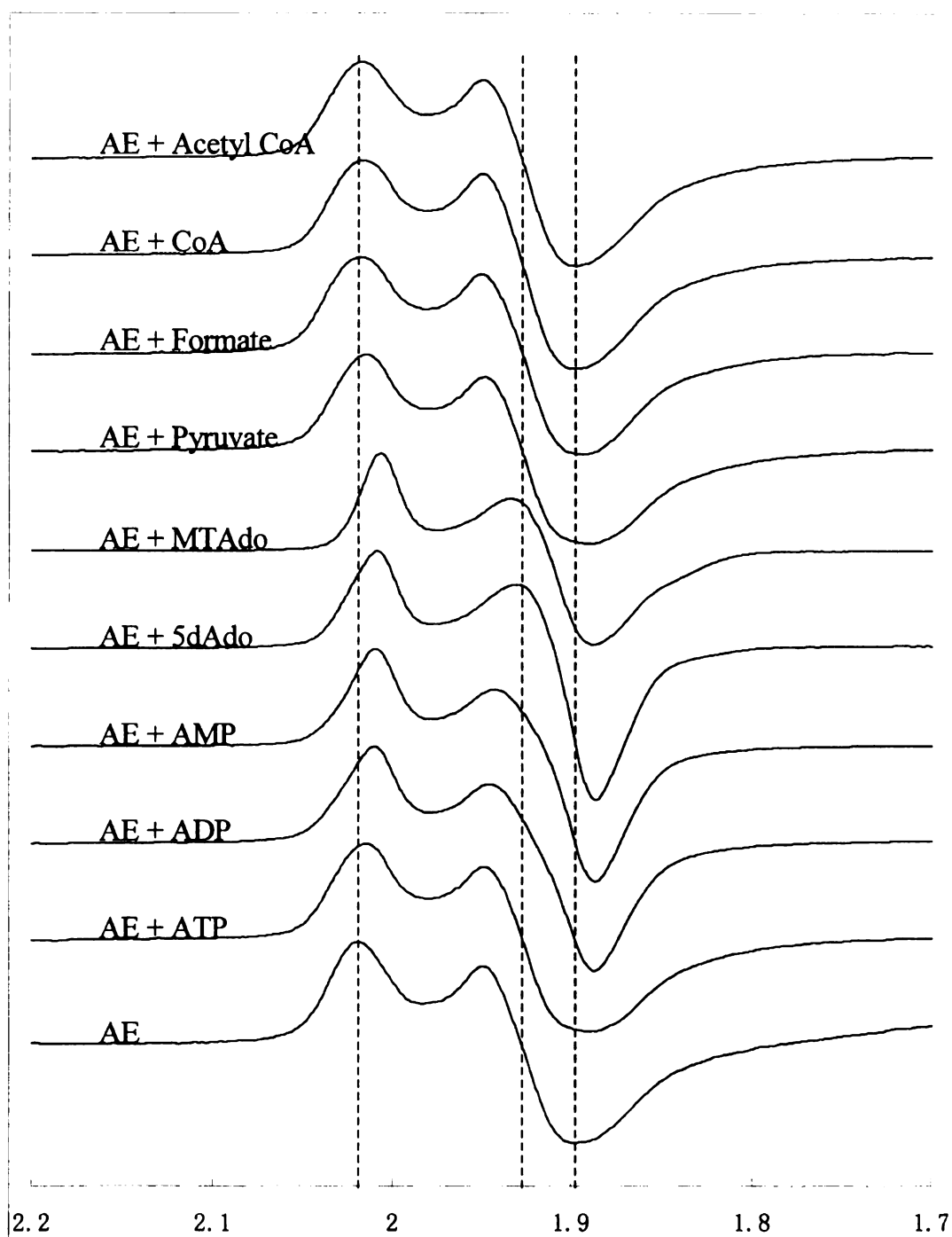


Figure II.3.4.4. Effects of different small molecules on the X-band EPR spectra of the photoreduced $[4\text{Fe-4S}]^{1+}$ cluster of PFL-AE. Purified PFL-AE (100 μM) in buffer containing 100 μM 5-deazariboflavin, 1 mM DTT, 100 mM Tris-Cl (pH=7.6), 100 mM KCl, and 20 mM oxamate was illuminated for 1 h at 0°C to reduce the $[4\text{Fe-4S}]$ cluster to the 1+ state. Each of the small molecules was added to 2 mM final concentration. The EPR samples were then frozen in liquid nitrogen. Conditions of measurement, $T = 12 \text{ K}$; microwave power, 2 mW; modulation amplitude, 10 G. The dashed vertical lines indicate the most representative features at g values 2.02, 1.93, and 1.89, respectively.

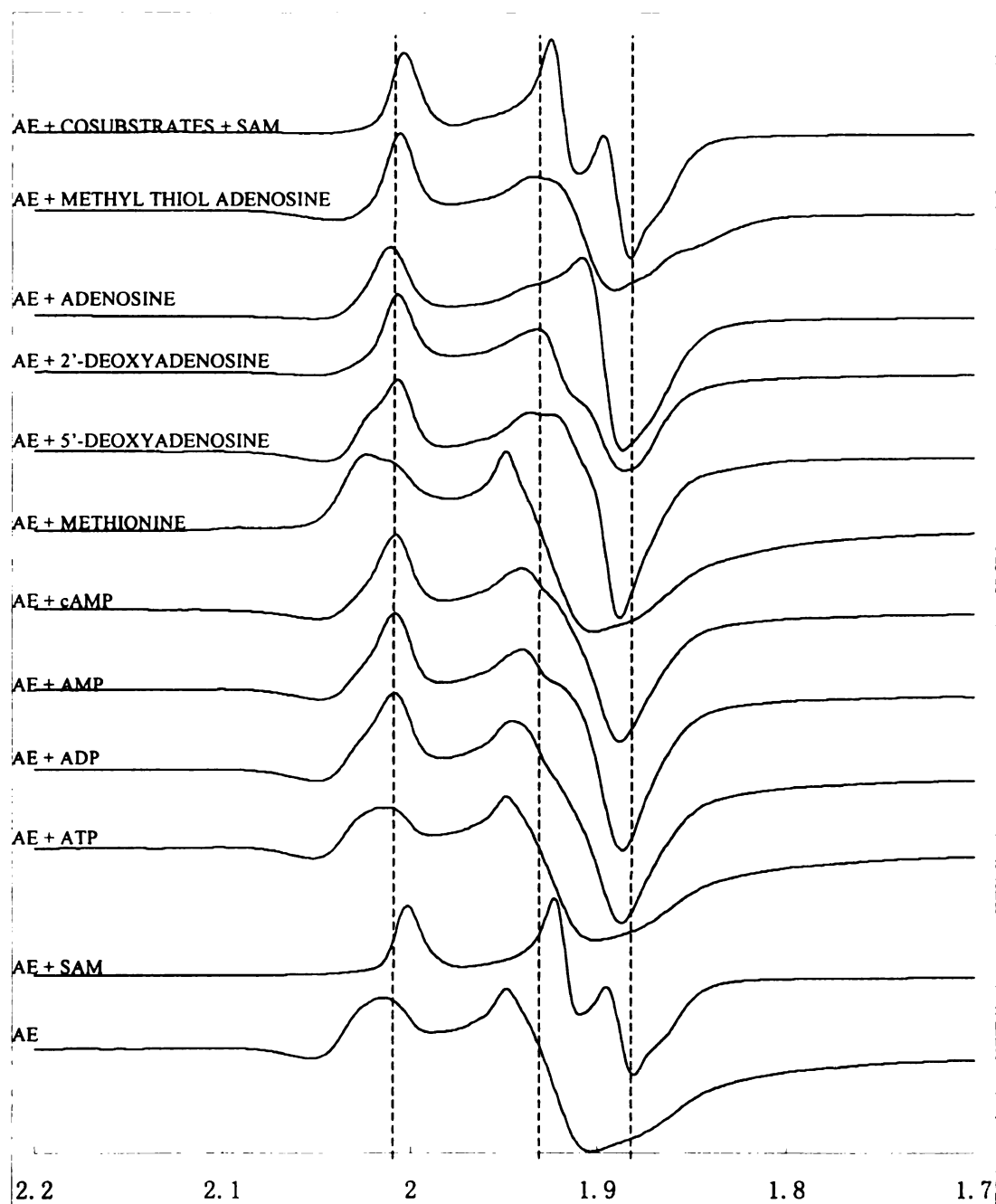


Figure II.3.4.5. Effects of different small molecules on the X-band EPR spectra of the photoreduced $[4\text{Fe-4S}]^{1+}$ cluster of PFL-AE. Shown are spectra of the enzyme in the presence of metabolites (ATP, ADP, AMP, cAMP, Methionine, 5dAdo, 2dAdo, Ado, and MTAdo). Purified PFL-AE (100 μM) in buffer containing 100 μM 5-deazariboflavin, 1 mM DTT, 100 mM Tris-Cl (pH=7.6), 100 mM KCl, and 20 mM oxamate was illuminated for 1 h at 0°C to reduce the $[4\text{Fe-4S}]$ cluster to the 1+ state. Each of the small molecules was added to 2 mM final concentration. The EPR samples were then frozen in liquid nitrogen. After measuring the EPR spectra, the samples were thawed and SAM was added to 2 mM final concentration followed by flash-freezing the samples again. The dashed vertical lines indicate the most representative features at g values 2.01, 1.93, and 1.88, respectively.

II.3.5. Stability of the $[4\text{Fe-4S}]^{2+}$ Cluster and the Valence-Localized Site in Whole Cells.

Addition of SAM to PFL-AE in whole cells or in crude lysate has no affect on the Mössbauer spectrum (Figure II.3.5.1.), suggesting that, unlike the case with the purified protein, AdoMet does not readily displace the molecule binding to PFL-AE and causing the valence localization. Addition of AdoMet in conjunction with the other PFL-AE substrate PFL or the PFL homolog YfiD also had no affect on the Mössbauer spectrum (data not shown). These results suggest that the valence-localized state of the PFL-AE $[4\text{Fe-4S}]^{2+}$ cluster is stabilized in whole cells with respect to interaction with its substrates. This cluster also appears to be stabilized with respect to oxidative cluster degradation, as prolonged 30 min exposure to air resulted in no change in the cluster composition. By comparison, the purified PFL-AE $[4\text{Fe-4S}]^{2+}$ cluster is rapidly degraded to the $[3\text{Fe-4S}]^+$ form upon exposure to air. However, there is another simpler explanation for this phenomenon that the difference is caused by the reducing conditions in the cell extract and may not be a function of molecules binding to PFL-AE. Currently, we are further exploring this interesting phenomenon.

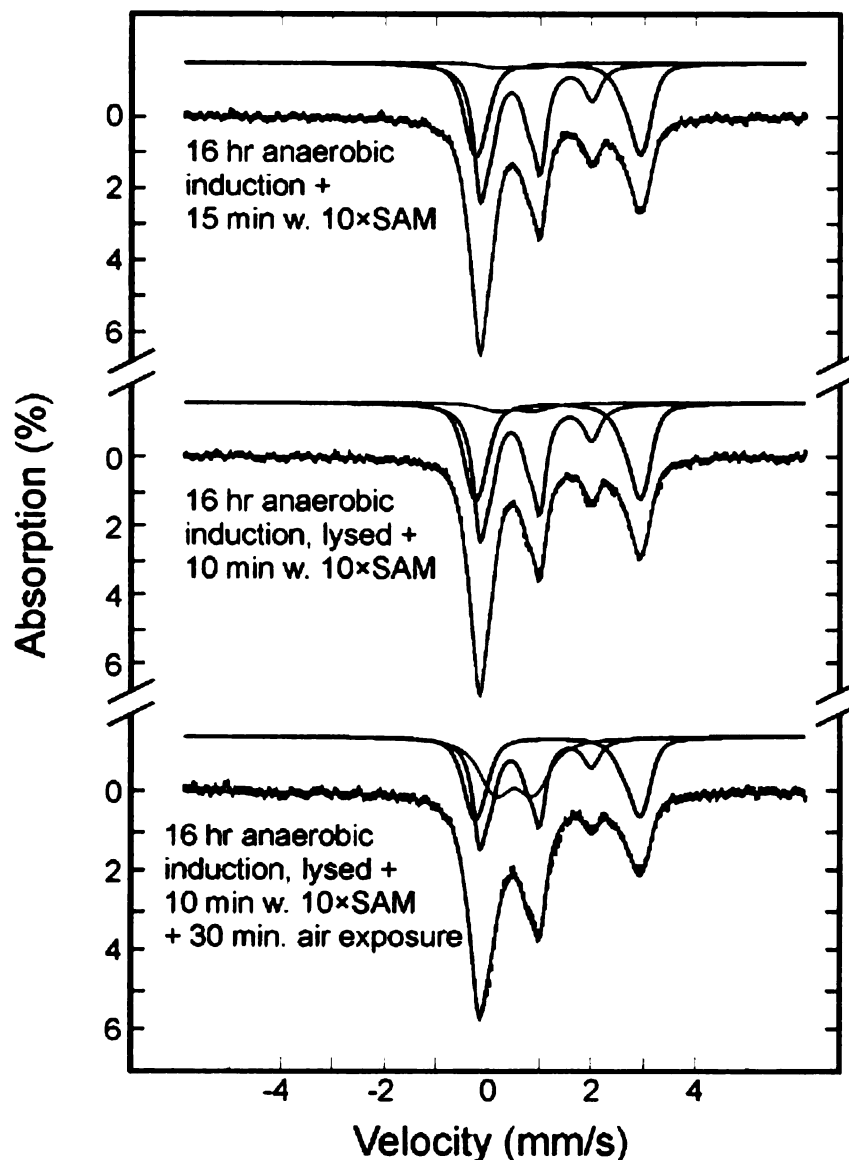


Figure II.3.5.1. Mössbauer spectra of whole cell PFL-AE in the presence of SAM. The colored lines are the theoretical simulations of component spectra that sum to a theoretical spectrum (black solid lines overlaying experimental data) in good agreement with the experimental data (black hatched lines). Component spectral simulations are color-coded as non-cluster Fe(II) (green), non-cluster Fe(III) (orange), $[2\text{Fe-2S}]^{2+}$ (red), and $[4\text{Fe-4S}]^{2+}$ (blue). The PFL-AE-expressing cells show, in addition to the ferrous and ferric signals, strong signals attributed to $[4\text{Fe-4S}]^{2+}$ clusters. Compared to the Mössbauer spectrum of whole cell PFL-AE, addition of SAM has no affect on the valence-localized $[4\text{Fe-4S}]^{2+}$ cluster (top and middle spectra). Prolonged 30 min exposure to air, in the presence of SAM, resulted in no change in the cluster composition.

II.4. Conclusions

The results presented herein provide evidence for $[2\text{Fe-2S}]^{2+} \longleftrightarrow [4\text{Fe-4S}]^{2+}$ cluster interconversions occurring in PFL-AE in growing *E. coli* cells. Similar *in vivo* cluster interconversions were observed for FNR overexpressed in *E. coli*;⁹ in the case of FNR, the $[2\text{Fe-2S}]^{2+} \longleftrightarrow [4\text{Fe-4S}]^{2+}$ cluster interconversion is physiologically relevant, with the conversion of $[2\text{Fe-2S}]$ to $[4\text{Fe-4S}]$ cluster being accompanied by protein dimerization and onset of DNA-binding properties, all triggered by the conversion from aerobic to anaerobic conditions.⁹ Such cluster interconversions may be physiologically relevant for PFL-AE since more of the catalytically relevant $[4\text{Fe-4S}]$ state is produced under anaerobic culture conditions, conditions under which PFL-AE is expected to be catalytically active.^{3.}

4, 21

Our results also provide unequivocal evidence for the presence of an unusual, valence-localized $[4\text{Fe-4S}]^{2+}$ cluster in PFL-AE in whole cells. The cluster present in PFL-AE in whole cells is distinctly different from that in the purified protein, with the latter showing a typical $[4\text{Fe-4S}]^{2+}$ Mössbauer spectrum resulting from two delocalized $\text{Fe}^{2+}/\text{Fe}^{3+}$ pairs, while the former gives rise to a Mössbauer spectrum indicative of a valence-localized site in a $[4\text{Fe-4S}]^{2+}$ cluster. The $[4\text{Fe-4S}]^{2+}$ cluster of PFL-AE therefore has unusual properties *in vivo* that are lost upon protein purification, perhaps due to the loss of a small molecule ligand. The reason for the valence localization in whole cells has not been unequivocally determined, however studies presented herein on the purified protein demonstrate that valence localization can be induced by addition of

certain small molecules containing adenosyl moieties. Whether one of these small molecules tested might be responsible for the *in vivo* properties of the [4Fe-4S] cluster of PFL-AE has yet to be determined. The level of overexpression of PFL-AE in the *E. coli* cells used in these experiments is estimated to be ~ 0.5 mM, therefore a small molecule binding to PFL-AE and causing valence localization would have to be quite abundant, as 100% of the [4Fe-4S]²⁺ clusters in PFL-AE in whole cells are in the valence localized state. Of the molecules causing valence localization in the purified protein, only AMP is expected to be of sufficient abundance in the cell to bind all of the PFL-AE (estimated to be over 1 mM),¹⁸⁻²⁰ and thus our current working hypothesis is that AMP binding to PFL-AE is responsible for the unusual cluster properties *in vivo*.

The results presented herein provide only the second example of valence-localization in a protein-bound [4Fe-4S]²⁺ cluster. The first such example was for ferredoxin thioredoxin reductase (FTR), in which the valence-localized site is an iron coordinated by a cysteine thiolate and within van der Waals contact of a cysteine disulfide.

The [4Fe-4S]²⁺ cluster *in vivo* shows no evidence of SAM binding upon addition or AdoMet to lysed cells. The cluster in crude extracts in the presence of SAM also does not degrade upon exposure to oxygen for 30 min. Both of these observations point to protection of the cluster of PFL-AE *in vivo*. Such protection may be related to valence localization and may play a role in preventing reductive cleavage of AdoMet, and subsequent generation of adenosyl radicals, unless conditions favor activation of PFL.

II.5. References

1. Broderick, J. B.; Duderstadt, R. E.; Fernandez, D. C.; Wojtuszewski, K.; Henshaw, T. F.; Johnson, M. K., Pyruvate formate-lyase activating enzyme is an iron-sulfur protein. *Journal of the American Chemical Society* **1997**, 119, (31), 7396-7397.
2. Broderick, J. B.; Henshaw, T. F.; Cheek, J.; Wojtuszewski, K.; Smith, S. R.; Trojan, M. R.; McGhan, R. M.; Kopf, A.; Kibbey, M.; Broderick, W. E., Pyruvate formate-lyase-activating enzyme: Strictly anaerobic isolation yields active enzyme containing a [3Fe-4S]⁺ cluster. *Biochemical and Biophysical Research Communications* **2000**, 269, (2), 451-456.
3. Walsby, C. J.; Hong, W.; Broderick, W. E.; Cheek, J.; Ortillo, D.; Broderick, J. B.; Hoffman, B. M., Electron-Nuclear Double Resonance Spectroscopic Evidence That S-Adenosylmethionine Binds in Contact with the Catalytically Active [4Fe-4S]⁺ Cluster of Pyruvate Formate-Lyase Activating Enzyme. *Journal of the American Chemical Society* **2002**, 124, (12), 3143-3151.
4. Walsby, C. J.; Ortillo, D.; Yang, J.; Nnyepi, M. R.; Broderick, W. E.; Hoffman, B. M.; Broderick, J. B., Spectroscopic Approaches to Elucidating Novel Iron-Sulfur Chemistry in the "Radical-SAM" Protein Superfamily. *Inorganic Chemistry* **2005**, 44, (4), 727-741.
5. Krebs, C.; Henshaw, T. F.; Cheek, J.; Huynh, B. H.; Broderick, J. B., Conversion of 3Fe-4S to 4Fe-4S Clusters in Native Pyruvate Formate-Lyase Activating Enzyme: Moessbauer Characterization and Implications for Mechanism. *Journal of the American Chemical Society* **2000**, 122, (50), 12497-12506.
6. Bender, C. J.; Rosenzweig, A. C.; Lippard, S. J.; Peisach, J., Nuclear hyperfine coupling of nitrogen in the coordination sphere of the diiron center of methane monooxygenase hydroxylase. *J Biol Chem* **1994**, 269, (23), 15993-8.
7. Que, L., *Physical Methods in Bioinorganic Chemistry* University Science Books: Sausalito, CA, 2000.
8. Solomon, P. S.; Shaw, A. L.; Lane, I.; Hanson, G. R.; Palmer, T.; McEwan, A. G., Characterization of a molybdenum cofactor biosynthetic gene cluster in *Rhodobacter capsulatus* which is specific for the biogenesis of dimethylsulfoxide reductase. *Microbiology (Reading, United Kingdom)* **1999**, 145, (6), 1421-1429.
9. Popescu, C. V.; Bates, D. M.; Beinert, H.; Munck, E.; Kiley, P. J., Moessbauer spectroscopy as a tool for the study of activation/inactivation of the transcription regulator FNR in whole cells of *Escherichia coli*. *Proceedings of the*

National Academy of Sciences of the United States of America **1998**, 95, (23), 13431-13435.

10. Mulliez, E.; Ollagnier-De Choudens, S.; Meier, C.; Cremonini, M.; Luchinat, C.; Trautwein, A. X.; Fontecave, M., Iron-sulfur interconversions in the anaerobic ribonucleotide reductase from *Escherichia coli*. *JBIC, Journal of Biological Inorganic Chemistry* **1999**, 4, (5), 614-620.

11. Benda, R.; Bui, B. T. S.; Schuenemann, V.; Florentin, D.; Marquet, A.; Trautwein, A. X., Iron-Sulfur Clusters of Biotin Synthase In Vivo: A Moessbauer Study. *Biochemistry* **2002**, 41, (50), 15000-15006.

12. Cosper, M. M.; Jameson, G. N. L.; Eidsness, M. K.; Huynh, B. H.; Johnson, M. K., Recombinant *Escherichia coli* biotin synthase is a $[2\text{Fe}-2\text{S}]_2^+$ protein in whole cells. *FEBS Letters* **2002**, 529, (2-3), 332-336.

13. Walters, E. M.; Garcia-Serres, R.; Jameson, G. N. L.; Glauser, D. A.; Bourquin, F.; Manieri, W.; Schuermann, P.; Johnson, M. K.; Huynh, B. H., Spectroscopic Characterization of Site-Specific $[\text{Fe}_4\text{S}_4]$ Cluster Chemistry in Ferredoxin:Thioredoxin Reductase: Implications for the Catalytic Mechanism. *Journal of the American Chemical Society* **2005**, 127, (26), 9612-9624.

14. Gutlich, P.; Link, R.; Trautwein, A., *Mossbauer Spectroscopy and Transition Metal Chemistry*. Springer - Verlag: Berlin, 1979.

15. Park, J.; Tai, J.; Roessner, C. A.; Scott, A. I., Enzymatic synthesis of S-adenosyl-L-methionine on the preparative scale. *Bioorg Med Chem* **1996**, 4, (12), 2179-85.

16. Krebs, C.; Broderick, W. E.; Henshaw, T. F.; Broderick, J. B.; Huynh, B. H., Coordination of Adenosylmethionine to a Unique Iron Site of the $[\text{4Fe-4S}]$ of Pyruvate Formate-Lyase Activating Enzyme: A Moessbauer Spectroscopic Study. *Journal of the American Chemical Society* **2002**, 124, (6), 912-913.

17. Walsby, C. J.; Ortillo, D.; Broderick, W. E.; Broderick, J. B.; Hoffman, B. M., An Anchoring Role for FeS Clusters: Chelation of the Amino Acid Moiety of S-Adenosylmethionine to the Unique Iron Site of the $[\text{4Fe-4S}]$ Cluster of Pyruvate Formate-Lyase Activating Enzyme. *Journal of the American Chemical Society* **2002**, 124, (38), 11270-11271.

18. Makarchikov, A. F.; Brans, A.; Bettendorff, L., Thiamine diphosphate adenylyl transferase from *E. coli*: functional characterization of the enzyme synthesizing adenosine thiamine triphosphate. *BMC Biochem* **2007**, 8, 17.

19. Chapman, A. G.; Fall, L.; Atkinson, D. E., Adenylate energy charge in *Escherichia coli* during growth and starvation. *J Bacteriol* **1971**, 108, (3), 1072-86.

20. Schneider, D. A.; Gourse, R. L., Relationship between growth rate and ATP concentration in *Escherichia coli*: a bioassay for available cellular ATP. *J Biol Chem* **2004**, 279, (9), 8262-8.
21. Broderick, J. B., Iron-sulfur clusters in enzyme catalysis. *Comprehensive Coordination Chemistry II* **2004**, 8, 739-757.

CHAPTER III

SPECIFIC ACTIVATION OF PYRUVATE FORMATE-LYASE ACTIVATING ENZYME BY POTASSIUM ION

III.1 Introduction

Pyruvate formate lyase-activating enzyme (PFL-AE) is a representative member of the radical SAM superfamily. The function of PFL-AE is to generate a catalytically essential glycy radical on G734 of PFL.¹⁻⁴ The mechanism of PFL activation by PFL-AE is proposed to involve coordination of AdoMet to the $[4\text{Fe-4S}]^{2+}$ cluster of PFL-AE via a classic five-member chelate ring formed by the unique iron of the cluster and the methionine moiety of AdoMet.⁵ Such interaction brings the sulfonium of AdoMet in orbital overlap with the $[4\text{Fe-4S}]^{2+}$ cluster.⁶ Then one-electron transfer from a reducing agent (reduced flavodoxin *in vivo*) reduces the $[4\text{Fe-4S}]^{2+}$ cluster to produce the $[4\text{Fe-4S}]^{1+}$ -AdoMet complex. Inner-sphere electron transfer from the $[4\text{Fe-4S}]^{1+}$ cluster to the sulfonium of AdoMet initiates homolytic S-C bond cleavage. Methionine, one of the two cleavage products of AdoMet, is left bound to the unique site of the oxidized $[4\text{Fe-4S}]^{2+}$ cluster, while the 5'-deoxyadenosyl radical intermediate, the other AdoMet cleavage product, activates PFL by abstracting the pro-S H from its residue

G734. The catalytic cycle is then repeated upon displacement of methionine and 5'-deoxyadenosine with a new AdoMet molecule. The activated PFL can then catalyze the conversion of pyruvate and CoA to acetyl CoA and formate by a mechanism that is still under debate ⁷⁻¹⁰.

Clearly, the iron-sulfur cluster of PFL-AE plays a very important role in PFL activation. Over the past few years, we have characterized the interaction of the $[4\text{Fe-4S}]^{2+/1+}$ cluster of PFL-AE with the cosubstrate AdoMet.^{5, 6, 11, 12} In this chapter, we focus on the role of monovalent ions in activating PFL-AE, and the corresponding effects of these monovalent ions on the EPR spectroscopic properties of the $[4\text{Fe-4S}]^{1+}$ cluster.

III.2 Materials and Methods

PFL-AE was purified according to the published procedures¹³ except that 1 mM DTT was included in all buffers. All buffers were deoxygenated using a vacuum/nitrogen gas manifold before being taken into the glove box. Solid chemicals were pumped in as solids. Ice was pre-chilled with liquid nitrogen before pumping into the glove box. Preparation of samples (EPR samples and PFL/PFL-AE activity assays) were carried out in a Mbraun box with oxygen level less than 2 ppm.

III.2.1 Preparation of EPR Samples.

All EPR samples were made according to the same procedure. Detailed components and their concentrations in each reaction mixture are provided in the Results section.

PFL-AE was mixed in a buffer to a final concentration of 200 μ M and a final volume of 600 μ L. The buffer was a combination of following components: Tris buffer (50 mM Tris pH 8.5 or 100 mM Tris pH 7.6), glassing agent (20 % (w/v) glycerol or 400 mM sucrose), pyruvate or oxamate (20 mM), and 200 mM salt (NaCl, KCl or NH_4Cl). To these mixtures were added 5-deazariboflavin (200 μ M final concentration from a 10mM stock solution in DMSO) in the dark. After the reaction mixtures were transferred into EPR tubes, they were capped and inserted in a beaker tightly packed with ice and water. Then all tubes were illuminated on ice for 1 hr using a 300 W halogen lamp situated 2 cm from the

samples. After illumination, 300 μ L of the PFL-AE mixture from the EPR tube was mixed with AdoMet to a final concentration of 2 mM while the remaining 300 μ L of the PFL-AE mixture was kept as control. Both +AdoMet and –AdoMet samples were then flash-frozen in liquid nitrogen for EPR analysis.

III.2.2. PFL and PFL-AE Activity Assays in the presence of different cations.

The PFL-AE activity was measured using modifications of previously published procedures.^{2, 14, 15} Anaerobic PFL-AE reaction mixes all contained in a final volume of 200 μ L: 0.1 M Tris-HCl pH 7.6, 0.1 M KCl (or NaCl or NH₄Cl), 10 mM oxamate, 8 mM DTT, ~0.06 μ M PFL-AE, ~6 μ M PFL, 0.2 mM AdoMet, and 50 μ M 5-deazariboflavin. For each PFL-AE activity assay, 5-deazariboflavin was added last, in the dark, and the reaction was initiated by illumination of the sample in an ice water bath with a 300 W halogen bulb. At time intervals after initiation of the reaction, typically 5 to 30 min, an aliquot (5 μ L) was removed for assay of active PFL through the coupling assay.

The coupling assay mix contained 0.1 M Tris-Cl pH 8.1, 3 mM NAD, 55 mM CoA, 0.1 mg BSA, 10 mM pyruvate, 10 mM malate, 20 units citrate synthase, 300 units malic dehydrogenase, and 10 mM DTT in a final volume of 20 mL. To assay PFL activity, 895 μ L of the coupling assay mix and 5 μ L of the PFL-AE activity mix were combined in a quartz cuvette, which was then sealed with a septum and brought out of the chamber to monitor the production of NADH by the increase in absorbance at 340 nm.

III.2.3. Photoreduction rate of PFL-AE in the presence of monovalent cations.

PFL-AE was mixed in a buffer containing 8 mM DTT, 10 mM oxamate, 100 mM Tris-HCl pH 7.6, and 100 mM salt (NaCl, NH₄Cl or KCl) to a final concentration of 100 μ M and a final volume of 1200 μ L. Photoreducing agent 5-deazariboflavin was added last in the dark to a final concentration of 100 μ M. Aliquots (300 μ L each) of the reaction mixtures were transferred into EPR tubes, and then capped and inserted in a beaker tightly packed with ice and water. All tubes were illuminated on ice using a 300 W halogen lamp situated 2 cm from the beaker. At specific time points, 5 to 30 min, EPR tubes were flash-frozen in liquid nitrogen for EPR analysis.

III.2.4 Estimation of K_D for Potassium Ion on PFL-AE using EPR.

PFL-AE was mixed in a series of buffers containing 1 mM DTT and 50 mM Tris buffer pH 8.5 to a final concentration of 200 μ M and a final volume of 600 μ L. This series of mixtures contained an increasing concentration of KCl (0, 1, 2, 5, 10, 20, 50, 100, and 200 mM) and a decreasing concentration of NaCl (200, 199, 198, 195, 190, 180, 150, 100, and 0 mM). Photoreducing agent 5-deazariboflavin (from a 10 mM stock solution in DMSO) was added last in the dark to a final concentration of 200 μ M. After the reaction mixtures were transferred into EPR tubes, they were capped and inserted in a beaker tightly packed with ice and water. Then all tubes were illuminated on ice for 1hr using a 300W halogen lamp situated 2 cm from the beaker. After illumination, 300 μ L

of the PFL-AE mixture from EPR tube was mixed with AdoMet to a final concentration of 2 mM, while the remaining 300 μ L of the PFL-AE mixture was kept as control without AdoMet. Both +AdoMet and –AdoMet samples were then flash-frozen in liquid nitrogen for EPR analysis.

III.2.5 EPR Spectroscopy.

All the EPR spectra were measured in a Bruker ESP300E EPR spectrometer equipped with a liquid He cryostat and a temperature controller from Oxford Instruments. Data were collected at 12 K with 2 mW microwave power and 10 G modulation amplitude. Spin concentrations for the $[4\text{Fe-4S}]^{1+}$ clusters in the protein samples were determined by calibrating double integrals of the EPR spectra recorded under nonsaturating conditions with a standard sample of 0.1 mM Cu(II), 1 mM EDTA and 10 % (w/v) glycerol solution.

III.3 Results and Discussion

III.3.1 Effect of Buffer Conditions on the EPR Spectra of PFL-AE.

The $[4\text{Fe-4S}]^{1+}$ cluster of PFL-AE, generated by photoreduced 5-deazariboflavin in PFL activation buffer, exhibits a strong, nearly axial signal ($g_{\parallel} = 2.02$, $g_{\perp} = 1.93$) (Figure III.3.1.1, upper panel). Addition of 10 molar equivalents of AdoMet to this $[4\text{Fe-4S}]^{1+}$ cluster of PFL-AE produces a dramatic change in the EPR spectral properties, resulting in a rhombic EPR signal ($g_z = 2.00$, $g_y = 1.92$, and $g_x = 1.88$) (Figure III.3.1.1, lower panel). These spectra are in marked contrast to those previously reported, in which the reduced $[4\text{Fe-4S}]^{1+}$ cluster with a rhombic signal ($g = 2.02, 1.94, 1.88$) converts to nearly axial upon addition of AdoMet.⁶ The only difference between the samples in Figure III.3.1.1 and those reported by Walsby et al.⁶ is the buffer conditions, with those reported here being in PFL activation buffer (100 mM Tris-HCl pH 7.6, 1 mM DTT, 100 mM KCl and 20 mM oxamate) and the latter being in 50 mM Tris-HCl pH 8.5, 200 mM NaCl, 1 mM DTT, and 20 % (w/v) glycerol. The discrepancy between the spectra in Figure III.3.1.1. and those previously published was perplexing, and led us to undertake a detailed study of the effects of buffer components on the EPR spectral properties of PFL-AE. As can be seen in Figure III.3.1.1, the buffer pH has little effect on the spectral properties, and thus cannot account for the differences between the current spectra and those previously reported.

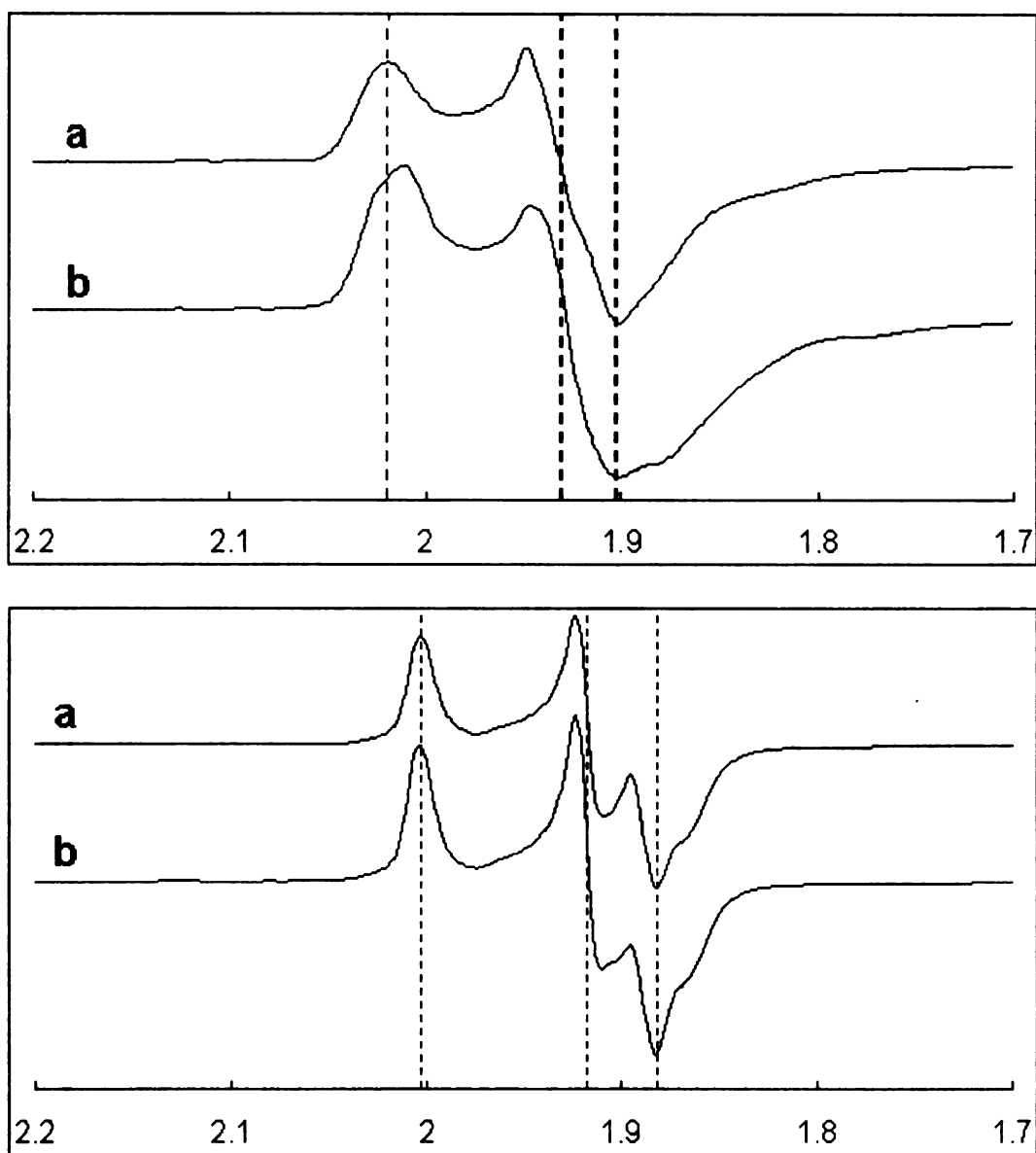


Figure III.3.1.1 X-band EPR spectra of reduced PFL-AE (top) and reduced PFL-AE in the presence of AdoMet (bottom). The protein was 200 μM in 100 mM Tris-HCl pH 7.6 (a) or 50 mM Tris-HCl pH 8.5 (b), as well as in 1 mM DTT, 100 mM KCl and 20 mM oxamate. 5-Deazariboflavin (200 μM) was added last in the dark followed by 1 hr illumination on ice. For the + AdoMet samples, AdoMet was added to 2 mM after photoreduction. Conditions of measurement $T = 12\text{ K}$; microwave power, 2 mW; modulation amplitude, 10 G. The dashed vertical lines indicate the most representative features at g values (Top: 2.02, 1.93, and 1.91. Bottom: 2.01, 1.92, and 1.88).

One of the differences between the samples whose spectra are presented in Figure III.3.1.1 and the earlier PFL-AE samples for which EPR spectra were reported,⁶ is that in Figure VI.3.1.1 the salt is KCl (as used in activity assays for PFL-AE) rather than NaCl (which in the past we have commonly used for ionic strength control in our spectroscopic samples). We therefore explored the effect of the monovalent cation on the EPR spectral properties of PFL-AE.

Photoreduction of PFL-AE in buffer containing Na^+ produced a strong, rhombic EPR signal essentially identical to that previously reported by us for PFL-AE ($g_z = 2.01$, $g_y = 1.93$, and $g_x = 1.87$) (Figure III.3.1.2, upper panel, c).⁶ Replacement of Na^+ with K^+ or NH_4^+ in the reaction mix caused striking effects on the line shape, changing the EPR spectrum to nearly axial ($g_{\parallel} = 2.02$, $g_{\perp} = 1.93$), as can be seen in Figure III.3.1.2 (upper panel, a and b). As expected, the addition of 10 molar equivalents of AdoMet to the photoreduced PFL-AE caused significant changes in the EPR spectra. The sample prepared in the presence of NaCl produced a nearly axial EPR signal ($g_{\parallel} = 2.00$, $g_{\perp} = 1.88$) (Figure III.3.1.2, lower panel, c) identical to that previously reported, however dramatic differences were observed when Na^+ was replaced with either K^+ or NH_4^+ (Figure III.3.1.2, lower panel, a and b). Together, these results demonstrated that the nature of the monovalent cation present in solution had a dramatic effect on the EPR spectral properties of the PFL-AE $[\text{4Fe-4S}]^+$ cluster, and accounts, at least in part, for the differences between the spectra

reported previously and those shown in Figure III.3.1.1.

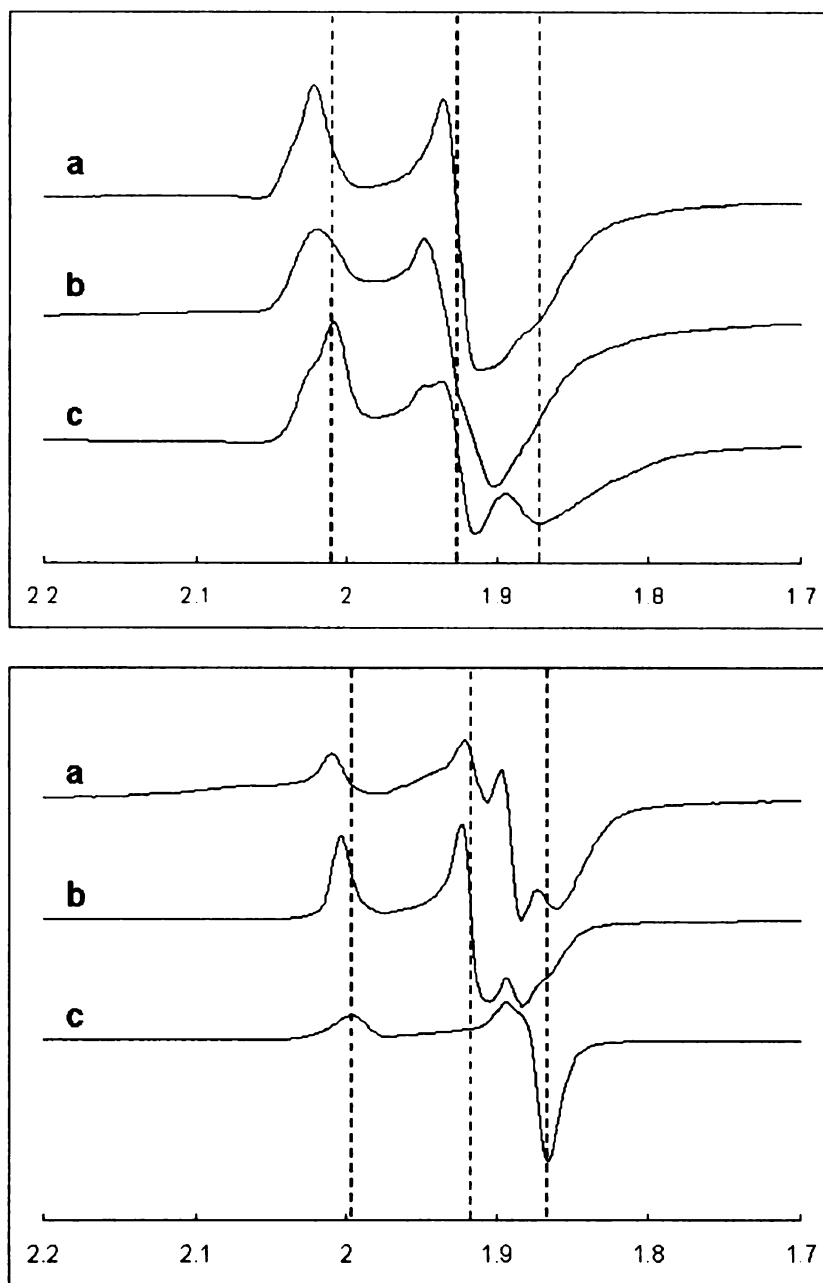


Figure III.3.1.2 Effects of different cations on the X-band EPR spectra of the photoreduced $[4\text{Fe-4S}]^{1+}$ cluster of PFL-AE. Shown are spectra of the enzyme in the absence (upper panel) and in the presence (lower panel) of AdoMet. The protein was 200 μM in 200 mM NH_4Cl (a), 200 mM KCl (b) and 200 mM NaCl (c), as well as in 50 mM Tris-HCl pH 8.5 and 1 mM DTT. 200 μM 5-deazariboflavin was added last in the dark followed by 1 hr illumination on ice. For the + AdoMet samples, AdoMet was added to 2 mM after photoreduction. Conditions of measurement $T = 12\text{ K}$; microwave power, 2 mW; modulation amplitude, 10 G. The dashed vertical lines indicate the most representative features at g values (Top: 2.01, 1.93, and 1.87. Bottom: 2.00, 1.92, and 1.87).

The presence of the PFL substrate pyruvate or substrate analog oxamate produced EPR spectra with subtle but reproducible changes in line shape (Figure III.3.1.3). In the presence of AdoMet, pyruvate or oxamate had very little effect on the EPR spectral properties of the $[4\text{Fe-4S}]^{1+}$ cluster (Figure III.3.1.3, lower panel), except for removing the small splitting in the g_{\perp} feature. In all these samples, the addition of AdoMet converts the rhombic signals ($g_z=2.01$, $g_y=1.93$, and $g_x=1.87$) to nearly axial signals ($g_{\parallel}=2.00$, $g_{\perp}=1.88$).

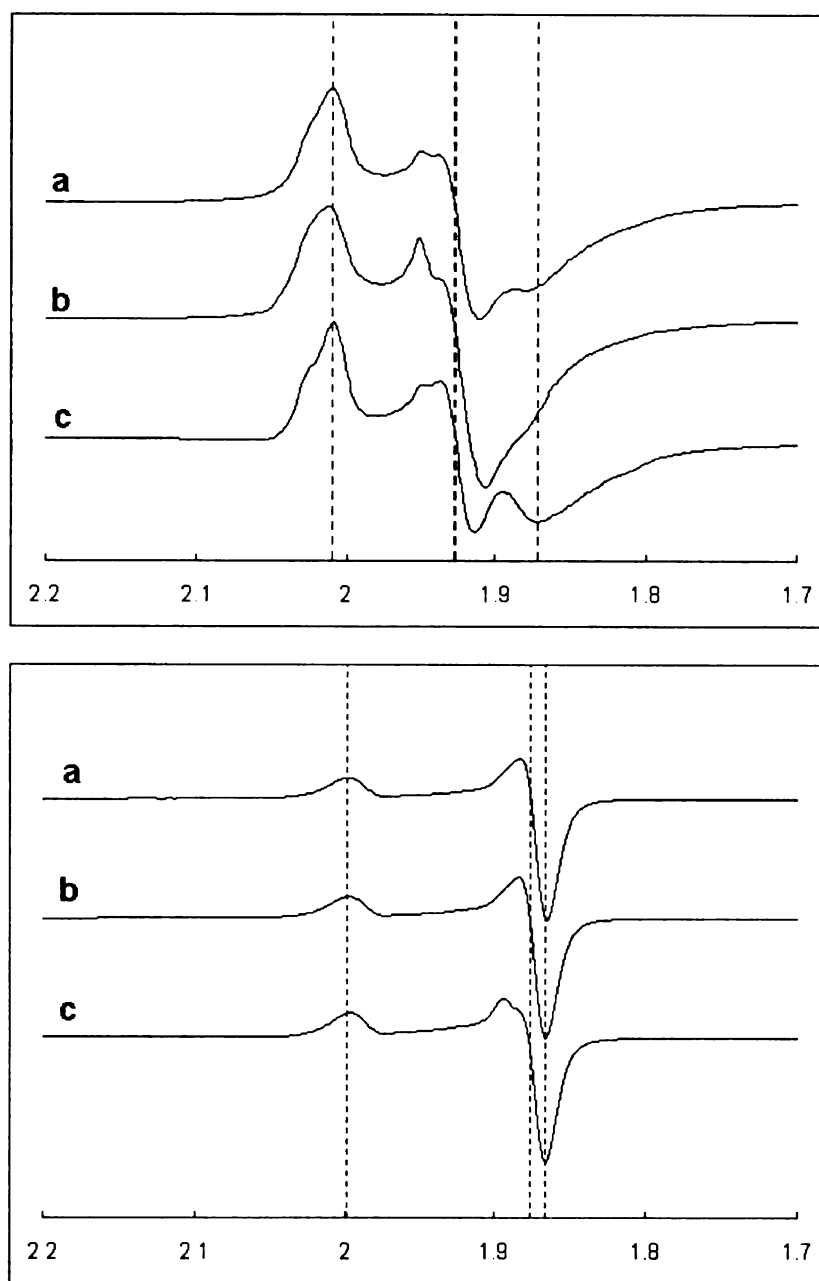


Figure III.3.1.3 Effects of oxamate or pyruvate on the X-band EPR spectra of the photoreduced $[4\text{Fe-4S}]^{1+}$ cluster of PFL-AE. Shown are spectra of the enzyme in the absence (upper panel) and in the presence (lower panel) of AdoMet. The protein was 200 μM in 20 mM pyruvate (a), 20 mM oxamate (b) or none of these two (c), as well as in 50 mM Tris-HCl pH 8.5, 1 mM DTT and 200 mM NaCl. 200 μM 5-deazariboflavin was added last in the dark followed by 1 hr illumination on ice. For the + AdoMet samples, AdoMet was added to 2 mM after photoreduction. Conditions of measurement $T = 12\text{ K}$; microwave power, 2 mW; modulation amplitude, 10 G. The dashed vertical lines indicate the most representative features at g values (Top: 2.01, 1.93, and 1.87. Bottom: 2.00, 1.88, and 1.87).

Glycerol and sucrose are the most commonly used cryoprotectants in spectroscopic studies of biological molecules to prevent proteins from being damaged while freezing. Both cryoprotectants were investigated because the size of the sucrose molecules ($C_{12}H_{22}O_{11}$, 342.3 g/mol) is much larger than that of the glycerol molecules ($C_3H_8O_3$, 92.1 g/mol), and therefore the two are unlikely to interact with PFL-AE in the same manner. The EPR spectrum of the $[4Fe-4S]^{1+}$ cluster of PFL-AE in buffer containing sucrose, glycerol, or neither are shown in Figure III.3.1.4, upper panel. All three samples show similar rhombic signals in the absence of AdoMet with moderate deviations in line shape and g values. Addition of AdoMet to these samples produces nearly identical spectra, regardless of the presence of glassing agent (Figure III.3.1.4, lower panel).

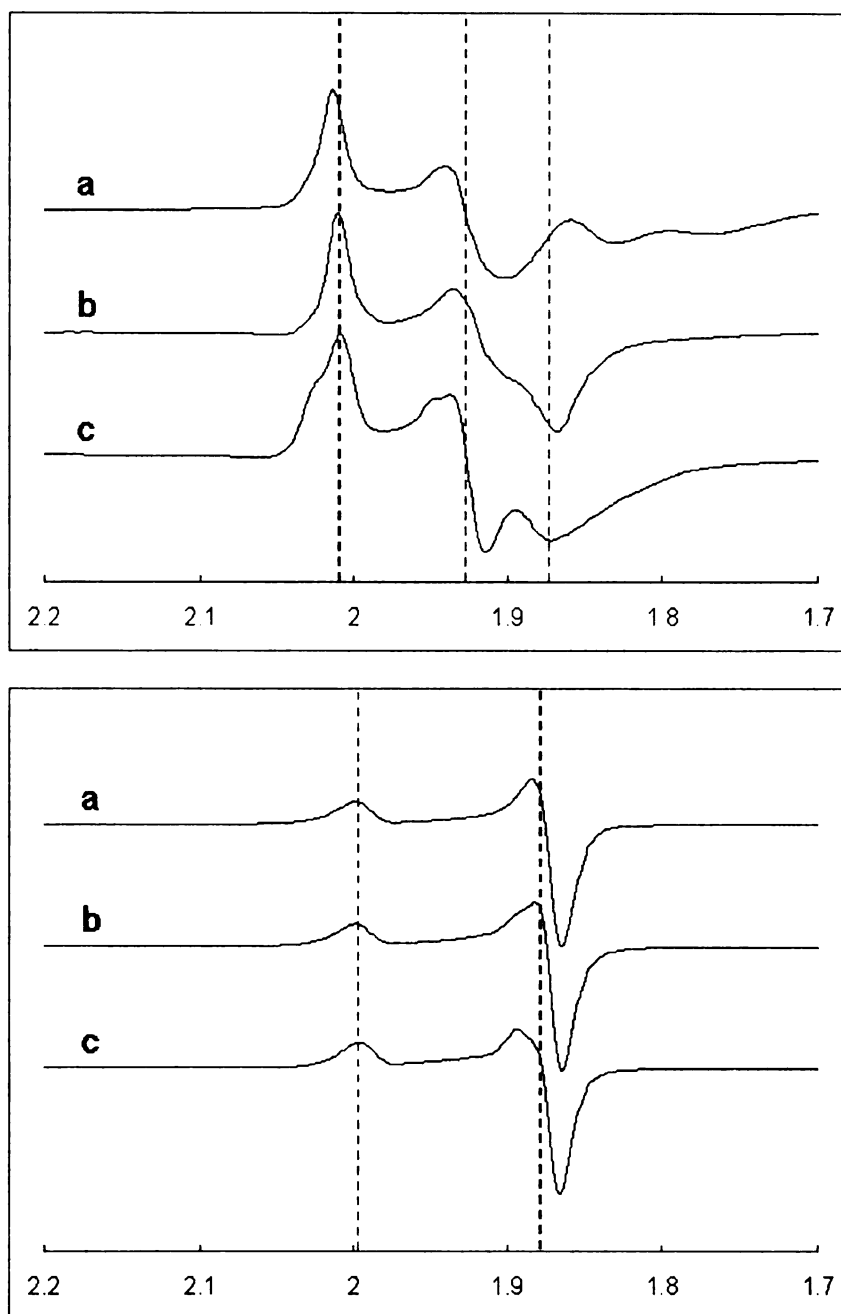


Figure III.3.1.4 Effects of different glassing agents on the X-band EPR spectra of the photoreduced $[4\text{Fe-4S}]^{1+}$ cluster of PFL-AE. Shown are spectra of the enzyme in the absence (upper panel) and in the presence (lower panel) of AdoMet. The protein was 200 μM in 0.4 M sucrose (a), 20% (v/v) glycerol (b) or none of these two (c), as well as in 50mM Tris-HCl pH 8.5, 1 mM DTT and 200 mM NaCl. 200 μM 5-deazariboflavin was added last in the dark followed by 1 hr illumination on ice. For the + AdoMet samples, AdoMet was added to 2 mM after photoreduction. Conditions of measurement $T = 12\text{ K}$; microwave power, 2 mW; modulation amplitude, 10 G. The dashed vertical lines indicate the most representative features at g values (Top: 2.01, 1.93, and 1.87. Bottom: 2.00 and 1.88).

Heretofore, we have identified the effects of several factors on the EPR characteristics of the photoreduced $[4\text{Fe-4S}]^{1+}$ cluster, including pH, pyruvate and oxamate, cations (Na^+ , K^+ , and NH_4^+), and glassing agents (glycerol, sucrose). In an effort to investigate whether these factors have mutual effects on each other, the photoreduced $[4\text{Fe-4S}]^{1+}$ cluster was measured in the following experimental conditions where only one factor was varied at a time while holding others constant.

The effect of Na^+ , K^+ , or NH_4^+ on the EPR spectrum of the $[4\text{Fe-4S}]^{1+}$ cluster was further investigated in a background buffer containing 20% (w/v) glycerol. Without AdoMet, several changes are observed upon replacement of Na^+ by K^+ or NH_4^+ , including changes in both the g values and line shape (Figure III.3.1.5, upper panel). Specifically, the g_z feature broadens while the g_x , g_y features narrow a bit and move to higher g values. For the samples in the presence of AdoMet, significant effects could also be identified when Na^+ is substituted by K^+ or NH_4^+ (Figure III.3.1.5, lower panel). The signal changes from nearly axial in the presence of sodium ion to much more rhombic in the presence of K^+ or NH_4^+ . As discussed earlier in this section (Figure III.3.1.2), the EPR spectra for samples PFL-AE/AdoMet in the presence of either K^+ or NH_4^+ also share striking similarities in the absence of any glassing agent. Taken together, these results suggest that the electronic structure of the $[4\text{Fe-4S}]^+$ cluster of PFL-AE is similar in the presence of K^+ or NH_4^+ , but different from that in the presence of Na^+ , regardless of the presence of other

components in the buffer.

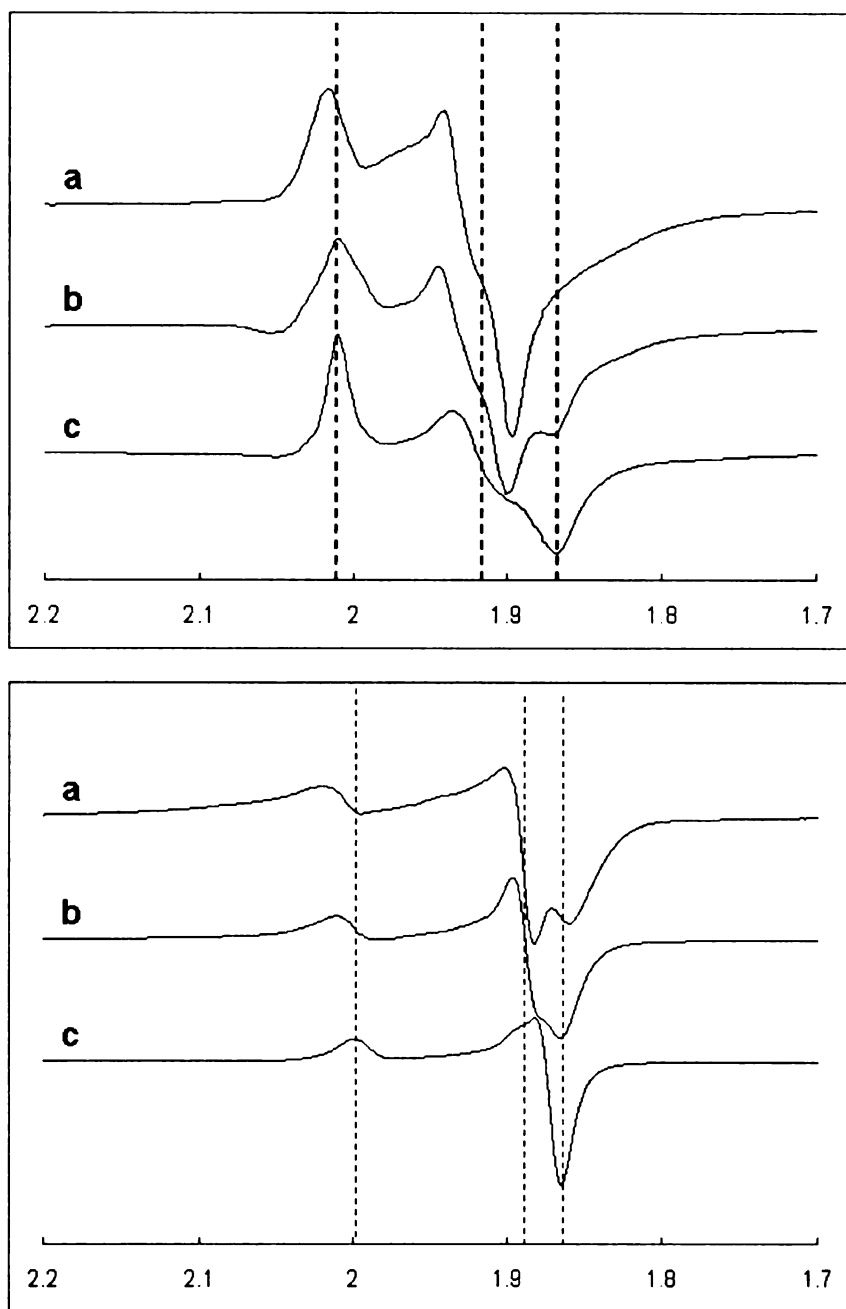


Figure III.3.1.5 Effects of different cations on the X-band EPR spectra of the photoreduced $[4\text{Fe-4S}]^{1+}$ cluster of PFL-AE in the presence of glycerol. Shown are spectra of the enzyme in the absence (upper panel) and in the presence (lower panel) of AdoMet. The protein was 200 μM in 200 mM NH_4Cl (a), 200 mM KCl (b) and 200 mM NaCl (c). All samples contained 50 mM Tris-HCl pH 8.5, 1 mM DTT and 20 % (v/v) glycerol. 200 μM 5-deazariboflavin was added last in the dark followed by 1hr illumination on ice. For the + AdoMet samples, AdoMet was added to 2 mM after photoreduction. Conditions of measurement $T = 12\text{ K}$; microwave power, 2 mW; modulation amplitude, 10 G. The dashed vertical lines indicate the most representative features at g values (Top: 2.01, 1.92, and 1.87. Bottom: 2.00, 1.89, and 1.87).

The effect of different glassing agents on the EPR spectra of the $[4\text{Fe-4S}]^{1+}$ cluster of PFL-AE was further investigated in a background buffer containing 200 mM KCl and 20 mM oxamate. In the absence of AdoMet, the presence of either glassing agent led to a sharpening of the EPR features as well as the emergence of a shoulder (glycerol: $g = 1.87$; sucrose: $g = 1.83$), making the EPR characteristics more rhombic (Figure III.3.1.6, upper panel). In the presence of AdoMet, the distinctly rhombic signal ($g_z = 2.00$, $g_y = 1.92$, and $g_x = 1.88$) became an intense, nearly axial signal ($g_{\parallel} = 2.01$, $g_{\perp} = 1.89$) with the incorporation of any glassing agent (Figure III.3.1.6, lower panel). Both glycerol and sucrose had the same effect on in the presence of AdoMet.

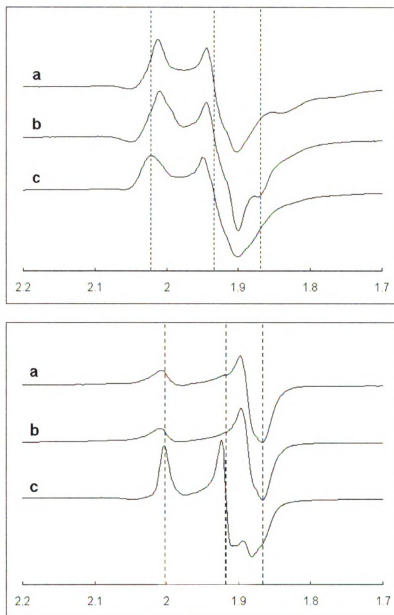


Figure III.3.1.6 Effects of different glassing agents on the X-band EPR spectra of the photoreduced $[4\text{Fe-4S}]^{1+}$ cluster of PFL-AE in the presence of oxamate and KCL. Shown are spectra of the enzyme in the absence (upper panel) and in the presence (lower panel) of AdoMet. The protein was 200 μM in 0.4 M sucrose (a), 20 % (v/v) glycerol (b) or none of these two (c). All samples also contained 50 mM Tris-HCl pH 8.5, 1 mM DTT, 200 mM KCl and 20 mM oxamate. 200 μM 5-deazariboflavin was added last in the dark followed by 1 hr illumination on ice. For the + AdoMet samples, AdoMet was added to 2 mM after photoreduction. Conditions of measurement $T = 12\text{ K}$; microwave power, 2 mW; modulation amplitude, 10 G. The dashed vertical lines indicate the most representative features at g values (Top: 2.02, 1.94, and 1.87. Bottom: 2.00, 1.92, and 1.87).

III.3.2. Effect of cations on PFL and PFL-AE Activity.

PFL-AE catalyzes the generation of the active form of PFL via the [4Fe-4S]¹⁺/AdoMet complex.⁵ Previous studies in our laboratory have documented in some detail the EPR spectral characteristics of the PFL-AE-[4Fe-4S]¹⁺ and its complex with AdoMet, however as revealed in the previous section, these EPR spectral characteristics are significantly affected by the identity of monovalent ions present. Because all activity assays in our laboratory had previously been carried out in the presence of K⁺ ions, while all previously published spectroscopic studies were done in the presence of Na⁺, but not K⁺ ions, we began to question the correlation between activity and spectroscopic properties. We therefore designed a set of activity assays to investigate the effects of monovalent cations on PFL-AE activity.

In general, our approach was to activate PFL using PFL-AE in a reaction medium containing only one of the monovalent cations at a time (Na⁺, K⁺, or NH₄⁺). Then, under strictly anaerobic conditions, the PFL activity was monitored as a function of time to probe the rate of activation by PFL-AE, if any, in the presence of the different monovalent cations (Figure III.3.2.1). The results showed that over the time course of the experiment, the activity of the PFL in all cases increased but did not reach saturation. The rate of PFL activation, and thus the activity of PFL-AE, was highest in the presence of K⁺ (4.3 U/mg, based on the time point at 25 min and PFL activation at 0 °C). In the presence of NH₄⁺ the activity (3.0 U/mg, based on the time point at 25 min and PFL activation at 0 °C) was approximately two thirds of that in the presence of

K^+ . PFL-AE had the lowest activity in the presence of Na^+ ions, with only approximately one third the activity in the presence of K^+ (1.3 U/mg, based on the time point at 25 min and PFL activation at 0 °C).

The results just described would be consistent with an affect of monovalent cations on PFL-AE activity. However, due to the complex nature of the PFL-AE activity assay, it is also possible that the differences observed were a result of effects on the rate of PFL-AE photoreduction. In an effort to demonstrate whether the cation effect was correlated with the photoreduction rate of PFL-AE, a photoreduction time course experiment was carried out in the presence of different cations. PFL-AE was photoreduced in a reaction mix containing only one of the cations (Na^+ , K^+ or NH_4^+) at a time, and in the absence of AdoMet and PFL. Then, the amount of the $[4Fe-4S]^{1+}$ cluster was monitored as a function of time in order to probe the photoreduction rate of PFL-AE in the presence of the different cations. The results showed that PFL-AE incubated with Na^+ or K^+ under otherwise identical conditions exhibited the same rates of photoreduction to the $[4Fe-4S]^{1+}$ state; the sample containing NH_4^+ exhibited a slightly lower rate of photoreduction, approximately 80% of that of the potassium ion (Table III.3.2.1). Therefore, the effects of monovalent cations on the rates of PFL was attributed to the PFL-AE catalyzed reaction, not the photoreduction of PFL-AE.

Monocations	Spin quantification of EPR signal at 5 min (μM)	Spin quantification of EPR signal at 10 min (μM)	Spin quantification of EPR signal at 20 min (μM)
K^+	52	56	41
Na^+	56	60	48
NH_4^+	40	40	39

Table III.3.2.1. Time course of the generation of glycy radical in the presence of different cations. PFL-AE was mixed in a buffer containing 8 mM DTT, 10 mM oxamate, 100 mM Tris-HCl pH 7.6, 100 μM 5-deazariboflavin, and 100 mM salt (NaCl, NH_4Cl or KCl) to a final concentration of 100 μM . At time intervals after tubes were illuminated on ice using a 300 W halogen lamp situated 2 cm from the beaker, an aliquot (300 μL) was flash-frozen in liquid nitrogen for EPR analysis. Conditions of measurement T = 12 K; microwave power, 2 mW; modulation amplitude, 10 G.

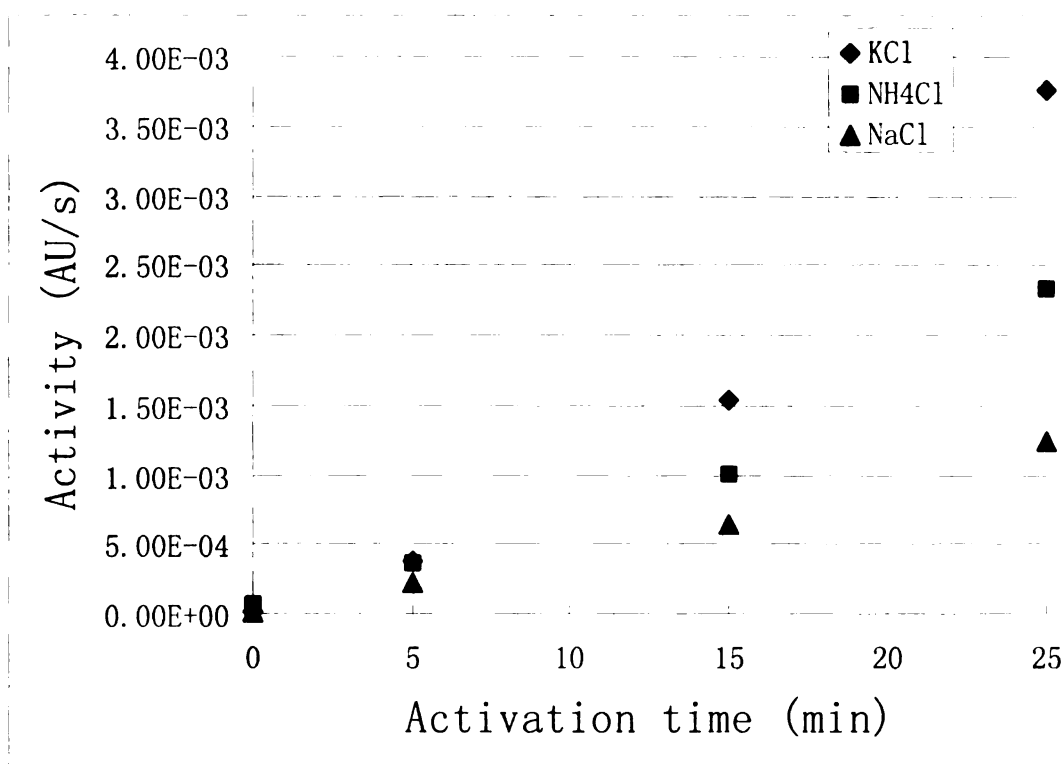


Figure III.3.2.1 Time course of PFL activation in the presence of different cations. PFL was activated by PFL-AE under anaerobic conditions in a final volume of 200 μ L containing 0.1 M Tris-Cl pH 7.6, 0.1 M salt (KCl, NaCl, or NH₄Cl), 10 mM oxamate, 8 mM DTT, ~0.06 μ M PFL-AE, ~6 μ M PFL, 0.2 mM AdoMet, and 50 μ M 5-deazariboflavin. At time intervals after initiation of the reaction, an aliquot (5 μ L) was removed for assay of active PFL through the coupling assay.

III.3.3. K_D for Potassium Ion on PFL-AE.

Potassium ion has a significant impact on the EPR line shape of the photoreduced $[4\text{Fe-4S}]^{1+}$ cluster of PFL-AE, both in the absence and presence of AdoMet. In addition, K^+ increased the activation rate of PFL by PFL-AE considerably. It is not unusual for enzymes to exhibit higher activity in the presence of potassium ion, and this is not surprising given that K^+ concentrations in cells can reach as high as 211 mM (*E. coli* cells).¹⁶ However the observation of changes in the EPR spectra of PFL-AE in the presence of potassium ion argue that the potassium effect in PFL-AE is a specific effect that produces significant electronic changes to the active site of the enzyme. To investigate and quantify the possible specific binding of K^+ to PFL-AE, we have examined EPR spectra for the photoreduced $[4\text{Fe-4S}]^{1+}$ cluster as a function of potassium ion concentration (Figure III.3.3.1.a. and Figure III.3.3.1.b). In the presence of AdoMet, the EPR spectra were dramatically altered with increasing $[\text{K}^+]$, changing from a nearly axial signal in the absence of K^+ to a rhombic signal at 200 mM K^+ (Figure III.3.3.1.b.). In contrast, similar experiments performed in the absence of AdoMet (Figure III.3.3.1.a.) showed a less dramatic effect. Therefore, the loss of the feature at $g = 1.86$ from the EPR spectra containing AdoMet (Figure III.3.3.2.) was used to determine the apparent binding constant (6.2 mM) of K^+ on PFL-AE by estimating the midpoint of its EPR intensities at $g = 1.86$. This K_d is well within the range of other proteins in the literature with specific potassium ion binding sites.¹⁷⁻²¹

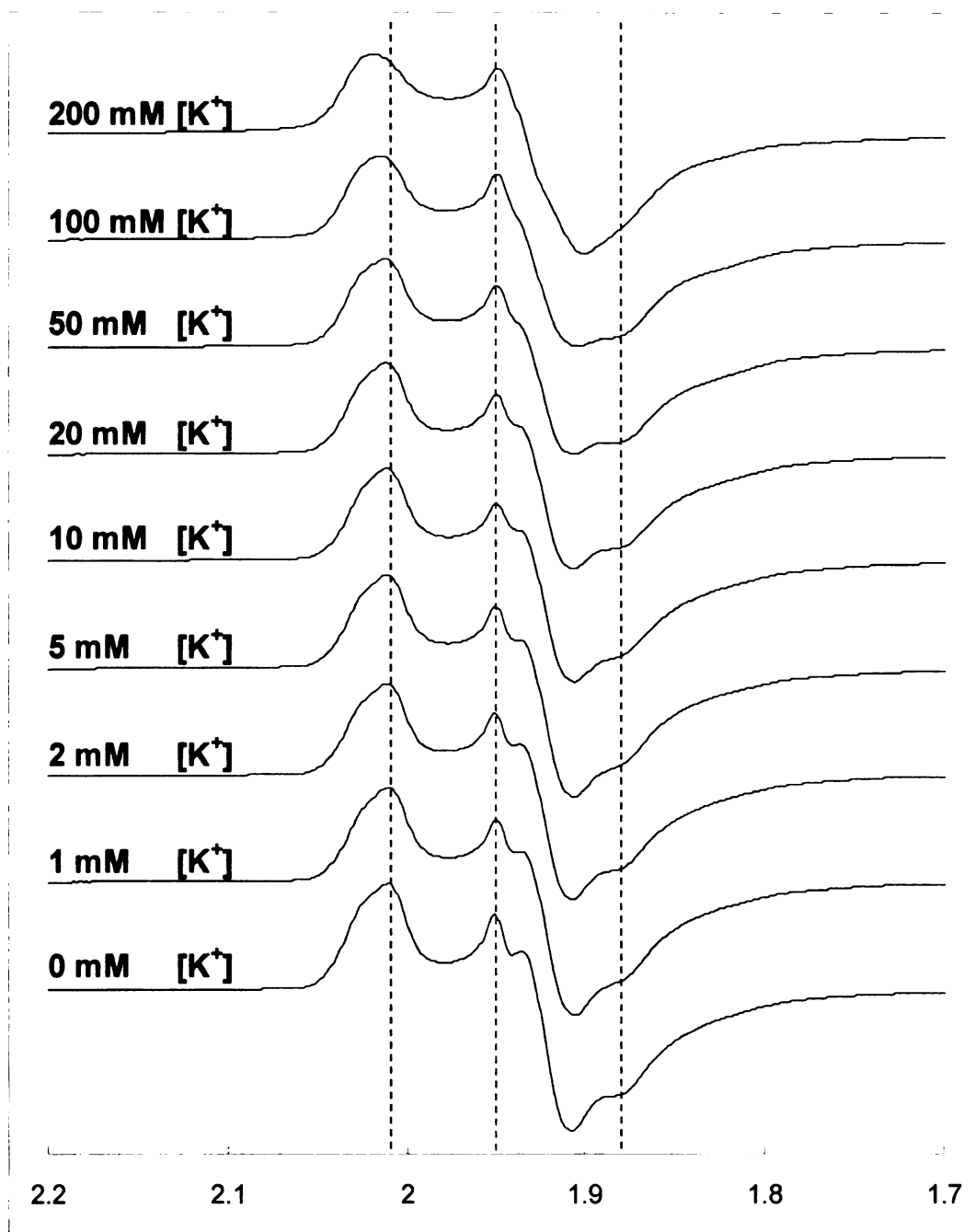


Figure III.3.3.1.a. EPR titration of the photoreduced $[4\text{Fe-4S}]^{1+}$ cluster of PFL-AE with potassium ion. The protein was $200\ \mu\text{M}$ in $50\ \text{mM}$ Tris-HCl pH 8.5 and $1\ \text{mM}$ DTT. A combination of $x\ \text{mM}$ KCl (as indicated on the left side of each spectrum) and $200-x\ \text{mM}$ NaCl was added in order to keep constant ionic strength. $200\ \mu\text{M}$ 5-deazariboflavin was added last in the dark followed by 1 hr illumination on ice. Conditions of measurement $T = 12\ \text{K}$; microwave power, $2\ \text{mW}$; modulation amplitude, $10\ \text{G}$. The dashed vertical lines indicate the most representative features at g values 2.01, 1.96, and 1.88, respectively.

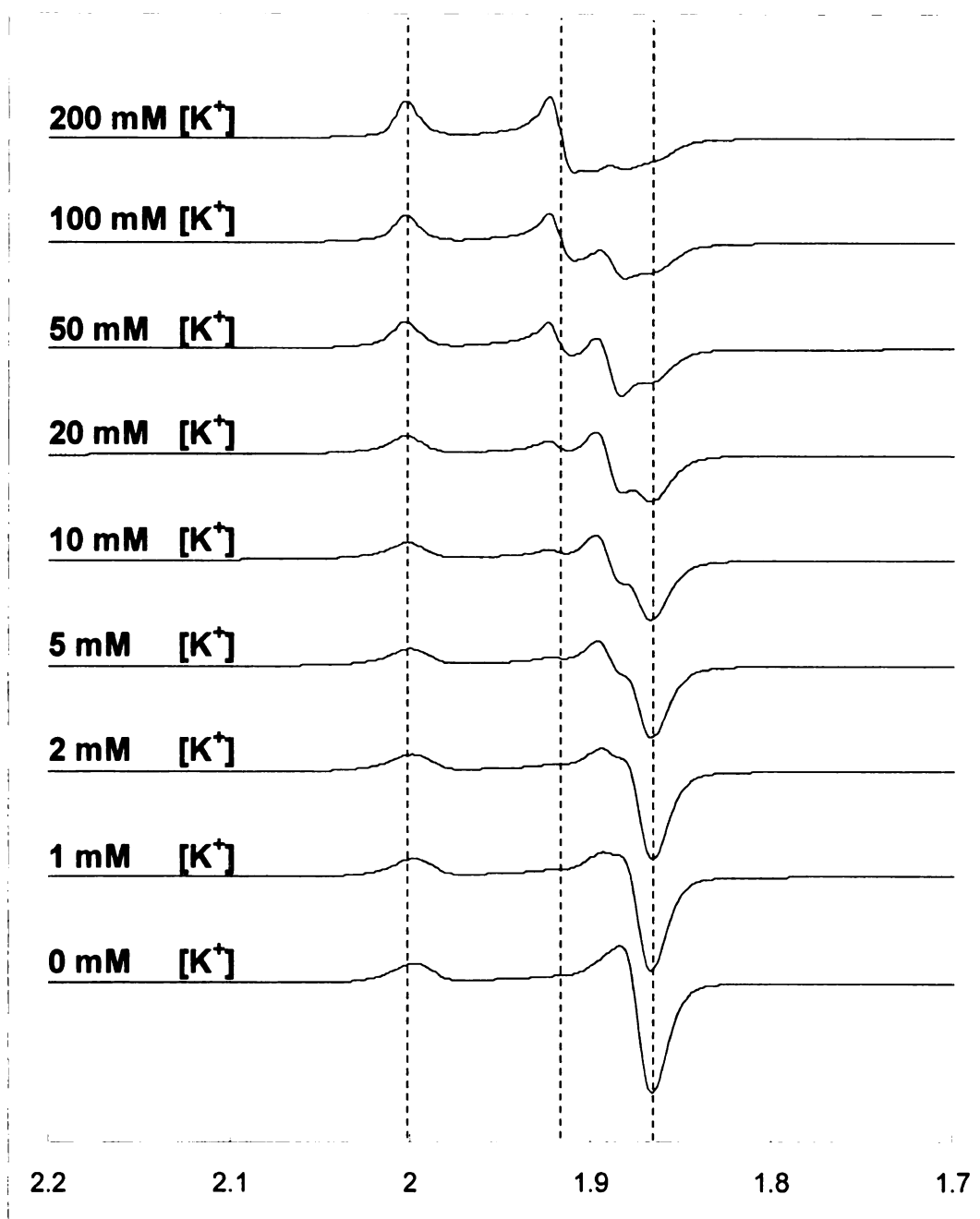


Figure III.3.3.1.b. EPR titration of the photoreduced $[4\text{Fe-4S}]^{1+}$ cluster of PFL-AE with potassium ion in the presence of AdoMet. The protein was 200 μM in 50 mM Tris-HCl pH 8.5 and 1 mM DTT. A combination of x mM KCl (as indicated on the left side of each spectrum) and $200-x$ mM NaCl was added in order to keep constant ionic strength. 200 μM 5-deazariboflavin was added last in the dark followed by 1 hr illumination on ice. AdoMet was added to 2 mM after photoreduction. Conditions of measurement $T = 12$ K; microwave power, 2 mW; modulation amplitude, 10 G. The dashed vertical lines indicate the most representative features at g values 2.00, 1.92, and 1.87, respectively.

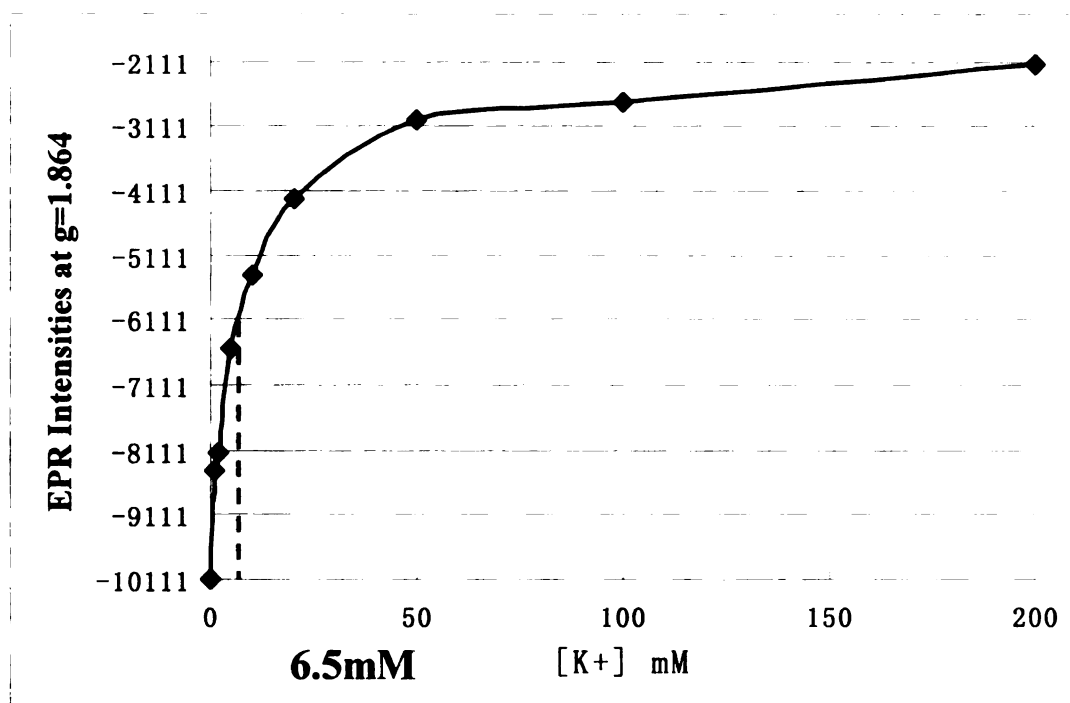


Figure III.3.3.2. Plot of EPR intensity at $g = 1.86$ vs. $[K^+]$ for PFL-AE/[4Fe-4S] $^+$ in the presence of AdoMet (Figure III.3.3.1.b.)

III.4 Conclusions

We provide here the first detailed investigation of the spectroscopic properties of the catalytically active form of pyruvate formate lyase-activating enzyme (PFL-AE), a radical SAM enzyme that contains a [4Fe-4S] cluster and utilizes S-adenosylmethionine (AdoMet) to generate the catalytically essential glycy radical of pyruvate formate lyase (PFL). The EPR characteristics of this cluster can be modified by several factors, including pH, pyruvate or oxamate, cations, and glassing agents. Our data demonstrates for the first time that the potassium ion (K^+) not only interacts with PFL-AE with an apparent K_d of 6.5 mM but also dramatically alters the electronic properties of the active-site [4Fe-4S]⁺ cluster and cause up to a three-fold increase in the enzymatic activity.

PFL-AE has been purified as the holo-form enzyme from *E. coli* BL21(DE3)pLysS cells containing an overexpressing vector pCal-n-AE3 as previously described ⁶. The purification procedure was carried out under strictly anaerobic conditions, resulting in an enzyme containing one [4Fe-4S]²⁺ cluster per protein monomer. All of our studies have been done on this "as-isolated" protein; no artificial cluster reconstitution has been required to achieve any of the results described herein. Reduction of PFL-AE using photoreduced 5-deazariboflavin yielded nearly 100 % conversion of [4Fe-4S]²⁺ clusters to the EPR active [4Fe-4S]¹⁺ clusters. Regardless of the presence of other components in the buffer, addition of AdoMet produced dramatic effects

on the EPR signal of the $[4\text{Fe-4S}]^{1+}$ cluster, as shown in Figure III.3.1.1-6. Such a dramatic change in the EPR characteristics is consistent with our previous results that AdoMet coordinates the $[4\text{Fe-4S}]$ cluster of PFL-AE.^{5, 6, 11, 12} AdoMet binding produces a change of the electronic structure of the $[4\text{Fe-4S}]^{1+}$ cluster of PFL-AE. As a result, rhombic or nearly axial signals have been repeatedly cited as characteristic of PFL-AE alone or PFL-AE in complex with AdoMet respectively.⁴⁻⁶ However, the results described herein demonstrated that the EPR signal of the $[4\text{Fe-4S}]^{1+}$ cluster is very sensitive to its environment and can be affected by several other factors, including pH, pyruvate and oxamate, cations (Na^+ , K^+ , and NH_4^+), and glassing agents (glycerol and sucrose). Therefore, great care must be taken when referring to the EPR signals of the iron sulfur clusters of PFL-AE as a standard or for the purpose of comparison; similar conclusions may also apply to its fellow members of radical SAM superfamily. Currently, we are working on investigation the correlation between the PFL-AE/PFL activity and the presence of these small molecules, including pH, more cations, and glassing agents (glycerol and sucrose).

K^+ , one of the most abundant physiologically available cations, can accumulate to as high as 211 mM in *E. coli* cells¹⁶. The primary cellular function of K^+ is the maintenance of proper fluid balance and nerve impulse function in complex organisms. We report herein the first experimental evidence for the effect of K^+ on the PFL-AE activity. The presence of K^+

dramatically alters the EPR characteristics of the $[4\text{Fe-4S}]^{1+}$ cluster and results in a three-fold increase in the PFL-AE enzymatic activity. Similar EPR and PFL-AE activity results were also observed when NH_4^+ , the cation analogue of K^+ , was utilized.

To further investigate the binding strength of K^+ as a cofactor/modulator on PFL-AE, we performed a series of EPR measurements, varying concentrations of K^+ in each reaction mix, with or without cosubstrate AdoMet. The results clearly supported a tight interaction of K^+ as a cofactor/modulator on PFL-AE with an apparent binding constant (k_D) of 6.5 mM. Considering the intracellular concentration of K^+ is well above this k_D , we believed PFL-AE must be fully saturated with K^+ *in vivo*. Indeed, a few enzymes have shown similar binding affinity for K^+ , such as arsenate reductase ($K_d = 0.3$ mM, calculated from the published result $K_a = 3.8 \times 10^3 \text{ M}^{-1}$),¹⁸ ribokinase ($k_d = 5$ mM),¹⁹ Kex2 protease ($K_D \sim 20$ mM),²⁰ and tyrosyl-tRNA synthetase ($K_D = 32$ mM).²¹ So far, two general types of binding sites have been proposed in an effort to elucidate the coordination chemistry of K^+ on proteins.²² In the first type of binding site, K^+ is octahedrally surrounded by 6 electronegative oxygen ligands (“oxygen cage”) donated by main chain carbonyls, side chain carboxyls, and/or bound water molecules. In contrast, the second binding site involves the π electrons at the face of four aromatic side chains serving as the electronegative source for the interaction with K^+ .

Besides those mentioned above, many other enzymes are also known

to contain a K^+ binding site and utilize it to modify the enzymatic activities, such as uridine phosphorylase,^{18, 21, 23} tyrosyl-tRNA synthetase,²⁴ tyrosine phenol-lyase,²⁵ MnmE,²⁶ and diol dehydratase.^{27, 28} Based on their functions, these enzymes can be divided into two major categories. The first kind of function is more structural, where the binding of K^+ causes a configurational change resulting in an affinity change of other substrates of the enzyme. In the case of adenosylcobalamin-dependent enzymes, K^+ has been thought to be required for the tight binding of cobalamins to apoenzyme by affecting the structure of the TIM barrel.^{29, 30} An approximately 20-fold increase in binding affinity between diol dehydrase and adenosylcobalamin was found when the potassium ion was included in the experiments.³¹ The second function involves K^+ being directly involved in the enzymatic reactions. For adenosylcobalamin-dependent enzymes, K^+ participates directly in the reaction with substrates, such as diol dehydratase,^{27, 28} helping migrate the hydroxyl group of 1,2-diols from C(2) to C(1) during the conversion reaction. Further studies are underway in our laboratory to address the function of K^+ in the activation of PFL by PFL-AE.

Glycerol or sucrose is the most commonly used cryoprotectant in biological studies to prevent freezing damage to living organisms or enzymes. That the presence of either one had a dramatic effect on the EPR spectra of PFL-AE was somewhat of a surprise, because no glassing agents had been reported to affect enzymatic activities in the radical SAM superfamily. It is

unknown at this time whether glassing agents have an affect on PFL-AE activity. At the very least these results serve as a warning to other investigators, demonstrating the need to consider the effects of all solution components when carrying out spectroscopic and activity studies on iron-sulfur enzymes.

III.5 References

1. Frey, M.; Rothe, M.; Wagner, A. F. V.; Knappe, J., Adenosylmethionine-dependent synthesis of the glycyl radical in pyruvate formate-lyase by abstraction of the glycine C-2 pro-S hydrogen atom. Studies of [2H]glycine-substituted enzyme and peptides homologous to the glycine 734 site. *Journal of Biological Chemistry* **1994**, 269, (17), 12432-7.
2. Conradt, H.; Hohmann-Berger, M.; Hohmann, H. P.; Blaschkowski, H. P.; Knappe, J., Pyruvate formate-lyase (inactive form) and pyruvate formate-lyase activating enzyme of *Escherichia coli*: isolation and structural properties. *Archives of Biochemistry and Biophysics* **1984**, 228, (1), 133-42.
3. Wagner, A. F. V.; Demand, J.; Schilling, G.; Pils, T.; Knappe, J., A dehydroalanyl residue can capture the 5'-deoxyadenosyl radical generated from S-adenosylmethionine by pyruvate formate-lyase-activating enzyme. *Biochemical and Biophysical Research Communications* **1999**, 254, (2), 306-310.
4. Henshaw, T. F.; Cheek, J.; Broderick, J. B., The [4Fe-4S]¹⁺ Cluster of Pyruvate Formate-Lyase Activating Enzyme Generates the Glycyl Radical on Pyruvate Formate-Lyase: EPR-Detected Single Turnover. *Journal of the American Chemical Society* **2000**, 122, (34), 8331-8332.
5. Walsby, C. J.; Ortillo, D.; Yang, J.; Nnyepi, M. R.; Broderick, W. E.; Hoffman, B. M.; Broderick, J. B., Spectroscopic Approaches to Elucidating Novel Iron-Sulfur Chemistry in the "Radical-SAM" Protein Superfamily. *Inorganic Chemistry* **2005**, 44, (4), 727-741.
6. Walsby, C. J.; Hong, W.; Broderick, W. E.; Cheek, J.; Ortillo, D.; Broderick, J. B.; Hoffman, B. M., Electron-Nuclear Double Resonance Spectroscopic Evidence That S-Adenosylmethionine Binds in Contact with the Catalytically Active [4Fe-4S]⁺ Cluster of Pyruvate Formate-Lyase Activating Enzyme. *Journal of the American Chemical Society* **2002**, 124, (12), 3143-3151.
7. Becker, A.; Fritz-Wolf, K.; Kabsch, W.; Knappe, J.; Schultz, S.; Wagner, A. F. V., Structure and mechanism of the glycyl radical enzyme pyruvate formate-lyase. *Nature Structural Biology* **1999**, 6, (10), 969-975.

8. Becker, A.; Kabsch, W., X-ray Structure of Pyruvate Formate-Lyase in Complex with Pyruvate and CoA. *Journal of Biological Chemistry* **2002**, 277, (42), 40036-40042.
9. Parast, C. V.; Wong, K. K.; Lewisch, S. A.; Kozarich, J. W.; Peisach, J.; Magliozzo, R. S., Hydrogen Exchange of the Glycyl Radical of Pyruvate Formate-Lyase Is Catalyzed by Cysteine 419. *Biochemistry* **1995**, 34, (8), 2393-9.
10. Lehtioe, L.; Leppaenen, V. M.; Kozarich, J. W.; Goldman, A., Structure of Escherichia coli pyruvate formate-lyase with pyruvate. *Acta Crystallographica, Section D: Biological Crystallography* **2002**, D58, (12), 2209-2212.
11. Krebs, C.; Broderick, W. E.; Henshaw, T. F.; Broderick, J. B.; Huynh, B. H., Coordination of Adenosylmethionine to a Unique Iron Site of the [4Fe-4S] of Pyruvate Formate-Lyase Activating Enzyme: A Moessbauer Spectroscopic Study. *Journal of the American Chemical Society* **2002**, 124, (6), 912-913.
12. Walsby, C. J.; Ortillo, D.; Broderick, W. E.; Broderick, J. B.; Hoffman, B. M., An Anchoring Role for FeS Clusters: Chelation of the Amino Acid Moiety of S-Adenosylmethionine to the Unique Iron Site of the [4Fe-4S] Cluster of Pyruvate Formate-Lyase Activating Enzyme. *Journal of the American Chemical Society* **2002**, 124, (38), 11270-11271.
13. Broderick, J. B.; Henshaw, T. F.; Cheek, J.; Wojtuszewski, K.; Smith, S. R.; Trojan, M. R.; McGhan, R. M.; Kopf, A.; Kibbey, M.; Broderick, W. E., Pyruvate formate-lyase-activating enzyme: Strictly anaerobic isolation yields active enzyme containing a [3Fe-4S]⁺ cluster. *Biochemical and Biophysical Research Communications* **2000**, 269, (2), 451-456.
14. Wong, K. K.; Murray, B. W.; Lewisch, S. A.; Baxter, M. K.; Ridky, T. W.; Ulissi-DeMario, L.; Kozarich, J. W., Molecular properties of pyruvate formate-lyase activating enzyme. *Biochemistry* **1993**, 32, (51), 14102-10.
15. Brush, E. J.; Lipsett, K. A.; Kozarich, J. W., Inactivation of Escherichia coli pyruvate formate-lyase by hypophosphite: evidence for a rate-limiting phosphorus-hydrogen bond cleavage. *Biochemistry* **1988**, 27, (6), 2217-22.

16. Schultz, S. G.; Solomon, A. K., Cation transport in *Escherichia coli*. I. Intracellular Na and K concentrations and net cation movement. *Journal of General Physiology* **1961**, 45, 355-69.
17. Suelter, C. H.; Snell, E. E., Monovalent cation activation of tryptophanase. *Journal of Biological Chemistry* **1977**, 252, (6), 1852-7.
18. Lah, N.; Lah, J.; Zegers, I.; Wyns, L.; Messens, J., Specific Potassium Binding Stabilizes p1258 Arsenate Reductase from *Staphylococcus aureus*. *Journal of Biological Chemistry* **2003**, 278, (27), 24673-24679.
19. Andersson, C. E.; Mowbray, S. L., Activation of ribokinase by monovalent cations. *Journal of Molecular Biology* **2002**, 315, (3), 409-419.
20. Rockwell, N. C.; Fuller, R. S., Specific modulation of Kex2/furin family proteases by potassium. *J Biol Chem* **2002**, 277, (20), 17531-7.
21. Austin, J.; First, E. A., Potassium functionally replaces the second lysine of the KMSKS signature sequence in human tyrosyl-tRNA synthetase. *J Biol Chem* **2002**, 277, (23), 20243-8.
22. Miller, C., Potassium selectivity in proteins: oxygen cage or in the F ace. *Science (Washington, DC, United States)* **1993**, 261, (5129), 1692-3.
23. Caradoc-Davies, T. T.; Cutfield, S. M.; Lamont, I. L.; Cutfield, J. F., Crystal structures of *Escherichia coli* uridine phosphorylase in two native and three complexed forms reveal basis of substrate specificity, induced conformational changes and influence of potassium. *J Mol Biol* **2004**, 337, (2), 337-54.
24. Austin, J.; First, E. A., Catalysis of tyrosyl-adenylate formation by the human tyrosyl-tRNA synthetase. *J Biol Chem* **2002**, 277, (17), 14812-20.
25. Milic, D.; Matkovic-Calogovic, D.; Demidkina Tatyana, V.; Kulikova Vitalia, V.; Sinitzina Nina, I.; Antson Alfred, A., Structures of apo- and holo-tyrosine phenol-lyase reveal a catalytically critical closed conformation and suggest a mechanism for activation by K⁺ ions. *Biochemistry* **2006**, 45, (24), 7544-52.

26. Scrima, A.; Wittinghofer, A., Dimerisation-dependent GTPase reaction of MnmE: how potassium acts as GTPase-activating element. *Embo J* **2006**, 25, (12), 2940-51.
27. Shibata, N.; Masuda, J.; Tobimatsu, T.; Toraya, T.; Suto, K.; Morimoto, Y.; Yasuoka, N., A new mode of B12 binding and the direct participation of a potassium ion in enzyme catalysis: X-ray structure of diol dehydratase. *Structure* **1999**, 7, (8), 997-1008.
28. Masuda, J.; Shibata, N.; Morimoto, Y.; Toraya, T.; Yasuoka, N., How a protein generates a catalytic radical from coenzyme B(12): X-ray structure of a diol-dehydratase-adeninylpentylcobalamin complex. *Structure* **2000**, 8, (7), 775-88.
29. Toraya, T.; Sugimoto, Y.; Tamao, Y.; Shimizu, S.; Fukui, S., Propanediol dehydratase system. Role of monovalent cations in binding of vitamin B 12 coenzyme or its analogs to apoenzyme. *Biochemistry* **1971**, 10, (18), 3475-84.
30. Toraya, T.; Kondo, M.; Isemura, Y.; Fukui, S., Coenzyme B 12 dependent propanediol dehydratase system. Nature of cobalamin binding and some properties of apoenzyme-coenzyme B 12 analog complexes. *Biochemistry* **1972**, 11, (14), 2599-606.
31. Schwartz, P. A.; Frey, P. A., Dioldehydrase: an essential role for potassium ion in the homolytic cleavage of the cobalt-carbon bond in adenosylcobalamin. *Biochemistry* **2007**, 46, (24), 7293-301.

CHAPTER IV

X-RAY STRUCTURAL CHARACTERIZATION OF PFL-AE

IV.1 Introduction

Enzymes in the radical SAM superfamily play important roles in cellular metabolism. Although they catalyze a variety of reactions on many different substrates,^{1, 2} the common first step is believed to be a one electron transfer from the [4Fe-4S] cluster to the bound SAM, followed by subsequent cleavage of C(5')-S bond to generate a 5'-deoxyadenosyl radical intermediate. Structures of several radical SAM enzymes have been solved by X-ray crystallography, including coproporphyrinogen III oxidase,³ biotin synthase,⁴ MoaA,⁵ and LAM.⁶ These structures provide useful information regarding specific function of each enzyme.

Various techniques (EPR, ENDOR, Mössbauer spectroscopy etc) have been successfully used in the Broderick lab to investigate the iron-sulfur cluster of PFL-AE and the interaction of the cluster with SAM.⁷⁻¹⁴ In this chapter, I describe the results of X-ray crystallographic studies of PFL-AE carried out in collaboration with Jessica Vey and Catherine L. Drennan (MIT). The results both confirm and extend our understanding of PFL-AE, its active site, and its

interaction with SAM. Further, the results provide dramatic new insights into the interaction between PFL-AE and its substrate PFL.

IV.2 Materials and Methods

PFL-AE was purified according to the published procedures⁸ except that 1 mM DTT was included in all buffers. Peptides [7-mer (RVSGYAV, purity > 98 %) and 12-mer (Ac-IRVSGYAVRFNS-NH₂, purity > 80 %)] were ordered from Celteck Peptides. Preparation of PFL-AE samples was carried out in a Coy anaerobic chamber and/or an Mbraun anaerobic glove box with oxygen level less than 2 ppm. All buffers were deoxygenated using a vacuum/nitrogen gas manifold before being taken into the glove box. Solid chemicals were pumped in as solids. After preparation, all samples were flash-frozen in liquid nitrogen and sent to the Drennan lab at MIT.

IV.2.1 PFL-AE in Hepes buffer

After purification in a buffer containing 50 mM Hepes pH 7.4, 200 mM NaCl and 1 mM DTT, PFL-AE was concentrated in a Coy chamber to a final concentration of 1.57 mM using an Amicon concentrator equipped with a YM-10 membrane. PFL-AE was determined by SDS-PAGE to be over 95 % pure and had 3.6 Fe/AE.^{15, 16} A total volume of 1 mL was flash-frozen and sent to MIT.

IV.2.2 PFL-AE/SAM in Hepes buffer

PFL-AE (from IV.2.1) was mixed with SAM (from a 200 mM stock solution dissolved in 50 mM Hepes pH 7.5, 200 mM NaCl, and 1 mM DTT) to the final concentrations of 1.46 mM PFL-AE and 14.5 mM SAM. The resulting mixture (440 μ L) was flash-frozen and sent to MIT.

IV.2.3 PFL-AE/SAM/7-mer-Peptide in Hepes buffer

PFL-AE (from IV.2.1) was mixed with SAM (from a 200 mM stock solution dissolved in 50 mM Hepes pH 7.5, 200 mM NaCl, and 1 mM DTT), and then 7-mer-peptide (2.3 mg 7-mer-peptide dissolved in 50 mM Hepes pH 7.5, 200 mM NaCl, and 1 mM DTT) to the final concentrations of 1.35 mM PFL-AE, 13.6 mM SAM and 13.9 mM 7-mer peptide. The resulting mixture (220 μ L) was flash-frozen and sent to MIT.

IV.2.4 PFL-AE/SAM/PFL in Hepes buffer

PFL-AE (from IV.2.1) was mixed with SAM (from a 200 mM stock solution dissolved in 50 mM Hepes pH 7.5, 200 mM NaCl, and 1 mM DTT), and then PFL (from a 1.1 mM stock solution dissolved in 20 mM Hepes pH 7.2, 1mM DTT) to the final concentrations of 0.62 mM PFL-AE, 6.3 mM SAM and 0.62 mM PFL. The resulting mixture (240 μ L) was flash-frozen and sent to MIT.

IV.2.5 PFL-AE/SAM/YfiD in Hepes buffer

PFL-AE (from IV.2.1) was mixed with SAM (from a 200 mM stock solution dissolved in 50 mM Hepes pH 7.5, 200 mM NaCl, and 1 mM DTT), and then YfiD (from a 2.25 mM in 20mM Hepes pH 7.2, 1mM DTT) to the final concentrations of 0.88 mM PFL-AE, 9.1 mM SAM and 0.88 mM YfiD. The resulting mixture (440 μ L) was flash-frozen and sent to MIT.

IV.2.6 *PFL-AE in Tris-HCl buffer*

PFL-AE was purified in a buffer containing 50 mM Tris-HCl, pH 8.5, 200 mM NaCl and 1 mM DTT, and concentrated in a Coy chamber to a final concentration of 1.42 mM using an Amicon concentrator equipped with a YM-10 membrane. PFL-AE was determined by SDS-PAGE to be over 95 % pure and contained 4.1 Fe/AE.^{15, 16} A total volume of 1 mL was flash-frozen and sent to MIT.

IV.2.7 *PFL-AE/SAM/12-mer-Peptide in Tris-HCl buffer*

PFL-AE (from IV.2.6) was mixed with SAM (from a 200 mM stock solution dissolved in 50 mM Tris-HCl pH 7.4, 200 mM NaCl and 1 mM DTT), and then 12-mer-peptide (2.8 mg 12-mer-peptide pre-dissolved in 50 mM Tris-HCl pH 8.5, 200 mM NaCl and 1 mM DTT) to the final concentrations of 1.2 mM PFL-AE, 12 mM SAM and 3.6 mM 12-mer peptide. The resulting mixture (500 μ L) was flash-frozen and sent to MIT.

IV.3 Results and discussion

IV.3.1 Crystal structure of PFL-AE.

Protein crystals of the PFL-AE holoenzyme have been successfully grown from the PFL-AE/SAM in Hepes buffer sample under anaerobic conditions. The structure (Figure IV.3.1.1) shows that PFL-AE contains 10 α helices and 8 β sheets, most of which are part of a partial TIM barrel with the side and bottom open to the outside. The [4Fe-4S] cluster is located at the upper (C-terminal) side of this barrel. Three of the irons of the [4Fe-4S] cluster form additional covalent bonds to conserved cysteine residues (CX₃CX₂C). The fourth iron, designated as the unique iron, exhibits some electron density that may result from partial occupancy of the AdoMet binding site. The results are consistent with our previous results that PFL-AE contains a [4Fe-4S] cluster.^{8, 9} By far, PFL-AE has the most compact machinery for generation of 5'-deoxyadenosyl radical among AdoMet radical enzymes of known structure. However, the opening of this PFL-AE partial TIM barrel is the largest known in the superfamily and is thought to be related to the size of its substrate (170 kDa homodimeric PFL). PFL-AE has the largest substrate among all these radical enzymes, including coproporphyrinogen III oxidase,³ biotin synthase,⁴ MoaA,⁵ and LAM.⁶

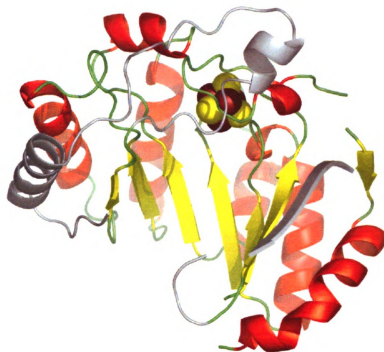


Figure IV.3.1.1. A ribbons diagram of the PFL-AE holoenzyme at 2.25Å resolution, viewing the barrel from "open" side. PFL-AE is a single domain enzyme with a partial TIM barrel (red/yellow) and very little other secondary structure (grey). The CxxCxxC motif, conserved in all Radical SAM proteins, is located at the top of the TIM barrel, coordinating three irons of the [4Fe-4S] cluster.

IV.3.2 Crystal Structure of PFL-AE with SAM and 7-mer peptide.

Crystals of PFL-AE with SAM and a 7-mer peptide (RVSGYAV) have been successfully grown under anaerobic conditions from the PFL-AE/SAM/peptide sample in Hepes buffer. The overall structure is similar to that of PFL-AE without SAM and peptide (Figure IV.3.2.1), however the opening of the barrel is now blocked by the binding of SAM and the 7-mer peptide. The amino and carboxylate groups of SAM coordinate the unique iron of the cluster, confirming the binding mode determined previously in our lab using ENDOR spectroscopy.^{12, 13} SAM is bound in between the iron-sulfur cluster and the 7-mer

peptide, and the distance between the 5' C of SAM and the G734 C α of the glycine residue is approximately 4 Å, suggesting a ready conformation for hydrogen abstraction from G734. This structure suggests that all the necessary components are well positioned prior to the formation of the 5'-deoxyadenosyl radical, and thus little movement of the extremely reactive 5'-deoxyadenosyl radical is required in order to abstract the hydrogen from the protein substrate.

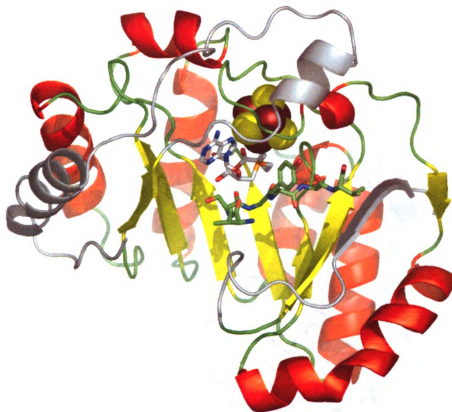


Figure IV.3.2.1. A ribbons diagram of the SAM and peptide bound form of PFL-AE at 2.88 Å resolution. View of the barrel from "open" side. SAM (white) and 7-mer peptide of PFL glycine loop (green) are shown in ball and stick.

IV.3.3 Comparison of the crystal structures of PFL-AE alone and with substrates bound.

The structures reported herein reveal that the only significant structural change upon binding SAM and peptide is the movement of a loop (Figure IV.3.3.1). The loop shown in blue moves in from the opening of the TIM barrel to the position shown in red upon binding of SAM and the peptide, and residues of the loop hydrogen bond to the bound peptide. This movement might imply that this loop serves as a gate to the TIM barrel, controlling the traffic of incoming substrates (SAM or the glycine loop of PFL). This movement might be related to

the activation of its protein substrate PFL. Further insight will require more crystal structures of PFL-AE with bound substrates.

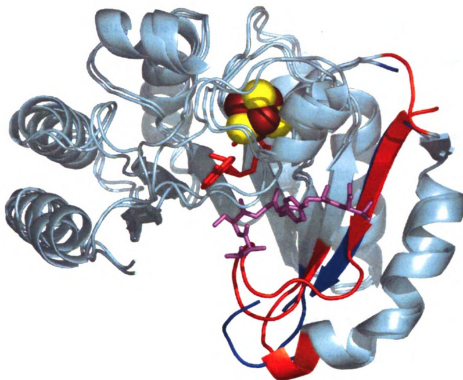


Figure IV.3.3.1. Structural comparison of the holoform and SAM/peptide bound form of PFL-AE. View of the barrel from "open" side. SAM (red) and 7-mer peptide of PFL glycine loop (purple) are shown in ball and stick. Upon binding of SAM and peptide, the β sheet and its adjacent loop (blue) is seen to move in from the opening side of PFL-AE (red).

IV.4 Conclusions

Spectroscopic methods have been successfully used in our lab over the past few years to investigate the structure and function of the iron sulfur cluster with or without its substrate SAM. Based on these results, we proposed a mechanism involving inner-sphere electron transfer with subsequent SAM cleavage and abstraction of a hydrogen atom from PFL G734.¹⁷

Crystallography is one of the best methods to structurally characterize enzymes and in so doing, to gain mechanistic insight. The focus of this research provided the first 3-D pictures of PFL-AE and its complex with substrates. We present herein the first crystal structures of PFL-AE, the holoform and the SAM/peptide bound form. The structures confirmed not only the presence of the iron-sulfur cluster at the top of the TIM barrel but also the binding mode between this cluster and the cosubstrate SAM. Structural comparison of the holoform and SAM/Peptide bound form of PFL-AE revealed an important conformational change of a small loop, which may gate the opening of the TIM barrel, strongly suggesting the involvement of this loop during the activation of PFL by PFL-AE.

IV.5 References

1. Cheek, J.; Broderick, J. B., Adenosylmethionine-dependent iron-sulfur enzymes: versatile clusters in a radical new role. *Journal of biological inorganic chemistry : JBIC : a publication of the Society of Biological Inorganic Chemistry* **2001**, 6, (3), 209-26.
2. Frey, P. A.; Magnusson, O. T., S-adenosylmethionine: A wolf in sheep's clothing, or a rich man's adenosylcobalamin? *Chemical Reviews (Washington, DC, United States)* **2003**, 103, (6), 2129-2148.
3. Layer, G.; Moser, J.; Heinz, D. W.; Jahn, D.; Schubert, W.-D., Crystal structure of coproporphyrinogen III oxidase reveals cofactor geometry of Radical SAM enzymes. *EMBO Journal* **2003**, 22, (23), 6214-6224.
4. Berkovitch, F.; Nicolet, Y.; Wan, J. T.; Jarrett, J. T.; Drennan, C. L., Crystal structure of biotin synthase, an S-adenosylmethionine-dependent radical enzyme. *Science (Washington, DC, United States)* **2004**, 303, (5654), 76-80.
5. Haenzelmann, P.; Schindelin, H., Crystal structure of the S-adenosylmethionine-dependent enzyme MoaA and its implications for molybdenum cofactor deficiency in humans. *Proceedings of the National Academy of Sciences of the United States of America* **2004**, 101, (35), 12870-12875.
6. Lepore, B. W.; Ruzicka, F. J.; Frey, P. A.; Ringe, D., The x-ray crystal structure of lysine-2,3-aminomutase from *Clostridium subterminale*. *Proceedings of the National Academy of Sciences of the United States of America* **2005**, 102, (39), 13819-13824.
7. Broderick, J. B.; Duderstadt, R. E.; Fernandez, D. C.; Wojtuszewski, K.; Henshaw, T. F.; Johnson, M. K., Pyruvate formate-lyase activating enzyme is an iron-sulfur protein. *Journal of the American Chemical Society* **1997**, 119, (31), 7396-7397.
8. Broderick, J. B.; Henshaw, T. F.; Cheek, J.; Wojtuszewski, K.; Smith, S. R.; Trojan, M. R.; McGhan, R. M.; Kopf, A.; Kibbey, M.; Broderick, W. E., Pyruvate formate-lyase-activating enzyme: Strictly anaerobic isolation yields active enzyme containing a [3Fe-4S]⁺ cluster. *Biochemical and Biophysical Research Communications* **2000**, 269, (2), 451-456.
9. Henshaw, T. F.; Cheek, J.; Broderick, J. B., The [4Fe-4S]¹⁺ Cluster of Pyruvate Formate-Lyase Activating Enzyme Generates the Glycyl Radical on Pyruvate Formate-Lyase: EPR-Detected Single Turnover. *Journal of the American Chemical Society* **2000**, 122, (34), 8331-8332.

10. Krebs, C.; Henshaw, T. F.; Cheek, J.; Huynh, B. H.; Broderick, J. B., Conversion of 3Fe-4S to 4Fe-4S Clusters in Native Pyruvate Formate-Lyase Activating Enzyme: Moessbauer Characterization and Implications for Mechanism. *Journal of the American Chemical Society* **2000**, 122, (50), 12497-12506.
11. Broderick, J. B.; Walsby, C.; Broderick, W. E.; Krebs, C.; Hong, W.; Ortillo, D.; Huynh, B. H.; Hoffman, B. M., [4Fe-4S] cluster of pyruvate formate-lyase activating enzyme and its interaction with S-adenosylmethionine. *Abstracts of Papers, 223rd ACS National Meeting, Orlando, FL, United States, April 7-11, 2002* **2002**, INOR-132.
12. Walsby, C. J.; Hong, W.; Broderick, W. E.; Cheek, J.; Ortillo, D.; Broderick, J. B.; Hoffman, B. M., Electron-Nuclear Double Resonance Spectroscopic Evidence That S-Adenosylmethionine Binds in Contact with the Catalytically Active [4Fe-4S]⁺ Cluster of Pyruvate Formate-Lyase Activating Enzyme. *Journal of the American Chemical Society* **2002**, 124, (12), 3143-3151.
13. Walsby, C. J.; Ortillo, D.; Broderick, W. E.; Broderick, J. B.; Hoffman, B. M., An Anchoring Role for FeS Clusters: Chelation of the Amino Acid Moiety of S-Adenosylmethionine to the Unique Iron Site of the [4Fe-4S] Cluster of Pyruvate Formate-Lyase Activating Enzyme. *Journal of the American Chemical Society* **2002**, 124, (38), 11270-11271.
14. Krebs, C.; Broderick, W. E.; Henshaw, T. F.; Broderick, J. B.; Huynh, B. H., Coordination of Adenosylmethionine to a Unique Iron Site of the [4Fe-4S] of Pyruvate Formate-Lyase Activating Enzyme: A Moessbauer Spectroscopic Study. *Journal of the American Chemical Society* **2002**, 124, (6), 912-913.
15. Fish, W. W., Rapid colorimetric micromethod for the quantitation of complexed iron in biological samples. *Methods Enzymol* **1988**, 158, 357-64.
16. Beinert, H., Micro methods for the quantitative determination of iron and copper in biological material. *Methods Enzymol* **1978**, 54, 435-45.
17. Walsby, C. J.; Ortillo, D.; Yang, J.; Nnyepi, M. R.; Broderick, W. E.; Hoffman, B. M.; Broderick, J. B., Spectroscopic Approaches to Elucidating Novel Iron-Sulfur Chemistry in the "Radical-SAM" Protein Superfamily. *Inorganic Chemistry* **2005**, 44, (4), 727-741.

CHAPTER V

SAM CLEAVAGE ASSAYS OF PFL-AE

V.1 Introduction

The function of PFL-AE is to generate a catalytically essential glycy radical on the residue G734 of PFL. Our current working hypothesis for PFL activation by PFL-AE is as follows.¹ The $[4\text{Fe-4S}]^{2+}$ cluster of PFL-AE situates AdoMet in the catalytic site of PFL-AE by forming a classic five-member chelate ring between the unique iron of the cluster and the methionine moiety of AdoMet. Such interaction brings the sulfonium of AdoMet in orbital overlap with the $[4\text{Fe-4S}]^{2+}$ cluster. The physiological reducing agent (reduced flavodoxin *in vivo*) then reduces the iron sulfur cluster to form the $[4\text{Fe-4S}]^{1+}$ -AdoMet complex. The inner-sphere electron transfer from the $[4\text{Fe-4S}]^{1+}$ cluster to the sulfonium of AdoMet initiates the homolytic S-C bond cleavage. Methionine, one of the two cleavage products of AdoMet, is left bound to the unique site of the oxidized $[4\text{Fe-4S}]^{2+}$ cluster, while the 5'-deoxyadenosyl radical intermediate, the other AdoMet cleavage product, activates PFL by abstracting the pro-S H from its residue G734. The catalytic

cycle is then repeated upon displacement of methionine and 5'-deoxyadenosine with a new AdoMet molecule. The activated PFL will then catalyze the conversion of pyruvate and CoA to acetyl CoA and formate by a mechanism that is still under debate.²⁻⁵

One interesting question regarding this proposed mechanism is: what is the trigger to induce electron transfer from the cluster to AdoMet to initiate the radical reaction? One possibility is that the interaction between PFL-AE/AdoMet and PFL provides the trigger, however other possibilities exist and the details of this initiation event remain unresolved. In 1994, Knappe and coworkers reported a weak SAM cleavage activity of PFL-AE in the absence of PFL.⁶ However, this result is questionable because the PFL-AE they used was purified aerobically and thus, presumably, had no iron-sulfur cluster (it was not even known at this time that PFL-AE contained an iron-sulfur cluster). In subsequent years, native PFL-AE was used in our lab to investigate the interaction of the iron sulfur cluster and cosubstrate SAM, and no evidence for SAM cleavage activity was observed.⁷⁻⁹ These latter experiments, however, were mostly carried out at 0 °C (which would slow any SAM cleavage reactions) and in the presence of excess SAM (which would drive PFL-AE to the SAM-bound state even if some of the SAM was cleaved). Furthermore, our only means of detecting SAM cleavage was via spectroscopic changes, since HPLC was not used routinely to monitor SAM cleavage. In addition, as reported in the previous chapter, the EPR spectra and catalytic activity of

PFL-AE have been shown to be significantly altered by the presence of potassium ion, a component that may be important to SAM cleavage and that was missing from essentially all earlier spectroscopic studies. In this chapter, we are going to use HPLC to monitor the SAM cleavage activity of PFL-AE in the presence of various small molecules and/or PFL. The correlation between the amount of the $[4\text{Fe-4S}]^{1+}$ cluster and the SAM cleavage activity of PFL-AE is another subject of this research.

V.2 Materials and Methods

PFL-AE was purified according to the published procedures¹⁰ except that 1 mM DTT was included in all buffers. Radiolabeled [2, 5', 8 – ³H] SAM was synthesized by other lab members according to the published procedures.¹¹ All buffers were deoxygenated using a vacuum/nitrogen gas manifold before being taken into the glove box. Solid chemicals were pumped in as solids. Ice was pre-chilled with liquid nitrogen before pumping into the glove box. Preparation of SAM cleavage samples was carried out in a Mbraun box with oxygen level less than 2 ppm.

V.2.1. SAM cleavage by as-isolated and reduced PFL-AE.

PFL-AE was mixed to a final concentration of 28.4 μ M in a buffer containing 150 mM Tris pH 7.5, 100 mM KCl, 5 mM DTT, 100 μ M 5-deazariboflavin, 10 mM oxamate, and 250 μ M [2, 5', 8 – ³H] SAM in a final volume of 100 μ L. One half of the reaction (50 μ L) was kept in the dark on ice as control. The other half (50 μ L) was transferred to an EPR tube and illuminated on ice for 1 hr. The resulting samples were then passed through a Microcon 3 kDa spin column. An aliquot (20 μ L) was loaded onto a C18 column and separated using the program described in section V.2.5.

The control experiment without PFL-AE was carried out exactly as described above except that PFL-AE was not included in the reaction mixture.

V.2.2 *Time course and stoichiometry for SAM cleavage by reduced PFL-AE.*

PFL-AE was mixed to a final concentration of 250 μ M in a buffer containing 150 mM Tris 7.5, 100 mM KCl, 5 mM DTT, 100 μ M 5-deazariboflavin, and 10 mM oxamate to a final volume of 2 mL. The reaction mixture was then transferred to an EPR tube and illuminated on ice for 0, 15, 30, 45, and 60 min. At each time point, 300 μ L was taken out of the EPR tube and flash-frozen in liquid nitrogen for EPR analysis. Meanwhile, 95 μ L this reaction was added to 5 μ L of [2,5',8 – 3 H] SAM (from a 5 mM stock solution) to make a final concentration of 250 μ M SAM. The resulting reactions were then incubated on ice in the dark for 1 hr, and passed through a Microcon 3 kDa spin column. An aliquot (20 μ L) was loaded onto the C18 column and separated using the program described in section V.2.5.

PFL-AE was mixed to a final concentration of 250 μ M in a buffer containing 150 mM Tris 7.5, 100 mM KCl, 5 mM DTT, 100 μ M 5-deazariboflavin, and 10 mM oxamate to a final volume of in a 600 μ L. The reaction mixture was then transferred to an EPR tube and illuminated on ice for 1 hr. After illumination, 300 μ L of this reaction was flash-frozen directly in liquid nitrogen for EPR analysis, and meanwhile 285 μ L of this reaction was added to 15 μ L of [2,5',8 – 3 H] SAM (from a 5 mM stock solution) to make a final concentration of 250 μ M SAM. After the resulting reaction was incubated on ice in the dark for 1, 5, 10, 20, 40, and 60 min, 50 μ L of the final reaction mixture was terminated by mixing with 5 μ L 1 M HCl, and then passed through

a Microcon 3 kDa spin column. An aliquot (20 μ L) was loaded onto a C18 column and separated using the program described in section V.2.5.

V.2.3 Effects of salt, glassing agent, and substrate on SAM cleavage.

The detailed components of each reaction are provided in the Results section associated with the relevant figure. In general, PFL-AE was mixed to a final concentration of 28.4 μ M in a buffer containing 150 mM Tris pH 7.5, 100 mM KCl (or NaCl, or none of these two), 5 mM DTT, 100 μ M 5-deazariboflavin, 10 mM oxamate (or none), 20 % (v/v) glycerol (or none), and 250 μ M [2, 5', 8 – 3 H] SAM to a final volume of 100 μ L. PFL, PFL R753K, or 12mer peptide (glycine loop mimic of PFL, Ac-IRVSGYAVRFNS-NH₂, purity >80 %) was added to a final concentration of 250 μ M to some of the reactions. After the reaction mixture was transferred to an EPR tube and illuminated on ice for 1 hr, it was then passed through a Microcon 3 kDa spin column. An aliquot (20 μ L) was loaded onto the C18 column and separated using the program described in section V.2.5.

V.2.4 Time course for substrate effects on SAM cleavage.

PFL-AE was mixed to a final concentration of 28.4 μ M in a buffer containing 150 mM Tris 7.5, 100 mM KCl, 5 mM DTT, 100 μ M 5-deazariboflavin, 10 mM oxamate, 250 μ M [2, 5', 8 – 3 H] SAM, and 250 μ M PFL (PFL, PFL R753K, PFL G734A, 12mer peptide, or none of these) to a final

volume of 100 μ L. After the reaction mixture was illuminated on ice for 0, 5, 10, 15, and 20 min, an aliquot (30 μ L) was removed and passed through a Microcon 3 kDa spin column. The resulting sample was then loaded onto a C18 column for separation using the program described in section V.2.5.

V.2.5. HPLC analysis of SAM cleavage.

The samples prepared as described above were thawed for 1 min, and then a portion (20 μ L) was loaded onto a C-18 column [Waters Spherisorb Reversed-Phase C18] and run with the following program. Elution was performed at 1 mL/min with a step gradient (3 min at 100 % buffer A (MQ, 0.1 % TFA), 14 min at 82 % buffer A, 6 min at 100 % buffer B (100 % Acetonitrile, 0.1 % TFA)). Under these conditions, SAM elutes at 3.0 mL and 5dAdo elutes at 6.8 mL. Fractions off the column were collected every 1 min and were added to 15 mL scintillation fluid (High Flash Point Cocktail Safety-Solve #111177, Research Products International Corp.). Liquid scintillation counting (LSC) was performed on each fraction using a Wallac 1414-001 Liquid Scintillation Counter.

V.3 Results and Discussion

V.3.1 SAM cleavage by PFL-AE occurs in the absence of PFL.

An important question regarding our current working hypothesis for PFL activation by PFL-AE is whether the interaction with PFL triggers the electron transfer from the cluster to AdoMet and resulting homolytic S-C bond cleavage. In an effort to solve this problem, experiments as described in section V.2.1 were carried out to investigate the SAM cleavage activity in the absence of PFL. The results are presented in Figure V.3.1.1. In the absence of PFL-AE, SAM was stable on ice in the reaction medium containing Tris pH 7.5, KCl, DTT, 5-deazariboflavin, and oxamate under both dark and illumination conditions. In the presence of as-isolated PFL-AE (containing $[4\text{Fe-4S}]^{2+}$ clusters), no significant SAM cleavage activity was observed. In contrast, after PFL-AE was reduced to the $[4\text{Fe-4S}]^{1+}$ state, the amount of SAM cleaved was greatly increased. The results demonstrate that SAM cleavage occurs in the presence of PFL-AE/ $[4\text{Fe-4S}]^{1+}$, even in the absence of substrate PFL.

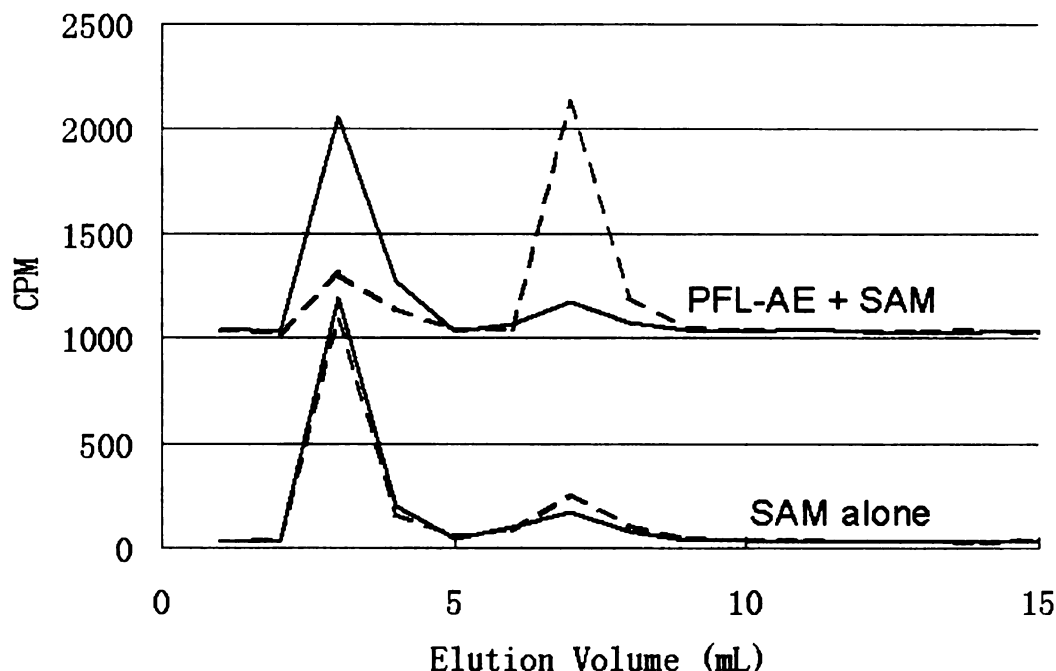


Figure V.3.1.1. HPLC chromatograms of SAM cleavage assays in the absence of PFL. Shown are CPMs of fractions vs. elution volumes in the absence (lower two lines) and in the presence (upper two lines) of PFL-AE. PFL-AE was 28.4 μ M in a buffer containing 150 mM Tris 7.5, 100 mM KCl, 5 mM DTT, 100 μ M 5-deazariboflavin, 10 mM oxamate, and 250 μ M [2, 5', 8 - 3 H] SAM. One half of the reaction was kept in the dark on ice as control (solid lines). The other half (dashed lines) was illuminated on ice for 1 hr. The resulting samples were then passed through a Microcon 3 kDa spin column. An aliquot (20 μ L) was loaded onto the C18 column and separated using the program described in section V.2.5. Under these conditions, SAM elutes at 3.0 mL and 5dAdo elutes at 6.8 mL.

V.3.2 One SAM is cleaved per [4Fe-4S] $^{1+}$ cluster in PFL-AE.

In the experiments described in the previous section (Figure V.3.1.1), the reduced PFL-AE was shown to cleave SAM in the absence of PFL. However, it was possible that this activity was caused by contaminants in the purified PFL-AE. In an effort to rule out this possibility, the iron-sulfur clusters of PFL-AE were first photoreduced to the +1 state, and then mixed with SAM in the dark to monitor the SAM cleavage activity. The amount of [4Fe-4S] $^{1+}$

cluster in each sample prior to addition of SAM was quantified by EPR, and the amount of SAM cleaved by each sample was quantified by HPLC analysis. The samples after addition of SAM and incubation in the dark for 1 hour were loaded onto a C-18 column and run with the program described in section V.2.5. Under these conditions, SAM eluted at 3.0 mL and 5dAdo eluted at 6.8 mL. The remaining amount of SAM and 5dAdo were calculated based on their radioactivity (CPM) in corresponding fractions. The results (Figure V.3.2.1) show that the cleavage of SAM is stoichiometric with the amount of the $[4\text{Fe-4S}]^{1+}$ clusters present in PFL-AE. These results are consistent with our previous report that one $[4\text{Fe-4S}]^{1+}$ cluster generates one PFL glycyl radical.⁹ Now we can fill in the details implied by the earlier studies: that one $[4\text{Fe-4S}]^{1+}$ cluster of PFL-AE cleaves one SAM, generating one 5'-deoxyadenosyl radical, which generates one glycyl radical on PFL.

Figure V.3.2.2. is the time course for SAM cleavage by reduced PFL-AE. After PFL-AE was photoreduced on ice for 1 h, the amount of $[4\text{Fe-4S}]^{1+}$ cluster was 234 μM based on the quantification of its EPR signal. Subsequent incubation of this reduced PFL-AE/ $[4\text{Fe-4S}]^{1+}$ cluster on ice in dark in the presence of added 250 μM SAM resulted in a steady cleavage of SAM. After 60 min incubation in dark on ice, the amount of SAM cleaved in the sample containing PFL-AE was 167 μM more than the control sample based on HPLC separation of the final components of the reactions. These experiments revealed that SAM cleavage in the absence of PFL was not a fast

reaction, and moreover the slow rate of cleavage is likely the reason we did not notice this activity in our previous studies.

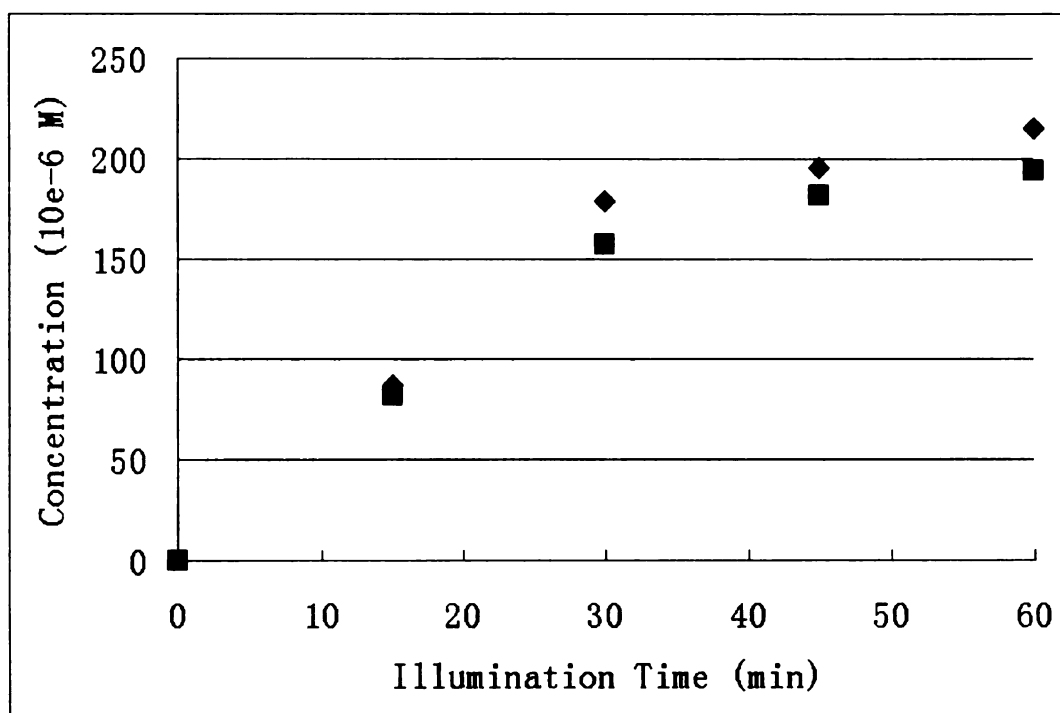


Figure V.3.2.1. Stoichiometry of SAM cleavage by PFL-AE [4Fe-4S]¹⁺. Shown are the quantitation of the [4Fe-4S]¹⁺ cluster (◆) and 5dAdo (■) as a function of illumination time. The amount of the [4Fe-4S]¹⁺ cluster was quantified by the double integration of its EPR signal. The amount of SAM being cleaved was calculated based on CPMs of the fractions after HPLC separation of the reaction components. PFL-AE was 250 μM in a buffer containing 150 mM Tris 7.5, 100 mM KCl, 5 mM DTT, 100 μM 5-deazariboflavin, and 10 mM oxamate. After the reaction was illuminated on ice for 0, 15, 30, 45, 60 min, 300 μL was flash-frozen in liquid nitrogen for EPR analysis. Meanwhile, 95 μL this reaction was added with 5 μL SAM to a final concentration of 250 μM SAM. Afterwards, the resulting reaction was incubated on ice in the dark for 1hr. The final reactions were then passed through a Microcon 3 kDa spin column. An aliquot (20 μL) was loaded onto the C18 column and separated using the program described in section V.2.5.

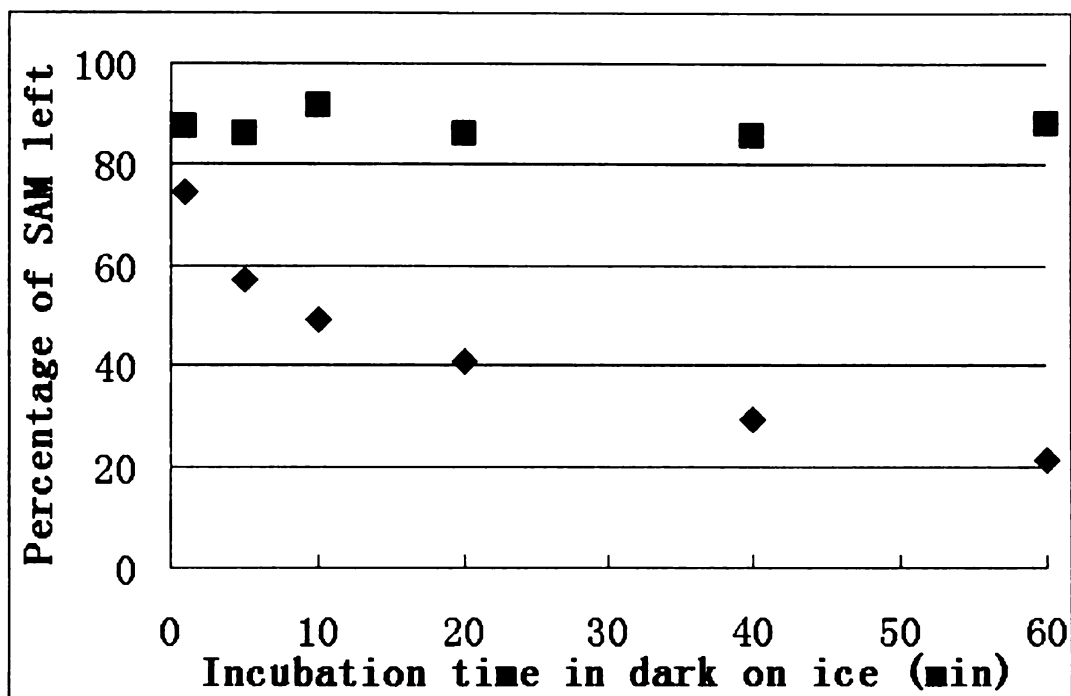


Figure V.3.2.2. Time course for SAM cleavage by reduced PFL-AE. Shown are percentages of SAM left after various time of incubation in dark on ice in the absence (■) and in the presence (◆) of reduced PFL-AE. PFL-AE was 250 μ M in a buffer containing 150 mM Tris 7.5, 100 mM KCl, 5 mM DTT, 100 μ M 5-deazariboflavin, and 10 mM oxamate. After the reaction was illuminated on ice for 1 hr, 300 μ L was flash-frozen directly in liquid nitrogen for EPR analysis, and meanwhile 285 μ L of this reaction was added with 15 μ L SAM to a final concentration of 250 μ M [2, 5', 8 - 3 H] SAM. After the resulting reaction was incubated on ice in dark for different time (1, 5, 10, 20, 40, and 60 min as indicated above), 50 μ L of the final reactions were removed and terminated by mixing with 5 μ L 1 M HCl, and then passed through a Microcon 3 kDa spin column. An aliquot (20 μ L) was loaded onto the C18 column and separated using the program described in section V.2.5. The amount of $[4\text{Fe-4S}]^{1+}$ cluster was 234 μ M based on the quantification of its EPR signal. After 60 min incubation in dark on ice, the amount of SAM cleaved in the sample containing PFL-AE is 167 μ M more than the control sample based on HPLC separation of the final components of the reactions.

V.3.3 Effects of buffer components and substrates on rates of SAM cleavage.

So far, we have found that many components in the reaction medium, including glycerol, KCl and oxamate, can affect the EPR spectra of PFL-AE in the presence or absence of SAM. The following set of experiments was designed to investigate whether these components have any effects on the SAM cleavage activity (Figure V.3.3.1).

Reaction mixtures containing PFL-AE, SAM (~ 9 fold excess over PFL-AE), and other components were photoreduced for one hour, and the amount of SAM remaining was analyzed by HPLC. The results are summarized in Figure V.3.3.1. In the absence of PFL-AE 76 % of the SAM remained, indicating that SAM alone is fair stable under these conditions. In contrast, only 22 % of the original SAM remained after one hour photoreduction in the presence of PFL-AE. Several molecules that were reported in the previous chapter to affect PFL-AE activity and spectral properties (e.g. glycerol, KCl, and oxamate) all had significant effects on the rate of SAM cleavage. The presence of KCl and oxamate increased the SAM cleavage activities while glycerol inhibited this activity; these results parallel those reported in the previous chapter. The sample (PFL-AE + SAM + glycerol – KCl – oxamate), the condition most similar to most of our previous PFL-AE spectroscopic experiments, showed almost no SAM cleavage activity above background.

The common feature of the last three samples shown in Figure V.3.3.1 compared to all previous samples is that they all contain the catalytically essential protein core, the glycine loop, either as PFL, PFL R753K, or the 12-mer glycine loop peptide. All these samples show much higher rates of SAM cleavage, suggesting the glycine loop increases the rate of SAM cleavage by PFL-AE. A more detailed study of PFL mutants is discussed in the next section.

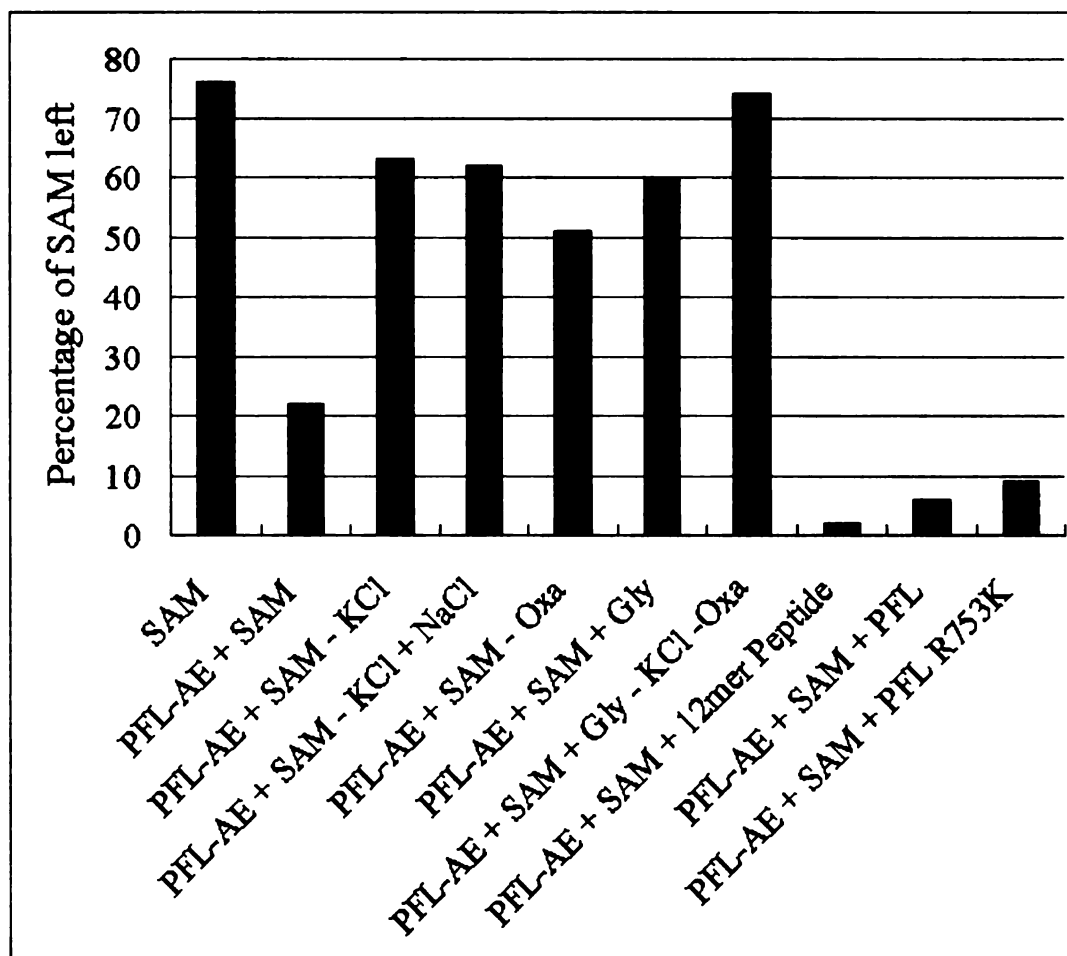


Figure V.3.3.1. Effects of various components on the SAM cleavage activity. Shown are the percentages of SAM left after 1 hr illumination on ice in the presence of various components. PFL-AE was 28.4 μ M in a buffer reaction containing 150 mM Tris 7.5, 100 mM KCl (or NaCl, or none of these two), 5 mM DTT, 100 μ M 5-deazariboflavin, 10 mM oxamate (or none), 20 % (v/v) glycerol (or none), and 250 μ M [2, 5', 8 - 3 H] SAM. PFL, PFL R753K and 12mer peptide (glycine loop mimic of PFL) were added to the last three samples to a final concentration of 250 μ M. After the reaction was illuminated on ice for 1 hr, it was then passed through a Microcon 3 kDa spin column. An aliquot (20 μ L) was loaded onto the C18 column and separated using the program described in section V.2.5. Oxa, oxamate; Gly, 20 % (v/v) glycerol.

Sample	SAM	PFL-AE + SAM	PFL-AE + SAM - KCl	PFL-AE + SAM - KCl + NaCl	PFL-AE + SAM - Oxa
PFL-AE		28.4 μ M	28.4 μ M	28.4 μ M	28.4 μ M
Tris pH 7.5	150 mM	150 mM	150 mM	150 mM	150 mM
KCl	100 mM	100 mM			100 mM
NaCl				100 mM	
DTT	5 mM	5 mM	5 mM	5 mM	5 mM
5-deaza- riboflavin	100 μ M	100 μ M	100 μ M	100 μ M	100 μ M
Oxamate	10 mM	10 mM	10 mM	10 mM	
[2, 5', 8 – ³ H] SAM	250 μ M	250 μ M	250 μ M	250 μ M	250 μ M

Sample	PFL-AE + SAM + Gly	PFL-AE + SAM + Gly - KCl - Oxa	PFL-AE + SAM + 12-mer Peptide	PFL-AE + SAM + PFL	PFL-AE + SAM + PFL R753K
PFL-AE	28.4 μ M	28.4 μ M	28.4 μ M	28.4 μ M	28.4 μ M
Tris pH 7.5	150 mM	150 mM	150 mM	150 mM	150 mM
KCl	100 mM		100 mM	100 mM	100 mM
DTT	5 mM	5 mM	5 mM	5 mM	5 mM
5-deaza- riboflavin	100 μ M	100 μ M	100 μ M	100 μ M	100 μ M
Oxamate	10 mM		10 mM	10 mM	10 mM
[2, 5', 8 – ³ H] SAM	250 μ M	250 μ M	250 μ M	250 μ M	250 μ M
Glycerol	20 % (w/v)	20 % (w/v)			
12-mer peptide			250 μ M		
PFL				250 μ M	
PFL R753K					250 μ M

Table V.3.3.1. Components and corresponding concentrations for each of the sample in Figure V.3.3.1.

V.3.4 PFL mutants affect SAM cleavage by PFL-AE.

As was mentioned in the previous section, the presence of the PFL glycine loop greatly increases the rates of SAM cleavage by PFL-AE. In an effort to further investigate this phenomenon, the rates of SAM cleavage in the presence of PFL, PFL homologs, and PFL mutants was investigated. SAM was incubated with PFL-AE (0.1 x SAM concentration), buffer components (as indicated in Figure V.3.4.1), and PFL or homologs or mutants (at 1.0 x SAM concentration). Samples were illuminated for 20 minutes, with aliquots taken every 5 min to test for SAM cleavage. The results are summarized in Figure V.3.4.1.

In the absence of any glycine loop (sample PFL-AE), the rate of SAM cleavage by PFL-AE was $0.124 \mu\text{M}(\text{SAM}) \text{ min}^{-1} \mu\text{M}(\text{PFL-AE})^{-1}$. In the presence of the intact glycine loop (PFL, YfiD, or PFL R753K), the rate of SAM cleavage is increased. PFL, the natural substrate of the PFL activation reaction, is the most efficient protein in enhancing SAM cleavage activity, resulting in a rate of $0.324 \mu\text{M}(\text{SAM}) \text{ min}^{-1} \mu\text{M}(\text{PFL-AE})^{-1}$. Although both PFL R753K and YfiD also contain the same glycine loop as PFL, their reactions showed a slightly lower enhancement of the rate of SAM cleavage (rates of $0.247 \mu\text{M}(\text{SAM}) \text{ min}^{-1} \mu\text{M}(\text{PFL-AE})^{-1}$ and $0.305 \mu\text{M}(\text{SAM}) \text{ min}^{-1} \mu\text{M}(\text{PFL-AE})^{-1}$, respectively). This suggests that mutation of a residue close to the glycine loop (PFL R753K) or the lack of the other domains of PFL (YfiD) may affect the overall configuration of PFL, which in turn may affect the interaction with PFL-AE that results in enhancement of the rate of SAM cleavage. Such results were expected

because the glycine loop is the target substrate of the 5'-deoxyadenosyl radical, which is generated by the homolytic cleavage of S-C bond of SAM by PFL-AE. Interestingly, however, PFL G734A, which has a mutated glycine loop, inhibits SAM cleavage ($0.053 \mu\text{M}(\text{SAM}) \text{ min}^{-1} \mu\text{M}(\text{PFL-AE})^{-1}$) relative to the rate with PFL-AE alone. This suggests that some of the rate enhancement of SAM cleavage may be a result of a concerted reaction requiring an abstractable hydrogen at G734.

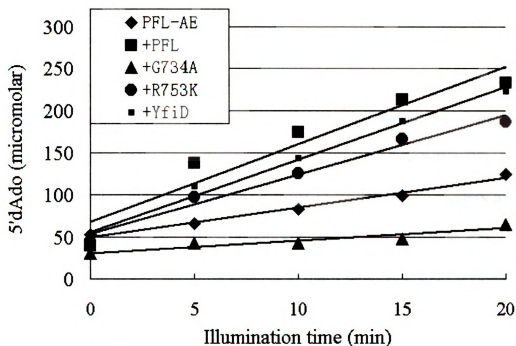


Figure V.3.4.1. Time course of the SAM cleavage by PFL-AE in the presence of PFL, YfiD, and PFL mutants. PFL-AE was 28.4 μM in a buffer containing 150 mM Tris 7.5, 100 mM KCl, 5 mM DTT, 100 μM 5-deazariboflavin, 10 mM oxamate, 250 μM [2, 5', 8- ^3H] SAM, and 250 μM PFL (PFL, PFL R753K, PFL G734A, YfiD, or none of these). After the reaction was illuminated on ice for 0, 5, 10, 15, and 20 min, an aliquot (30 μL) was then passed through a Microcon 3 kDa spin column and loaded onto a C18 column for separation using the program described in section V.2.5.

Sample	Linear fitting of above SAM cleavage data	Calculated SAM cleavage rate $\mu\text{M}(\text{SAM}) \text{ min}^{-1} \mu\text{M}(\text{PFL-AE})^{-1}$
PFL-AE + PFL	$y = 9.214x + 67.62$ $R^2 = 0.9136$	0.324
PFL-AE + YfiD	$y = 8.664x + 55.24$ $R^2 = 0.9858$	0.305
PFL-AE + PFL R753K	$y = 7.028x + 54.08$ $R^2 = 0.9784$	0.247
PFL-AE	$y = 3.534x + 49.94$ $R^2 = 0.9860$	0.124
PFL-AE + PFL G734A	$y = 1.498x + 30.88$ $R^2 = 0.8802$	0.053

Table V.3.4.1. Linear fitting of the time course of the SAM cleavage by PFL-AE in the presence of PFL, YfiD, and PFL mutants.

V.4 Conclusions

Homolytic cleavage of the S-C bond of SAM is a mandatory step in producing the catalytically essential 5'-deoxyadenosyl radical, the intermediate radical responsible for abstracting a hydrogen atom from various substrates in the radical SAM superfamily enzymes. In this chapter, we show that in PFL-AE, the SAM cleavage reaction is the direct result of the $[4\text{Fe-4S}]^{1+}$ clusters and this reaction can proceed in the absence of its protein substrate PFL. In addition, the rate of this reaction is affected by many other seemingly unrelated components, such as glycerol, oxamate, and the potassium ion. These results are consistent with the enzyme activity and EPR spectroscopic results described in the previous chapter, in which these components affect the EPR signal of the reduced PFL-AE. The intact glycine loop of PFL, as seen in several PFL mutants, increases the efficiency of SAM cleavage. In contrast, PFL G734A, which includes a mutated glycine loop, inhibits this activity, suggesting the importance of the G734 residue in the SAM cleavage reaction.

V.5 References

1. Walsby, C. J.; Ortillo, D.; Yang, J.; Nnyepi, M. R.; Broderick, W. E.; Hoffman, B. M.; Broderick, J. B., Spectroscopic Approaches to Elucidating Novel Iron-Sulfur Chemistry in the "Radical-SAM" Protein Superfamily. *Inorganic Chemistry* **2005**, *44*, (4), 727-741.
2. Becker, A.; Fritz-Wolf, K.; Kabsch, W.; Knappe, J.; Schultz, S.; Wagner, A. F. V., Structure and mechanism of the glycyl radical enzyme pyruvate formate-lyase. *Nature Structural Biology* **1999**, *6*, (10), 969-975.
3. Becker, A.; Kabsch, W., X-ray Structure of Pyruvate Formate-Lyase in Complex with Pyruvate and CoA. *Journal of Biological Chemistry* **2002**, *277*, (42), 40036-40042.
4. Parast, C. V.; Wong, K. K.; Lewisch, S. A.; Kozarich, J. W.; Peisach, J.; Magliozzo, R. S., Hydrogen Exchange of the Glycyl Radical of Pyruvate Formate-Lyase Is Catalyzed by Cysteine 419. *Biochemistry* **1995**, *34*, (8), 2393-9.
5. Lehtioe, L.; Leppaenen, V. M.; Kozarich, J. W.; Goldman, A., Structure of Escherichia coli pyruvate formate-lyase with pyruvate. *Acta Crystallographica, Section D: Biological Crystallography* **2002**, *D58*, (12), 2209-2212.
6. Frey, M.; Rothe, M.; Wagner, A. F. V.; Knappe, J., Adenosylmethionine-dependent synthesis of the glycyl radical in pyruvate formate-lyase by abstraction of the glycine C-2 pro-S hydrogen atom. Studies of [2H]glycine-substituted enzyme and peptides homologous to the glycine 734 site. *Journal of Biological Chemistry* **1994**, *269*, (17), 12432-7.
7. Krebs, C.; Broderick, W. E.; Henshaw, T. F.; Broderick, J. B.; Huynh, B. H., Coordination of Adenosylmethionine to a Unique Iron Site of the [4Fe-4S] of Pyruvate Formate-Lyase Activating Enzyme: A Moessbauer Spectroscopic Study. *Journal of the American Chemical Society* **2002**, *124*, (6), 912-913.
8. Walsby, C. J.; Ortillo, D.; Broderick, W. E.; Broderick, J. B.; Hoffman, B. M., An Anchoring Role for FeS Clusters: Chelation of the Amino Acid Moiety of S-Adenosylmethionine to the Unique Iron Site of the [4Fe-4S] Cluster of Pyruvate Formate-Lyase Activating Enzyme. *Journal of the American Chemical Society* **2002**, *124*, (38), 11270-11271.
9. Henshaw, T. F.; Cheek, J.; Broderick, J. B., The [4Fe-4S]¹⁺ Cluster of

Pyruvate Formate-Lyase Activating Enzyme Generates the Glycyl Radical on Pyruvate Formate-Lyase: EPR-Detected Single Turnover. *Journal of the American Chemical Society* **2000**, 122, (34), 8331-8332.

10. Broderick, J. B.; Henshaw, T. F.; Cheek, J.; Wojtuszewski, K.; Smith, S. R.; Trojan, M. R.; McGhan, R. M.; Kopf, A.; Kibbey, M.; Broderick, W. E., Pyruvate formate-lyase-activating enzyme: Strictly anaerobic isolation yields active enzyme containing a [3Fe-4S]⁺ cluster. *Biochemical and Biophysical Research Communications* **2000**, 269, (2), 451-456.

11. Walsby, C. J.; Hong, W.; Broderick, W. E.; Cheek, J.; Ortillo, D.; Broderick, J. B.; Hoffman, B. M., Electron-Nuclear Double Resonance Spectroscopic Evidence That S-Adenosylmethionine Binds in Contact with the Catalytically Active [4Fe-4S]⁺ Cluster of Pyruvate Formate-Lyase Activating Enzyme. *Journal of the American Chemical Society* **2002**, 124, (12), 3143-3151.

CHAPTER VI

INVESTIGATION ON THE INTERACTION OF PFL-AE AND PFL

VI.1 Introduction

PFL and its activating enzyme (PFL-AE) are critical for facultative anaerobes to survive oxygen stress by switching on anaerobic glucose metabolism. This process is composed of two separate steps: Step 1 is the post-translational modification of PFL by PFL-AE, which activates PFL by generating a glycyl radical on its residue G734; this reaction occurs only under anaerobic conditions. In step 2, the activated PFL catalyzes the reaction of pyruvate with CoA to formate and acetyl CoA. Much has been learned about these two proteins individually, however little is known about how PFL-AE and PFL interact with each other during the activation reaction. In this chapter, two PFL mutants (PFL G734A and PFL R753K) and a PFL homolog (YfiD) are utilized to address the interaction during activation.

PFL G734A is a catalytic site mutant of the wildtype PFL. The primary reason for using this mutant is that the G734 residue of the wildtype PFL harbors a pro-S hydrogen, which is abstracted to generate a stable glycyl radical on G734. Replacement of G734 by alanine abolishes the pro-S hydrogen; as a

result, no glycy radical can be generated in this PFL G734A mutant.¹ The use of this mutant is thus expected to allow us to preserve the catalytically active [4Fe-4S]¹⁺/AdoMet complex in the presence of PFL G734A to form a ternary activation complex. Because a glycine to alanine mutation represents a small structural change, the mutation of G734 to alanine is expected to preserve the overall conformation of PFL, an essential prerequisite to investigate the ternary complex.

PFL R753K is another interesting mutant of wildtype PFL. The residue R753 is located at the surface of PFL with its side chain pointing toward the catalytic site. The primary function, based on the crystal structures of the inactive form of PFL, is to form a hydrogen bond with V752, one of the glycine loop residues. As a result of this interaction, it stabilizes the glycine loop of PFL. There are two reasons this residue has been mutated to K753. First, the PFL-AE/PFL system is similar to that of the glycerol dehydratase (GD) and the GD-activating enzyme (GD-AE).² The GD/GD-AE system catalyzes the dehydration of glycerol to 3-hydroxypropionaldehyde (3-HPA).³ GD-AE, a radical SAM enzyme like PFL-AE, activates GD by generating a stable glycy radical on GD under strictly anaerobic conditions.² GD, which also adopts a similar 10-stranded α/β barrel motif as PFL and ARNR (anaerobic ribonucleotide reductase),² is the actual catalytic enzyme for the dehydration of glycerol mediated by a thiyl radical transferred from a glycy radical.² Second, the C-terminal domains (Figure VI.1.1) of both GD and PFL align well and exhibit structural properties consistent with these domains being the docking sites for the activating enzyme. Interestingly, a single point mutation at a strictly conserved arginine residue (R782K) in the GD

results in the formation of a tight GD/GD-AE complex *in vivo*. Therefore, by analogy we proposed that mutation of the corresponding residue of PFL (R753) to lysine might result in the formation of a similar tight complex between PFL-AE and PFL. Formation of this complex would be of interest because it might allow us to investigate the interaction between PFL and PFL-AE, and perhaps trap important intermediates as well.

```

GD  731-GFHVQFNVIDKKILLAAQKNPEKYQDLIVRVAGYSAQFISLDKSIQNDIART-783
      : : : : : : : : : : : : : : : : : : : : : : : : : : : : : : : :
PFL 703-GQHLLNVNMNREMLLDAMENPEKYPQLTIRVSGYAVRFNSLTKEQQQDVITRT-754

```

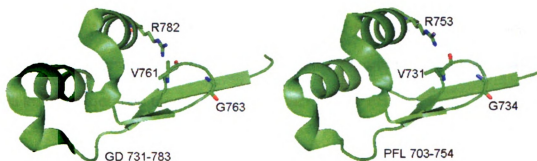


Figure VI.1.1. Sequence and structural comparison of the C-terminal domains of PFL and GD. In the sequence comparison (top), identical residues are colored red and similar residues blue. In the structural comparison, the strictly conserved residues in the GD and PFL models are represented as sticks with the carbon atoms colored green, oxygen atoms colored red, and nitrogen atoms colored blue. The distance between the side chain of R782 and the backbone carbonyl oxygen of residue 761 in GD is 2.76 Å. The distance between the side chain of R753 and the backbone carbonyl oxygen of residue 732 in PFL is 2.75 Å. PFL and GD structures were made from PDB files 1H16 and 1R9D, respectively.^{2,4}

As has been mentioned in the introduction part of this dissertation, the PFL glycy radical remains very stable under strict anaerobic conditions ($t_{1/2} > 24\text{hr}$).⁵ However, this radical is extremely susceptible to oxygen and

exposure to oxygen results in protein cleavage into two smaller pieces (PFL1-733 and PFL734-760).⁶⁻⁸ YfiD, which shares significant sequence homology with the C-terminus of PFL (Figure VI.1.2), contains the important glycine loop of PFL and salvages this oxygen damaged species PFL1-733.⁹ Based on crystal structures of PFL,^{4, 10} the C-terminal region forms a relatively independent domain and may be the docking area of PFL-AE. Taken together, these results suggest that YfiD has a good possibility of forming a tight binding complex with PFL-AE. YfiD R120K, the corresponding mutation to PFL R753K, was also made in an effort to take advantage of both the minimal potential docking domain and the conserved arginine residue, which results in the tight complex between GD and GD-AE. We are hoping that by investigating PFL, YfiD, and their mutants, we can better understand the interaction between PFL and PFL-AE. Eventually, this will lead to a detailed mechanistic proposal for the PFL activation.

YfiD 70-GQHLLNVNVLRR^{LEDAVKHPEKYPQLT}IRVSGYAVRFNSLTPEQQRDVIARTFTESL-126

 PFL 703-GQHLLNVNVMNR^{EMLLDAMENPEKYPQLT}IRVSGYAVRFNSLTKEQQQDVI^{TRTFTQSM}-759

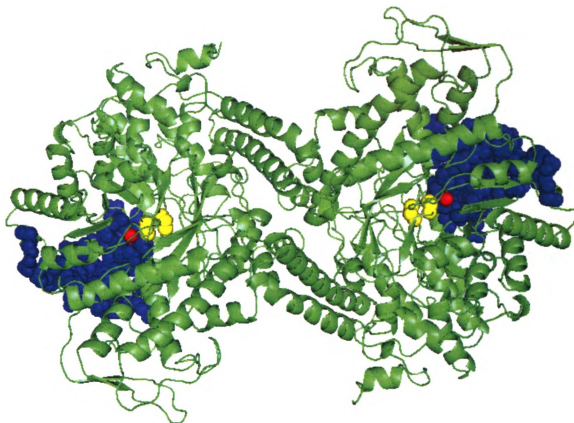


Figure VI.1.2. Top, sequence comparison of the C-terminal domains of PFL and the YfiD. Identical residues are colored red and similar residues blue. Bottom, cartoon diagram of PFL with the C-terminal region corresponding to YfiD shown as a blue space-filled model. G734 is shown in red, while C418 and C419 are shown in yellow.

VI.2 Materials and Methods

Materials

All chemicals used were commercially obtained except when noted otherwise and were of the highest purity. BL21(DE3)pLysS competent cells were purchased from NovagenTM. QuikChange Site-Directed Mutagenesis Kit was purchased from Stratagene. All columns and resins were purchased from Amersham Biosciences and Waters Corporations. SDS-PAGE gels were commercially obtained from Bio-Rad Scientific.

Preparation of EPR and ENDOR samples were carried out in an anaerobic glove box (Mbraun) with oxygen level less than 2 ppm. All buffers were deoxygenated using a vacuum/nitrogen gas manifold before being taken into the glove box. Solid chemicals were pumped in as solids. Ice was pre-chilled with liquid nitrogen before pumping into the glove box.

VI.2.1 Expression and Purification of PFL G734A

The pkk-pflG734A plasmid (hereafter designated pTHXI67) used in this work had been made in our lab by former members. A single colony of *E. coli* BL21(DE3)pLysS competent cells transformed with pTHXI67 was used to inoculate 50 mL of Luria/Bertani (Miller's Modification)¹¹ medium containing 50 µg/mL of ampicillin. This culture was grown to saturation at 37 °C and used to inoculate 1 L LB/ampicillin in a 2800 mL Fernbach flask (5 mL overnight culture per 1 L). The 1 L cultures were grown at 37 °C with shaking (250 rpm). When the culture reached an OD₆₀₀ = 0.7-0.8, isopropyl β-D-thiogalacto-pyranoside (IPTG)

was added to 1 mM final concentration to induce the overexpression of PFL G734A. The cultures were grown for an additional 3 hours, and then were harvested by centrifugation at 4 °C and stored under nitrogen at –80 °C for further use.

Cells pellets were resuspended in lysis buffer (20 g / 50 mL) containing 20 mM Hepes pH 7.2, 1% Triton X-100, 5% glycerol, 10 mM MgCl₂, 1 mM PMSF, 10 mg lysozyme, and 0.5 mg each of DNase I and RNase A. This suspension was agitated for one hour until homogenous and then centrifuged at 27,000 x g for 30 mins at 4 °C.

The resulting crude extract was separated into ~15 mL aliquots, which were loaded separately onto a HiLoad 26/10 Q Sepharose HP column that had been previously equilibrated with 20 mM Hepes pH 7.2, 1 mM DTT. Immediately following sample injection, the column was flushed with the low ionic strength buffer (buffer A: 20 mM Hepes pH 7.2, 1 mM DTT) for 10 minutes at a rate of 2 ml/min in order to wash out the proteins that were not bound specifically by the column. Following the initial wash, the column was eluted with a steadily increasing ionic strength starting from 100 % buffer A to 100 % buffer B (20 mM Hepes pH 7.2, 500 mM NaCl, 1mM DTT) over 80 mins with a total combined flow rate of 2 ml/min. When the eluent composition reached 100 % buffer B, it was kept isocratic for 10 minutes at a rate of 2 ml/min to clean the column. Under these conditions, PFL G734 started to elute out of the column at approximately 375 mM NaCl and was collected in 4 mL fractions. The fractions were analyzed using SDS-PAGE in order to determine the quantity and purity of PFL G734 in

each. Based on the SDS-PAGE results, fractions from all separate runs containing PFL G734A as > 50% of total protein were pooled together and concentrated down to ~ 10 mL. To the pooled fractions was then added 30 mL buffer C (20 mM Hepes pH 7.2, 1 M $(\text{NH}_4)_2\text{SO}_4$, 1 mM DTT) followed by concentrating down to ~ 10 mL using an Amicon concentrator equipped with a YM-30 membrane. After these two steps were repeated 2 more times, the protein was again concentrated down to less than 10 mL.

The resulting partially purified PFL G734A was then loaded onto a HiLoad 16/10 Phenyl Sepharose HP column that had been previously equilibrated with buffer C (20 mM Hepes pH 7.2, 1 M $(\text{NH}_4)_2\text{SO}_4$, 1 mM DTT). Immediately following sample injection, the column was flushed with the high ionic strength buffer C for 50 minutes at a rate of 1 ml/min in order to wash out the proteins that were not bound specifically by the column. Following the initial wash, the column was eluted with a steadily decreasing ionic strength starting from 100 % buffer C to 100 % buffer A over 50 mins with a total combined flow rate of 1 ml/min. When the eluent composition reached 100 % buffer A, it was kept isocratic for 50 minutes at a rate of 1 ml/min to elute all the remaining proteins from the column. Under these conditions, PFL G734 started to elute at approximately 0.05 M $(\text{NH}_4)_2\text{SO}_4$ and was collected in 1 mL fractions. The fractions were analyzed using SDS-PAGE in order to determine the quantity and purity of PFL G734A in each. Based on the SDS-PAGE results, fractions from all separate runs containing PFL G734A as > 90% of total protein were pooled together and concentrated down to ~ 1 mL. To the pooled fractions was then

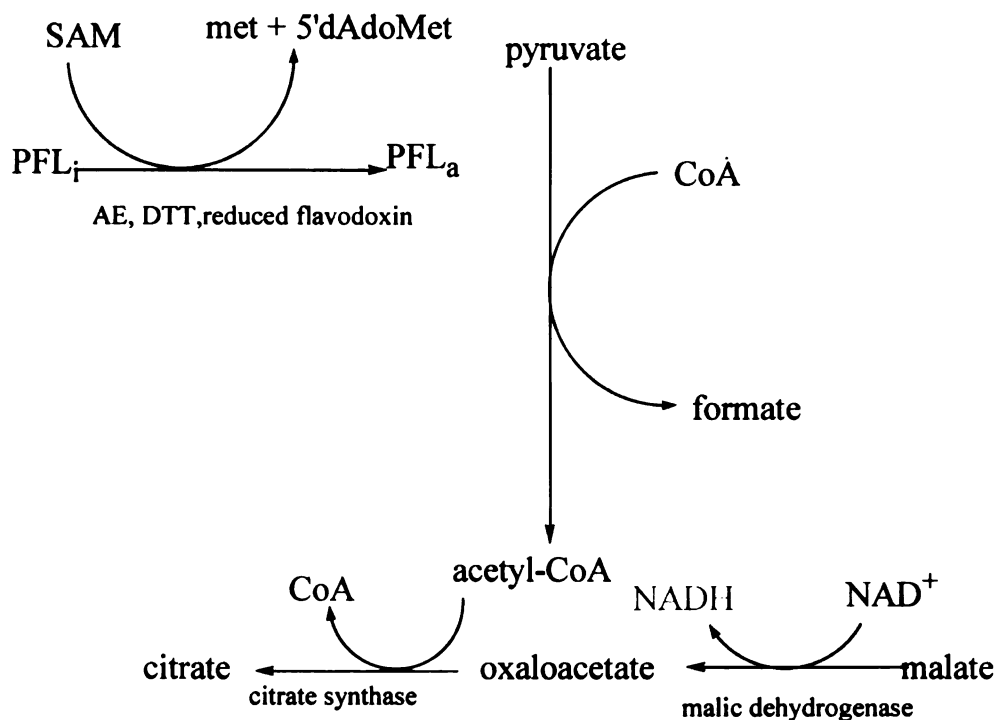
added 10 mL buffer A followed by concentrating down to ~ 1mL using an Amicon concentrator equipped with a YM-30 membrane. After these two steps were repeated 2 more times, the protein was again concentrated down to less than 1 mL. The protein was then flash-frozen and stored at -80°C .

VI.2.2 *Activity Assay of PFL G734A*

The activation of PFL or PFL G734A by PFL-AE was carried out in a final volume of 500 μL , containing 0.1 M Tris-HCl pH 7.6, 0.1 M KCl, 10 mM oxamate, 8 mM DTT, 1.5 μM PFL-AE, 1.5 μM PFL or PFL G734A, 0.2 mM AdoMet, and 50 μM 5-deazariboflavin. This mix was made in the anaerobic chamber by combining reagents from anaerobic stock solutions in the order listed to the final concentrations indicated. In all cases, 5-deazariboflavin was added last, in the dark, and the reaction was initiated by illumination of the sample with a 300 W halogen bulb in an ice water bath. After 30 mins illumination, an aliquot (5 μL) was removed for assay of active PFL through the coupling assay. The average absorbance changes of PFL G734A and PFL were 2.4×10^{-5} AU/s and 1.8×10^{-3} AU/s, respectively. These absorbance changes were corrected for a background UV absorbance change of 3.9×10^{-5} AU/s.

The coupling assay mix contained 0.1 M Tris-HCl pH 8.1, 3 mM NAD^{+} , 55 μM CoA, 0.1 mg BSA, 10 mM pyruvate, 10 mM malate, 20 units citrate synthase, 300 units malic dehydrogenase, and 10 mM DTT in a final volume of 10mL. All reagents were combined from previously anaerobic stock solutions. To assay PFL activity, 895 μL of this mix and 5 μL of the activated PFL described

above were combined in a quartz cuvette, which was then sealed with a septum and brought out of the chamber to monitor the production of NADH by the increase in absorbance at 340 nm. Scheme VI.2.2.1 is a graphic representation of all the reactions involved in this activity assay.



Scheme VI.2.2.1. Schematic depiction of the coupled enzymatic assay for PFL activity.

VI.2.3 Preparation of EPR and ENDOR samples of PFL-AE/PFL G734A/(¹³C-Methyl)-AdoMet

PFL-AE was mixed with 40 % glycerol in a buffer containing 50 mM Tris-HCl pH 8.5, 200 mM NaCl and 2.68 mM DTT to a final volume of 149 μ L and a final concentration of 1.21 mM. Photoreducing agent 5-deazariboflavin (from a 10 mM stock solution in DMSO) was added in the dark to a final concentration of 402 μ M. Dithionite was added to 1.61 mM from a freshly made 60 mM stock

solution in 50 mM Tris-HCl pH 8.5, 200 mM NaCl, and this reaction mixture was then transferred to an EPR tube. Meanwhile, PFL G734A was mixed with 1.8 mM dithionite and 301 μ M 5-deazariboflavin to a final volume of 133 μ L and a final concentration of 1.36 mM, and transferred to a second EPR tube. Both EPR tubes were then capped and inserted in a beaker tightly packed with ice and water. After both tubes were illuminated on ice for 1 h using a 300 W halogen lamp situated 2 cm from the beaker, methyl- 13 C-SAM (2.16 mM final concentration) was added to the PFL-AE mixture in the first EPR tube. The PFL G734A mixture from the second EPR tube was then added to the resulting PFL-AE/SAM mixture and mixed. The final concentrations of major components in this final mixture (400 μ L) were 600 μ M PFL-AE, 600 μ M PFL G734A, 1.61 mM dithionite, 330 μ M 5-deazariboflavin, 1.33 mM DTT, 1.2 mM Methyl- 13 C-SAM and 20 % glycerol in a buffer containing 50 mM Tris pH 8.5, and 100 mM NaCl. Aliquots of this mixture, 100 μ L and 300 μ L, were transferred to an ENDOR tube and an EPR tube, respectively. Both tubes were then flash-frozen in liquid nitrogen in the glove box for further analysis.

VI.2.4 *Site-directed mutagenesis of PFL to produce PFL R753K.*

Site-directed mutagenesis of PFL using pKK-PFL (a generous gift from Kozarch's group^{12, 13}) double-stranded (ds) DNA was performed as described by the protocol of Stratagene QuikChange Site-Directed Mutagenesis Kit (Catalog # 200519b). The oligonucleotide sequences used in this mutagenesis reaction are shown below, with the mutated codon highlighted in red.

Primer I: 5'-G,CAG,GAC,GTT,ATT,ACT,AAG,ACC,TTC,ACT,CAA,TCT,ATG-3'
and,

Primer II: 5'-CAT,AGA,TTG,AGT,GAA,GGT,CTT,AGT,AAT,AAC,GTC,CTG,C-3'

In brief, purified ds pKK-PFL plasmid (25 ng) was mixed with the above two primers (125 ng each), dideoxynucleotides (1 μ L from the supplied stock solution) and *Pfu Turbo* DNA polymerase (2.5 U) to a final volume of 50 μ L in a 100 μ L PCR tube containing other components required by the mutagenesis kit. The ds pKK-PFL plasmid was then denatured by heating to 95 °C for 30 seconds. The reaction mix was cooled down to 55 °C for 1 min to allow the two separated pKK-PFL strands to anneal to the two primers. Then the temperature was raised to 68 °C and the reaction was kept at this temperature for 15 min to let the polymerase synthesize the complete complementary strands of pKK-PFL with mutated codons. After the PCR cycling was repeated for 16 times, the mutagenesis was stopped by lowering the temperature to 4 °C. Restriction enzyme DpnI (1 μ L from the supplied stock solution) was then added to the reaction mix to digest away the original pKK-PFL plasmids at 37 °C. The mutated plasmid was subsequently transformed into XL1-Blue competent cells for amplification. The amplified mutated plasmid pKK-PFL R753K (hereafter designated pJYVII123) was confirmed by DNA sequencing in the Research Technology Support Facility at Michigan State University.

VI.2.5 *Expression and Purification of PFL R753K.*

A single colony of the overexpression strain *E. coli* BL21(DE3)plysS transformed with pJYVII123 was used to inoculate 50 mL of Luria/Bertani (Miller's Modification)¹¹ medium containing 50 µg/mL of ampicillin. This culture was grown to saturation at 37 °C and then 5 mL of this overnight culture was used to inoculate each 1L LB/ampicillin in a 2800 mL Fernbach flask. The 1 L cultures were grown at 37 °C with shaking at 250rpm. When the culture reached an OD₆₀₀ = 0.7-0.8, IPTG was added to 1 mM final concentration to induce the overexpression of PFL R753K. The cultures were grown for an additional 3 hours, and then were harvested by centrifugation at 4 °C and stored under nitrogen at – 80 °C for further use.

Pelleted cells were resuspended in lysis buffer (20 g / 50 mL) containing 20 mM Hepes pH 7.2, 1% Triton X-100, 5% glycerol, 10 mM MgCl₂, 1 mM PMSF, 10 mg lysozyme, and 0.5 mg DNase I and RNase A. This suspension was agitated for one hour and then centrifuged at 27,000 x g for 30 min at 4 °C.

The resulting crude extract was loaded onto a Waters AP5-50/30 column with Accell Plus QMA anion exchange media that had been previously equilibrated with 20 mM Hepes pH 7.2, 1 mM DTT. Immediately following sample injection, the column was flushed with the low ionic strength buffer (buffer A: 20 mM Hepes pH 7.2, 1 mM DTT) for 60 minutes at a rate of 5 ml/min in order to wash out the proteins that were not bound specifically by the column. Following the initial wash, the column was eluted with a steadily increasing ionic strength starting from 100% buffer A to 100% buffer B (20 mM Hepes pH 7.2, 500 mM NaCl, 1 mM DTT) over 180 min with a total combined flow rate of 5 ml/min. When

the eluent composition reached 100% buffer B, it was kept isocratic for 60 minutes at a rate of 5 ml/min to clean the column. Under these conditions, PFL R753K started to elute out of the column at approximately 375 mM NaCl and was collected in 4 mL fractions. The fractions were analyzed using SDS-PAGE in order to determine the quantity and purity of PFL R753K in each. Based on the SDS-PAGE results, fractions from all separate runs containing PFL R753K as > 75% of total protein were pooled together and concentrated down to ~ 10 mL. To the pooled fractions was then added 30mL buffer C (20 mM Hepes pH 7.2, 1 M $(\text{NH}_4)_2\text{SO}_4$, 1 mM DTT) followed by concentrating down to ~ 10 mL using an Amicon concentrator equipped with a YM-30 membrane. After these two steps were repeated 2 more times, the protein was again concentrated down to less than 10 mL.

The resulting partially purified PFL R753K was then loaded onto a HiLoad 16/10 Phenyl Sepharose HP column that had been previously equilibrated with buffer C (20 mM Hepes pH 7.2, 1 M $(\text{NH}_4)_2\text{SO}_4$, 1 mM DTT). Immediately following sample injection, the column was flushed with the high ionic strength buffer C for 50 minutes at a rate of 1 ml/min in order to wash out the proteins that were not bound specifically by the column. Following the initial wash, the column was eluted with a steadily decreasing ionic strength starting from 100% buffer C to 100% buffer A over 50 min with a total combined flow rate of 1 ml/min. When the eluent composition reached 100% buffer A, it was kept isocratic for 50 minutes at a rate of 1 ml/min to elute all the remaining proteins from the column. Under these conditions, PFL R753K started to elute at

approximately 0.05 M $(\text{NH}_4)_2\text{SO}_4$ and was collected in 1 mL fractions. The fractions were analyzed using SDS-PAGE in order to determine the quantity and purity of PFL R753K in each. Based on the SDS-PAGE results, fractions from all separate runs containing PFL R753K as > 90% of total protein were pooled together and concentrated down to ~ 1 mL. To the pooled fractions were then added 10 mL buffer A followed by concentrating down to ~ 1 mL using an Amicon concentrator equipped with a YM-30 membrane. After these two steps were repeated 2 more times, the protein was again concentrated down to less than 1 mL. The protein was then flash-frozen and stored at -80°C .

VI.2.6 *Binding assay of PFL-AE with PFL R753K.*

One mL of 200 – 320 μM purified PFL-AE (2 x relative to the concentration of PFL R753K) and 100 – 160 μM purified PFL R753K (dimer) were mixed together in a Coy anaerobic chamber (Coy Laboratories, Grass Lake, MI), and then incubated at 4°C for 1 hr to allow the proteins to interact with each other. Then this mixture was loaded onto a HiLoad 26/50 Superose 12 column that was preequilibrated with buffer containing 20 mM Hepes pH 7.4, 1 mM DTT in the absence or presence of 150 mM NaCl. The proteins were eluted using the same buffer at a flow rate of 1 mL/min for 90 min. The fractions (1.5 mL per tube) were analyzed using UV-vis at both 280 nm and 426 nm, and by SDS-PAGE in order to determine which ones contained PFL R753K, PFL-AE, and the relative amounts of them in each fraction. Bio-Rad gel filtration standards were loaded and run under the above conditions to calibrate the column.

VI.2.7 *Sample preparation for EPR spectroscopy of PFL R753K with PFL-AE*

The EPR samples of PFL R753K have been prepared by two methods. In the first method, purified PFL-AE was mixed to a final concentration of 290 μM in buffer containing 200 μM 5-deazariboflavin, 10 mM DTT, 100 mM Tris-Cl pH 7.6, 100 mM KCl, and 20 mM oxamate in a final volume of 500 μL . This mixture was then illuminated for 1 h at 0 °C to reduce the [4Fe-4S] cluster to the 1+ state. After the reduced enzyme was mixed with SAM (3 mM final concentration), a 300 μL aliquot was flash-frozen to measure the concentration of the [4Fe-4S]¹⁺ cluster. The remaining 200 μL was mixed with PFL R753K to a 200 μM final concentration. The final concentrations of major components in this final mixture (300 μL) were 200 μM PFL-AE, 200 μM PFL R753K, 2 mM SAM, 140 μM 5-deazariboflavin, 7 mM DTT, 70 mM Tris-Cl pH 7.6, 70 mM KCl, and 14 mM oxamate. The EPR sample was then flash-frozen in liquid nitrogen for EPR spectroscopy.

In the second method, purified PFL-AE was mixed to a final concentration of 200 μM in a buffer containing 200 μM 5-deazariboflavin, 10 mM DTT, 100 mM Tris-Cl pH 7.6, 100 mM KCl, 20 mM oxamate, 2 mM SAM and 200 μM PFL R753K in a final volume of 400 μL . This mixture was illuminated for 1 h at 0 °C to reduce the [4Fe-4S] cluster to the 1+ state in the presence of PFL R753K and SAM. The EPR sample was then flash-frozen in liquid nitrogen for EPR spectroscopy.

VI.2.8 *PFL R753K Crystallization by Microdialysis*

Growth of PFL R753K crystals were attempted by three methods.

The first method was based on work done by Knappe's group.¹⁴ Purified PFL R753K (10 mg/mL) was first dialyzed into buffer containing 25 mM MOPS/NH₃ pH 7.3, 50 mM NH₄Cl, 10 mM DTT, 3 mM NaN₃ and 16% (w/v) PEG1000. This protein solution (40 µL) was then dialyzed against 1.5 mL reservoir solutions containing 25 mM MOPS/NH₃ pH 7.3, 50 mM NH₄Cl, 1 mM DTT, 1 mM EDTA, 3 mM NaN₃, 2 mM MgCl₂, 24, 26, 28 or 30% (w/v) PEG1000 at 20°C. The second method was based on work done by Kozarich's group.¹⁰ PFL R753K (10 or 25 mg/mL) was first dialyzed into buffer containing 50 mM MOPS/NH₃ pH 7.3, and 20 mM DTT. This protein solution (40 µL) was then dialyzed against 1.5 mL reservoir solutions which included 25 mM MOPS/NH₃ pH 7.3, 25 mM NH₄Cl, 10mM DTT, 1 mM EDTA, 2 mM MgCl₂, and 25% (w/v) PEG1000 at 20 °C.

The third method was essentially a revision of the second method. PFL R753K (10 or 25 mg/mL) was first dialyzed into buffer containing 50 mM MOPS/NH₃ pH 7.3, and 20 mM DTT. This protein solution (40 µL) was then dialyzed against 1.5 mL reservoir solutions which included 25 mM MOPS/NH₃ pH 7.3, 25 mM NH₄Cl, 10mM DTT, 1 mM EDTA, 2 mM MgCl₂, 25% (w/v) PEG1000, a 5-deoxyadenosine (10 mM), sodium pyruvate (10 mM) or sodium oxamate (10 mM) at 20°C.

VI.2.9 *Cloning of yfiD gene into pCAL-n-EK and pET44a(+) vectors:*

The *yfiD* gene was amplified by the polymerase chain reaction (PCR) technique using *E.coli* BL21 chromosomal DNA as a template. The synthetic oligonucleotide primers had the sequences shown below:

Nde I

Primer I: 5'-GCC,GCC,**CAT,ATG**,ATT,ACA,GGT,ATC,CAG,ATT-3'

Hind III

Primer II: 5'-GCC,GCC,**AAG,CTT**,TTA,CAG,GCT,TTC,AGT,AAA-3'

The bold letters indicate the restriction enzyme recognition sequences, with the corresponding restriction enzyme used at each site indicated in italics above each restriction site sequence. The PCR product was digested with the restriction enzymes *Nde I* and *Hind III* and then cloned into a PET-44a(+) expression vector (Novagen) or pCAL-n-EK, which were also digested with the same set of restriction enzymes. The recombinant DNA [pJYVII127-1 (pCAL-n-EK-*yfiD*) or pJYVII127-2 (pET44a-*yfiD*)] obtained from above was first transformed into XL1 Blue competent cells. Then the transformation mix was plated on LB-agar containing 50 µg/ml ampicillin and incubated overnight at 37 °C. Single colonies were identified and used to inoculate a Falcon tube containing 5 ml of liquid LB medium containing 50 µg/ml ampicillin. All tubes were incubated overnight at 37°C with shaking at 250 rpm.

From each of the overnight cultures, a total of 1 - 5 ml was centrifuged in order to obtain a cell pellet. Plasmid DNA was then extracted from each cell pellet using a commercially available DNA extraction kit (Stratagen). In order to ascertain its genetic identity, the recombinant plasmid DNA purified as above was checked and confirmed by DNA sequencing in the Research Technology Support Facility at Michigan State University.

VI.2.10 *Site-directed mutagenesis of YfiD to generate YfiD R120K.*

Site directed mutagenesis of YfiD was performed essentially the same as described for PFL as described in VI.2.4. The template DNA used was pJYVII127-1 (VI.2.9). The two primers used are indicated below, with the mutated codon highlighted in red.

Primer I: 5'-CGC,GAC,GTT,ATC,GCT,CGT,ACC,TTT,ACT,GAA,AGC-3',

Primer II: 5'-GCT,TTC,AGT,AAA,GGT,CTT,AGC,GAT,AAC,GTC,GCG-3'

The resulting mutant plasmid pJYVII139-1 (pCAL-n-EK-yfiD R120K) was amplified in XL1-Blue competent cells and the sequence was confirmed by DNA sequencing in the Research Technology Support Facility at Michigan State University.

VI.2.11 *Expression and Purification of YfiD and YfiD R120K.*

The method used for expression and purification of YfiD and YfiD R120K was carried out the same as for PFL G734A (VI.2.1). The plasmids used were pJYVII127-1 and pJYVII139-1 respectively.

VI.2.12 *Binding assay of PFL-AE with YfiD and YfiD R120K*

Purified PFL-AE (100 μ M final concentration) and purified YfiD or YfiD R120K (100 μ M final concentration) were mixed to a final volume of 1 mL in a Coy anaerobic chamber, and incubated at 4 °C for 1 hr to allow the proteins

interact with each other. Then this mixture was loaded onto a HiLoad 16/60 Superdex 75 column that was pre-equilibrated with buffer containing 50 mM Hepes pH 7.4, 1 mM DTT in the same anaerobic chamber. YfiD or YfiD R120K and PFL-AE were eluted using the same buffer at a flow rate of 1 ml/min for 90 min. The fractions (1.5 mL per tube) were analyzed using UV-vis at both 280 nm and 426 nm and SDS-PAGE in order to determine which ones contained YfiD, YfiD R120K, and PFL-AE and the relative amounts of them in each fraction. Bio-Rad gel filtration standards were loaded and run under the above conditions to calibrate the column.

VI.2.13 Activation and oxygen cleavage of PFL

The PFL-AE/PFL reaction was mixed in a final volume of 500 μ L containing 0.1 M Tris-HCl pH 7.6, 0.1 M KCl, 10 mM oxamate, 1 mM DTT, 10 μ M PFL-AE, 50 μ M PFL, 0.4 mM SAM, and 100 μ M 5-deazariboflavin. This mix was made in the anaerobic chamber by combining reagents from anaerobic stock solutions in the order listed to the final concentrations indicated. In all cases, 5-deazariboflavin was added last, in the dark, and the reaction was initiated by illumination of the sample with a 300 W halogen bulb in an ice water bath. After 60 min illumination, this reaction mixture was taken out of the anaerobic chamber. The reaction mixture, including PFL-AE and activated PFL, were exposed to air by pipetting the mixture up and down many times on a glass dish situated on ice to keep the reaction cold. To this reaction mixture was added 10 mL buffer (20 mM Hepes pH 7.2, 1 mM DTT), and then the solution was concentrated down to

~ 1mL using an Amicon concentrator equipped with a YM-30 membrane. After these two steps were repeated 2 more times, the protein was again concentrated down to less than 0.5 mL. This protein solution was then deoxygenated using a vacuum/nitrogen gas manifold and flash-frozen in liquid nitrogen. Protein concentration was determined by the method of Bradford and purity was checked using SDS-PAGE.

VI.2.14 Salvage of PFL activity by YfiD.

The activation reaction for oxygen-damaged PFL was mixed in a final volume of 500 μ L containing 0.1 M Tris-HCl pH 7.6, 0.1 M KCl, 10 mM oxamate, 8 mM DTT, 0.05 μ M PFL-AE, 5 μ M oxygen damaged PFL (VI.2.13), 0.2 mM AdoMet, 0 – 50 μ M YfiD and 50 μ M 5-deazariboflavin. This mix was made in the anaerobic chamber by combining reagents from anaerobic stock solutions in the order listed to the final concentrations indicated. In all cases, 5-deazariboflavin was added last, in the dark, and the reaction was initiated by illumination of the sample with a 300 W halogen bulb in an ice water bath. After 30 min illumination, an aliquot (5 μ L) was removed for assay of active PFL through the coupling assay.

The coupling assay mix contained 0.1 M Tris-HCl pH 8.1, 3 mM NAD⁺, 55 mM CoA, 0.1 mg BSA, 10 mM pyruvate, 10 mM malate, 20 units citrate synthase, 300 units malic dehydrogenase, and 10 mM DTT in a final volume of 10mL. All reagents were combined from previously anaerobic stock solutions by freeze–pump–thaw cycles. To assay PFL activity, 895 μ L of this mix and 5 μ L of

the activated PFL described above were combined in a quartz cuvette, which was then sealed with a septum and brought out of the chamber to monitor the production of NADH by the increase in absorbance at 340 nm.

VI.2.15 EPR monitored salvage of PFL by YfiD

Purified PFL-AE was mixed to a final concentration of 50 μ M in buffer containing 100 μ M 5-deazariboflavin, 10 mM DTT, 100 mM Tris-HCl pH 7.6, 100 mM KCl, 20 mM oxamate and 2 mM SAM. Oxygen damaged PFL (50 μ M final concentration, section VI.2.13), 250 μ M YfiD or both oxygen damaged PFL and YfiD were also included in the activation mix. This mix was then illuminated for 40 min at 0 °C to reduce the [4Fe-4S] cluster to the 1+ state and to generate the glycyl radical. The EPR sample was then flash-frozen in liquid nitrogen for further analysis.

VI.3.16 EPR spectroscopy

All the EPR spectra were measured in a Bruker EPR spectrometer equipped with a liquid He cryostat and a temperature controller from Oxford Instruments. Spectra were recorded at 12 K for [4Fe-4S]¹⁺, at 60 K to detect glycyl radical, and at 80 K to detect thiyl radical. Spin concentrations in the protein samples were determined by calibrating double integrals of the EPR spectra recorded under nonsaturating conditions (i) with a standard sample of 0.1 mM Cu(II), 1 mM EDTA and 10 %(w/v) glycerol solution for the cluster signals, or (ii) with a K₂(SO₃)₂NO solution for the radical signals. The concentration of

$\text{K}_2(\text{SO}_3)_2\text{NO}$ standard was determined using the optical extinction coefficient.^{15, 16}

Microwave power and modulation amplitude are indicated with each EPR spectrum.

VI.3 Results and Discussion

VI.3.1 Overexpression and purification of PFL G734A.

The pTHXI67 plasmid has been successfully transformed into BL21(DE3)plysS cells using standard molecular cloning techniques. After the overexpressing cells were lysed using the enzymatic lysis procedure described in the experimental section, the crude clear lysate was first purified on an ionic exchange column as shown in Figure VI.3.1.1. PFL G734A eluted at approximately 44 % buffer B. Because the purity of this partially purified PFL G734A was not satisfactory, an additional purification on a hydrophobic interaction column was carried out (Figure VI.3.1.2). PFL G734A (> 90 % pure) eluted as a single peak at approximately 100 % buffer A. The overall yield of purified PFL G734A was 30 mg per 10 L of growth media.

Although the only difference between the wildtype PFL and mutant PFL G734A is the presence of a methyl in place of a hydrogen on amino acid 734, the amount of protein produced with mutant plasmid is significantly lower than that of the wildtype. Currently, we have not been able to identify the reason, however a few postulates can potentially explain this interesting phenomenon. For example, the overexpression of PFL G734A might be disrupted in protein synthesis. This can result from a low yield of mRNA transcript, the mutant mRNA being less stable, or difficulty in translation from mRNA into protein. Alternately, the PFL G734A might simply be unstable *in vivo*. Nevertheless, the low yield causes the purification to be more difficult. The overall yield of purified PFL G734A is only

approximately 30 mg per 10 L culture, as compared to > 300 mg / 10 L for wildtype PFL. The mutant and the wildtype PFL do, however, show almost the same behavior on both ion exchange and hydrophobic interaction columns, suggesting that the mutation of this G734 into A734 does not change the overall structure of PFL. Since surface properties of the protein are generally strongly associated with the internal milieu of a protein, a similar local configuration around the catalytic site can therefore be proposed for both PFL and PFL G734A.

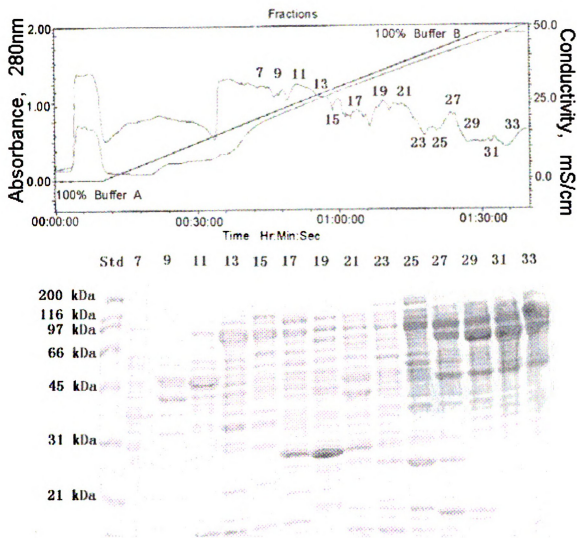


Figure VI.3.1.1. Purification of PFL G734A by ion exchange chromatography. Upper Panel: Chromatogram of PFL G734A purification by ion exchange chromatography. PFL G734A elutes in fractions 13-17, at approximately 44 % buffer B. Lower Panel: SDS-PAGE analysis of corresponding fractions from ion exchange column. The fraction numbers are indicated on top of the gel.

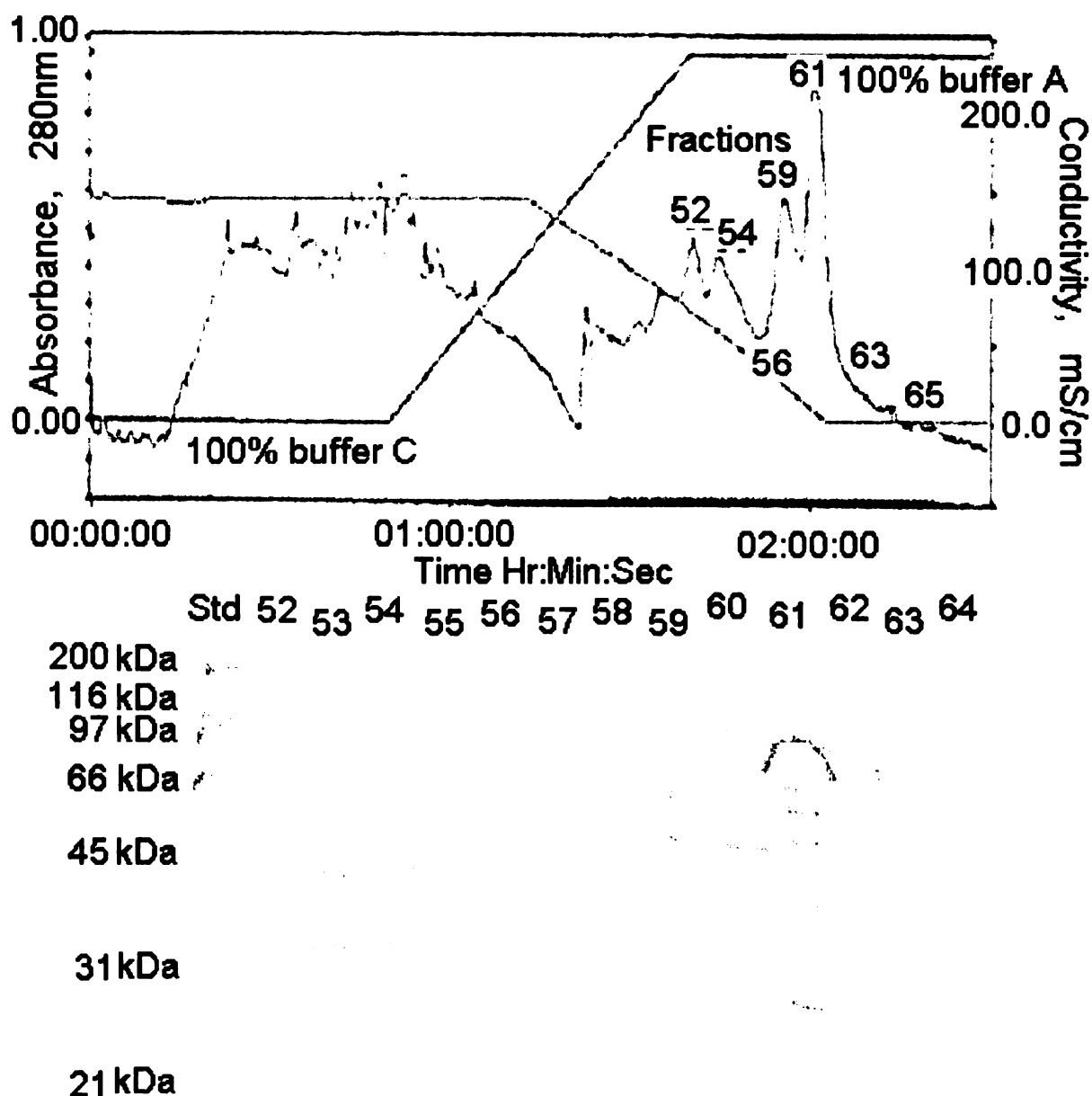


Figure VI.3.1.2. Purification of PFL G734A by hydrophobic interaction chromatography. Upper Panel: UV Chromatogram of PFL G734A purification by hydrophobic interaction chromatography. PFL G734A elutes in fractions 59-63, at approximately 100 % buffer A. Lower Panel: SDS-PAGE analysis of corresponding fractions from hydrophobic interaction column. The fraction numbers are indicated on top of the gel.

VI.3.2 Activity Assay of PFL and PFL G734A

The activity assay for PFL G734A was performed essentially the same as that for wildtype PFL using previously established procedures¹⁷ with a few modifications. Firstly, the amount of PFL-AE used in these activity assays was much higher than previous wildtype PFL activity assays in order to maximize activation of PFL. Secondly, a control assay of wildtype PFL was performed in parallel with the assay for PFL G734A, with both activated under identical conditions and the activity assays performed multiple times in order to verify reproducibility. The average activity of PFL G734A was 0.2 $\mu\text{mol}/\text{min}/\text{mg}$, while that of the wildtype PFL was 12.3 $\mu\text{mol}/\text{min}/\text{mg}$, thus the calculated activity of PFL G734A is approximately 1.4 % of that of wildtype PFL. The loss of activity is consistent with the fact that the pro-S hydrogen from PFL G734 residue has been replaced by a methyl group, thus removing the hydrogen atom abstracted to generate the glycyl radical. The 1.4 % residual activity is likely the result of contamination with wildtype PFL, which is constitutively expressed in *E. coli*. As was previously discussed (VI.3.1), the elution time of PFL G734A is identical to that of wildtype PFL on both ion exchange and hydrophobic interaction columns. As a result, wildtype PFL expressed from genomic DNA coelutes with PFL G734A during purification, and becomes an inevitable impurity of the purified PFL G734A.

VI.3.3 EPR and ENDOR spectroscopy of PFL-AE/PFL G734A/(¹³C-Methyl)-SAM

The PFL-AE/PFL G734A/(^{13}C -Methyl)-SAM sample has been investigated both by X-band and Q-band EPR spectroscopy. The sample exhibits a nearly axial signal at X-band (Figure VI.3.3.1), similar to that of the PFL-AE/(^{13}C -Methyl)-SAM complex.¹⁸ Only minor distinction can be spotted between these two spectra, where the small trough at approximately $g = 1.9$ in the presence of PFL G734A does not exist in the absence of PFL G734A. Meanwhile, the Q-band EPR spectrum of the same PFL-AE/PFL G734A/(^{13}C -Methyl)-SAM sample (collected by Dr. Brian Hoffman's group) shows a typical nearly axial signal with the same set of g values as that of the X-band EPR ($g=2.02, 1.89$) (Figure VI.3.3.1 and Figure VI.3.3.2). These results suggest to us that PFL G734A has little, if any, impact on the electronic structure of the iron-sulfur cluster of PFL-AE. These results are supported by the field dependence data of the PFL-AE/PFL G734A/(^{13}C -Methyl)-SAM sample as compared to that of the PFL-AE/(^{13}C -Methyl)-SAM sample; these two sets do not show any significant difference (Figure VI.3.3.3).

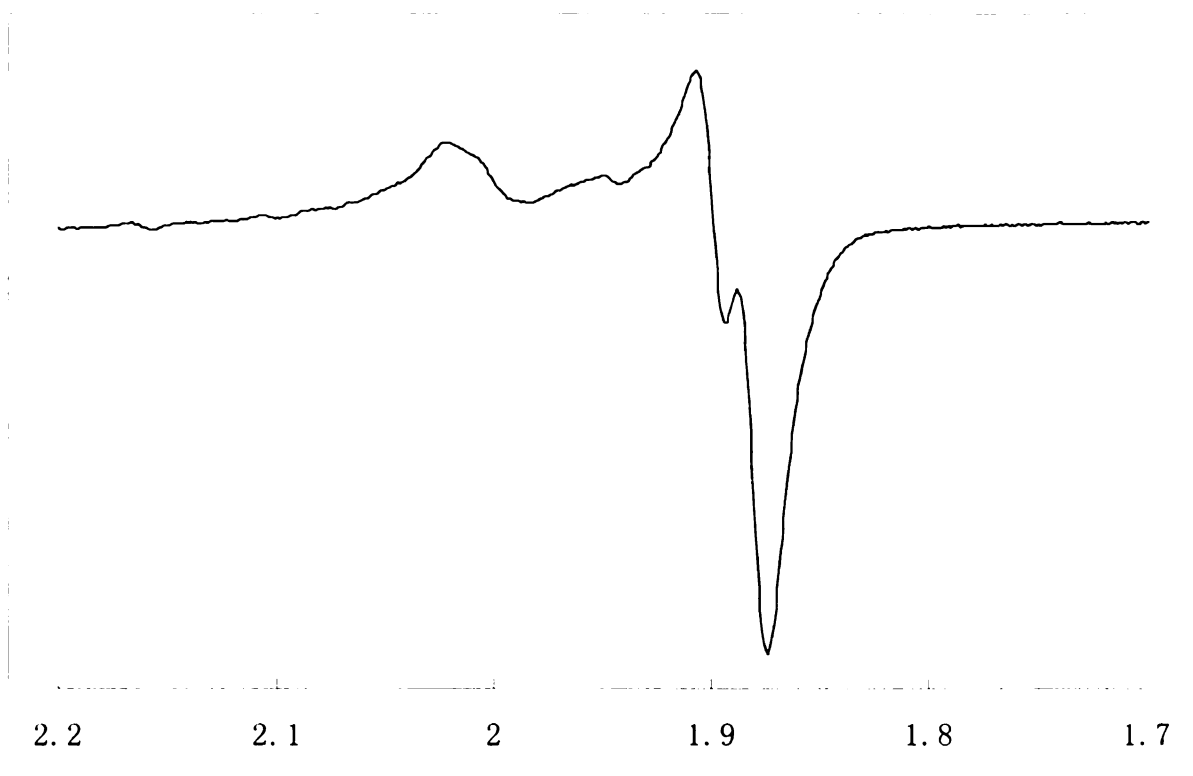


Figure VI.3.3.1. X-band EPR spectrum of PFL-AE/SAM/PFL G734A complex. The sample contains the following components: 600 μM PFL-AE, 600 μM PFL G734A, 1.6 mM dithionite, 330 μM 5-deazariboflavin, 1.3 mM DTT, 1.2 mM Methyl- ^{13}C -SAM, and 20 % glycerol in 50 mM Tris-HCl pH 8.5, 100 mM NaCl. Conditions of measurement, $T = 12\text{ K}$; microwave power, 2 mW; modulation amplitude, 10 G. Double integration of signal intensity: 460 μM

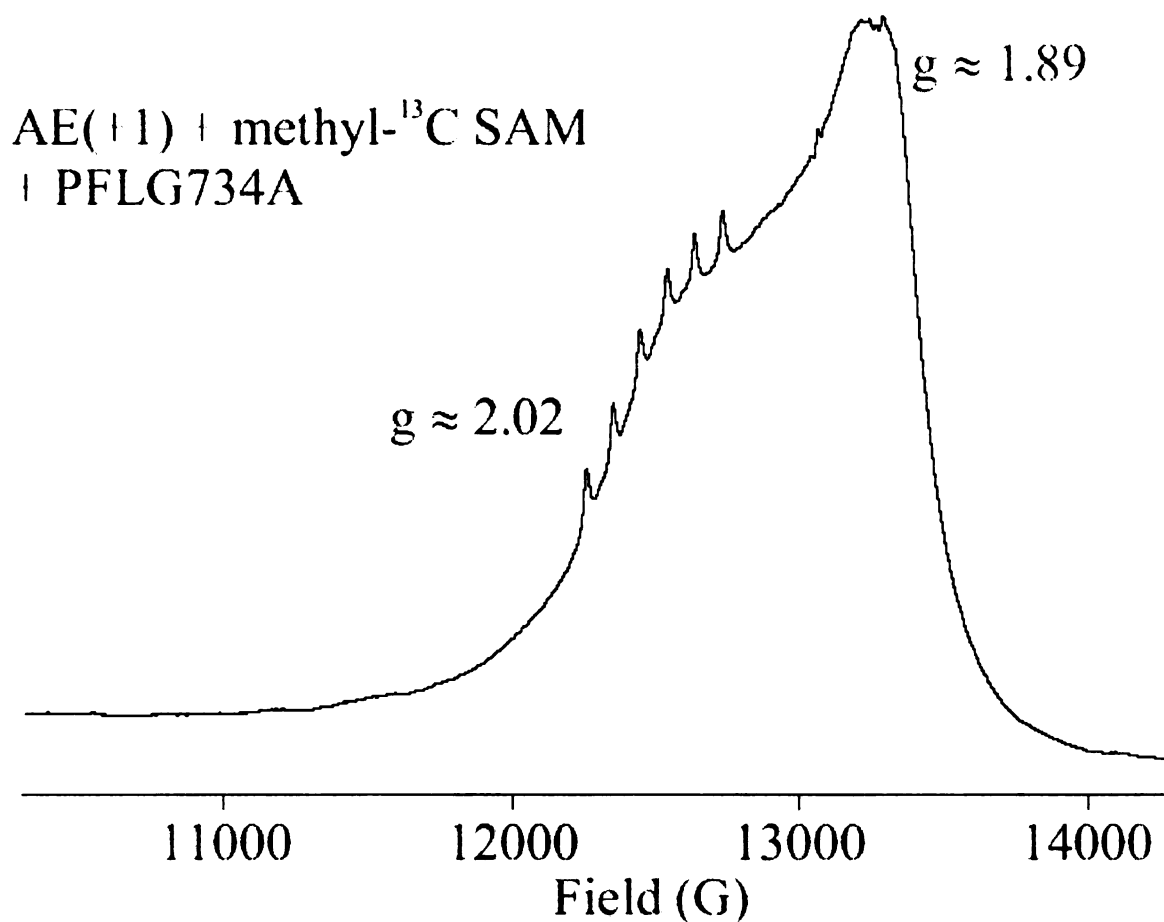


Figure VI.3.3.2. Q-band EPR spectrum of PFL-AE/SAM/PFL G734A complex. The sample contains the following components: 600 μM PFL-AE, 600 μM PFL G734A, 1.6 mM dithionite, 330 μM 5deazariboflavin, 1.3 mM DTT, 1.2 mM Methyl- ^{13}C -SAM, and 20 % glycerol in 50 mM Tris-HCl pH 8.5, 100 mM NaCl. Conditions of measurement, $T = 2$ K; microwave power, 1 mW; modulation amplitude, 2 G. The six line spectrum centered around $g = 2$ is indicative of Mn (II) (100 % $I = 5/2$) contamination.

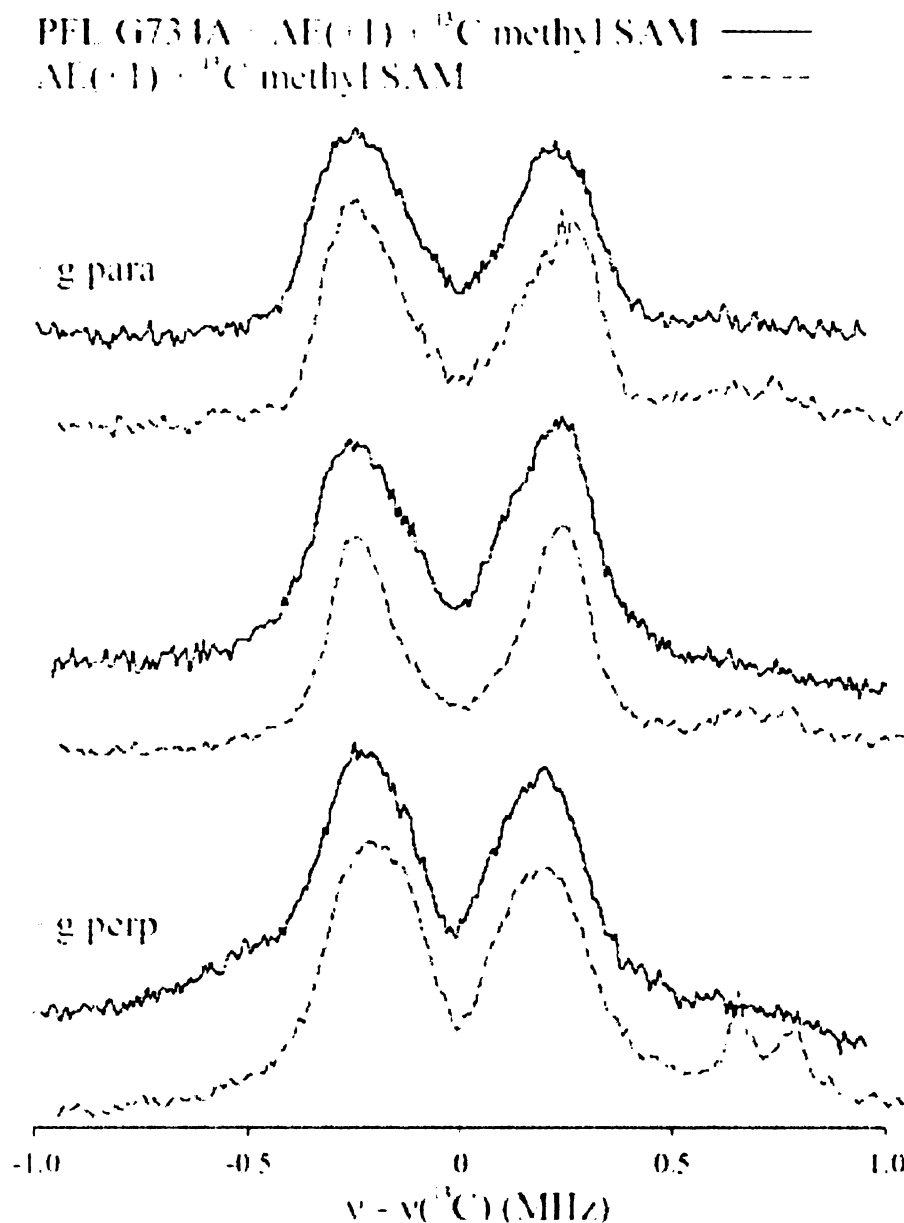


Figure VI.3.3.3. The field dependence data comparison of the PFL-AE/(^{13}C -Methyl)-SAM/PFL G734A complex (solid line) and the PFL-AE/(^{13}C -Methyl)-SAM complex¹⁸ (dashed line). The sample [PFL-AE/(^{13}C -Methyl)-SAM/PFL G734A] contains the following components: 600 μM PFL-AE, 600 μM PFL G734A, 1.6 mM dithionite, 330 μM 5deazariboflavin, 1.3 mM DTT, 1.2 mM Methyl- ^{13}C -SAM, and 20 % glycerol in 50 mM Tris-HCl pH 8.5, 100 mM NaCl. Conditions of measurement: $T = 2 \text{ K}$, $\nu_{\text{MW}} = 34.8 \text{ GHz}$, MW pulse lengths = 80 ns, $\tau = 600 \text{ ns}$, RF pulse length = 60 μs , repetition rate = 30 Hz, and number of transients = 600.

VI.3.4 Mutagenesis, transformation, overexpression, and purification of PFL R753K.

The pJYVII123 plasmid containing the gene for PFL R753K was successfully generated from pKK-PFL using site directed mutagenesis. Subsequent transformation of this plasmid into BL21(DE3)plysS created the overexpressing strain. PFL R753K was overexpressed by inducing with 1 mM IPTG after normal aerobic growth. Interestingly, the purification of this mutant is essentially the same as that of wildtype PFL in terms of elution time on both ion exchange and hydrophobic interaction columns. This is a clear sign to us that the overall structure of this mutant is similar to that of the wildtype PFL, an important prerequisite to any future experiments. The side chain of either R753 or K753 is expected to point inside toward the catalytic site of PFL, therefore modifications should be only around the catalytic site and the surface of the protein should remain similar (Figure VI.3.4.1).

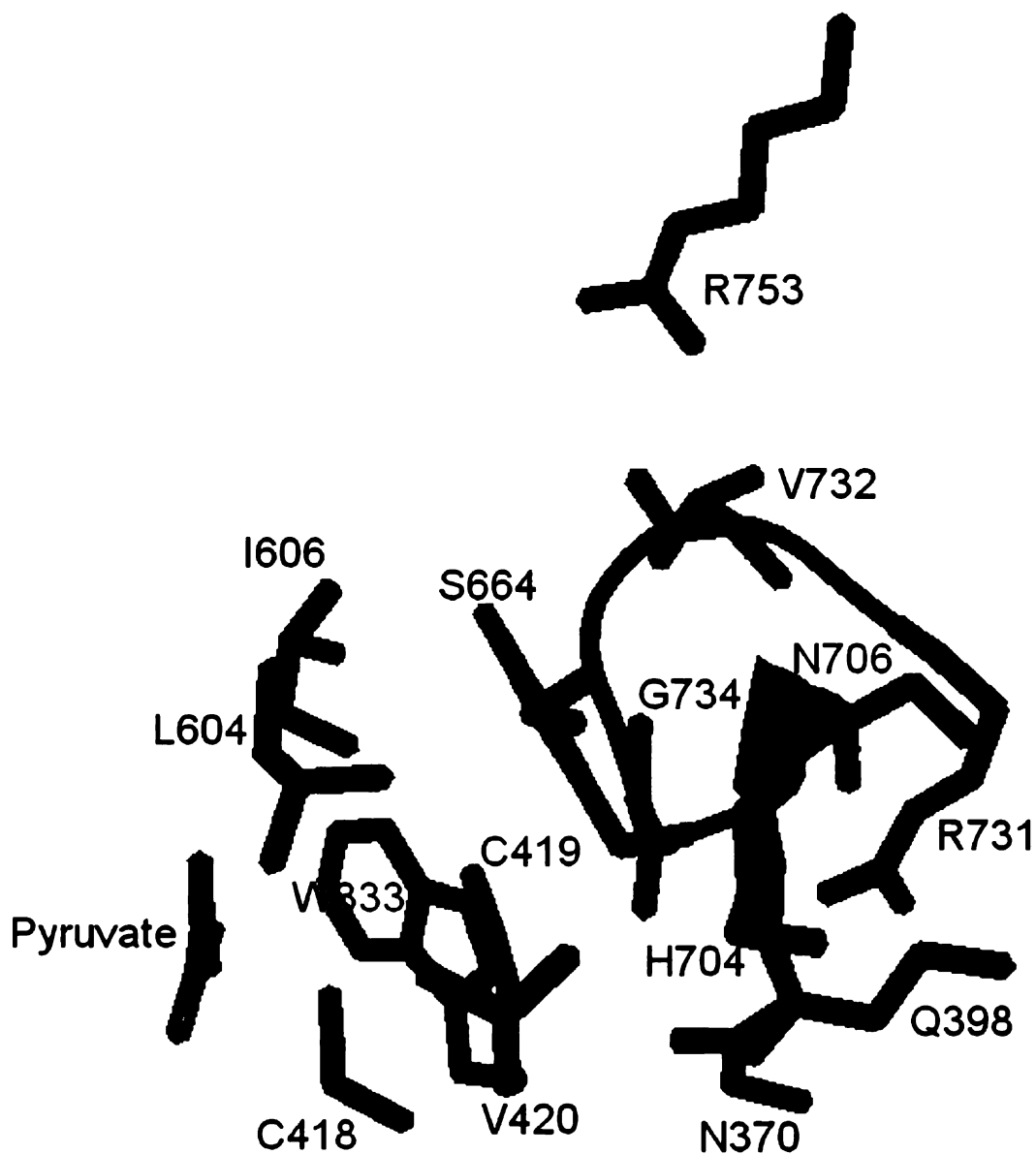


Figure VI.3.4.1. The structural topology of the local residues surrounding glycine loop of PFL. The side chains of local residues in the PFL model are represented as sticks with the carbon atoms colored green, oxygen atoms colored red, and nitrogen atoms colored blue. The side chain of R753 comes within 3.0 Å of the backbone carbonyl oxygen of residue V732.

VI.3.5 Binding assay of PFL-AE with PFL R753K

According to a recent report on glycerol dehydratase (GD) and its activating enzyme (GD-AE),² single mutation of GD into GD R782K results in the formation of a tight complex between GD and GD-AE *in vivo*. Considering both GD and PFL adopt the similar 10-stranded α/β barrel motif and their C-terminal domains align well, it is reasonable to propose that the single mutation of PFL at the same conserved arginine residue (R753) into lysine will result in the formation of a similar tight complex between PFL-AE and PFL.

The sample (mixture of PFL-AE and PFL R753K) was prepared in an anaerobic Coy chamber at 4 °C to avoid degradation of the iron-sulfur cluster of PFL-AE. Then this mixture was given 1 hour to allow PFL-AE and PFL R753K to interact with each other. After the PFL-AE and PFL R753K mixture was separated by gel filtration, two well-resolved peaks were identified based on UV-vis detection at 426 and 280 nm. The first peak was centered at 46.5 mL with an apparent molecular weight approximately 170 kDa, identical to that of the PFL R753K homodimer. The second peak was centered at 61.5 mL with an apparent molecular weight of approximately 30 kDa, similar to that of PFL-AE (28 kDa). There is no peak consistent with a PFL-AE and PFLR753K complex (expected molecular weight of approximately 200 kDa. Moreover, the elution volumes of both PFL-AE and PFL R753K remain the same when samples containing either PFL-AE or PFL R753K are tested individually on the same gel filtration column, further suggesting that PFL-AE and PFL R753K do not interact with each other.

This result is contradictory to that of GD/GD-AE system where a tight GD/GD-AE complex is observed.

Although the PFL R753K mutant was made in an effort to form a tight complex between PFL-AE and PFLR753K, the negative result described above suggests to us that PFL is different from GD and the tight complex may be an exception for the GD/GD-AE system. Based on the crystal structures of PFL, the residue R753 is located at the surface and positions its side chain toward the catalytic site. It is questionable that a single mutation, which is likely to cause minor modification in the catalytic site, will have significant effect on the overall structure of PFL and therefore change the binding properties with PFL-AE. In fact, crystal structures suggest that the primary function of this highly conserved R753 residue is to hold the glycine loop in place as a result of the hydrogen bond between the side chain of Arg753 and the glycine loop residue Val732. Mutation of R753 into K753 may only make the side chain one atom (approximately 0.7 Å) shorter, and thus may disrupt the configuration of the glycine loop but is unlikely to significantly change the overall configuration of PFL to form a tight complex with PFL-AE.

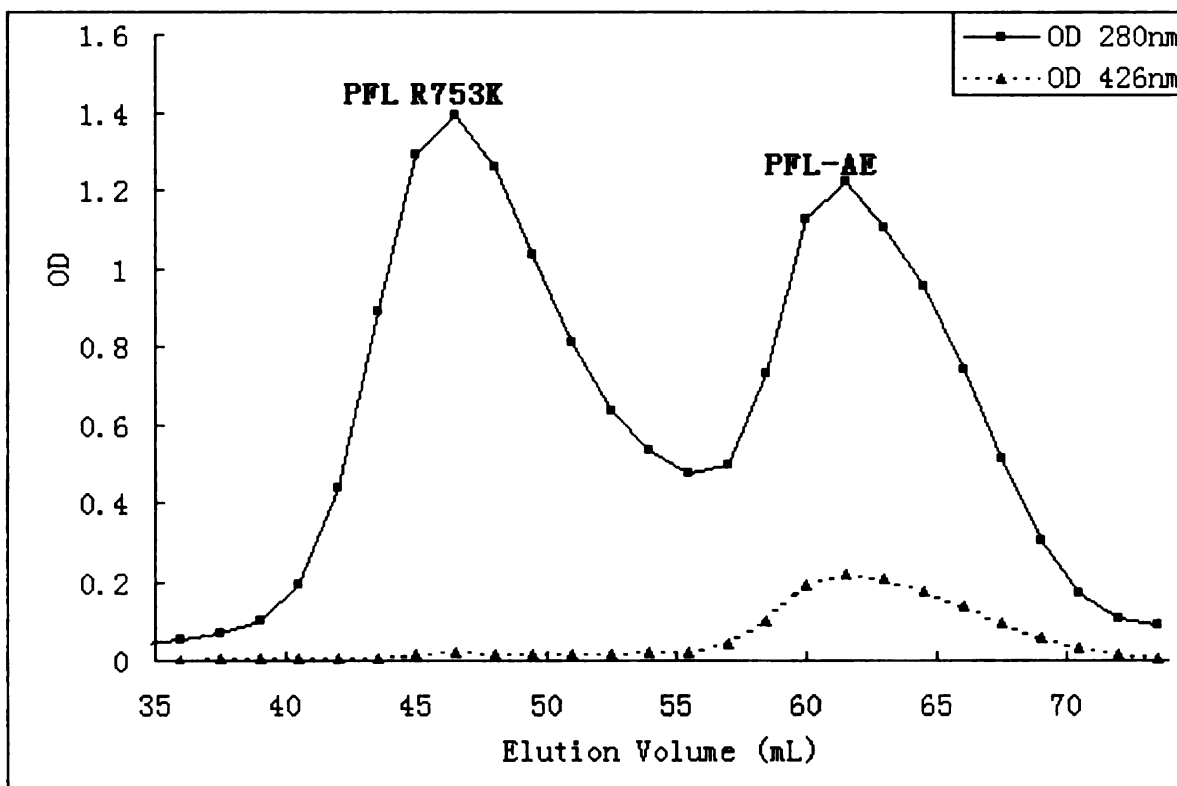


Figure VI.3.5.1. Gel filtration chromatography of PFL R753K and PFL-AE mixture on a SepharoseTM 12 column. An equimolar mixture of PFL R753K and PFL-AE was loaded onto the gel filtration column and run with isocratic flow. Two well-resolved symmetric peaks are observed with molecular weights of 170 kDa for PFL R753K and 30 kDa for PFL-AE.

VI.3.6 EPR of PFL-AE with PFL R753K

We probed the ability to activate PFL R753K by using EPR spectroscopy. Two methods were employed to investigate the interaction between PFL R753K and the PFL-AE/SAM complex. In the first method, PFL-AE was first photoreduced to generate the $[4\text{Fe-4S}]^{1+}$ cluster followed by addition of a 10-fold excess of SAM and a equimolar PFL R753K. In such a single turnover experiment, each photoreduced PFL-AE can only provide one electron (from the reduced $[4\text{Fe-4S}]^{1+}$ cluster) for activation, and thus a maximum of one glycy radical per PFL-AE can be produced. The second method involves starting with a

mixture containing everything including PFL-AE, a 10-fold excess of SAM and a equimolar PFL R753K, and performing photoreduction on the entire mixture. Because photoreduced 5-deazariboflavin in the presence of light can continuously provide electrons to reduce the PFL-AE cluster, PFL-AE may be reduced multiple times and provide more than one electron for PFL activation. Therefore the second method can be considered as a multiple turnover experiment.

In the single turnover experiment, the EPR spectrum of photoreduced PFL-AE in the presence of SAM exhibited a typical rhombic signal (Figure VI.3.6.1). Upon addition of PFL R753K, this $[4\text{Fe-4S}]^{1+}/\text{SAM}$ signal disappeared, suggesting that the $[4\text{Fe-4S}]^{1+}$ cluster has been consumed by PFL R753K. There was, however, no glycy radical generated in this sample. This result was different from that obtained with wildtype PFL, where the consumption of the $[4\text{Fe-4S}]^{1+}$ cluster produced equimolar glycy radical.¹⁹

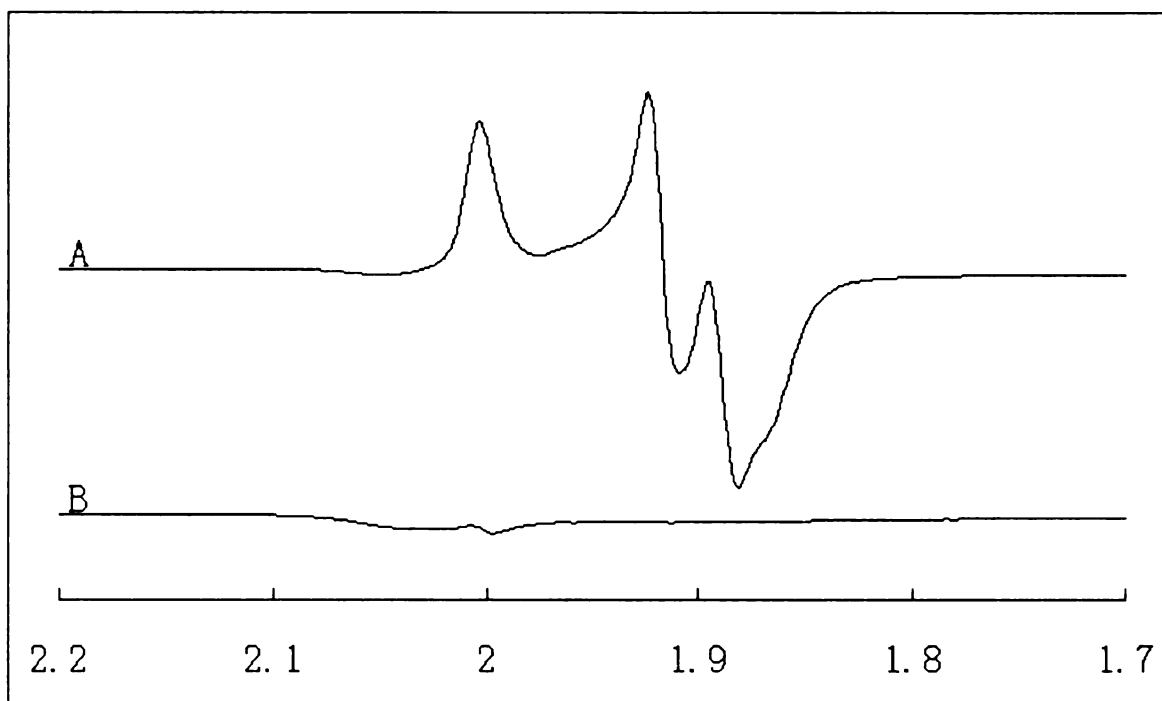


Figure VI.3.6.1. X-band EPR spectra of the single turnover samples before (A) and after (B) addition of PFL R753K to the photoreduced PFL-AE/SAM complex. The final concentrations of major components in sample A are: 290 μ M PFL-AE, 3 mM SAM, 200 μ M 5-deazariboflavin, 10 mM DTT, 100 mM Tris-Cl pH 7.6, 100 mM KCl, and 20 mM oxamate. The final concentrations of major components in sample B are: 200 μ M PFL-AE, 200 μ M PFL R753K, 2 mM SAM, 140 μ M 5-deazariboflavin, 7 mM DTT, 70 mM Tris-Cl pH 7.6, 70 mM KCl, and 14 mM oxamate. Conditions of measurement: T = 12 K; microwave power, 2 mW; modulation amplitude, 10 G. Double integration of signal intensity: A 114 μ M, B N/A.

In the multiple turnover experiment (Figure VI.3.6.2), after PFL-AE, SAM, and PFLR753K were all illuminated together for 1 hr, we observed a signal typical of the $[4\text{Fe-4S}]^{1+}$ /SAM complex at 12 K. EPR spectra recorded at 60 K showed a weak asymmetric signal. The same sample was also measured at 80 K in order to detect any thiyl radical. We see a new asymmetric signal with low intensity (10 μ M at -80 K), however the signal does not look similar to published EPR spectra of thiyl radicals.

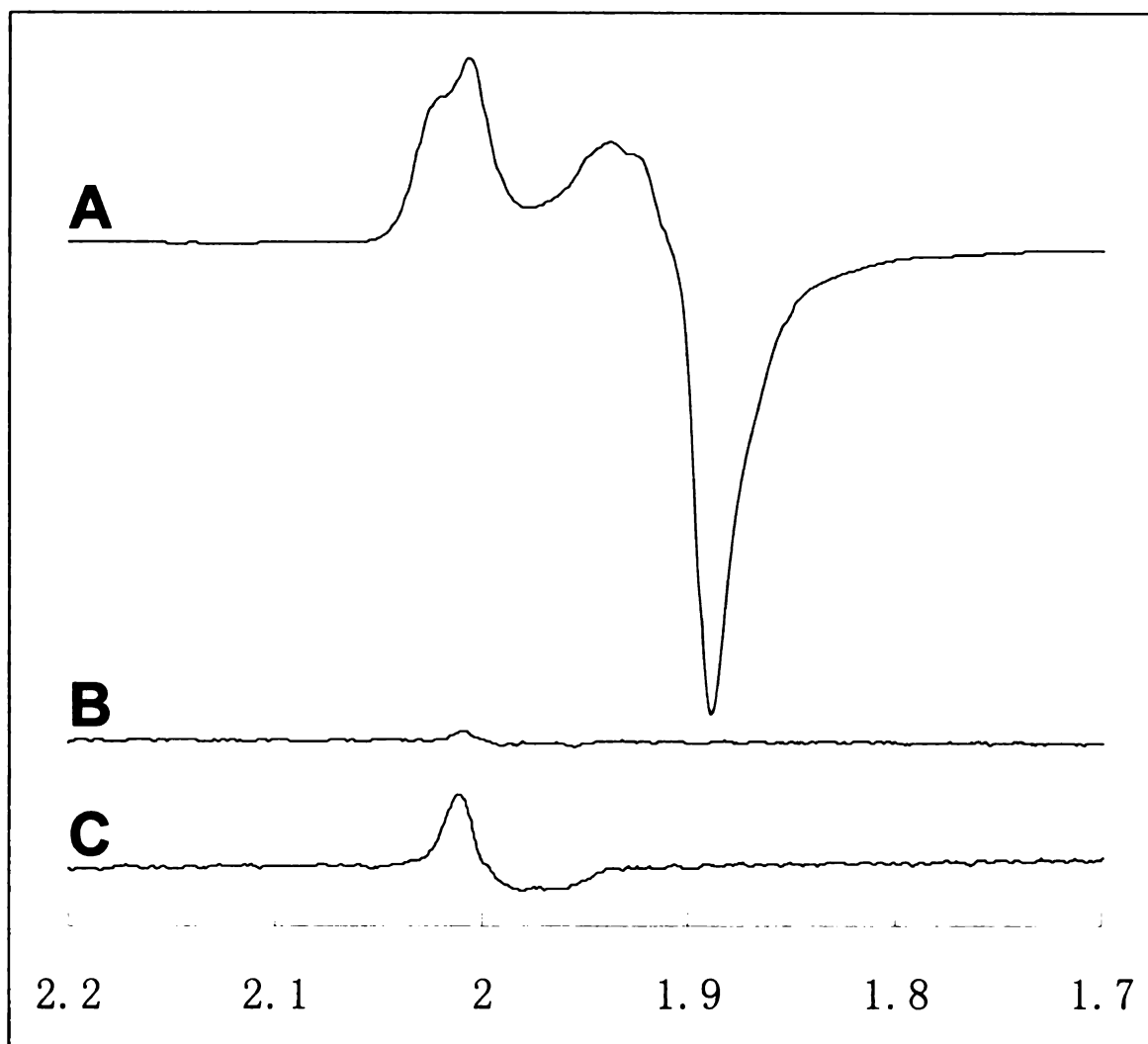


Figure VI.3.6.2. X-band EPR spectra of the multiple turnover samples containing photoreduced PFL-AE, SAM and PFL R753K under three different conditions. The final concentrations of the major components are: 200 μM PFL-AE, 200 μM PFL R753K, 2 mM SAM, 200 μM 5-deazariboflavin, 10 mM DTT, 100 mM Tris-Cl pH 7.6, 100 mM KCl, and 20 mM oxamate. Conditions of measurement: (A), $T = 12\text{ K}$; microwave power, 2 mW; modulation amplitude, 10 G; (B), $T = 60\text{ K}$; microwave power, 0.02 mW; modulation amplitude, 5 G; (C), $T = 80\text{ K}$; microwave power, 2 mW; modulation amplitude, 5 G. Double integration of signal intensity: A 120 μM , B 6 μM , C 10 μM

The apparent difference of the $[4\text{Fe}4\text{S}]^{1+}/\text{SAM}$ EPR spectra in the single turnover and the multiple turnover was caused by the presence of added PFL R753K in the multiple turnover samples. This phenomenon has been discussed in the previous chapter III.

VI.3.7 Attempted crystallization of PFL R753K by Microdialysis.

As can be seen from previous sections, PFL R753K has different properties compared to the wildtype PFL. Although PFL R753K appears to induce the radical transfer from the $[4\text{Fe-4S}]^{1+}$ /SAM complex, it perhaps can not stabilize the subsequent glycyl radical. In an effort to further understand the effect of this mutation on the mechanism, the crystal structure of this PFL R753K would be helpful.

Three different methods have been attempted to grow PFL R753K crystals. The first two methods were exactly the same as the methods published by Knappe and coworkers¹⁴ and Kozarich and coworkers¹⁰ for wildtype PFL. In these methods, PFL R753K was dialyzed against a reservoir solution containing various concentrations of PEG1000 at room temperature. During the first week all the solutions were clear while during the second week all of them became cloudy. The cloudiness was proportional to the concentration of the protein and PEG1000. To improve the crystallization conditions, 5'dAdo, oxamate and pyruvate were introduced into the reservoir solution in hope that these molecules may interact with PFL R753K, therefore increasing the chance to form crystals. Unfortunately, no crystals have been successfully grown under any of these conditions.

VI.3.8 Construction of plasmids to express YfiD, and YfiD R120K.

The YfiD gene was synthesized by the standard PCR techniques with both ends modified with restriction enzymes NdeI and Hind III. After the PCR

product and the vectors were digested by the same two restriction enzymes, they were ligated together and transformed into XL1 Blue competent cells for amplification of the plasmids. The plasmid was then purified from these cells, and DNA sequences were confirmed by DNA sequencing. The mutated plasmid pJYVII139-1 was made from pJYVII127-1 by the same site directed mutagenesis method used for pJYVII123 (Section VI.3.4). DNA sequencing confirmed the presence of the mutation.

VI.3.9 Expression and purification of YfiD and YfiD R120K

YfiD and YfiD R120K were both transformed into the same BL21(DE3)pLysS competent cells. Subsequent overexpression and purification were performed essentially the same as described for PFL R753K. Figure VI.3.9.1 is an example of YfiD purification on ion exchange column. YfiD and YfiD R120K showed the same behavior in terms of the elution profile from ion exchange column, suggesting they are similar in overall protein structure. The overall yield of purified YfiD and YfiD R120K was 20 mg per 1 L of growth media.

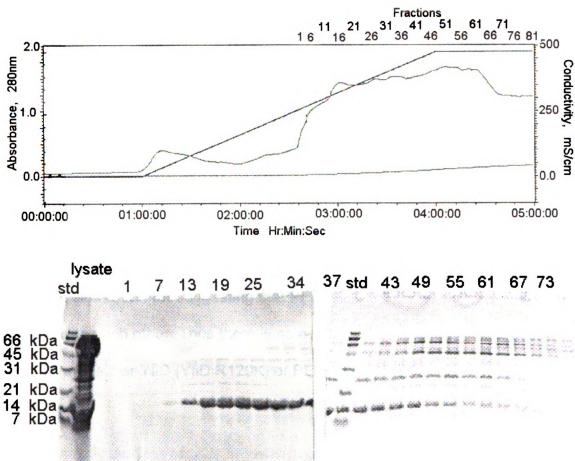


Figure VI.3.9.1. Purification of YfiD by ion exchange chromatography. Upper Panel: UV Chromatogram of YfiD purification by ion exchange chromatography. YfiD elutes in fractions 13-34, at approximately 56 % buffer B. Lower Panel: SDS-PAGE analysis of corresponding fractions from ion exchange column. The fraction numbers are indicated on top of the gel.

VI.3.10 Binding assay of PFL-AE with YfiD and YfiD R120K

The binding assay of PFL-AE with YfiD (or YfiD R120K) was carried out essentially as described for that of PFL-AE with PFL R753K (Section VI.3.5).

Upon separation of the mixture of PFL-AE with YfiD (or YfiD R120K) by gel filtration chromatography, there were two well-resolved peaks. The first peak was centered at 70.5 mL with an apparent molecular weight approximately 30 kDa, consistent with that of the PFL-AE monomer (28 kDa). The second peak was

centered at 75 mL with an apparent molecular weight approximately 14 kDa, identical to that of YfiD (or YfiD R120K) (14 kDa). There was no peak consistent with the PFL-AE and YfiD (or YfiD R120K) complex (expected molecular weight of 42 kDa). These results were also confirmed by SDS-PAGE of the fractions off the gel filtration column, which showed each protein eluting in a separate peak (Figure VI.3.10.1 and Figure VI.3.10.2). Moreover, the elution volumes of both PFL-AE and YfiD (or YfiD R120K) remain the same when samples containing either PFL-AE or YfiD (or YfiD R120K) were tested individually on the same gel filtration column, further suggesting that PFL-AE and YfiD (or YfiD R120K) do not interact with each other. Thus there is no evidence for complex formed between PFL-AE and either YfiD (YfiD R120K) or PFL (PFL R753K).

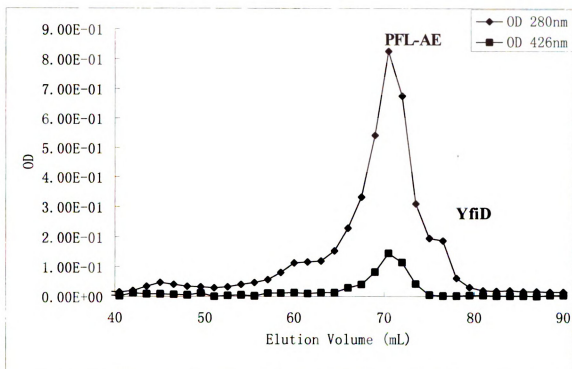


Figure VI.3.10.1. Gel filtration chromatography of YfiD and PFL-AE mixture on a Sepharose™ 12 column. An equimolar mixture of YfiD and PFL-AE was loaded onto the gel filtration column and run with isocratic flow. Two peaks are observed with molecular weights of 14 kDa for YfiD and 30 kDa for PFL-AE.

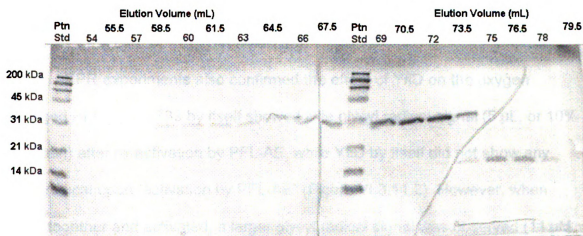


Figure VI.3.10.2. SDS-PAGE analysis of fractions off the gel filtration column showing separation of PFL-AE and YfiD. The elution volumes are indicated on top of the gel.

VI.3.11 *Salvage of PFL by YfiD: EPR and activity assays*

The oxygen damaged products (the larger piece PFL1-733 and the smaller piece PFL734-760) of the activated PFL were made by cleaving the peptide bond between G734 and S733 (Section VI.2.13).⁸ When the mixture of PFL1-733 and PFL734-760 was tested by the regular PFL-AE/PFL activity assay, only little activity (2.0 $\mu\text{mol}/\text{min}/\text{mg}$) was observed compared to that of the wildtype PFL (12.3 $\mu\text{mol}/\text{min}/\text{mg}$, Section VI.3.2). The small activity observed is likely caused by the trace amount of residual PFL that was not initially activated; that is, PFL is rarely 100% activated during an activation reaction, and therefore remains unaffected by oxygen exposure and is capable of being “reactivated”. The activity of oxygen-cleaved and reactivated PFL was greatly increased in the presence of YfiD, suggesting YfiD is able to interact with PFL1-733 and restore the enzymatic activity (Figure VI.3.11.1). The specific activity of this YfiD/PFL1-733 sample is 9.1 $\mu\text{mol}/\text{min}/\text{mg}$ in the presence of 10 x excess amount of YfiD over PFL1-733. This is consistent with literature reports showing the association of YfiD with the core of PFL (Ser1-Ser733).⁹

EPR experiments also confirmed the effect of YfiD on the oxygen damaged PFL. PFL1-733 by itself showed little glycy radical signal (5 μL , or 10% of protein) after re-activation by PFL-AE, while YfiD by itself did not show any glycy radical upon “activation by PFL-AE” (Figure VI.3.11.2). However, when mixed together and activated, a larger glycy radical signal was observed (11 μM , or 20% of protein), suggesting the production of glycy radical is the result of the mixture of PFL1-733 and YfiD.

To summarize, the activity of the oxygen damaged PFL can be salvaged by addition of excess amount of YfiD. Maximal increase of PFL1-733 activity requires an excess of YfiD, suggesting that YfiD and PFL1-733 don't form tight complex. EPR experiment with a 5-fold excess of YfiD significantly increased the amount of glycyl radical generated, further supporting the salvage function of YfiD for oxygen damaged PFL1-733.

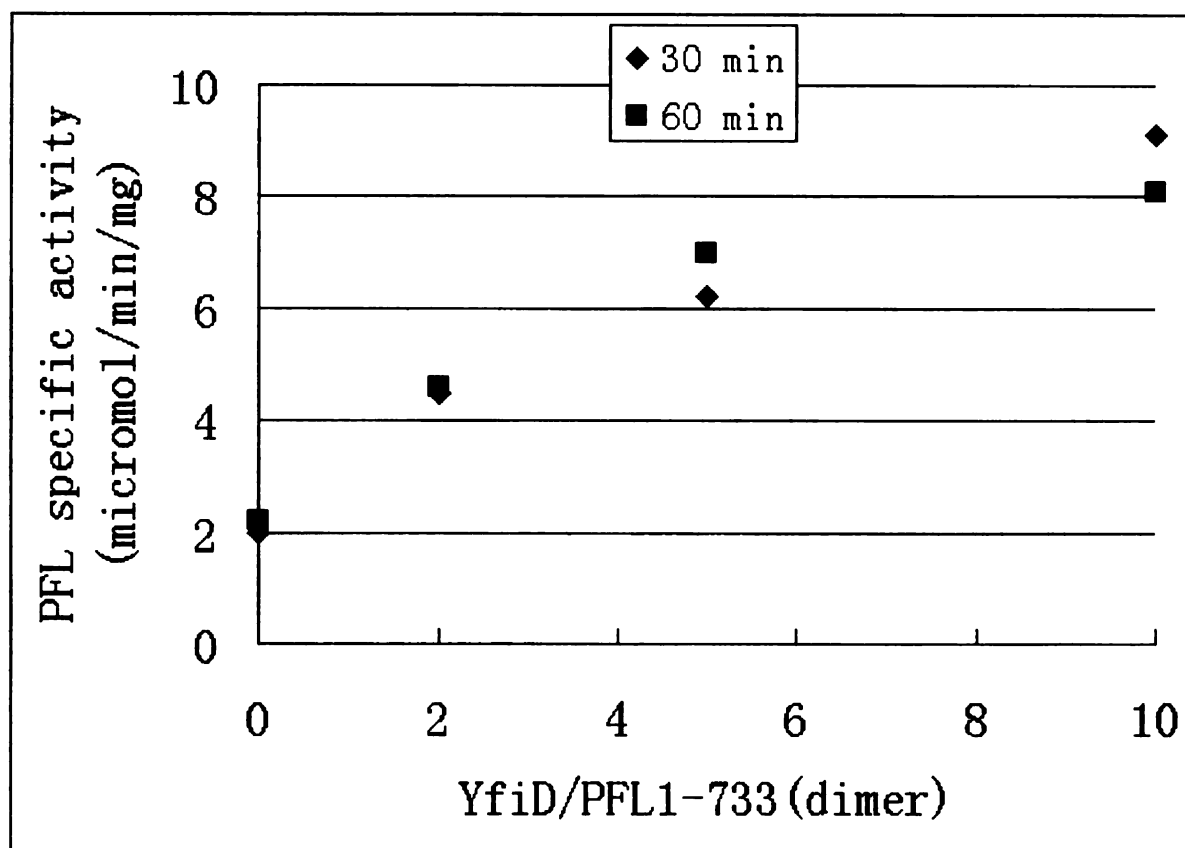


Figure VI.3.11.1. Plot of PFL specific activity as a function of YfiD/PFL ratio. The activation reaction includes 0.1 M Tris-HCl pH 7.6, 0.1 M KCl, 10 mM oxamate, 8 mM DTT, 0.05 μ M PFL-AE, 5 μ M oxygen damaged PFL, 0.2 mM AdoMet, 0 – 50 μ M YfiD (as indicated by the above YfiD/PFL ratio) and 50 μ M 5-deazariboflavin. After 30 min (■) and 60 min (▲) illumination on ice, an aliquot was removed for assay of active PFL through the coupling assay.

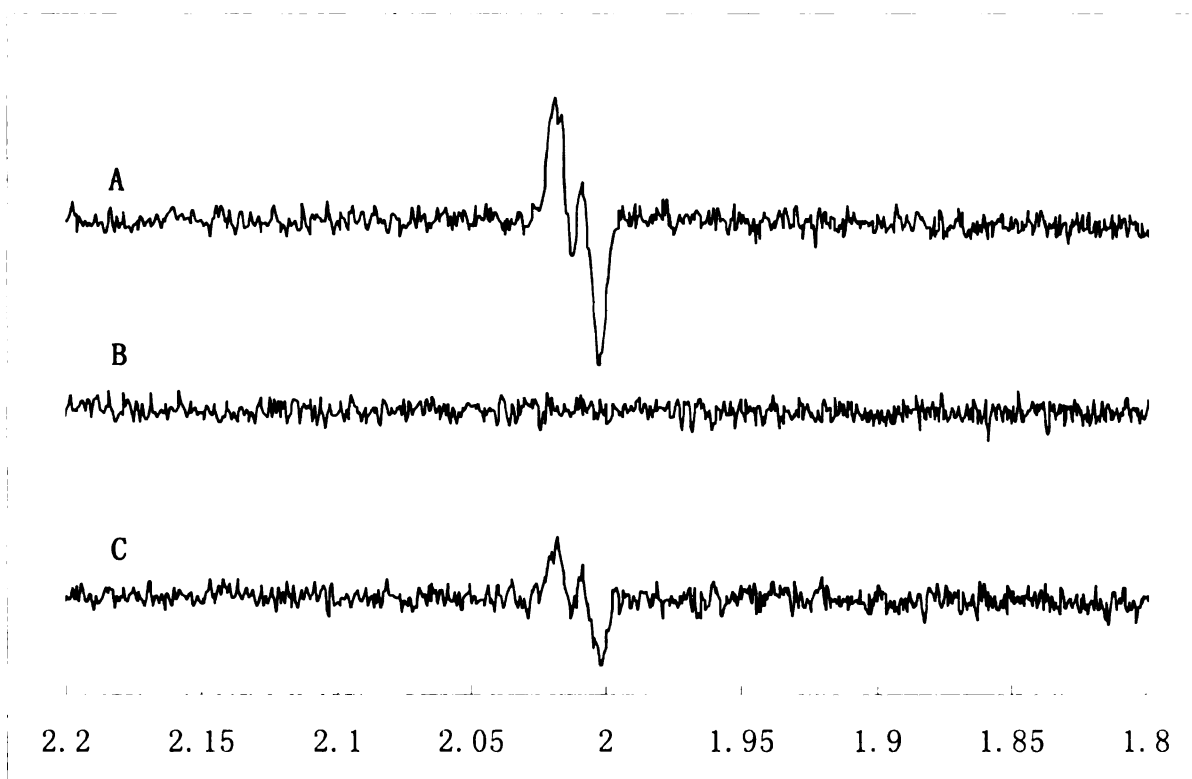


Figure VI.3.11.2. X-band EPR spectra of the PFL1-733 (A), a 5-fold excess of YfiD (B) and the mixture of both (C) after “activation” by PFL-AE. The final concentrations of the major components in these samples are 50 μ M PFL-AE, 100 μ M 5-deazariboflavin, 10 mM DTT, 100 mM Tris-HCl pH 7.6, 100 mM KCl, 20 mM oxamate, 2 mM SAM, 50 μ M oxygen damaged PFL (C), 250 μ M YfiD (B) or both oxygen damaged PFL and YfiD (A). Conditions of measurement T = 60 K; microwave power, 0.02 mW; modulation amplitude, 5 G. Double integration of signal intensity: A 11 μ M, B N/A, C 5 μ M.

VI.4 Conclusions

In this chapter, the interaction between PFL-AE and PFL has been investigated by using the methods of gel filtration, EPR and ENDOR spectroscopy, and activity assays in the presence of PFL mutants and homologs. None of the results provide evidence for the presence of a tight complex with PFL-AE.

PFL G734A was investigated in hope that this mutant would allow us to probe the interaction of the catalytically active $[4\text{Fe-4S}]^{1+}$ /AdoMet complex with its substrate during the activation reaction. Both EPR and ENDOR results show that PFL G734A has little impact on the electronic structure of the $[4\text{Fe-4S}]^{1+}$ /AdoMet complex. The field dependence of the ENDOR of the PFL-AE/(^{13}C -Methyl)-SAM complex does not change in the presence of PFL G734A, suggesting that the interaction between ^{13}C -methyl group and the iron sulfur cluster in PFL-AE remains the same regardless of the addition of PFL G734A.

PFL R753K does not form tight complex with PFL-AE as was reported for the corresponding GD R782K and GD-AE.² PFL R753K appears to be able to cause oxidation of the $[4\text{Fe-4S}]^{1+}$ cluster, but no glycyl radical is observed afterwards. To our surprise, when PFL-AE, SAM and PFL R753K are illuminated together, a new weak signal appears, which can not be definitively assigned as either a glycyl radical or a thiyl radical.

As previously reported,⁹ YfiD is able to salvage the oxygen damaged PFL. However, YfiD as well as its mutant YfiD R120K can not form tight complex

with PFL-AE even though YfiD is the smallest independent domain proposed to provide the surface for the docking of PFL-AE on PFL during activation.²

VI.5 References

1. Frey, M.; Rothe, M.; Wagner, A. F. V.; Knappe, J., Adenosylmethionine-dependent synthesis of the glycyl radical in pyruvate formate-lyase by abstraction of the glycine C-2 pro-S hydrogen atom. Studies of [2H]glycine-substituted enzyme and peptides homologous to the glycine 734 site. *Journal of Biological Chemistry* **1994**, 269, (17), 12432-7.
2. O'Brien, J. R.; Raynaud, C.; Croux, C.; Girbal, L.; Soucaille, P.; Lanzilotta, W. N., Insight into the Mechanism of the B12-Independent Glycerol Dehydratase from *Clostridium butyricum*: Preliminary Biochemical and Structural Characterization. *Biochemistry* **2004**, 43, (16), 4635-4645.
3. Toraya, T., Radical catalysis in coenzyme B12-dependent isomerization (eliminating) reactions. *Chem Rev* **2003**, 103, (6), 2095-127.
4. Becker, A.; Kabsch, W., X-ray Structure of Pyruvate Formate-Lyase in Complex with Pyruvate and CoA. *Journal of Biological Chemistry* **2002**, 277, (42), 40036-40042.
5. Walsby, C. J.; Ortillo, D.; Yang, J.; Nnyepi, M. R.; Broderick, W. E.; Hoffman, B. M.; Broderick, J. B., Spectroscopic Approaches to Elucidating Novel Iron-Sulfur Chemistry in the "Radical-SAM" Protein Superfamily. *Inorganic Chemistry* **2005**, 44, (4), 727-741.
6. Knappe, J.; Neugebauer, F. A.; Blaschkowski, H. P.; Gaenzler, M., Post-translational activation introduces a free radical into pyruvate formate-lyase. *Proceedings of the National Academy of Sciences of the United States of America* **1984**, 81, (5), 1332-5.
7. Unkrig, V.; Neugebauer, F. A.; Knappe, J., The free radical of pyruvate formate-lyase. Characterization by EPR spectroscopy and involvement in catalysis as studied with the substrate-analogue hypophosphite. *European Journal of Biochemistry* **1989**, 184, (3), 723-8.
8. Wagner, A. F. V.; Frey, M.; Neugebauer, F. A.; Schaefer, W.; Knappe, J., The free radical in pyruvate formate-lyase is located on glycine-734. *Proceedings of the National Academy of Sciences of the United States of America* **1992**, 89, (3), 996-1000.
9. Wagner, A. F. V.; Schultz, S.; Bomke, J.; Pils, T.; Lehmann, W. D.; Knappe, J., YfiD of *Escherichia coli* and Y06I of Bacteriophage T4 as Autonomous Glycyl Radical Cofactors Reconstituting the Catalytic Center of

Oxygen-Fragmented Pyruvate Formate-Lyase. *Biochemical and Biophysical Research Communications* **2001**, 285, (2), 456-462.

10. Lehtioe, L.; Leppaenen, V. M.; Kozarich, J. W.; Goldman, A., Structure of Escherichia coli pyruvate formate-lyase with pyruvate. *Acta Crystallographica, Section D: Biological Crystallography* **2002**, D58, (12), 2209-2212.
11. Miller, J. H., *Experiments in Molecular Genetics*. C. S. H. Press: New York, 1972.
12. Leppanen, V.-M.; Parast, C. V.; Wong, K. K.; Kozarich, J. W.; Goldman, A., Purification and crystallization of a proteolytic fragment of Escherichia coli pyruvate formate-lyase. *Acta Crystallographica, Section D: Biological Crystallography* **1999**, D55, (2), 531-533.
13. Parast, C. V.; Wong, K. K.; Lewisch, S. A.; Kozarich, J. W.; Peisach, J.; Magliozzo, R. S., Hydrogen Exchange of the Glycyl Radical of Pyruvate Formate-Lyase Is Catalyzed by Cysteine 419. *Biochemistry* **1995**, 34, (8), 2393-9.
14. Becker, A.; Fritz-Wolf, K.; Kabsch, W.; Knappe, J.; Schultz, S.; Wagner, A. F. V., Structure and mechanism of the glycyl radical enzyme pyruvate formate-lyase. *Nature Structural Biology* **1999**, 6, (10), 969-975.
15. Aasa, R.; Vanngard, T.; Dunford, H. B., EPR studies on compound I of horseradish peroxidase. *Biochim Biophys Acta* **1975**, 391, (2), 259-64.
16. Murib, J. H.; Riter, D. M., *Journal of the American Chemical Society* **1952**, 74, 339.
17. Broderick, J. B.; Henshaw, T. F.; Cheek, J.; Wojtuszewski, K.; Smith, S. R.; Trojan, M. R.; McGhan, R. M.; Kopf, A.; Kibbey, M.; Broderick, W. E., Pyruvate formate-lyase-activating enzyme: Strictly anaerobic isolation yields active enzyme containing a [3Fe-4S]⁺ cluster. *Biochemical and Biophysical Research Communications* **2000**, 269, (2), 451-456.
18. Walsby, C. J.; Hong, W.; Broderick, W. E.; Cheek, J.; Ortillo, D.; Broderick, J. B.; Hoffman, B. M., Electron-Nuclear Double Resonance Spectroscopic Evidence That S-Adenosylmethionine Binds in Contact with the Catalytically Active [4Fe-4S]⁺ Cluster of Pyruvate Formate-Lyase Activating Enzyme. *Journal of the American Chemical Society* **2002**, 124, (12), 3143-3151.
19. Henshaw, T. F.; Cheek, J.; Broderick, J. B., The [4Fe-4S]¹⁺ Cluster of Pyruvate Formate-Lyase Activating Enzyme Generates the Glycyl Radical on Pyruvate Formate-Lyase: EPR-Detected Single Turnover. *Journal of the American Chemical Society* **2000**, 122, (34), 8331-8332.

CHAPTER VII

INVESTIGATION ON THE MECHANISM OF PFL BY VARIOUS CYSTEINE MUTANTS: PFL C418A, PFL C419A, AND PFL C418A/C419A.

VII.1 Introduction

The crystal structure of PFL has been described in the introduction part of this dissertation (I.3). In an effort to make the study of this chapter clearer, a few key features of this enzyme are reemphasized here. 1. PFL is homodimeric protein with a molecular weight of 170 KDa. 2. Each PFL protomer forms a G-barrel, which consists of 10-stranded α/β barrel assembled in an anti-parallel manner from two parallel five-stranded β -sheets. 3. The catalytic site of PFL is located at the center of this G-barrel. 4. Two opposing hairpin loops, which are designated as the glycine loop and the cysteine loop respectively, protrude from the top and bottom surfaces of the barrel and meet at the center of this barrel. 5. The relative positions of three key residues, G734 of the glycine loop, and C418 and C419 of the cysteine loop, are illustrated in the Figure VII.1.1.

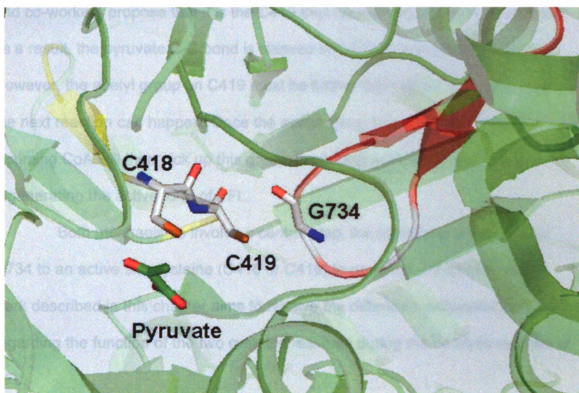


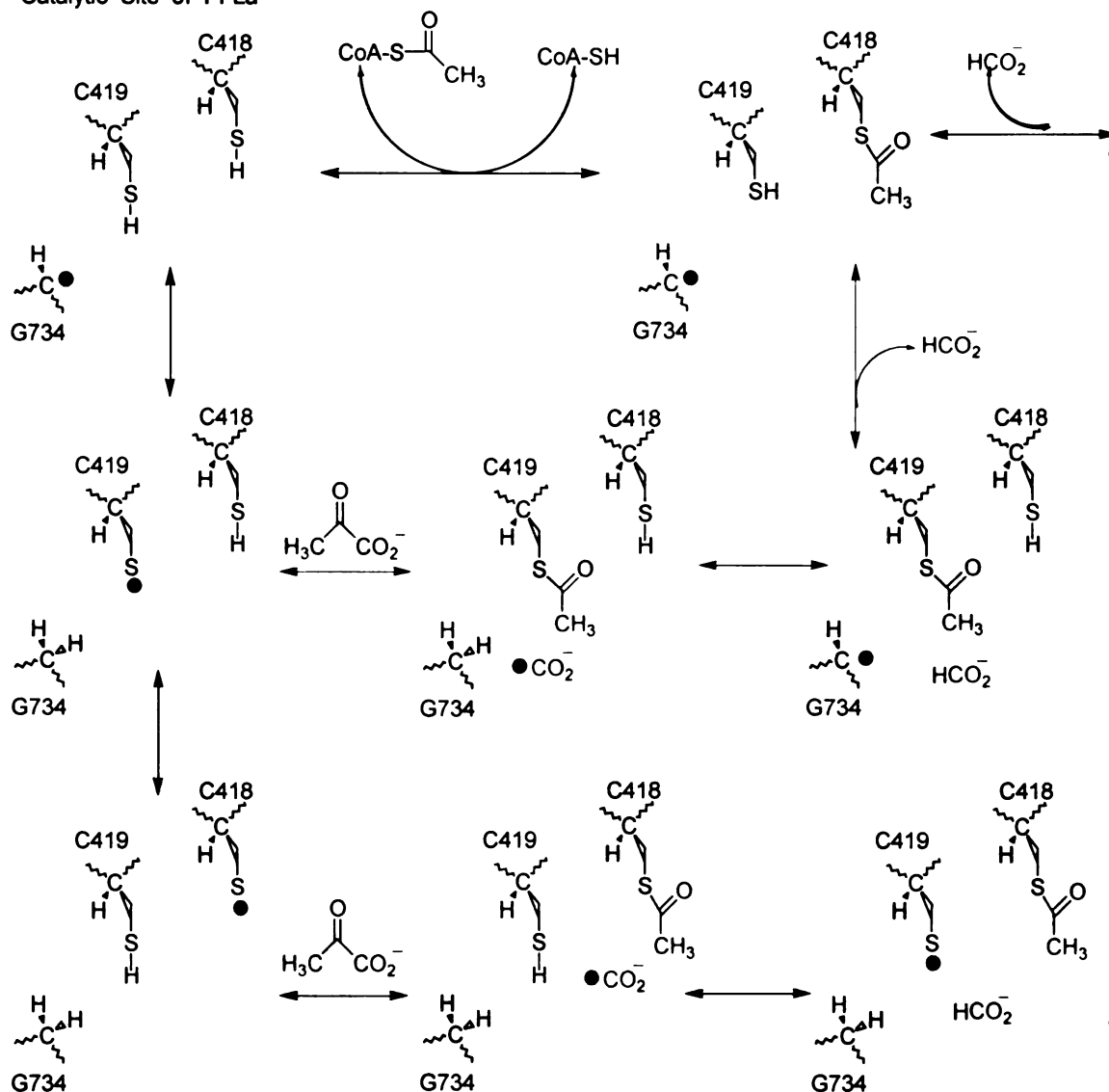
Figure VII.1.1 Catalytic site of PFL. Residues G734, C418, C419, and the bound pyruvate molecule are shown as sticks and indicated in the graph. The catalytic cysteine loop and the radical-bearing glycine loop are colored in yellow and red, respectively.

Although the glycy radical is initially generated on the residue G734 of PFL, G734 is not believed to be directly involved in catalysis. Instead, G734 is able to relay the glycy radical to the adjacent cysteine residues to form a C418 thiyl radical or a C419 thiyl radical. Depending on which thiyl radical is directly involved in the homolytic cleavage of the pyruvate C-C bond, two mechanisms have been proposed as summarized in Scheme VII.1.1.¹⁻⁴ Knappe and coworkers believe that it is the C418 thiyl radical that initially attacks pyruvate, resulting in homolytic cleavage of its C-C bond. In this mechanism, the function of C419 is simply to relay the radical from G734 to C418. In contrast, Kozarich

and co-workers propose that it is the C419 thiyl radical that attacks pyruvate first; as a result, the pyruvate C-C bond is cleaved and PFL is acetylated at C419. However, the acetyl group on C419 must be further transferred to C418 before the next reaction can happen. Once the acetyl group is located on C418, the incoming CoA will then pick up this group, producing acetyl-CoA and regenerating the active form of PFL.

Both mechanisms involve a central step, the transfer of a radical from G734 to an active site cysteine (C418 or C419) to generate a thiyl radical. The work described in this chapter aims to resolve the different mechanistic proposal regarding the function of the two cysteine residues during the catalytic reaction of PFL.

Catalytic Site of PFLa



Scheme VII.1.1. Summary of two PFL mechanisms. Inner loop: the mechanism proposed by Kozarich and co-workers.^{3, 4} Outer loop: mechanism proposed by Knappe and co-workers.^{1, 2}

VII.2 Materials and Methods

Materials

All chemicals used were commercially obtained except when noted otherwise and were of the highest available purity. BL21(DE3)pLysS competent cells were purchased from NovagenTM. QuikChange Site-Directed Mutagenesis Kit was purchased from Stratagene. All columns and resins were purchased from Amersham Biosciences and Waters Corporations. SDS-PAGE gels were commercially obtained from Bio-Rad Scientific.

Preparation of EPR samples were carried out in an anaerobic glove box (Mbraun) with oxygen level less than 2 ppm. All buffers were deoxygenated using a vacuum/nitrogen gas manifold before being taken into the glove box. Solid chemicals were pumped in as solids. Ice was pre-chilled with liquid nitrogen before pumping into the glove box.

VII.2.1 Site-directed mutagenesis of PFL.

Site directed mutagenesis of PFL cysteine residues was performed essentially the same as that to generate PFL R753K (section VI.2.4). The oligonucleotide sequences used in these mutagenesis reactions are shown below, with the mutated codon highlighted in red.

PFL C418A:

Primer I: 5'-GAC,TAC,GCT,ATT,GCT,GCA,TGC,GTA,AGC,CCG,ATG,ATC-3'
and

Primer II: 5'-GAT,CAT,CGG,GCT,TAC,GCA,TGC,AGC,AAT,AGC,GTA,GTC-3'

PFL C419A

Primer I: 5'-GAC,TAC,GCT,ATT,GCT,TGC,GCA,GTA,AGC,CCG,ATG,ATC-3'
and

Primer II: 5'-GAT,CAT,CGG,GCT,TAC,TGC,GCA,AGC,AAT,AGC,GTA,GTC-3'

PFL C418A/C419A

Primer I: 5'-GAC,TAC,GCT,ATT,GCT, GCA,GCA,GTA,AGC,CCG,ATG,ATC-3'
and

Primer II: 5'-GAT,CAT,CGG,GCT,TAC,TGC,TGC,AGC,AAT,AGC,GTA,GTC-3'

Mutated plasmids [pJYVII119-1 (PFL C418A), pJYVII119-2 (PFL C419A), and pJYVII119-3 (PFL C418A/C419A)] were confirmed by DNA sequencing in the Research Technology Support Facility at Michigan State University.

VII.2.2 Transformation, overexpression and purification of PFL cysteine mutants

All PFL cysteine mutant plasmids (pJYVII119-1, pJYVII119-2, and pJYVII119-3) were transformed into BL21(DE3)plysS cells using the same procedure as for pJYVII123 (PFL R753K). The overexpression and purification were also performed essentially the same as PFL R753K (VI.2.5).

VII.2.3. Mechanistic studies of cysteine mutants.

PFL cysteine mutants (PFL C418A or PFL C419A) and PFL-AE were mixed in a buffer containing 100 mM Tris-HCl pH 7.6, 100 mM KCl, 10 mM DTT, and 20 mM oxamate to a final volume of 400 μ L and a final concentration of 200 μ M each. Photoreducing agent 5-deazariboflavin (from a 10 mM stock solution in DMSO) was added in the dark to a final concentration of 200 μ M and the samples were transferred to EPR tubes. Then the EPR tubes were capped and inserted in a beaker tightly packed with ice and water. After the reaction mixtures

were illuminated on ice for 30 min using a 300 W halogen lamp situated 2 cm from the beaker, the resulting mixtures were divided into 4 identical aliquots (75 μ L each). Aliquot I was diluted with 225 μ L H₂O buffer (100 mM Tris-HCl pH 7.6, 100 mM KCl) and flash-frozen in liquid nitrogen as the H₂O control (A). Aliquot II was diluted with 225 μ L D₂O buffer (100 mM Tris-HCl pD 8.0, 100 mM KCl) and flash-frozen in liquid nitrogen as D₂O control (B). To aliquot III was added pyruvate to a final concentration of 20 mM (from a 1 M pyruvate stock solution in MQ water), and this solution was incubated at room temperature for 10 min. The resulting reaction mixture was then diluted with 225 μ L H₂O buffer (100 mM Tris-HCl pH 7.6, 100 mM KCl), and flash-frozen as H₂O/Pyruvate (C). To aliquot IV was added pyruvate to a final concentration of 20 mM, and this solution was incubated at room temperature for 10 min. The resulting reaction mixture was then diluted with 225 μ L D₂O buffer (100 mM Tris-HCl pD 8.0, 100 mM KCl), and flash-frozen as D₂O/Pyruvate (D). All EPR samples were flash-frozen in liquid nitrogen in the glove box for further analysis.

VII.2.4 Photolysis to generate thiyl radical on PFL cysteine mutants

The as-isolated PFL cysteine mutants (PFL C418A, PFL C419A, and PFL C418A/C419A) were first dialyzed into a buffer containing 200 mM potassium phosphate pH 7.0, and concentrated in an Amicon concentrator equipped with a YM-30 membrane in the Coy chamber. The concentrations were determined by the method of Bradford. The resulting concentrated PFL cysteine mutants were mixed with 200 mM potassium phosphate pH 7.0 to a final volume of 300 μ L and

a final concentration of 500 μM , and transferred to EPR tubes in the anaerobic glove box and flash-frozen in liquid nitrogen.

Thiyl radicals were generated by UV photolysis at low temperature.⁵ Samples in EPR quartz tubes were irradiated at 77 K by UV for 8 min with a 175 W Xe arc lamp in a quartz finger cryostat filled with liquid nitrogen. In two-minute intervals the sample was turned by 90° to ensure a homogeneous irradiation of the surface of the sample. These EPR tubes were then kept under liquid nitrogen until being measured by EPR.

VII.3 Results and Discussion

VII.3.1 Mutagenesis of PFL to produce PFL C418A, PFL C419A, and PFL C418A/C419A.

The PFL mutants C418A, C419A, and C418A/C419A have all been successfully produced from wildtype PFL using site directed mutagenesis. The sequences of all mutants have been confirmed by DNA sequencing in the Research Technology Support Facility at Michigan State University.

VII.3.2 Expression and purification of PFL mutants.

Subsequent transformation of these plasmids into BL21(DE3)plysS created the overexpressing strains. PFL C418A, PFL C419A and PFL C418A/C419A were overexpressed by inducing with 1 mM IPTG after normal aerobic growth. Interestingly, the purification of these mutants were essentially the same as that of wildtype PFL in terms of elution volumes on both ion exchange and hydrophobic interaction columns (Figure VII.3.2.1 and Figure VII.3.2.2 are an example for the purification of C418A). The overall yield of purified PFL cysteine mutants were 30 mg per 1 L of growth media. This is a clear sign to us that the overall structure of these mutants is very similar to that of wildtype PFL, which is expected since this each single mutation replaces the C418 or C419 residue by a similarly sized alanine residue.

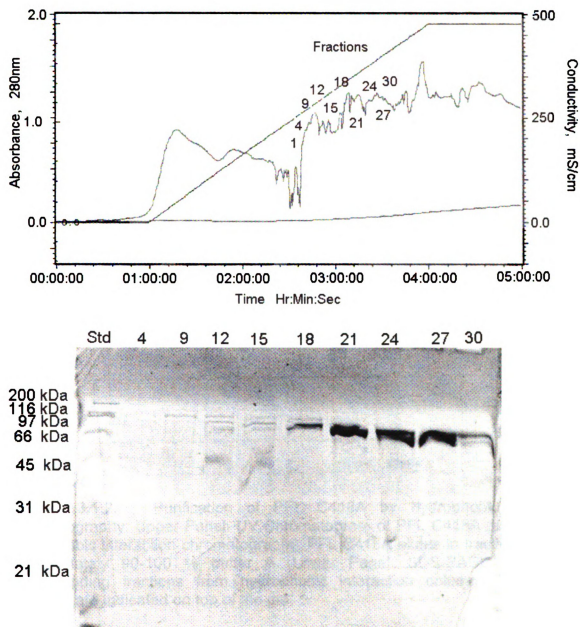


Figure VII.3.1.1. Purification of PFL C418A by ion exchange chromatography. Upper Panel: Chromatogram of PFL C418A purification by ion exchange chromatography. PFL C418A elutes in fractions 21-27, at approximately 45 % buffer B. Lower Panel: SDS-PAGE analysis of corresponding fractions from ion exchange column. The fraction numbers are indicated on top of the gel.

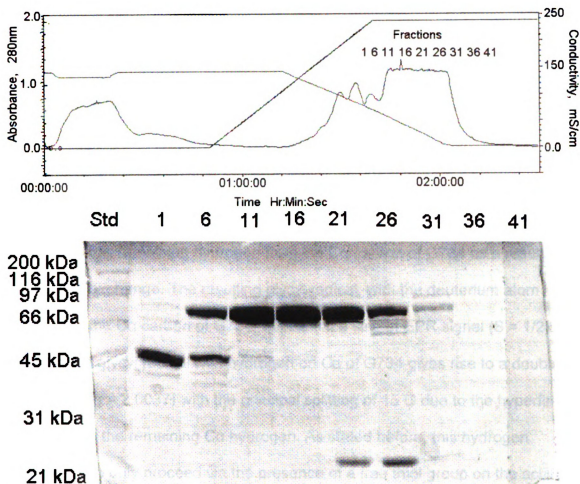


Figure V.3.1.2. Purification of PFL C418A by hydrophobic interaction chromatography. Upper Panel: UV Chromatogram of PFL C418A purification by hydrophobic interaction chromatography. PFL C418A elutes in fractions 6-26, at approximately 90-100 % buffer A. Lower Panel: SDS-PAGE analysis of corresponding fractions from hydrophobic interaction column. The fraction numbers are indicated on top of the gel.

VII.3.3D₂O exchange in the PFL cysteine mutants.

It has been shown that once the PFL glycyl radical is generated on residue G734, it remains stable under strict anaerobic conditions ($t_{1/2} > 24\text{hr}$).^{6, 7} One of the intriguing properties of this glycyl radical is that the remaining C α hydrogen of the G734 residue can exchange with solvent via the free thiol group of the active-site residue C419.³ In the presence of D₂O buffer, a deuterium atom will replace this remaining hydrogen from the C α carbon of G734 as a result of this solvent exchange. The resulting glycyl radical, with the deuterium atom attached to the C α carbon of G734, will exhibit a singlet EPR signal ($S = 1/2$). In contrast, the glycyl radical with hydrogen on C α of G734 gives rise to a doublet EPR signal ($g = 2.0037$) with the principal splitting of 15 G due to the hyperfine coupling with the remaining C α hydrogen. As stated before, this hydrogen exchange can only proceed via the presence of a free thiol group on the active site residue C419.³ If the thiol is removed by mutagenesis or the free thiol group is occupied by an acetyl group as a result of PFL reaction with pyruvate (the first step in the ping-pong mechanism of PFL), the hydrogen exchange is disrupted and the glycyl radical EPR spectra appear as doublets. In the work described in this section, we take advantage of this property to solve the discrepancy regarding different functions of the two cysteines (C418 and C419) arising from the mechanisms proposed by Knappe and Kozarich.¹⁻⁴

Both PFL cysteine mutants (PFL C418A or PFL C419A) were activated by PFL-AE under strict anaerobic conditions, and then 4 samples were made (\pm pyruvate and \pm D₂O). The EPR spectra of these samples are summarized in

Figure VII.3.3.1 (C418A) and VII.3.3.2 (C419A). In both figures, spectrum A is the sample in H₂O buffer with no pyruvate. The results show that samples containing either PFL C418A or PFL C419A are almost 100% activated into the active form with a doublet glycy radical indicating the presence of a hydrogen on G734 as expected. Spectra labeled B are the same samples diluted with D₂O. The sample containing PFL C419A shows a doublet as expected because the mutation of C419A removes the free thiol group responsible for the hydrogen exchange between C α of the glycy radical and solvent. In contrast, the spectrum for PFL C418A shows a singlet, which is also expected, because the mutation of C418A has no effect on the free thiol group of C419, and therefore no effect on the hydrogen exchange reaction. Spectra C are for the same samples incubated with pyruvate at room temperature to acetylate the free thiol (if possible for each mutant). Spin quantifications of both EPR spectra show almost 100 % preservation of the original doublet glycy radical signals, suggesting the acetylation of PFL mutants does not consume the glycy radical, as has been previously reported.³ Spectra D are of samples that were first reacted with pyruvate and then diluted with D₂O buffer. Depending on which cysteine (C418 or C419) initiates the reaction on pyruvate, the possible outcomes will vary, as described below and summarized in Scheme VII.3.3.1 and VII.3.3.2.

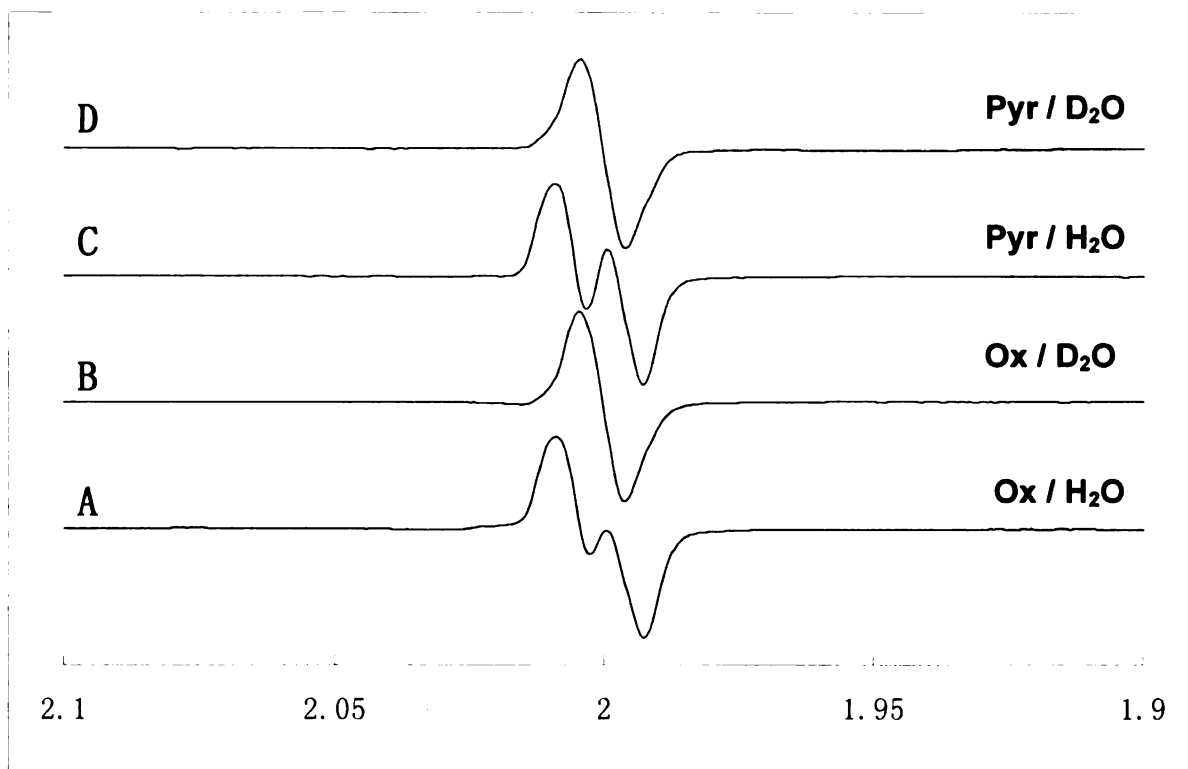


Figure VII.3.3.1. X-band EPR spectra of activated PFL C418A with different amount of pyruvate and D₂O. The final concentrations of major components in these samples are: A, 50 μ M PFL C418A, 100 mM Tris-HCl pH 7.6, 100 mM KCl, 2.5 mM DTT, and 5 mM oxamate; B, 50 μ M PFL C418A, 100 mM Tris-HCl pD 8.0, 100 mM KCl, 2.5 mM DTT, 5 mM oxamate, and 75 % (v/v) D₂O; C, 50 μ M PFL C418A, 100 mM Tris-HCl pH 7.6, 100 mM KCl, 2.5 mM DTT, 5 mM oxamate, and 5 mM pyruvate; D, 50 μ M PFL C418A, 100 mM Tris-HCl pD 8.0, 100 mM KCl, 2.5 mM DTT, 5 mM oxamate, 5 mM pyruvate, and 75 % (v/v) D₂O. Condition of measurement: T = 60 K; microwave power, 0.02 mW; modulation amplitude, 10 G. Double integration of signal intensity: A 47 μ M, B 40 μ M, C 70 μ M, D 53 μ M.

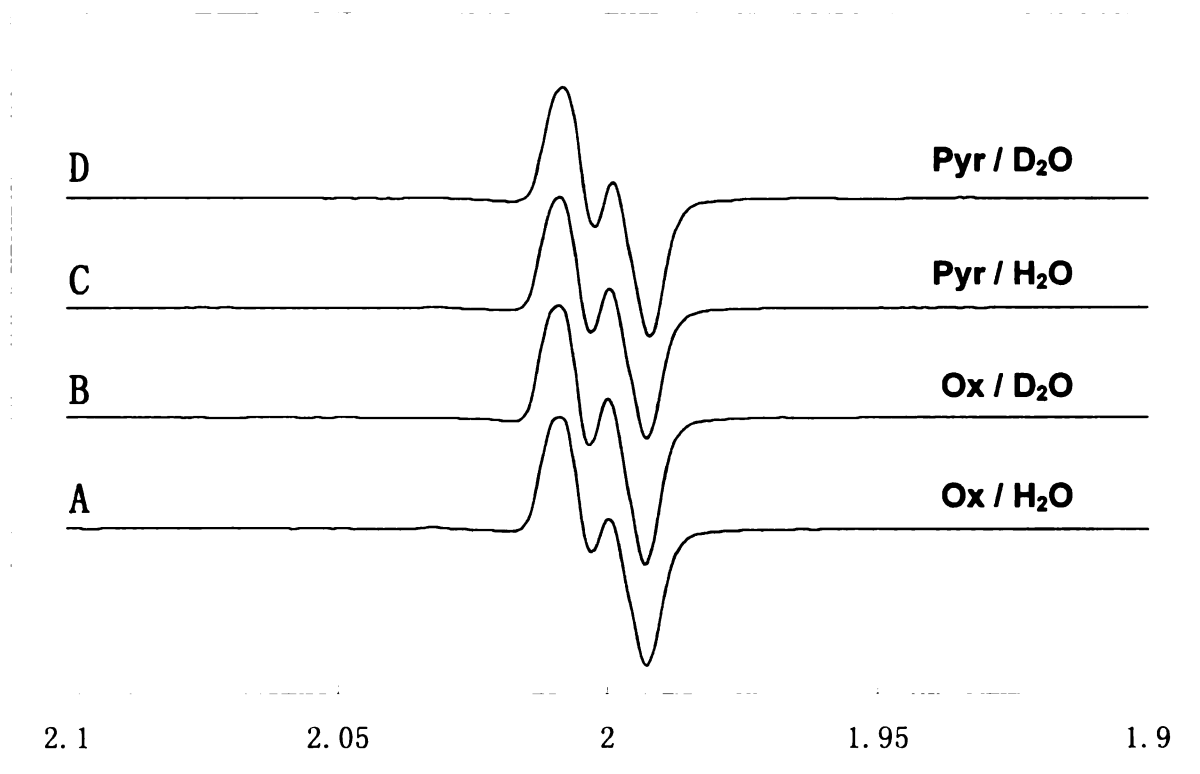


Figure VII.3.3.2. X-band EPR spectra of activated PFL C419A with different amount of pyruvate and D₂O. The final concentrations of major components in these samples are: A, 50 μ M PFL C419A, 100 mM Tris-HCl pH 7.6, 100 mM KCl, 2.5 mM DTT, and 5 mM oxamate; B, 50 μ M PFL C419A, 100 mM Tris-HCl pD 8.0, 100 mM KCl, 2.5 mM DTT, 5 mM oxamate, and 75 % (v/v) D₂O; C, 50 μ M PFL C419A, 100 mM Tris-HCl pH 7.6, 100 mM KCl, 2.5 mM DTT, 5 mM oxamate, and 5 mM pyruvate; D, 50 μ M PFL C419A, 100 mM Tris-HCl pD 8.0, 100 mM KCl, 2.5 mM DTT, 5 mM oxamate, 5 mM pyruvate, and 75 % (v/v) D₂O. Condition of measurement: T = 60 K; microwave power, 0.02 mW; modulation amplitude, 10 G. Double integration of signal intensity: A 51 μ M, B 49 μ M, C 45 μ M, D 39 μ M.

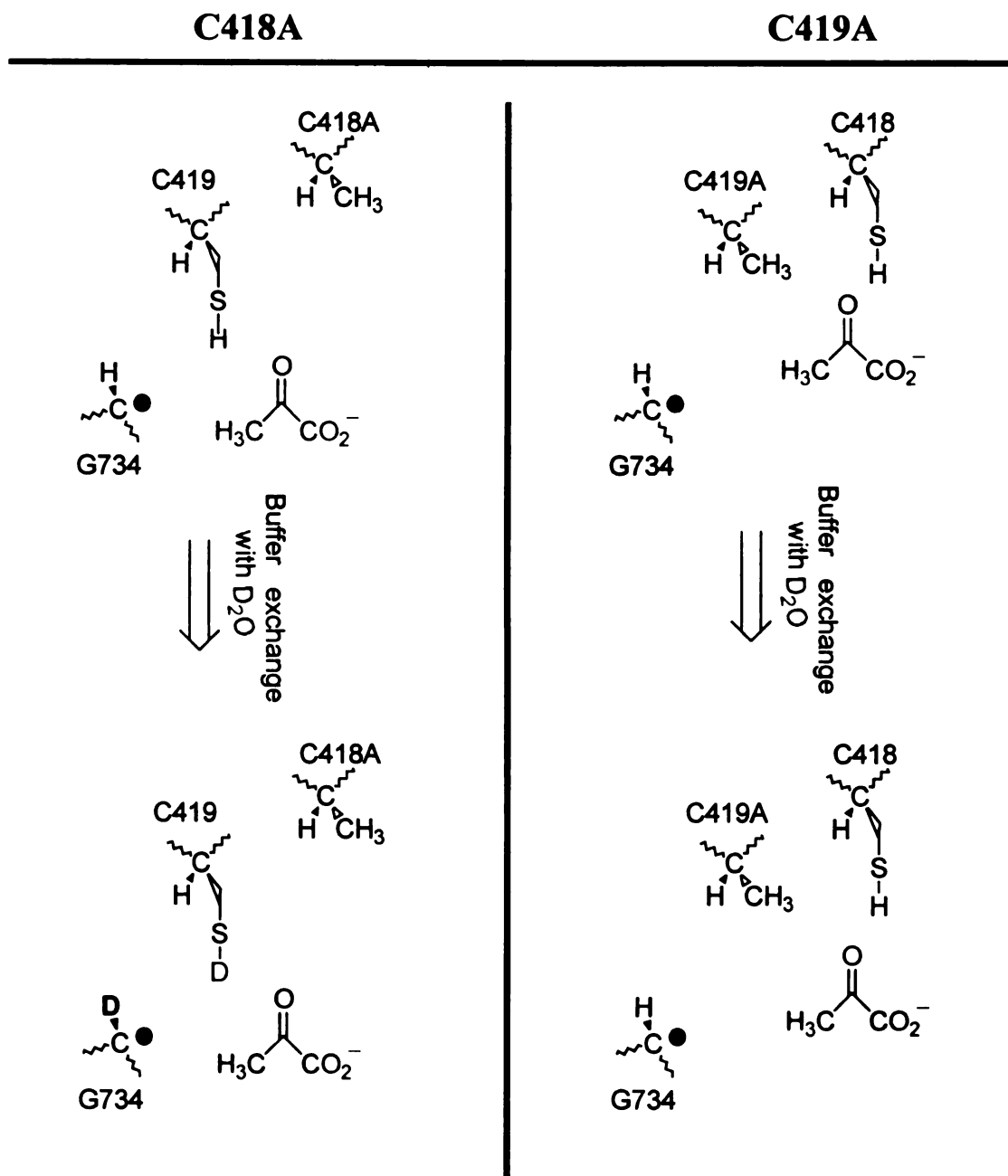
In Scheme VII.3.3.1 and this paragraph, we assume the initial reaction with pyruvate is via C418. In the case of the PFL C418A sample, the mutation of C418 into an alanine results in the loss of the free thiol group. As a result of this mutation, the acetylation reaction would be disrupted due to the fact that no thiyl radical can be generated on C418A. The C419 residue, which still contains a free thiol group but can not react with pyruvate, can still catalyze hydrogen exchange

and also the EPR spectrum of C418A in D₂O is expected to be a singlet. In the case of the PFL C419A sample, the mutation of C419 into an alanine results in the loss of the free thiol group at C419 and therefore the loss of hydrogen exchange, resulting in a doublet EPR signal for C419A in D₂O. To summarize, if C418 is responsible for the initial reaction with pyruvate, we will observe a singlet signal for the C418A mutant and a doublet signal for the C419A mutant in D₂O.

In Scheme VII.3.3.2 and this paragraph, we assume the initial attack on pyruvate is from the C419 thiyl radical. In the case of the PFL C418A sample, the mutation of C418 into an alanine results in the loss of the free thiol group at residue C418. C419, which still contains the free thiol group and is assumed to attack the pyruvate molecule, remains catalytically active and therefore is acetylated. As a result of this acetylation reaction, the C419 free thiol group is occupied and no longer available to catalyze the hydrogen exchange reaction. Therefore, the C418A/pyruvate in D₂O is expected to exhibit a doublet signal because of the retention of the C α hydrogen of the G734 glycyl radical. In the case of the PFLC419A sample, the mutation of C419 into an alanine results in the loss of the free thiol group. Therefore no free thiol group of C419 is available to catalyze the acetylation reaction nor the hydrogen exchange reaction. The EPR spectrum of this sample is expected to be a doublet signal because of the retention of the C α hydrogen of the G734 glycyl radical. To summarize, if C419 is responsible for the initial reaction with pyruvate, we will observe a doublet signal for the C418A mutant and a doublet signal for the C419A mutant.

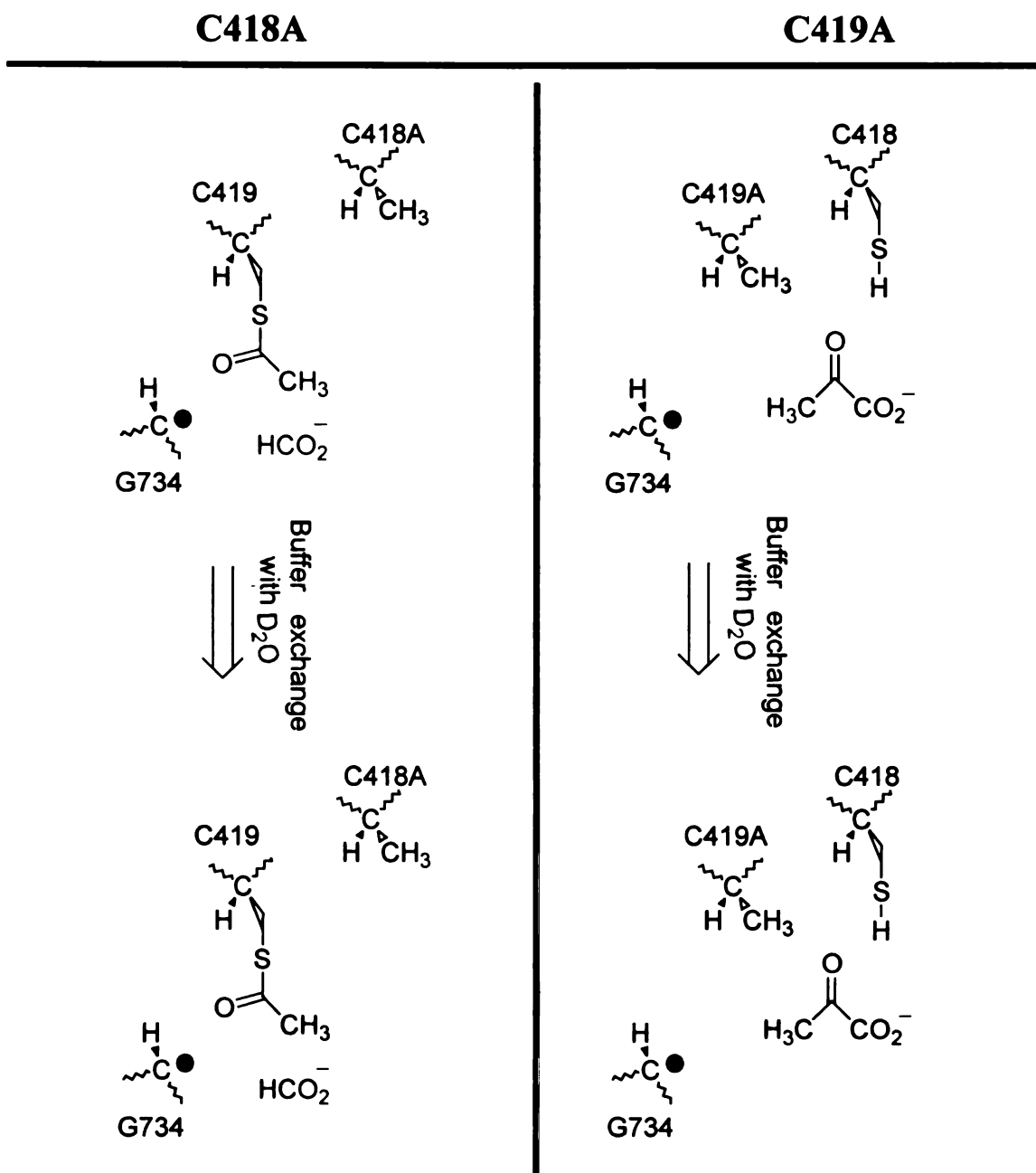
Our experimental results are that the C418A mutant exhibits a singlet signal in D₂O while the C419A mutant shows a doublet signal in D₂O. This is consistent with the results predicted by Scheme VII.3.3.1. Therefore, we propose that the PFL reaction is initiated by the thiyl radical of C418, and C419 functions as a radical shuttle between G734 and C418.

If C418 attacks



Scheme VII.3.3.1. Theoretical results of C418A and C419A mutants reaction with pyruvate followed by buffer exchange with D₂O assuming the initial attack is from C418 thiol radical.

If C419 attacks



Scheme VII.3.3.2. Theoretical results of C418A and C419A mutants reaction with pyruvate followed by buffer exchange with D₂O assuming the initial attack is from C419 thiol radical.

VII.3.4 *Photolysis to generate thiyl radicals on PFL cysteine mutants.*

In the experiments described in the previous section, we have provided evidence that C418 is responsible for the initial attack on pyruvate. The evidence provided, however, is somewhat inconclusive. We have proposed that C419 acts as a radical shuttle between the G734 and C418 residues. Based on this proposal, the C418 thiyl radical can not be generated in the absence of C419 and therefore C418 could not attack the pyruvate molecule even in the C419A mutant. This leaves the interpretation of the EPR results in question. In an effort to conquer this dilemma, we have attempted to generate the thiyl radical directly on C418 so that it is not dependent on a C419 radical shuttle. Here we have utilized UV photolysis at low temperature to directly generate thiyl radicals on PFL.

Three PFL cysteine mutants were examined. C418A, which contains a free thiol group on C419, C419A, which contains a free thiol group on C419, and the double mutant C418A/C419A, which has eliminated both C418 and C419 thiol groups, were photolyzed. The EPR spectra of all PFL cysteine mutants clearly show similar signals centered at $g = 2.002$, suggesting the presence of possible thiyl radicals after UV photolysis.⁵ However, there are two major problems. 1: The overall yields of photolysis for all the mutants are very low. 2: The amount of the thiyl radical generated from the double mutant C418A/C419A is slightly higher than any single mutant (C418A or C419A), suggesting that this method of generating thiyl radical by UV-irradiation is limited to the surface of the frozen sample and not very consistent from sample to sample. There is no doubt that further experiments are required to increase the yield and the reliability of the

photolysis method. Due to the low yields of radical generation, these experiments were not pursued further.

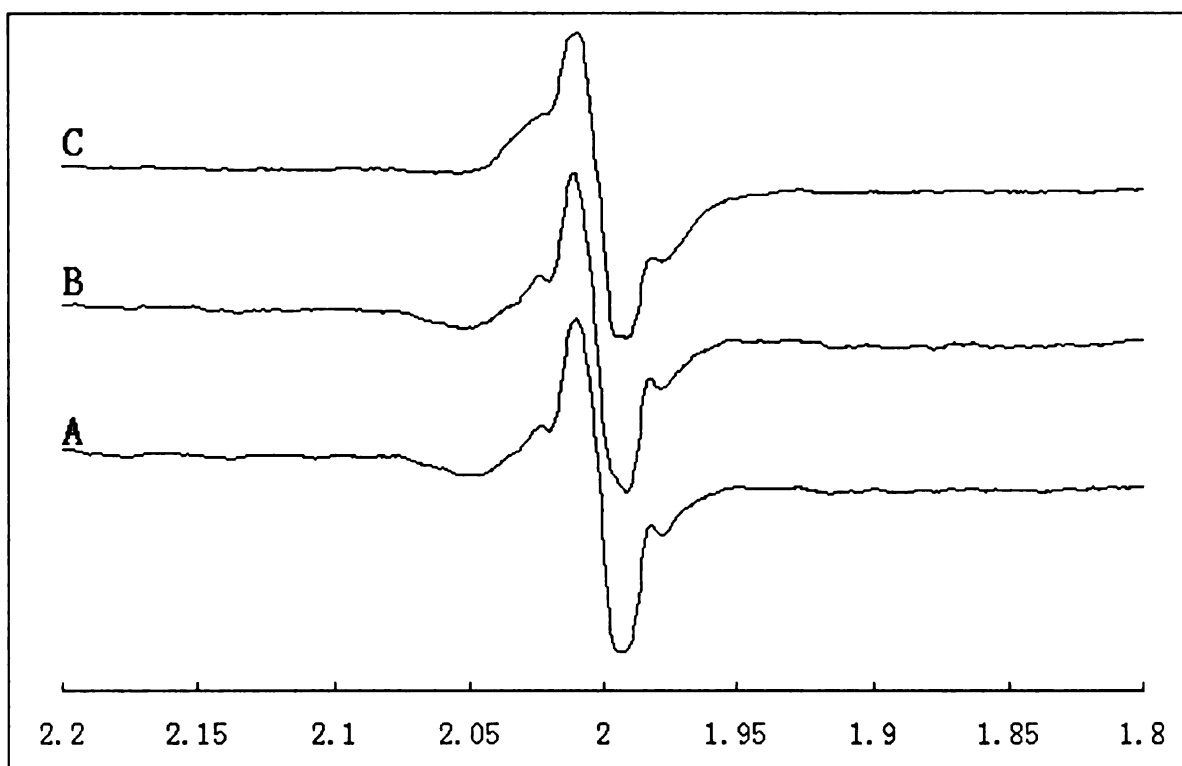


Figure VII.3.4.1. X-band EPR spectra of thiyl radicals of PFL cysteine mutants generated by UV photolysis. C418A (A), C419A (B) and C418A/C419A (C). Condition of measurement $T = 80$ K; microwave power, 2 mW; modulation amplitude, 10 G. Double integration of signal intensity: A C418A 3.8 μ M, B C419A 4.0 μ M, C C418A/C419A 10 μ M.

VII.4 Conclusions

PFL cysteine mutants have been successfully constructed in order to investigate the roles of two cysteines (C418 and C419) in the PFL catalytic reaction. Interestingly, the purification of these mutants is essentially the same as that of the wildtype PFL in terms of the elution volumes on both ion exchange and hydrophobic interaction columns. This is a clear sign to us that the overall structures of these cysteine mutants are very similar to that of the wildtype PFL.

We have provided evidence that C419 serves as a radical shuttle between G734 and C418, and that it is the C418 thiyl radical that attacks pyruvate to initiate the reaction. In fact, the crystal structure of PFL in complex with pyruvate also supports this mechanism, indicating that the pyruvate carbonyl carbon is 2.6 Å away from C418 Sγ. C419 is located in between G734 and C418, and the distance between G734 Cα and C419 Cα, which receives the radical from G734, is only about 4.8 Å. Our work is most consistent with the mechanism proposed by Knappe and coworkers.^{1, 2}

UV photolysis has been used to generate thiyl radicals on PFL in order to achieve a more direct evidence for which cysteine residue serves as the attacking thiol group. EPR spectra of the photolysed cysteine mutants at low temperature clearly show the well defined symmetric thiyl radical signals with $g = 2.00252$. However, the overall yields of photolysis for all the mutants are very low suggesting this method of generating the thiyl radical by UV-irradiation is not efficient and that more experiments are required to improve the experimental conditions.

VII.5 References

1. Becker, A.; Fritz-Wolf, K.; Kabsch, W.; Knappe, J.; Schultz, S.; Wagner, A. F. V., Structure and mechanism of the glycyl radical enzyme pyruvate formate-lyase. *Nature Structural Biology* **1999**, 6, (10), 969-975.
2. Becker, A.; Kabsch, W., X-ray Structure of Pyruvate Formate-Lyase in Complex with Pyruvate and CoA. *Journal of Biological Chemistry* **2002**, 277, (42), 40036-40042.
3. Parast, C. V.; Wong, K. K.; Lewisch, S. A.; Kozarich, J. W.; Peisach, J.; Magliozzo, R. S., Hydrogen Exchange of the Glycyl Radical of Pyruvate Formate-Lyase Is Catalyzed by Cysteine 419. *Biochemistry* **1995**, 34, (8), 2393-9.
4. Lehtioe, L.; Leppaenen, V. M.; Kozarich, J. W.; Goldman, A., Structure of Escherichia coli pyruvate formate-lyase with pyruvate. *Acta Crystallographica, Section D: Biological Crystallography* **2002**, D58, (12), 2209-2212.
5. Lassmann, G.; Kolberg, M.; Bleifuss, G.; Graeslund, A.; Sjoeborg, B.-M.; Lubitz, W., Protein thiyl radicals in disordered systems: a comparative EPR study at low temperature. *Physical Chemistry Chemical Physics* **2003**, 5, (11), 2442-2453.
6. Walsby, C. J.; Ortillo, D.; Yang, J.; Nnyepi, M. R.; Broderick, W. E.; Hoffman, B. M.; Broderick, J. B., Spectroscopic Approaches to Elucidating Novel Iron-Sulfur Chemistry in the "Radical-SAM" Protein Superfamily. *Inorganic Chemistry* **2005**, 44, (4), 727-741.
7. Nnyepi, M. R.; Peng, Y.; Broderick, J. B., Inactivation of E. coli pyruvate formate-lyase: role of AdhE and small molecules. *Arch Biochem Biophys* **2007**, 459, (1), 1-9.

CHAPTER VIII

INVESTIGATION ON THE FIRST STEP OF THE BIOSYNTHESIS OF MOCO

VIII.1. Introduction

Molybdenum cofactor (Moco) containing enzymes are found in almost all organisms and are involved in global circulation of carbon, oxygen, hydrogen, nitrogen and sulfur.¹ Based on sequence similarities of their polypeptides, molybdenum enzymes are classified into four families, the DMSO reductase, xanthine oxidase, sulfite oxidase and aldehyde ferredoxin oxidoreductase (AOR) families.² The protein sequences are much more similar among the members in the same family than between the members from different families

Another way to classify molybdenum enzymes is based on the reaction catalyzed, which can be one of two general types.¹ Hydroxylases catalyze the oxidative hydroxylation of a diverse range of aldehydes and aromatic heterocycles in reactions that necessarily involve the cleavage of a C-H bond, although product tautomerization in reactions involving heterocyclic substrates usually results in the keto rather than enol form predominating in aqueous solution. The second category comprises the oxotransferases, which catalyze

proper oxygen atom transfer reactions to or from an available electron lone pair of substrate.

Compared to the variety and the wide applications of the members of this family, the structure of the organic or metal-free part of the Moco (named MPT, molybdopterin) and the biosynthesis of this organic ligand is highly conserved. It is well believed to be one of the ancient inventions of nature.³

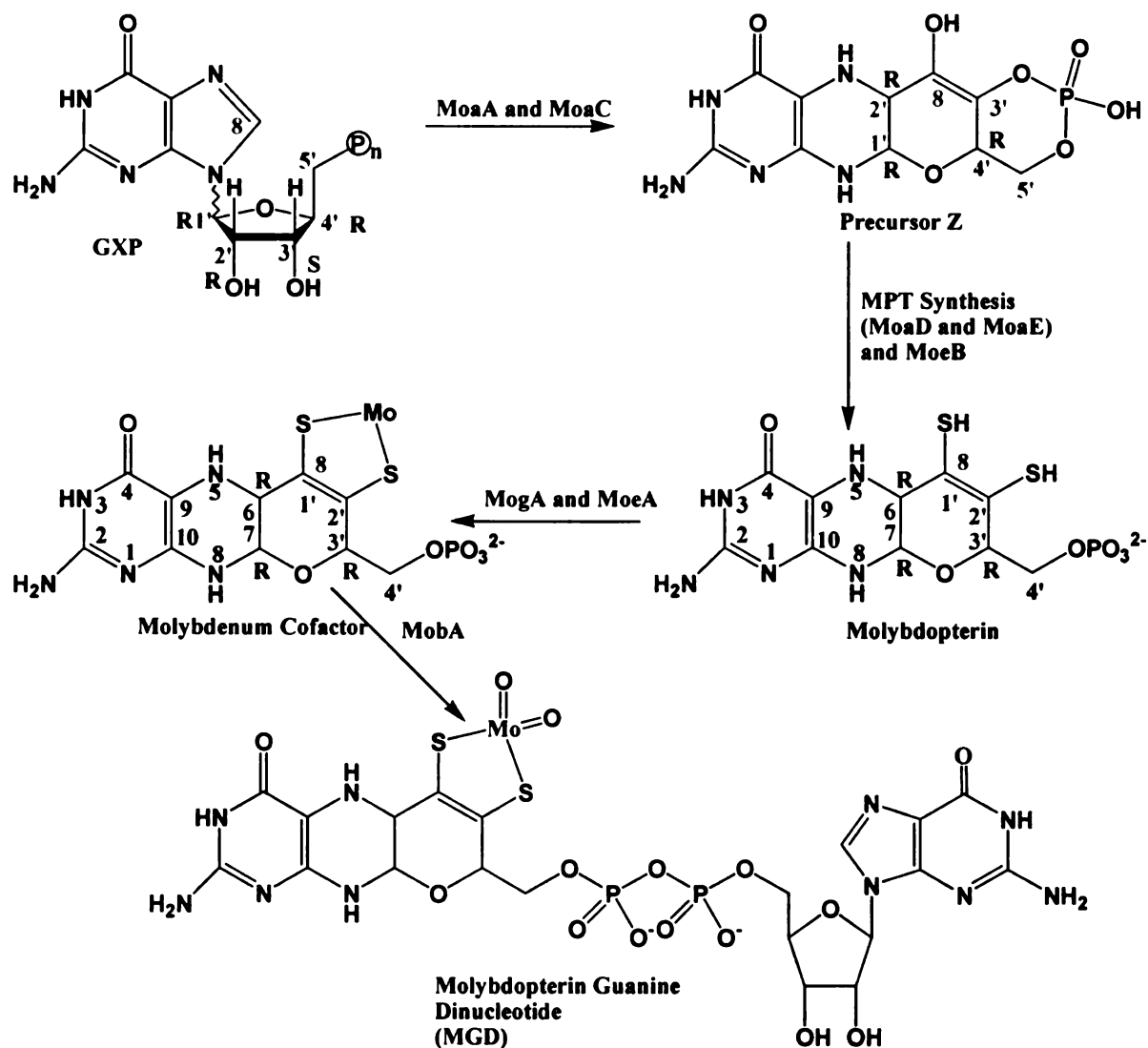
In *E. coli*, more than 15 genes from five operons (*moa*, *mob*, *mod*, *moe* and *mog*) are known to be involved in the biosynthesis of Moco. Four biosynthetic stages have been determined based on the excellent work from Rajagopalan and Johnson (Scheme VIII.4.1):⁴

Step 1: Conversion of GTP to Precursor Z,

Step 2: Conversion of Precursor Z to Molybdopterin (MPT),

Step 3: Formation of active Moco, and

Step 4: Formation of dinucleotide form of Moco (not needed for plants and human beings).



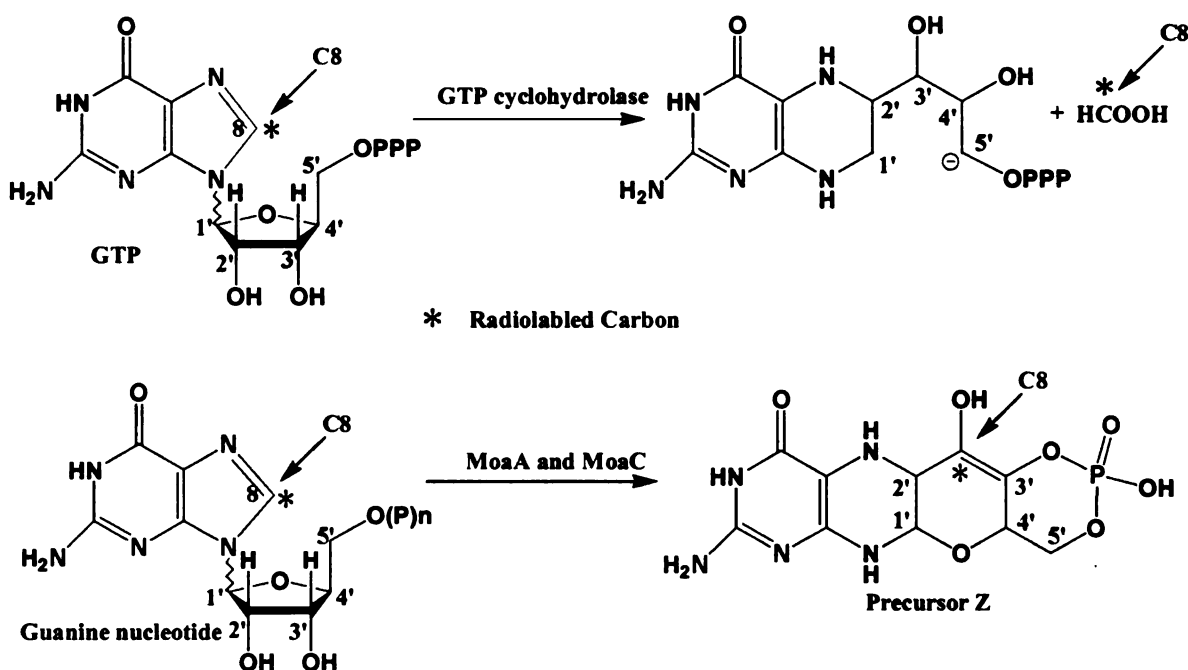
Scheme VIII.4.1. Biosynthesis of Moco

From the lowest bacteria to human beings, the first step of Moco biosynthesis is quite similar in terms of the genes and the pathway involved (Table VIII.4.1). In all cases a MoaA-like protein and a MoaC-like protein appear to be involved. MoaB is found only in bacteria and its role in MPT synthesis is uncertain.

Bacteria ^{5, 6}	Fungi ⁷	Plants ⁸	Humans ⁹
<i>E. coli</i>	<i>A. nidulans</i>	<i>A. thaliana</i>	<i>H. sapiens</i>
MoaA	CnxA	Cnx2	MOCS1A
MoaB (uncertain)	--	--	--
MoaC	CnC	Cnx3	MOCS1B

Table VIII.4.1. Genes involved in the first step of biosynthesis of Moco

Compared to the biosynthesis of pteridines and flavines,¹⁰ which have three-carbon side chains (C3', C4' and C5' in the product of the top reaction in Scheme VIII.4.2), Moco is quite unique because of its four-carbon side chain (C8, C3', C4' and C5' in the product of the bottom reaction in Figure VIII.4.2), which results in the formation of a pyrano ring. The biosynthesis Moco is a new and novel reaction with the preservation of C8 (Scheme VIII.4.2).¹¹



Scheme VIII.4.2. Comparison of pterin biosynthesis pathways. (Top) Formation of neopterin triphosphate from GTP in the pathways of folic and biopterin biosynthesis. (Bottom) Formation of precursor Z from a guanine nucleotide in *E. coli*.

Comparing the proposed substrate with its corresponding product, precursor Z, the following facts must hold although in an unknown order. First, the destabilization and breakage of both the imidazole ring and the ribose ring must happen. Second, the bond between the C2' and C3' is the target of the incoming C8, most likely to be in the formate form. Third, in the intermediate, the C8 must be preserved in a reasonably close site to where it needs to go in the final product. Last, stereochemical control must be involved due to substrate binding to a chiral protein active site.

MoaA has two cysteine-rich regions; the one close to the N terminus is highly conserved and shows sequence similarity to radical SAM superfamily enzymes.¹² The similarity to these enzymes may indicate that a radical-based reaction mechanism is involved in MoaA. Chemical analysis and EPR studies

suggested the existence of a [3Fe-xS] cluster in the *Arthrobacter nicotinovorans* MoaA and a [3Fe-4S] cluster in the *Rhodobacter capsulatus* MoaA.^{13, 14}

The crystal structure of MoaC has been solved and found to be a homohexamer.⁶ Even though the active site has been proposed to be located between pairs of monomers, little is known about the binding and the mechanism involved or even the specific reaction catalyzed by MoaC.

Due to the lack of a MoaB counterpart in other organisms, the function of MoaB in the biosynthesis of Moco in bacteria may be suspect. However, the location of *moaB* gene in the *moa* operon might imply the necessity of this protein. Besides the hexameric crystal structure solved, nothing more is known about the function of MoaB.¹⁵

In order to investigate the mechanism of Moco biosynthesis, we undertook efforts to clone the proteins that are involved in the reaction including MoaA, MoaB and MoaC. A wide variety of methods and factors were considered to increase the overexpression and the solubility of the proteins, such as the *E. coli* overexpression strains being used, the cell lysis procedures, the buffering conditions including pH, salt concentration, glycerol and detergent content, the expression vectors in which the genes were inserted, the temperatures of the cell growth, the presence of affinity tags, and co-expression.

In this chapter, we describe the cloning of a series of *moaA* and *moaC* genes from *E. coli* genomic DNA with and without tags attached. Our results show that MoaA was overexpressed as inclusion bodies that are located in the cell pellet after lysis. Subsequent purification was difficult due to its insolubility.

Although many of the above methods have been employed in an attempt to increase protein solubility, most of them were unsuccessful.

VIII.2. Material and Methods

Materials

All chemicals were obtained from commercial sources and were of the highest purity available. Expression vectors pETBlue-1 and pET44a were purchased from NovagenTM. Expression vector pMAL-p2x was purchased from NEBTM. PETBlue-1 Perfectly Blunt Cloning Kit was purchased from NovagenTM. Pfu Turbo Polymerase was purchased from StratageneTM. T4 DNA ligase was purchased from NEBTM. DNA ladder (100b and 1kb) was purchased from InvitrogenTM and NEBTM. Restriction Endonucleases were purchased from NEBTM. Compass DNA Purification Kit was purchased from American BioanalyticalTM. Wizard Genomic DNA Purification Kit was purchased from PromegaTM. Wizard Plus SV Minipreps DNA Purification System was purchased from PromegaTM. *E. Coli* strains of Novablue, Tuner(DE3)pLacI, and BL21(DE3)plysS were purchased from Novagen. SDS-PAGE gels were obtained from BioRad Scientific.

VIII.2.1 Purification of genomic DNA from E. coli BL21 cells

An isolated *E. coli* BL21 colony was used to inoculate 50 mL LB medium, which was then incubated at 37 °C with shaking (250 rpm) overnight. The genomic DNA was purified according to the procedure of Promega's Wizard Genomic DNA Purification Kit. The concentration of the purified genomic DNA was measured in an HP UV-Vis 8453 system at 260 nm and 280 nm respectively to check the concentration and the purity. The equation used to check the

concentration is 1Au (260 nm) = 50 µg/mL. The purify was thought to be good if the ratio of 260 nm / 280 nm was greater than 1.6.

VIII.2.2 Cloning of *E. coli moaA* and *moaC* gene into pETBlue-1 vector.

The *moaA* and *moaC* genes were amplified by the polymerase chain reaction (PCR) technique using *E.coli* BL21 chromosomal DNA as a template.

The synthetic oligonucleotide primers had the sequences shown below:

moaA:

primer I: 5'-ATG,GCT,TCA,CAA,CTG,ACT,GAT,GCA,TTT,GCG-3'

primer II: 5'-TTA,GCC,GCC,AAT,GTA,CGA,TAA,ATT,TTG,CGT-3'

moaC:

primer I: 5'-ATG,TGG,CAA,CTG,ACC,CAT,ATC,AAC,GCC,GCT-3'

primer II: 5'-TTA,ATC,ATC,CGC,TTC,CAC,CTT,AAA,GTC,ACC-3'

The PCR products were then cloned into a pETBlue-1 vector supplied in Novagen PETBlue-1 Perfectly Blunt Cloning Kit. The resulting recombinant DNA JYI58 (*pETBlue-1-Ecoli-moaA*) and JYIII139 (*pETBlue-1-Ecoli-moaC*) were then transformed into NovaBlue competent cells. The transformation mix was plated on LB-agar containing 50 µg/mL ampicillin and incubated overnight at 37° C. Single colonies were identified and used to inoculate 5 mL of liquid LB medium containing 50 µg/mL ampicillin. All tubes were incubated overnight in a shaker at 37° C and 250 rpm.

From each of the overnight cultures, a total of 1 - 5 mL was centrifuged in order to obtain a cell pellet. Plasmid DNA was then extracted from each cell pellet using a commercially available DNA extraction kit (Stratagen). In order to ascertain its identity, the recombinant plasmid DNA (JYI58) purified as above

was digested using restriction endonucleases *Sca*I. The recombinant plasmid DNA (JYIII139) purified as above was digested using restriction endonucleases *Sca*I and *Eco*R I.

VIII.2.3 Transformation and overexpression of JYI58 and JYIII139 in

Tuner(DE3)placI cells

A single colony of the overexpression strain *E. coli* Tuner(DE3)placI transformed with JYI58 or JYIII139 was used to inoculate 50 mL of LB medium containing 50 µg/mL of ampicillin. This culture was grown to saturation at 37 °C and 5 mL of this overnight culture was used to inoculate each 1 L LB/ampicillin in a 2800 mL Fernbach flask. The 1 L cultures were grown at 37 °C with shaking at 250 rpm. When the culture reached an OD₆₀₀ = 0.7 - 0.8, IPTG was added to 1 mM final concentration to induce the overexpression of MoaA or MoaC. The cultures were grown for an additional 3 hours, and then were harvested by centrifugation at 4 °C and stored under nitrogen at – 80 °C.

VIII.2.4 Lysis of cells expressing MoaA.

Pelleted cells were resuspended in various lysis buffer (shown below) (15 g / 50 mL) containing 1 mM PMSF, 10 mg lysozyme, and 0.5 mg DNase I and RNase A. This suspension was agitated for one hour on ice in glove box and then centrifuged at 27,000 x g for 30 min at 4 °C. SDS-PAGE was used to check the solubility of MoaA in each lysis buffer.

Lysis buffers:

Tris/Triton lysis buffer: 50 mM Tris pH 8.5, 200 mM NaCl, 10 mM MgCl₂, 5 - 50% (w/v) glycerol, 1 – 5 % Triton X - 100.

Tris/CHAPS lysis buffer: 50 mM Tris pH 7.5 or pH 8.0, 300 mM NaCl, 10 mM MgCl₂, 20% (w/v) glycerol, 2 -10mM CHAPS.

0.2 M Phosphate buffer: 0.2 M phosphate pH 7.2, 200 mM NaCl, 10 mM MgCl₂, 5 % (w/v) glycerol, 1 - 5% Triton X – 100.

0.4 M Phosphate buffer: 0.4 M phosphate pH 7.2, 200 mM NaCl, 10 mM MgCl₂, 5 % (w/v) glycerol, 1 - 5% Triton X - 100.

VIII.2.5 *Partial denaturation of MoaA*

Pelleted cells were resuspended in lysis buffer (15 g / 50 mL) containing 50 mM Tris pH 8.0, 300 mM NaCl, 10 mM MgCl₂, 20 % (w/v) glycerol and 1 mM PMSF, 10 mg lysozyme, and 0.5 mg DNase I and RNase A. This suspension was agitated for one hour on ice in glove box and then centrifuged at 27,000 x g for 30 min at 4 ° C. The lysis pellet was then denatured in 50 mM Tris pH 8.0, 1 mM βME buffer in the presence of urea or guanidine (2 M or 6 M). This suspension was agitated for one hour at room temperature in glove box and then centrifuged at 27,000 x g for 30 min at 4 ° C. Each clear lysate was then dialyzed against 1 L 50 mM Tris pH 8.0 and 1 mM βME at room temperature for 8 hrs. SDS-PAGE was used to check the solubility of MoaA under these conditions.

VIII.2.6 *Overexpression of MoaA under different conditions*

A single colony of the overexpression strain *E. coli* Tuner(DE3)placI transformed with JYI58 was used to inoculate 50 mL of LB medium containing 50 µg/mL of ampicillin. This culture was grown to saturation at 37 ° C and 5 mL of

this overnight culture was used to inoculate each 1 L LB or MM (minimal medium as described before¹⁶) containing 50 µg/mL ampicillin in a 2800 mL Fernbach flask under different conditions as shown below. The 1 L cultures were grown at either 25 °C or 37 °C with shaking (250 rpm). When the culture reached an OD₆₀₀ = 0.5-0.8, IPTG was added to a final concentration of 0.2, 0.5 or 1 mM to induce the overexpression of MoaA. Sometimes this culture was cooled down to 4 °C, 16 °C or 25 °C before IPTG was used to induce the overexpression of MoaA. After IPTG was added, the cultures were grown for an additional 3 hours with or without the addition of 0.075 g of ferrous ammonium sulfate hexahydrate per liter culture (to a final concentration of approximately 0.2 mM). Same cultures were then supplemented with additional 0.075 g of ferrous ammonium sulfate per liter culture and incubated overnight at 4 °C under anaerobic condition with a continuous nitrogen purge. The cells were then harvested by centrifugation at 4 °C and stored at -80 °C for further use.

VIII.2.7 Purification of MoaA.

Pelleted cells were resuspended in lysis buffer (15 g / 50 mL) containing 50 mM Tris pH 8.0, 300 mM NaCl, 10 mM MgCl₂, 20% (w/v) glycerol and 1 mM PMSF, 10 mg lysozyme, and 0.5 mg DNase I and RNase A. This suspension was agitated for one hour on ice in a glove box and then centrifuged at 27,000 x g for 30 min at 4 °C. The pellet was then denatured in 50 mM Tris pH 8.0, 1 mM βME buffer with 6 M urea. This suspension was agitated for one hour at room temperature in a glove box and then centrifuged at 27,000 x g for 30 min at 4 °C.

Each clear lysate was dialyzed against 1 L 50 mM Tris pH 8.0 and 1 mM β ME at room temperature for 8 hrs.

The resulting crude extract containing MoaA was aliquoted, with each aliquot being loaded separately onto a column that had been previously equilibrated with starting buffer. Immediately following sample injection, the programs shown in Table VIII.2.7.1) were run. Fractions were collected and analyzed using SDS-PAGE in order to determine the quantity and purity of MoaA in each.

Columns	Loading Amount mL	Buffers	Program	Fraction Size mL
Waters AP-5 Superdex 75 Gel Filtration column	30	50mM Tris pH8.0 200mM NaCl, 1mM DTT	Flow Rate: 3mL/min	9
Pharmacia Mono S HR 5/5 Cation Exchange column	5	Low salt buffer(A): 20mM Tris pH 7.0-8.0 high salt buffer(B): 20mM Tris pH 7.0-8.0 1M NaCl.	Flow Rate: 1mL/min 1 st 15min A 2 nd 25min Gradient from 100%A to 100%B 3 rd 20min B	1
Pharmacia Mono Q HR 5/5 Anion Exchange column	5	Low salt buffer(A): 20mM Tris pH 8.0-8.7 High salt buffer(B): 20mM Tris pH 8.0-8.7 1M NaCl.	Flow Rate: 1mL/min 1 st 15min A 2 nd 25min Gradient from 100%A to 100%B 3 rd 20min B	1
Waters AP-5 Accell Plus QMA Anion Exchange column	10	Low salt buffer(A): 20mM Tris pH 8.0, High salt buffer(B): 20mM Tris pH 8.0 1M NaCl.	Flow Rate: 5mL/min 1 st 40min A 2 nd 40min Gradient from 100%A to 100%B 3 rd 40min B	5
Pharmacia HiLoad 26/10 Q Sepharose HP column	10	Low salt buffer(A): 20mM Tris pH 8.0 High salt buffer(B): 20mM Tris pH 8.0 1M NaCl	Flow Rate: 3mL/min 1 st 15min A 2 nd 100min Gradient from 100%A to 100%B 3 rd 15min B	3

Table VIII.2.7.1 The variance of columns and buffering conditions for purification of MoaA.

VIII.2.8 *Cloning of E. coli moaA gene with restriction site on 3' end into pMAL-p2x vector*

The *moaA* gene with one end modified with a *Hind III* restriction site was amplified by the polymerase chain reaction (PCR) technique using *E.coli* BL21 chromosomal DNA as a template. The synthetic oligonucleotide primers had the sequences shown below:

Primer I: 5'-ATG,GCT,TCA,CAA,CTG,ACT,GAT,GCA,TTT,GCG-3'

Hind III

Primer II: GCC,GCC,**AAG,CTT**,TTA,GCC,GCC,AAT,GTA,CGA-3'

The bold letters indicate the restriction enzyme recognition sequences, with the corresponding restriction enzyme used indicated in italics above restriction site sequence. The PCR product was digested with the restriction enzyme *Hind III* and then cloned into a pMAL-p2x vector, which was pre-digested with enzymes *HindIII* and *XmnI*. The recombinant DNA JYIV145 (pMAL-p2x-moaA) obtained from above was first transformed into NovaBlue competent cells. Then the transformation mix was plated on LB-agar containing 50 µg/mL ampicillin and incubated overnight at 37 °C. Single colonies were identified and used to inoculate 5 mL of liquid LB medium containing 50 µg/mL ampicillin. All tubes were incubated overnight at 37 °C with shaking (250 rpm).

From each of the overnight cultures, a total of 1 - 5 mL was centrifuged in order to obtain a cell pellet. Plasmid DNA was then extracted from each cell pellet using a commercially available DNA extraction kit (Stratagen). In order to ascertain its identity, the recombinant plasmid DNA purified as above was checked by DNA fingerprinting with *NdeI* and *HindIII*.

VIII.2.9 Transformation and overexpression of JYIV145 into Tuner(DE3)placI competent cells.

A single colony of the overexpression strain *E. coli* Tuner(DE3)placI transformed with JYIV145 was used to inoculate 50 mL of LB medium containing 50 µg/mL of ampicillin. This culture was grown to saturation at 37 °C and 5 mL of this overnight culture was used to inoculate each 1 L LB/ampicillin in a 2800 mL Fernbach flask. The 1 L cultures were grown at 37 °C with shaking (250 rpm). When the culture reached an OD₆₀₀ = 0.7 - 0.8, IPTG was added to 1 mM final concentration to induce the overexpression of MoaA. The cultures were grown for an additional 3 hours, and then were harvested by centrifugation at 4 °C and stored under nitrogen at – 80 °C for further use.

VIII.2.10. Western blotting of the overexpressed fusion protein MoaA-MBP.

Cell paste, which was collected from 1 mL of the previously described (VIII.2.9) was resuspended in 200 µL SDS loading buffer (50 mM Tris, pH 6.8, 100 mM βME, 2 % (w/v) SDS, 0.1 % (w/v) bromophenol blue, and 10 % (w/v) glycerol). The sample was then boiled for 5 mins and cooled to room temperature. After the condensation on the tube walls was brought down by flash spin at top speed for a few seconds, 20 µL of this sample was loaded into a well of a 10 % Bio-rad ready gel, which was then run at constant voltage (180 V) for 40 min. The resulting gel was then placed next to a nitrocellulose membrane; and sandwiched by additional tissue papers soaked with semi-dry transfer buffer (50 mM Tris, pH

8.0, 0.3 % (w/v) glycerol, 0.37 % (w/v) SDS, and 20 % (v/v) methanol). Under constant voltage (12 V) for 90 min, proteins from the SDS gel were then transferred to the nitrocellulose membrane. The membrane was then blocked with 4 % (w/v) nonfat dry milk, which was dissolved in TBST buffer (10 mM Tris, pH 8.0, 150 mM NaCl, and 0.05 % Tween 20), at 4 °C overnight. After the membrane was thoroughly washed by TBST buffer, a dilute solution of primary antibody (4 µL Anti-MBP antiserum, NEB) in TBST buffer (5 mL) containing 4 % nonfat dry milk was incubated with the membrane under gentle agitation for 1 h at room temperature. After the membrane was rinsed to remove unbound primary antibody, it was exposed to the anti-rabbit antibody coupled to horseradish peroxidase as a secondary antibody (3 µL Anti-rabbit IgG, Amersham Biosciences) diluted in TBST buffer (10 mL) under gentle agitation for 1.5 hr at room temperature. The proteins were finally visualized via enhanced chemiluminescence (ECL Kit, Amersham).

VIII.3 Results and Discussion

VIII.3.1 Purification of genomic DNA from E. coli BL21 cells.

The genomic DNA of *E. coli* was successfully purified from *E. coli* BL21 cells. UV-vis characterization of the purified DNA provided a 260 nm/ 280 nm absorbance ratio of larger than 1.6, indicating DNA good purity. This DNA was used for all the subsequent PCR reactions to amplify the target genes including *moaA* and *moaC*.

VIII.3.2 Construction of the recombinant plasmids JYI58 and JYIII139.

Both *moaA* and *moaC* genes were cloned from *E. coli* genomic DNA using PCR reaction with good quality as show in Figure VIII.3.2.1. The PCR products were then blunt end-ligated into the linear vector of pETBlue-1 to construct the recombinant plasmids JYI58 and JYIII139. The recombinant plasmids were then confirmed by DNA fingerprinting as shown in Figure VIII.3.2.2. Some of the bands shown in lane 2, 3, and 4 of the *moaC* confirmatory DNA fingerprints were probably caused by the incomplete digestion of Sca I and EcoR I from lane 1.

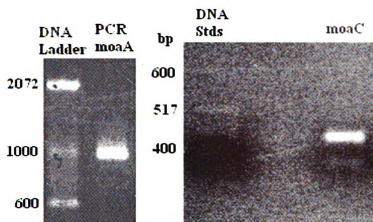


Figure VIII.3.2.1. PCR products of *moaA* and *moaC* genes from *E. coli* genomic DNA. Left panel: *moaA* with expected size of 990 bp. Right panel: *moaC* with expected size of 493 bp. The PCR products (10 μ L) were thoroughly mixed with approximately the same volume of loading buffer before loading onto an agarose gel containing 10 μ g mL⁻¹ ethidium bromide.

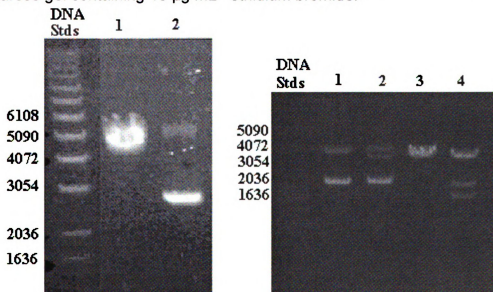


Figure VIII.3.2.2. Confirmatory DNA fingerprints of plasmids JYI58 (*pETBlue-1-Ecoli-moaA*) and JYIII139 (*pETBlue-1-Ecoli-moaC*). Left panel: JYI58 Lane 1: Digested with *Scal*. Expected size: 4438 bp. Lane 2: Undigested plasmid. Right panel: JYIII139 Lane 1: Undigested plasmid. Lane 2: Digested with *Scal*. Expected size: 3969 bp. Lane 3: Digested with *EcoR* I. Expected size: 3969 bp. Lane 4: Digested with *Scal* and *EcoR* I. Expected size: 1760 bp and 2209 bp. The undigested and digested plasmids (10 μ L) were thoroughly mixed with approximately the same volume of loading buffer before loading into an agarose gel containing 10 μ g mL⁻¹ ethidium bromide.

VIII.3.3 Transformation and overexpression of plasmids JYI58 and JYIII139 into Tuner(DE3)placI cells.

The plasmids JYI58 and JYIII139 were successfully transformed into *E. coli* Tuner(DE3)placI competent cells and grown as described in the experimental section. Typical whole cell SDS-PAGE gels are shown in Figure VIII.3.3.1. Significant overexpression of MoaA and MoaC were achieved by addition of 1 mM IPTG.

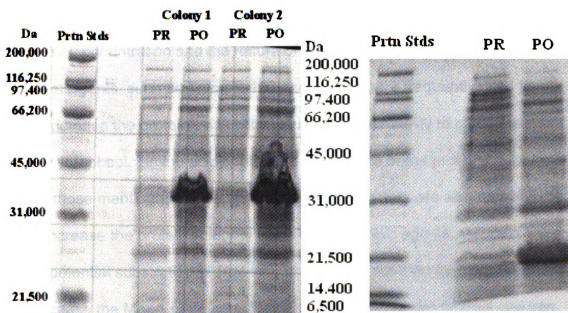


Figure VIII.3.3.1. SDS-PAGE of MoaA and MoaC overexpression. Left panel: MoaA. PR: uninduced. PO: induced. The large band shown at ~ 37 kDa matches the predicted MW of MoaA (37,346 Da). Right panel: MoaC. The large band shown at ~ 17 kDa matches the predicted MW of MoaC (17,467 Da).

VIII.3.4 Solubilization and purification of MoaA.

The solubility of proteins in aqueous buffers depends on the distribution of hydrophilic and hydrophobic amino acid residues on the protein's surface.

Charged and polar surface residues interact with ionic groups in the solvent, increasing the protein's solubility. In contrast, proteins that have high hydrophobic amino acid content on the surface have low solubility in an aqueous solvent. In order to increase the solubility of MoaA protein in aqueous solvent, a variety of factors must be considered, such as

- 1 A protein is minimally soluble near its isoelectric point (pI). The theoretical isoelectric point of MoaA is about 8.15.
- 2 The addition of salt can increase solubility (salting in) or decrease solubility (salting out) depending on the nature of the protein and on both the concentration and the nature of the salt.
- 3 Detergents, such as Triton X-100 and CHAPS, are frequently used to increase the protein's solubility because of their ability to cover the hydrophobic amino acid content on the surface of the protein.

Besides those mentioned above, a number of other factors are also known to be able to increase the protein solubility, such as chaotropic agents, reducing agents, potential substrate etc. However, these were not tried for the preliminary tests because the MoaA protein has been proposed to contain at least one iron sulfur cluster, which may be unfolded or modified upon addition of the chaotropic agents.

After MoaA was overexpressed from the culture containing 1 mM IPTG at 37 °C, a variety of lysis buffers had been tried according to the above mentioned factors in order to solubilize the protein. Unfortunately, MoaA remained in the inclusion bodies and none of the buffers yielded soluble MoaA.

Since the moderate lysis methods mentioned above had no effect on its solubility, the next step was to denature MoaA to help solubilization using chaotropic agents, such as urea or guanidine. These chaotropic agents can disrupt hydrogen bonds and hydrophobic interactions both between and within proteins, and result in the disruption of the secondary structure and solubilization of proteins that are otherwise insoluble. The neutral chaotropic agent urea has been shown to dramatically increase the number of protein solubilized including MoaA, when used at concentration of 6 M (Figure VIII.3.4.1).

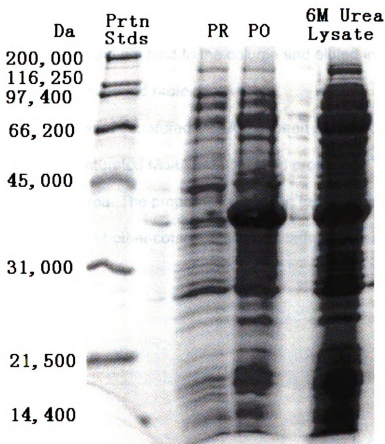


Figure VIII.3.4.1. SDS-PAGE of MoaA Denaturation by 6M Urea. PR: uninduced cells. PO: induced whole cells. 6M Urea Lysate: Clear lysate from 6M urea dialysed against 50 mM Tris pH 8.0 and 1 mM β ME buffer. The large band shown at ~37 kDa matches the predicted MW of MoaA 37,346 Da.

VIII.3.5 *Purification of denatured MoaA*

In order to properly identify and characterize the function and structure of MoaA, the pure form is vital and necessary. Separation of MoaA after denaturation was performed on different types of columns in order to exploit differences in protein size, physico-chemical property and binding affinity. These columns included gel filtration, anion exchange, cation exchange and hydrophobic interaction columns. Unfortunately, varying the types of columns as well as corresponding buffer conditions did not yield any improvement in protein purity. Figure VIII.3.5.1 is an example of MoaA purification on Q Sepharose HP column. Denatured MoaA did not bind to the column and eluted in the very first few fractions with other nonbound proteins.

That the purification of denatured MoaA has been shown to be so difficult may suggest that the renatured MoaA did not refold properly in Tris buffer after it was denatured in 6 M urea. The proper folding of the tertiary structure of MoaA may require the presence of other cofactors and/or scaffold proteins.

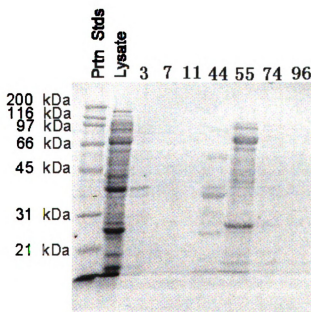
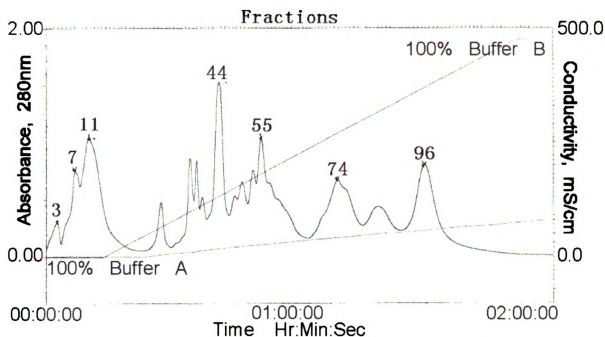


Figure VIII.3.5.1. Purification of denatured MoaA by ion exchange chromatography. Upper Panel: Chromatogram of MoaA purification on Q Sepharose HP column. Major fractions were indicated on the chromatogram. Lower Panel: SDS-PAGE analysis of corresponding fractions. The fraction numbers were indicated on top of the gel. Lysate: Denatured MoaA crude lysate renatured in Tris buffer after 6 M urea denaturation.

VIII.3.6. Construction of plasmid JYIV145 for maltose binding purification

The *moaA* gene was synthesized by standard PCR techniques with the 3' end modified with HindIII restriction site as shown in Figure VIII.3.6.1. After the PCR product and the *pMAL-p2x* vector were digested by restriction enzymes *Xmn I* and *Hind III*, they were ligated together to construct the plasmid JYIV145 (*pMAL-p2x-Ecoli-moaA*). The plasmid was then digested by restriction enzymes *Nde I* and *Hind III* in order to confirm the DNA sequence as shown in Figure VIII.3.6.1. The *moaA* gene has been cloned into the *pMAL-p2x* vector as we planned, immediately following MBP encoding sequence.

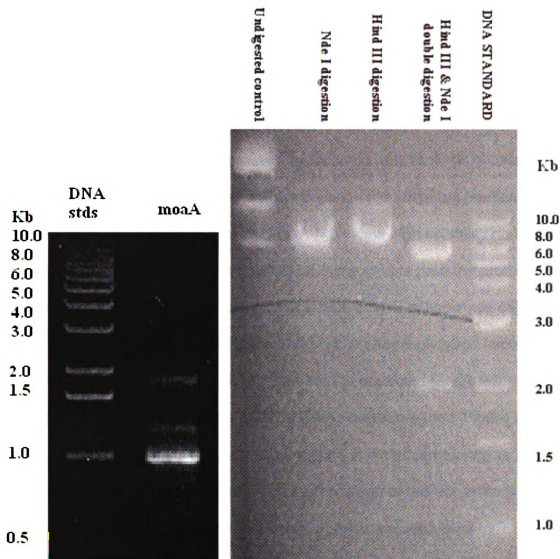


Figure VIII.3.6.1. PCR of *moaA* from *E. coli* genomic DNA and confirmatory DNA fingerprints of plasmids JYIV145. Left panel: PCR product *moaA* with expected size of 990 bp. Right panel: DNA fingerprints of plasmids JYIV145. Expected size for single digestion by *Nde*I or *Hind* III: 7654bp. Expected size for double digestion by *Nde*I and *Hind* III: 2208bp and 5446bp. The PCR product *moaA* and DNA digestions (10 μ L) were thoroughly mixed with approximately the same volume of loading buffer before loading into an agarose gel containing 10 μ g mL⁻¹ ethidium bromide.

VIII.3.7. Transformation and overexpression of the fusion protein MBP-MoaA.

The plasmid JYIV145 was successfully transformed into *E. coli* Tuner(DE3)placI competent cells to create the overexpressing strain. The fusion protein MBP-MoaA was overexpressed by inducing with 1 mM IPTG after normal aerobic growth. This method was chosen because the fused tag [maltose-binding protein (MBP)] of this fusion protein (MoaA-MBP) has high solubility on its own. As a result, MBP-MoaA was expected to be more soluble than the protein of interest by itself (MoaA). A typical analytical SDS-PAGE gel of whole cells before and after induction is shown in Figure VIII.3.7.1. A seemingly good fusion protein (MoaA-MBP) migrating at ~ 80 kDa (compared to predicted MoaA-MBP (79.5 kDa) = MBP (42.5 kDa) + MoaA (37 kDa)) was overexpressed (Figure VIII.3.7.1).

Western blotting is a widely used method in molecular biology to identify specific proteins in a given sample. The methodology of this experiment is stated as follows. First, crude samples containing proteins are separated by electrophoresis according to molecular properties such as size. Second, proteins (e.g. as bands on an SDS-PAGE gel) are transferred out of the SDS gel and onto a nitrocellulose membrane. Third, proteins with specific sequences are then "probed" using antibodies specific to the target proteins. Fourth, a reporter enzyme detects the antibodies, which are now attached to the proteins of interest. Last, the reporter enzyme (as well as antibodies or the original protein of interest) is then exposed to an appropriate substrate to develop bands. As a result, proteins with specific sequences can be detected from the background.

The whole cell sample containing the expected overexpressed fusion protein was tested by western blotting (Figure VIII.3.7.2). The overexpressed band was clearly seen in the SDS-PAGE gel with the predicted molecular weight of about 80 kDa. However, the western blotting did not detect the presence of MBP tag in this heavily overexpressed band. Instead, a band with an apparent molecular weight of 43 kDa was detected, matching the molecular weight of MBP by itself. This result suggested to us that the overexpressed band was not the fusion protein MoaA-MBP as we expected. The appearance of MBP by itself on the western blot might suggest that either MoaA-MBP was cleaved after overexpression or the plasmid was damaged during the transformation into the Tuner competent cells.

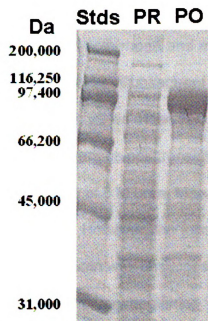


Figure VIII.3.7.1. SDS-PAGE of the overexpression of the MoaA-MBP fusion protein in whole cells. PR: uninduced cells. PO: induced whole cells. The large band shown at ~80 kDa matches the predicted MW of MoaA-MBP (79.5 kDa).

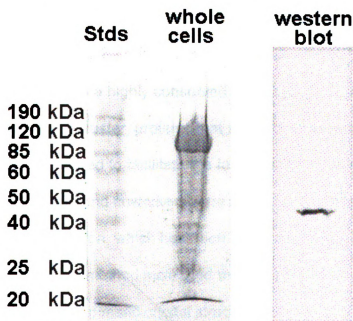


Figure VIII.3.7.2. SDS-PAGE and western blotting of whole cells containing MoaA-MBP fusion protein. Whole cell sample was acquired from 1 mL overexpressed culture. Lane 2: SDS-PAGE showing the resolved protein in whole cell sample. Lane 3: Western blotting of the same whole cell sample. The large band shown at ~80 kDa in the second lane matches the predicted MW of MoaA-MBP (79.5 kDa). The only band shown at ~45 kDa in the third lane matches the predicted MW of MBP (45 kDa).

VIII.4. Conclusions

We have successfully cloned both *moaA* and *moaC* genes from *E. coli* genomic DNA into the *pETBlue-1* vector. Subsequent transformations produced two overexpressing strains with high yields. However, the overexpressed MoaA was found in inclusion bodies and various posttranslational improvements did not yield soluble MoaA. In the presence of 6 M urea, MoaA was completely unfolded and brought into the soluble phase. However, the following purification of “refolded” MoaA on any type of column was unsuccessful; MoaA was always seen to elute out of the column at the very beginning, suggesting MoaA was not properly refolded during the renaturation step.

The extremely difficulty in solubilizing MoaA may suggest to us that the proper folding of MoaA requires some other accessory enzymes, such as MoaB or MoaC, which are encoded by genes located at the same ORF as *moaA* gene. Considering MoaA contains a highly conserved CX₃CX₂C motif, which coordinates an iron-sulfur cluster, proteins that are able to assemble the iron-sulfur cluster may be required to facilitate the formation of soluble form of MoaA.

In 2004, Schindelin and coworkers were able to coexpress MoaA in the presence of *E. coli suf* operon, which has been implicated in the iron-sulfur cluster assembly.^{17, 18} This method increased the solubility of MoaA. Since then, they were able to solve the dimeric crystal structures of MoaA, confirming the presence of two [4Fe-4S] clusters. The one close to the N terminus was a typical [4Fe-4S] for radical SAM superfamily enzymes, with its unique iron coordinated by SAM. The C terminal [4Fe-4S] cluster, which is unique to MoaA proteins,

bound the proposed substrate (5'-GTP) with high affinity.^{17, 19} In addition, the double glycine motif in the C-terminus of MoaA (Figure 6) has been suggested to be involved in the preservation of carbon in the substrate or the transfer of radical.⁶

VIII.5. References

1. Hille, R., The Mononuclear Molybdenum Enzymes. *Chemical Reviews* (Washington, D. C.) **1996**, 96, (7), 2757-2816.
2. Kisker, C.; Schindelin, H.; Rees, D. C., Molybdenum-cofactor-containing enzymes: structure and mechanism. *Annual Review of Biochemistry* **1997**, 66, 233-267.
3. Belikov, S. I.; Digas, S. E.; Khasnatinov, M. A., Detection of a new Rickettsia in ticks Dermacentor silvarum in the region of Baikal Lake. *Zhurnal Mikrobiologii, Epidemiologii i Immunobiologii* **2001**, (5), 8-11.
4. Rajagopalan, K. V.; Johnson, J. L., The pterin molybdenum cofactors. *Journal of Biological Chemistry* **1992**, 267, (15), 10199-202.
5. Wuebbens, M. M.; Rajagopalan, K. V., Investigation of the early steps of molybdopterin biosynthesis in Escherichia coli through the use of in vivo labeling studies. *Journal of Biological Chemistry* **1995**, 270, (3), 1082-7.
6. Wuebbens, M. M.; Liu, M. T.; Rajagopalan, K.; Schindelin, H., Insights into molybdenum cofactor deficiency provided by the crystal structure of the molybdenum cofactor biosynthesis protein MoaC. *Structure (London)* **2000**, 8, (7), 709-718.
7. Unkles, S. E.; Smith, J.; Kanan, G. J. M. M.; Millar, L. J.; Heck, I. S.; Boxer, D. H.; Kinghorn, J. R., The Aspergillus nidulans cnxABC locus is a single gene encoding two catalytic domains required for synthesis of precursor Z, an intermediate in molybdenum cofactor biosynthesis. *Journal of Biological Chemistry* **1997**, 272, (45), 28381-28390.
8. Hoff, T.; Schnorr, K. M.; Meyer, C.; Caboche, M., Isolation of two Arabidopsis cDNAs involved in early steps of molybdenum cofactor biosynthesis by functional complementation of Escherichia coli mutants. *Journal of Biological Chemistry* **1995**, 270, (11), 6100-7.
9. Reiss, J.; Cohen, N.; Dorche, C.; Mandel, H.; Mendel, R. R.; Stallmeyer, B.; Zabot, M.-T.; Dierks, T., Mutations in a polycistronic nuclear gene associated with molybdenum cofactor deficiency. *Nature Genetics* **1998**, 20, (1), 51-53.
10. Blakley, R. L.; Benkovic, S. J.; Editors, *Folates and Pterins, Vol. 2: Chemistry and Biochemistry of Pterins*. 1985; p 414 pp.

11. Wuebbens, M. M.; Rajagopalan, K. V., Structural characterization of a molybdopterin precursor. *Journal of Biological Chemistry* **1993**, 268, (18), 13493-8.
12. Rivers, S. L.; McNairn, E.; Blasco, F.; Giordano, G.; Boxer, D. H., Molecular genetic analysis of the moa operon of Escherichia coli K-12 required for molybdenum cofactor biosynthesis. *Molecular Microbiology* **1993**, 8, (6), 1071-81.
13. Menendez, C.; Siebert, D.; Brandsch, R., MoaA of Arthrobacter nicotinovorans pAO1 involved in Mo-pterin cofactor synthesis is an Fe-S protein. *FEBS Letters* **1996**, 391, (1,2), 101-103.
14. Solomon, P. S.; Shaw, A. L.; Lane, I.; Hanson, G. R.; Palmer, T.; McEwan, A. G., Characterization of a molybdenum cofactor biosynthetic gene cluster in Rhodobacter capsulatus which is specific for the biogenesis of dimethylsulfoxide reductase. *Microbiology (Reading, United Kingdom)* **1999**, 145, (6), 1421-1429.
15. Bader, G.; Gomez-Ortiz, M.; Haussmann, C.; Bacher, A.; Huber, R.; Fischer, M., Structure of the molybdenum-cofactor biosynthesis protein MoaB of Escherichia coli. *Acta Crystallographica, Section D: Biological Crystallography* **2004**, D60, (6), 1068-1075.
16. Broderick, J. B.; Henshaw, T. F.; Cheek, J.; Wojtuszewski, K.; Smith, S. R.; Trojan, M. R.; McGhan, R. M.; Kopf, A.; Kibbey, M.; Broderick, W. E., Pyruvate formate-lyase-activating enzyme: Strictly anaerobic isolation yields active enzyme containing a [3Fe-4S]⁺ cluster. *Biochemical and Biophysical Research Communications* **2000**, 269, (2), 451-456.
17. Haenzelmann, P.; Schindelin, H., Crystal structure of the S-adenosylmethionine-dependent enzyme MoaA and its implications for molybdenum cofactor deficiency in humans. *Proceedings of the National Academy of Sciences of the United States of America* **2004**, 101, (35), 12870-12875.
18. Outten, F. W.; Djaman, O.; Storz, G., A suf operon requirement for Fe-S cluster assembly during iron starvation in Escherichia coli. *Mol Microbiol* **2004**, 52, (3), 861-72.
19. Hanzelmann, P.; Schindelin, H., Binding of 5'-GTP to the C-terminal FeS cluster of the radical S-adenosylmethionine enzyme MoaA provides insights into its mechanism. *Proceedings of the National Academy of Sciences of the United States of America* **2006**, 103, (18), 6829-6834.

MICHIGAN STATE UNIVERSITY LIBRARIES



3 1293 02956 3263